THE NUMERICAL ANALYSIS OF

TURBULENT FREE JET FLOWS

A Thesis Submitted to the Council for National Academic Awards for the Degree of Master of Philosophy

by

Martin Downie

The Department of Civil Engineering
Sheffield City Polytechnic

October 1978

ACKNOWLEDGEMENTS

The author would like to express his gratitude to all those whose support have made this study possible. He is indepted to Prof. P Wolf and Dr K Arrumugam for their encouragement and assistance, particularly with regard to the experimental investigation which was conducted at City University. He also wishes to thank Mr A Kumar for his advice on aspects of the work involving fluid mechanics. Finally, the author would like to extend his grateful thanks to Dr N W Taylor for his patient and unflagging efforts in supervising this study.

ABSTRACT

During the past two decades, the dual development of the Generalised Discrete Methods of numerical analysis and the electronic digital computer has had an enormous impact on the field of engineering analysis. Its influence has been particularly evident in the field of linear structural analysis. The success of these methods, particularly that of the Ritz Finite Element Method, has aroused growing interest in their utilisation in the field of fluid mechanics. The proposed study is concerned with the application of a Generalised Discrete, or Finite Element, method of analysis to free turbulent jet flows.

This problem was considered to be appropriate for several reasons. First, a jet of fluid entrains and mixes with another fluid in a number of important engineering applications. Examples of these are legion and include their utilisation in the combustion chamber and other components of the reaction engine, the control of boundary layer seperation, film cooling in rocket and jet engines, various fluidic devices, ejector pumps and gas burners. Second, besides being of practical engineering significance, the free turbulent jet represents the simplest form of turbulence in which the effects of viscosity due to the presence of a solid wall have no influence. Third, the assumptions of modest non-homogeneity and high Reynolds number made in the proposed model of turbulence are satisfied. Finally, there is considerable data, both theoretical and experimental, with which to compare numerical results.

The proposed study entails the development of a standardised numerical approach to the solution of free turbulent jet flow problems. Particular emphasis is placed on the free plane turbulent jet from which further free jet studies may be extrapolated. Also included are corroborative experimental data and results obtained from alternative approaches to the problem.

CONTENTS

CHAPTER 5 : THE DISCRETE MODELLING OF THE TURBULENT PLANE JET

CHAPTER 6 : SOLUTION OF THE DISCRETE GLOBAL SYSTEM

CHAPTER 7 : THE CALCULATION PROCEDURE

CHAPTER 8 : CONCLUSIONS

APPENDICES

APPENDIX 1 : THE LASER DOPPLER ANEMOMETER

LIST OF FIGURES

APPENDIX I

LIST OF TABLES

CHAPTER 1

THE TURBULENT PLANE JET

1.1 Jet Flows

The jet has been classically defined as 'a stream of fluid shot forward or thrown upwards (either in a spurt or continuously), especially from a small orifice'[1]. This definition alone embraces many different flow configurations. Classification of jet flows with regard to four basic parameters allows for a precise definition of specific types of jet flow.

Firstly, the geometrical shape of a jet commonly falls into one of three catagories. The plane, or two-dimensional, jet has an efflux section which is effectively a long thin slot extending to infinity in a direction orthogonal to the axis of jet flow. The axisymmetric, or radial, jet flows from a circular orifice. The third geometrical configuration is of a three-dimensional mode and includes those cases which do not fall into the previous catagories.

Secondly, the boundaries of the jet flow may also be classified in three ways. In a free, or unbounded, jet the boundaries are assumed to be infinitely distant. The wall jet has one solid boundary, all others being infinitely distant, and the bounded jet is completely bounded in a manner commensurate with its dimensionality.

Thirdly, the jet may be mixing with a fluid that is stagnant, flowing in the same direction, or flowing in an adverse direction.

Finally, the basic properties of the fluid flow, such as whether or not the jet is turbulent, compressible or heated , may be delineated.

The jet flow to be considered in this study is the plane, unbounded, incompressible, iso-thermal turbulent jet exhausting into stagnant surroundings. For convenience this case will be simply referred to in the remainder of the study as the turbulent plane jet.

1.2 The Plane Jet Topology

The processes involved when a jet exhausts into stagnant surroundings may be most easily understood when considered in terms

of the conversion of kinetic energy[2]. The kinetic energy of the oncoming flow is steadily converted into the kinetic energy of turbulence, which in turn decays through the action of viscous shear. A simultaneous acceleration of the surrounding fluid is brought about by the deceleration of the jet. Thus the process continues as the distance from the jet increases and, due to the entrainment, the total rate of flow past successive sections becomes correspondingly larger.

The process is illustrated in Figure (1) in which the profiles represent the lateral distribution of 'U', the mean velocity in the X-direction. An initial zone of establishment exists beyond the efflux section. Due to the pronounced velocity discontinuity between the jet, which issues with uniform velocity, and the stagnant surrounding fluid, a lateral mixing process occurs in this zone of high shear. As a result the fluid within the jet is gradually decelerated and the surrounding fluid is entrained. Accordingly, the potential core of the jet steadily decreases in lateral extent whilst the breadth of the jet, 'b', increases with the distance from the efflux section. The structure of the potential core was demonstrated by Binnie[3] who set up an experiment in which a jet mixture of iodine and starch flowed into a region of sodium thiosulphate. The deep blue colour of the jet mixture was instantly annihilated on contact with the sodium thiosulphate, leaving the coloured zone clearly visible. The limit of the zone of establishment occurs when the mixing region has penetrated to the centre-line of the jet.

The fully established zone of flow occurs when the turbulent regime extends across the full breadth of the jet. Further entrainment of the surrounding fluid is balanced inertially by a continuous reduction in the velocity of the jet. This region was also demonstrated by Binnie by the introduction of black dye into the jet fluid[3]. This zone approaches, but never actually attains, a limit as the centre-line velocity becomes of negligible magnitude at a very great distance from the original efflux section of the jet. The process of entrainment is illustrated schematically in Figure (1) in which the streamlines represent the mean motion of the fluid[2]. It should be noted that although the direction of entrainment is

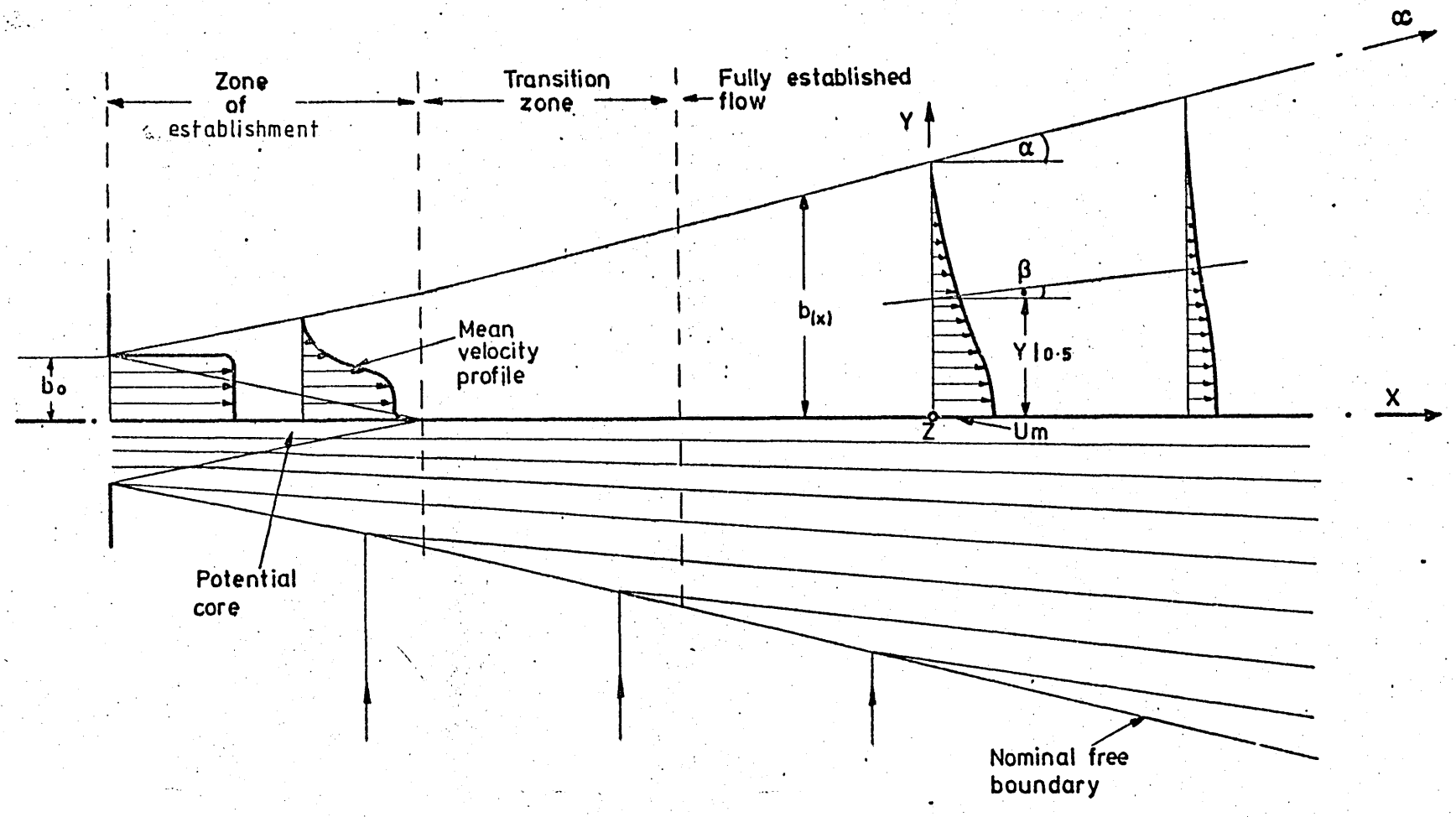

Figure 1.

Schematic Representation Of The Turbulent Plane Jet.

conventionally accepted to be an angle of 90° to the jet axis, it has been observed to vary from this figure[4].

Between these two well-defined flow regimes there is a transition zone. It owes its being to the fact that there is no precise point at which the mixing regions from opposite sides of the jet can be said to meet, for the statistical nature of the process makes it impossible to place more than an arbitary limit on its lateral range.

Similarly, the free boundaries, like the boundaries between the two zones, must be accepted as merely convenient nominations[2]. Whilst there is general agreement that the spread of the jet may be represented by a curve increasing linearly with distance from the efflux section, there is some disagreement relating to the angle of spread, 'α'. A literature survey[2][5][6][7][8][9][10] of those publications from which it is possible to extract a value for the angle of spread from either experimental results, theoretical derivations or from their interpretation, yields a value of ;

$$12.50^\circ \leqslant \alpha \leqslant 16.13^\circ \qquad \ldots\ldots\ldots \quad (1.1)$$

The angle of spread given in Figure (1) and later adopted for the numerical work is 14.04°, which gives ;

$$\alpha = \arctan(1/4) \qquad \ldots\ldots\ldots \quad (1.2)$$

and is in good agreement with the general concensus. The rate of spread of the jet is more commonly given in terms of 'β', the half-angle, where ;

$$\beta = \arctan(Y|_{0.5}/X) \qquad \ldots\ldots\ldots \quad (1.3)$$

where '$Y|_{0.5}$' is the ordinate at which the velocity is half the maximum velocity for any given value of X. The range of values to be found in the literature[4][11][12][13][14][15][16] is ;

$$5.00^\circ \leqslant \beta \leqslant 6.28^\circ \qquad \ldots\ldots\ldots \quad (1.4)$$

the mean value being in the region of 5.70°.

1.3 The Turbulent Plane Jet Flow Characteristics

In the mathematical description of turbulent flows, it is convenient to assume that the motion consists of a mean flow and a fluctuation about the mean flow[17]. Let the mean velocity components relative to the Cartesian axes 'X,Y,Z' be denoted by 'U,V,W', the fluctuating velocity components by u,v,w and the total velocity components by 'U,V,W' respectively. Thus ;

$$U = U + u \qquad \ldots\ldots\ldots \quad (1.5)$$

$$V = V + v \qquad \ldots\ldots\ldots \quad (1.6)$$

$$W = W + w \qquad \ldots\ldots\ldots \quad (1.7)$$

The temporal mean of any quantity f(X,Y,Z,t) at time 't_0', denoted by '$\bar{f}$', may be defined as ;

$$\bar{f} = \frac{1}{T}\int_{t_0 - \frac{T}{2}}^{t_0 + \frac{T}{2}} f \, dt \qquad \ldots\ldots\ldots \quad (1.8)$$

where 'T' is the period of sampling which is sufficiently large to include an adequate number of fluctuations but is short compared with some period representitive of long term variations in '$\bar{f}$'.

Consider now an elementary area co-planar with the 'Y-Z' plane of a turbulent fluid whose velocity components are 'U,V,W'. The superposition of the fluctuations on the mean motion gives rise to three additional stresses ;

$$\tau_{XX} = -\rho\overline{u^2} \qquad \ldots\ldots\ldots \quad (1.9)$$

$$\tau_{XY} = -\rho\overline{uv} \qquad \ldots\ldots\ldots \quad (1.10)$$

$$\tau_{XZ} = -\rho\overline{uw} \qquad \ldots\ldots\ldots \quad (1.11)$$

acting on the elementary surface[18]. The over-bar denotes the temporal mean of the relevant quantity and 'ρ' is the density of the fluid. Corresponding expressions apply in the case of elementary areas normal to the two remaining axes to provide a complete stress tensor for turbulent flow.

The stress components arising through the superposition of the fluctuations are known as eddy stresses. They are additional

to the viscous stresses which arise from the much smaller scale of random molecular movement. In two-dimensional turbulent shear flow in the 'X-Y' plane, the stress 'τ_{XY}' (the Reynolds stress) is of major importance and its magnitude is far greater than the viscous stress '$\mu\partial U/\partial Y$' - 'μ' is the fluid viscosity - or the other eddy stresses[19].

If the lateral distribution of the mean velocity, 'U', is measured at a number of stations along the X-axis of the jet and the results are plotted together, the diagram shown in Figure (2.a) is obtained[6]. The mean velocities decrease as the distance from the efflux section increases. If the same results are plotted non-dimensionally, as in Figure (2.b), they collapse onto a single curve[6]. The lateral distribution of 'U' retains the same functional form at all downstream locations while changing only in scale,

ie ;
$$U = U_m f(Y/b) \qquad \ldots\ldots\ldots \quad (1.12)$$

where 'U_m' is the maximum mean velocity at any one station and occurs on the jet axis. This phenomenon is known as similarity[20]. The plane free jet belongs to a class of flows, described as self-preserving flows[21], in which the whole structure of the flow is similar at all streamwise stations. The necessary conditions[22] of self-preservation in the plane free jet are,

$$\frac{db}{dX} = \text{constant} \qquad \ldots\ldots\ldots \quad (1.13)$$

$$U_m^2 = \text{constant}.X^{-1} \qquad \ldots\ldots\ldots \quad (1.14)$$

The decay of the centre-line velocity is illustrated in Figure (2.c).

The manner in which the fluctuating components are distributed across the jet is illustrated in Figures (3)(4) and (5). The turbulent intensity (ie: the ratio of the fluctuating to the mean velocity) increases significantly towards the edges of the jet, as shown in Figure (3)[15]. For this reason, inaccuracies inevitably occur in measurements taken in this region of the jet. The lateral distribution of the non-dimensionalised fluctuating velocity components is illustrated in Figures (4) and (5.a)[22]. The development of similar profiles is demonstrated in Figure (4.a) and

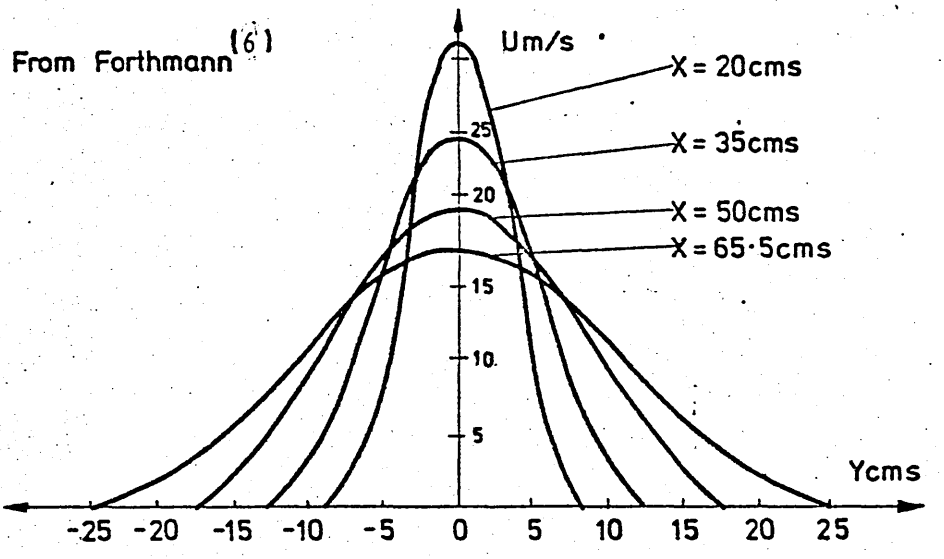

a) Mean Velocity Profiles.

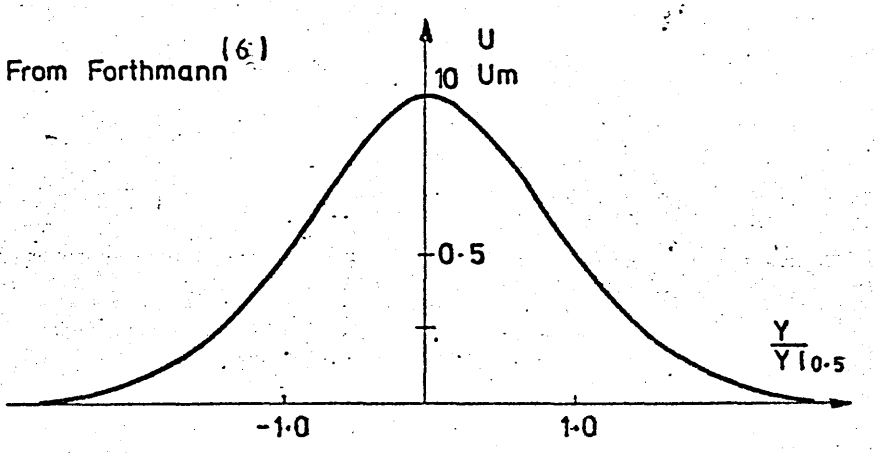

b) Similarity Of Velocity Profiles.

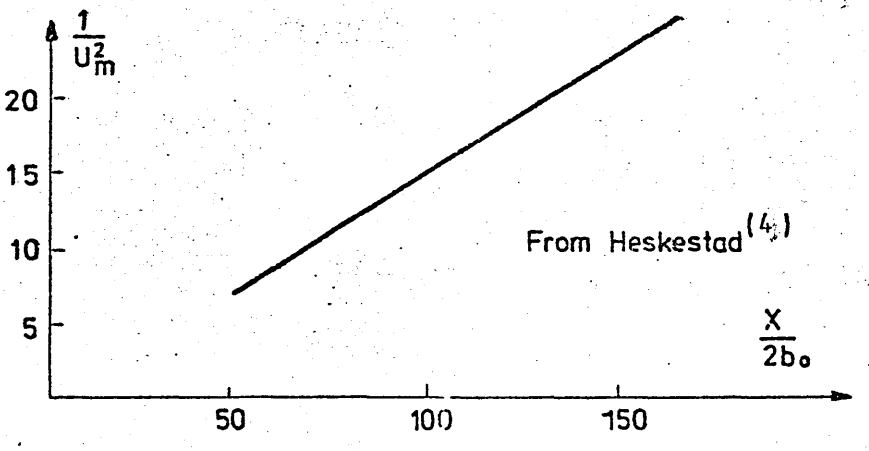

c) Decay Of Centre-line Velocity.

Figure 2

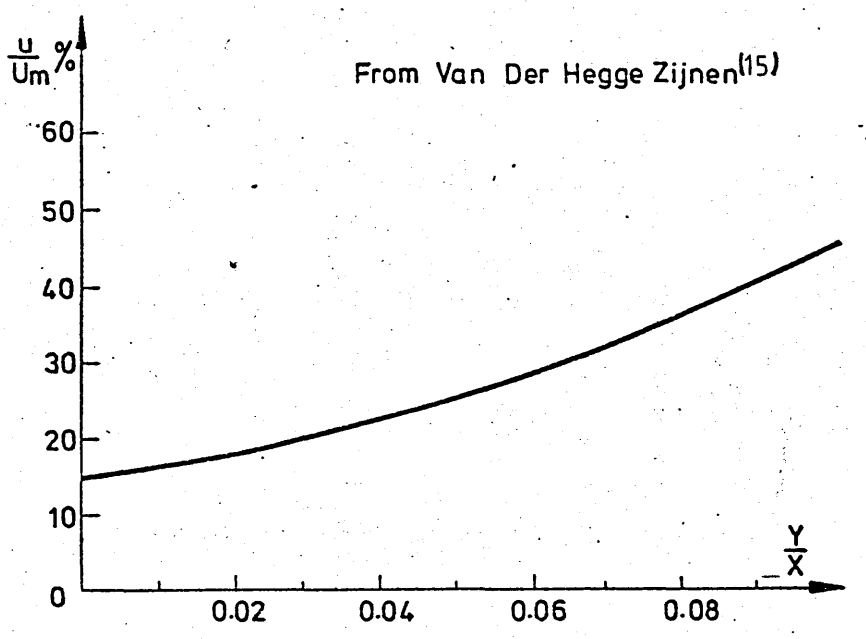

a) Axial Intensity Of Turbulence

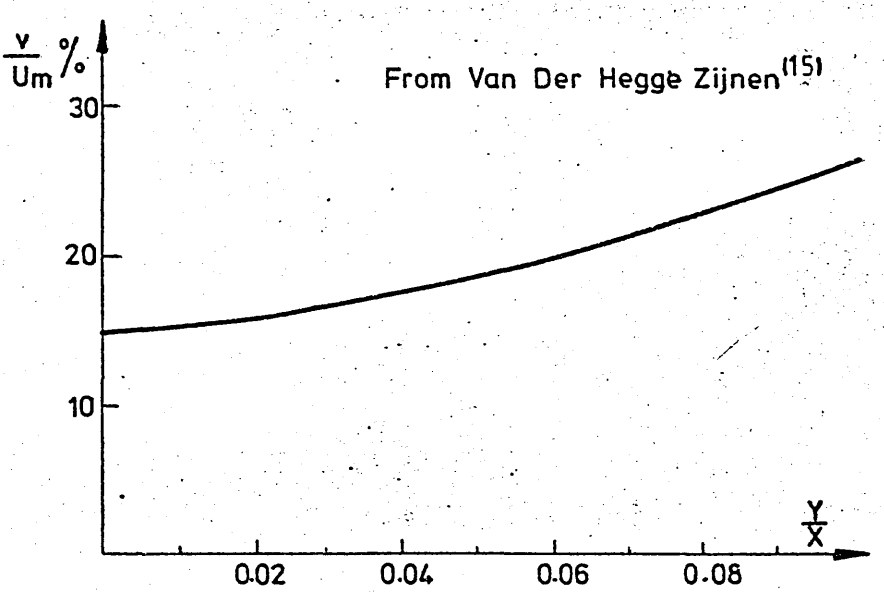

b) Transverse Intensity Of Turbulence

Figure 3

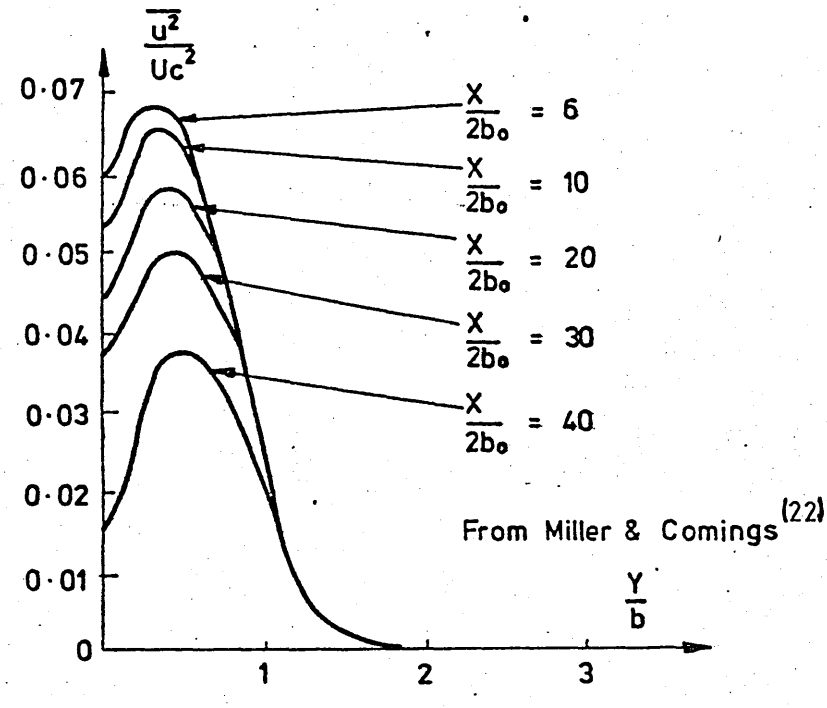

a) Turbulent X-stress Profiles.

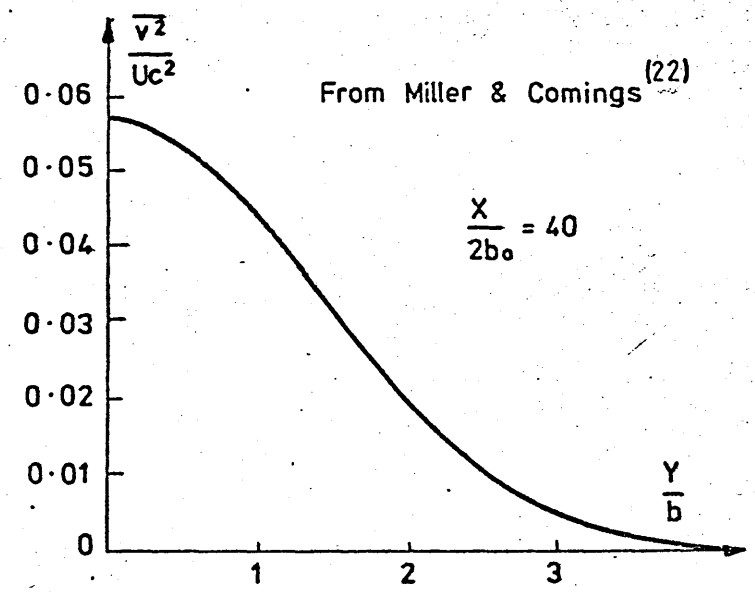

b) Turbulent Y-stress Profile.

Figure 4

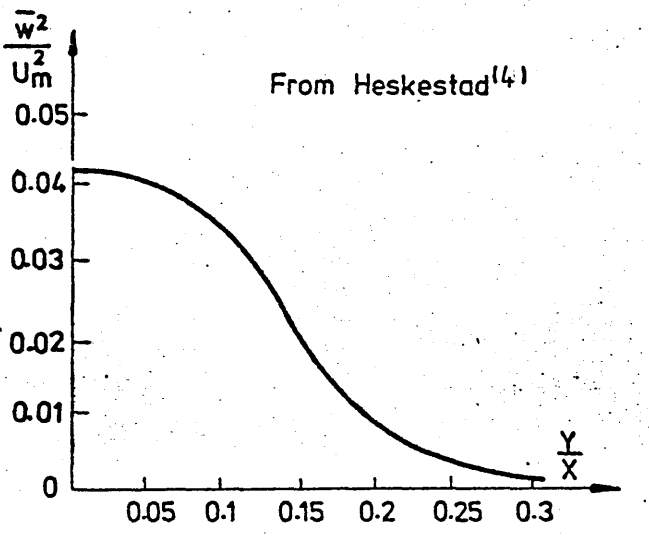

a) Turbulent $\overline{z}$-Stress Profile

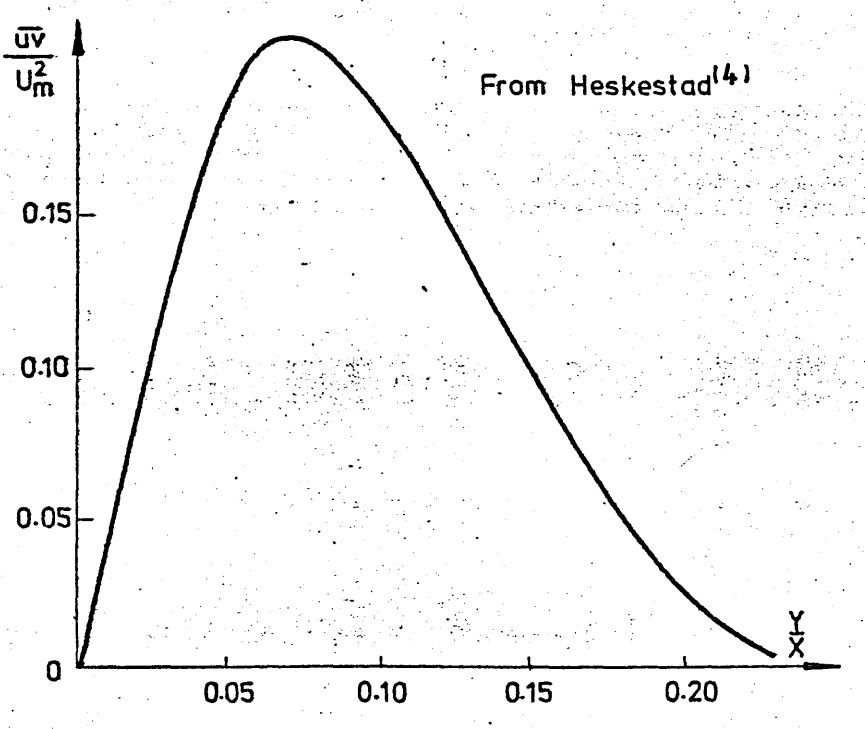

b) Reynolds Shear Stress Profile

Figure 5

it is interesting to note that 'partial self-preservation'[23] is exhibited in the outer region of the jet well before a complete similarity of profiles is obtained.

The lateral distribution of the Reynolds stresses, '$\overline{uv}$', is given in Figure (5.b)[22], which illustrates the manner in which the shear stresses disappear along the symmetry boundary at the centre of the jet. The development of the turbulent intensities along the axis of the jet is shown in Figure (6)[15]. Similarity of profiles is attained some forty nozzle-widths down stream of the efflux section, this result being slightly at variance with other investigations[16][22]. The magnitude of the turbulent intensities may be seen to approach the same value as the distance from the efflux section increases, thus giving credence to the theoretical assumptions of isotropic turbulence.

With the occurrence of shearing and tensile or compressive stresses, kinetic energy is withdrawn from the basic flow and partly reappears as kinetic energy of the disordered turbulence motion[24]. The time average of the kinetic energy of turbulence, 'k', referred to the unit mass, may be defined as,

$$k = \frac{1}{2}(\overline{u^2} + \overline{v^2} + \overline{w^2}) \qquad \ldots\ldots\ldots \quad (1.15)$$

The lateral distribution of 'k' is illustrated non-dimensionally in Figure (7)[16]. The minimum at the centre is characteristic of the plane jet and is largely due to the absence of shear stress at this point.

A further characteristic exhibited by turbulent jet flows is the phenomenon known as intermittency. Intermittancy may best be described by postulating a flow field in which an outer region of irrotational flow is seperated from an inner core of fully developed turbulence by an irregular boundary. Thus at points approaching the outer region of the jet, the irrotational flow is interupted by bursts of turbulence as the irregularities of the core boundary are carried downstream. 'A point of interest is whether the essentially irrotational flow that exists between the turbulent bursts has a mean velocity equal to the free stream velocity, or whether it is accelerated by pressure forces to have a mean velocity equal to that of the turbulent fluid'[16]. Bradbury tends to the view expressed by

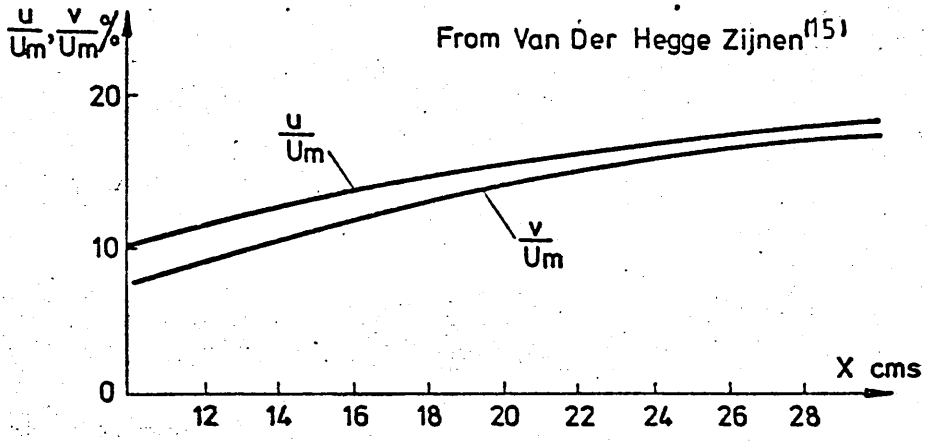

Figure 6 : Intensity Of Turbulence On Jet Axis

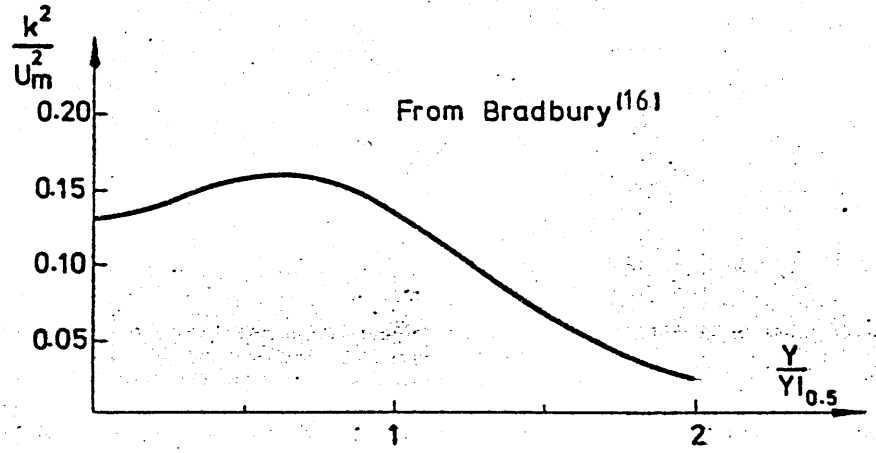

Figure 7: Turbulent Energy Distribution

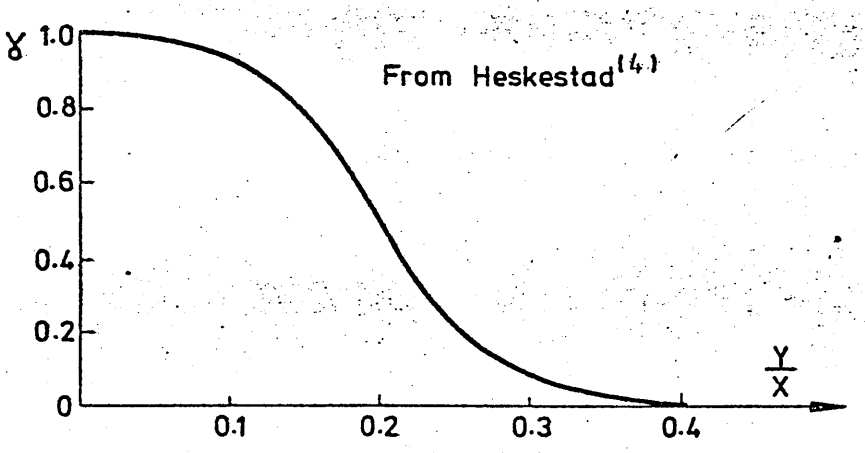

Figure 8 : Lateral Distribution Of Intermittency

Townsend, namely that the irrotational flow has the same mean velocity as the turbulent fluid.

The intermittency factor at a point may be defined as the fraction of the total time the point is immersed in the turbulent fluid. The lateral distribution of the intermittency factor is illustrated in Figure (8)[16], and it may be seen to decrease rapidly in the outer half of the jet. That is, the flow becomes increasingly intermittant as the jet boundaries are approached. It is necessary, therefore, to make allowance for the intermittency factor when taking measurements of properties associated with turbulent flow. For example, quantities such as the turbulent energy and the turbulent shear stress are small or zero in the irrotational flow occurring between the turbulent bursts. The measurement of these quantities, therefore, must be divided by the intermittency factor in order to obtain the average values within the turbulent field.

1.4 Mechanisms of Turbulence in the Plane Jet

Having established the basic properties of the jet flow, it is necessary to account for the mechanisms from which they stem. Many attempts have been made to provide a satisfactory explanation of the structure of shear flow turbulence and a number of different approaches have been proposed. The ideas currently in favour have been clearly and succinctly described by Bradshaw[25].

The basic structure of the flow may be thought of as a development of that proposed by Townsend[18]. This stated that it consisted of a series of large eddies, whose lateral dimensions are comparable to the width of the flow, with the remaining flow containing most of the turbulent motion and having a scale which is an order of magnitude smaller than the large eddies. Energy is passed from the mean flow to the large eddies from whence it is passed on again to the smaller eddies by a process known as vortex stretching[26][27]. For a significant part of their existence the large eddies dominating the flow are in energy equilibrium, gaining energy from the mean flow whilst losing it at an equal rate to the remaining turbulent motion. Energy enters the turbulence if the vortex elements are mainly orientated in the right sense to be stretched by the mean velocity gradients. The part of the motion

that might be expected to interact with the mean flow consists of those eddies which are not too small in comparison with the mean flow width. Thus, the larger scale motion carries most of the energy and the Reynolds stresses in the turbulence. This contradicts Townsend's original hypothesis but has been re-affirmed by Bradbury[16]. The latter noticed a close relationship between these eddies and the intermittancy. The motion of the large eddies is such that not only do they migrate across the flow, but they travel downstream a distance equivalent to many times its width. For this reason transport equations are required for an adequate description of the turbulent motion, since the Reynolds stress at any given position depends significantly upon the upstream history[25].

By relating the terms in the transport equations to the processes they represent (eg; energy dissipation), and the mechanisms associated with them (eg; the transfer of energy to viscosity-dependant eddies by vortex stretching), a more detailed picture of the flow may be gained. The transport equation for the Reynolds shear stress for steady incompressible flow in the X-Y plane may be written[25]

$$(U\frac{\partial}{\partial X} + V\frac{\partial}{\partial Y} - W\frac{\partial}{\partial Z})(-\overline{uv}) = \bar{\gamma}_1 - \bar{\gamma}_2 + \bar{\gamma}_3 + \bar{\gamma}_4 - \bar{\gamma}_5 \quad \ldots (1.16)$$

where $\bar{\gamma}_1$ represents generation by interaction with the mean flow,

ie ; $$\overline{v^2}\frac{\partial U}{\partial Y} + \overline{u^2}\frac{\partial V}{\partial X} + \overline{uv}(\frac{\partial U}{\partial X} + \frac{\partial V}{\partial Y}) + \overline{vw}\frac{\partial U}{\partial Z} + \overline{uw}\frac{\partial V}{\partial Z} = \bar{\gamma}_1 \quad \ldots (1.17)$$

$\bar{\gamma}_2$ represents redistribution by pressure fluctuations,

ie ; $$\overline{\frac{p}{\rho}(\frac{\partial u}{\partial Y} + \frac{\partial v}{\partial X})} = \bar{\gamma}_2 \quad \ldots (1.18)$$

(where 'p' is the fluctuation in pressure corresponding to u, v and w)

$\bar{\gamma}_3$ represents transport by velocity fluctuations,

ie ; $$(\frac{\partial \overline{u^2 v}}{\partial X} + \frac{\partial \overline{uv^2}}{\partial Y} + \frac{\partial \overline{uvw}}{\partial Z}) = \bar{\gamma}_3 \quad \ldots (1.19)$$

$\bar{\gamma}_4$ represents transport by pressure fluctuations,

$$\frac{1}{\rho}\left(\frac{\partial pu}{\partial Y} + \frac{\partial pv}{\partial X}\right) = \bar{\gamma}_4 \qquad \ldots\ldots\ldots \quad (1.20)$$

and $\bar{\gamma}_5$ represents transport and destruction by viscous forces,

$$\nu\left(u\nabla^2 v + v\nabla^2 u\right) = \bar{\gamma}_5 \qquad \ldots\ldots\ldots \quad (1.21)$$

(where 'ν' is the kinematic viscosity (μ/ρ) and '∇' is a differential operator).

In a two-dimensional thin shear layer (eg; a plane jet) only the under-lined terms of '$\bar{\gamma}_i$' ($i = 1,5$) remain. Clarification of the related assumptions is given in Chapter III.

The left-hand side of the equation (1.16) and '$\bar{\gamma}_1$' are straightforward in mathematical content and physical meaning. The term '$\bar{\gamma}_2$' is the rate at which '$\overline{uv}$' is destroyed by the interaction of the pressure fluctuations and the fluctuating rate of strain. The net rate of spatial transport of '$\overline{uv}$' by the turbulence is denoted by '$\bar{\gamma}_3$' and '$\bar{\gamma}_4$', the latter usually being ignored since it is much the smaller of the two. The term '$\bar{\gamma}_5$' is the sum of the net spatial transport and destruction of the Reynolds stresses by viscous effects. The presence of the second derivatives indicates that the process is associated with the smallest eddies. Thus the viscous transport of the Reynolds stress is negligible since these eddies contribute little to the Reynolds stress. The rate at which energy is dissipated by the small eddies is dependent on the rate at which it is supplied by the large eddies and, again, is independent of viscosity.

The transport equation for any other individual Reynolds stress has a similar structure to equation (1.16)[25]. The transport equation for half the sum of the Reynolds normal stresses, 'k', is known as the turbulent energy equation. It is the transport equation whose terms have been measured most extensively and, since it describes the balance of the kinetic energy contained in the velocity fluctuations, is physically the most graphic one[24]. The term in this equation analagous to the redistribution term '$\bar{\gamma}_2$' in equation (1.16) sums to zero. The left-hand side of the equation is termed advection and '$\bar{\gamma}_1$', '$\bar{\gamma}_3 + \bar{\gamma}_4$' and '$\bar{\gamma}_5$' are termed production diffusion and dissipation respectively. The equation may thus be written in the form[16];

advection | production from shear stresses | production from normal stresses | diffusion | dissipation

If the distribution of the advection, production and dissipation terms are known, the diffusion term can readily be obtained by the inherent difference. By plotting the lateral distribution of each term, their relative contributions, or the 'energy balance', may be easily appreciated. The energy balance obtained by Bradbury[16] is shown in Figure (9.a), the axial development along the centre-line of the jet from Heskestad's[4] study is shown in Figure (9.b).

The energy balance shows clearly that 'in the fully turbulent region, the rate of energy production by the action of Reynolds stresses, is greatest near the inflection points of the mean velocity profile; the energy dissipation is, on the other hand, more diffuse, being surprisingly uniform throughout the turbulent region'[28]. That the viscous dissipation and production terms are the most significant in the energy balance, has been shown quantitatively by Bradbury[16] who compared the integral values of the various terms over the jet width. He found the magnitudes of the integrals of the production, dissipation and the advection terms to be -0.0169, 0.0207 and -0.0038 respectively, the integral of the diffusion term being zero by definition. The relatively low values of advection, along with the absence of shear stress at the centre, are responsible for the characteristic minimum exhibited by 'k' on at the centre of the jet.

The chronological development of investigations leading to the discovery of the jet features described above is now considered.

1.5 A Review of Jets in their Historical Context

The jet has been employed in various forms as an engineering device throughout the history of civilised man. As long ago as 1000 B.C. it was used by the Egyptians in the form of bellows for primitive forges[29]. Ctesibius, a contemporary of Archimedes (287-212 B.C.), and who studied at Alexandria under the disciples of Euclid, is credited with the invention of a two-piston positive displacement pump which was eventually applied to the production of a water jet for fighting fires[30]. Hero (circa 100 A.D.) constructed

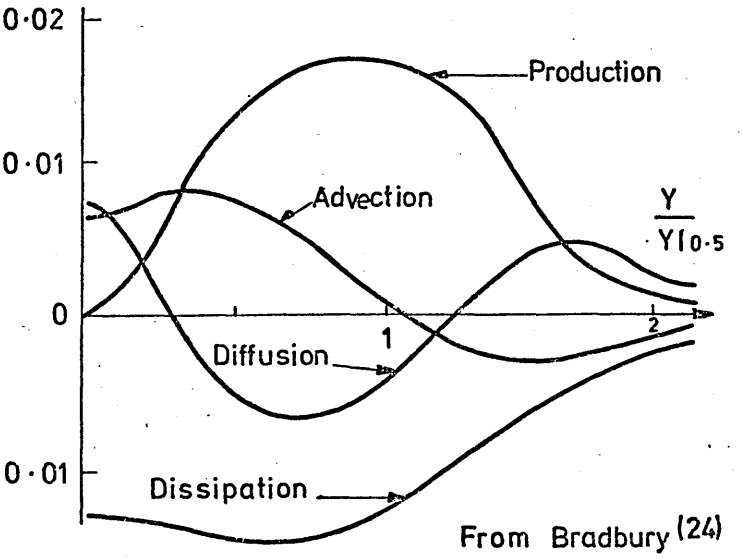

a) Turbulent Energy Balance

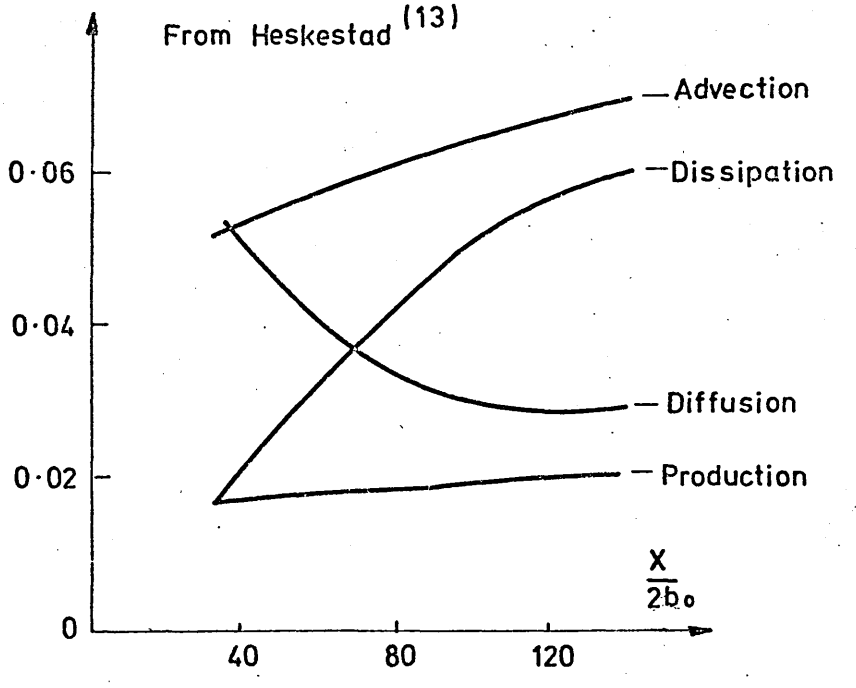

b) Axial Distribution Of Energy Balance On Jet Centre-line.

Figure 9

a rudimentary steam engine working on a jet reaction principle and consisting of a rotating steam driven device operating on the same basis as many present-day lawn sprinklers[31]. It was regarded by Hero as a curious toy rather than a useful machine[29]. In the twelth or thirteenth century an improvement of the foot-driven bellows of the Egytians appeared in Europe (probably imported by returning Crusaders), in the shape of furnace bellows driven by water wheels.

During the fifteenth century, the Rennaissance brought with it a gradual change in thought from the purely philosophical to observational science. Perhaps the most impressive of the early proponents of this approach was Leonardo da Vinci (1452-1519)[30]. Amongst his many achievements, he made a significant contribution to the development of hydraulics in his collected writings 'Del moto e misura dell'acqua'[29]. Included in the phenomena of which he was the first to sketch or describe, is that of the profiles of free jets.

Early in the seventeenth century, Evangelista Torricelli, in his work 'de moto gravium'[30] proposed a hypothysis relating to the efflux of a fluid from an orifice. In an attempt to prove his hypothesis, he conducted several experiments using water jets. In 1686, Marriotte's work 'Traite du movement des eaux et des autres corps fluides'[30] was published. It included in the section dealing with the 'equilibrium of fluid bodies by weight', a series of rules describing the deflection of a jet by a normal surface. He also produced analyses of the parabolic trajectories of jets discharged at different inclinations.

Isaac Newton (1642-1727) was also interested in the problem of efflux from an orifice. In his hypothysis postulated in his 1687 edition of 'Principia Mathematica Philosophiae Naturalis'[33], his computed rate of efflux differed from that actually measured by a factor approximately equal to the square root of two. In the second edition, published in 1713, he attributed the error to the contraction of the jet.

The treatise 'Hydrodynamica', by Daniel Bernoulli, was published in 1738; a section was devoted to 'the velocity of efflux and efflux under constant head'[32]. He originated the idea of jet propulsion for ships, although he was thinking only in terms of the

reaction produced by the efflux of water from a tank. Fifty years later this idea was to be improved upon by an American named James Rumsey. He employed the newly-developed steam engine to propel a boat on the Potomac River by utilising the reaction of a jet of water produced by a steam driven piston pump.

In 1766 Borda published a treatise entitled 'Memoire sur l'ecoulement des fluids par les orifices des vases'[30], in which he sought to remove certain discrepancies in Bernoulli's and d'Alembert's analyses of the efflux problem. Besides introducing the concept of elementary stream tubes, he also showed that not only the contraction of the jet, but also a loss of energy, must usually be taken into account in formulating the discharge rate.

The year 1854 saw the publication of a paper by G.H.L. Hagen 'Ueber den Einfluss der Temperatur auf die Bewegung des Wassers in Röhren'[30], in which he dealt with the effect of temperature upon the resistance to flow through pipes. In the course of his experimental work he noticed that the appearance of an efflux jet varied with temperature, remaining 'immovable as though it were a solid glass rod', at low temperature and exhibiting 'very noticable fluctuations of short period', as the temperature rose[29]. He went on to introduce sawdust into water flowing through glass tubes and observed similar phenomena to those described by Osborne Reynolds in the latter's famous paper of 1883[33]. The laws of instability of streamline motion and the fundamental facts of turbulent flow[30], as proposed by Reynolds, have provided one of the major contributions to contemporary fluid mechanics. One of the earliest papers published by Reynolds was concerned with the suspension of a ball by a jet of water[33].

The early part of the twentieth century saw the beginning of increasingly systematic and detailed investigations into jet flows. Interest in the field was heightened by a growing awareness of the potential of jet propulsion particularly with regard to aircraft[34]. The development of the jet engine, and related research into jet flows, was accelerated by the military implications. The extent of research in this field is such as to go beyond the scope of this study. The ensuing account will now be mainly confined to describing investigations relating to plane jet flows.

Probably the first significant investigation of the plane jet was carried out by Forthmann[6] in 1934 when he made a number of measurements of the mean velocity of a jet issuing into still air. Over the next two decades other similar investigations were made - Kuethe[7] in 1935, Albertson et al.[2] in 1948, and Abramovich[35] in 1957 - most of them being concerned with the development of phenomenological expressions for the prediction of the mean velocity distribution and the spread of the jet. A number of theoretical models were proposed over this period, ranging from Schlichting's approximate solution of a laminar jet[18], to be later developed by Bickley[36], to various analyses of the turbulent jet. Prominent amongst the latter were those of Tollmien and Gortler, employing different approaches utilising Prandtl's momentum transfer theories, Howarth, using Taylor's vorticity-transfer theory, and Reichardt, employing a molecular analogy theory. Detailed descriptions of these studies can be found in standard texts[26][10][18]. In the late fifties, a further advance in the knowledge in the nature of the turbulent jet was made by Miller and Comings[22], who investigated its static pressure distribution, and B.G. van der Hegge Zijnen[14][15], who investigated both the mean and the fluctuating velocity distributions.

The last decade has seen research directed towards the establishment of the actual structure of the jet[26][37][38][39] and investigation of such phenomena as intermittancy, self-preservation and the behaviour of the jet in a co-flowing stream[4][16]. The investigations have been very much associated with the large eddy hypothesis proposed by Townsend[20] and its ensuing development. The analytical work that has been carried out over this period has mainly been concerned with the solution of differential transport equations of various turbulent quantities. Such solutions have employed approximate numerical methods, notably the Finite Difference method, in conjunction with the electronic digital computer[40]. This topic is discussed further in Chapter Four.

1.6 Summary

The aim of this chapter has been three-fold; firstly, to delineate clearly and logically the problem to be considered in

this study and, secondly, to introduce, and where necessary define, the basic parameters to be encountered in the succeeding chapters. To this end, the classification of jet flows has been discussed, the topology of the problem domain has been outlined, and the mechanisms and corresponding flow characteristics have been considered. Finally, a review of the history of jets, and a chronological account of their more recent investigation have been given. The qualitative element in this chapter is to be substantiated more quantitatively, albeit in a somewhat simplified manner, in Chapter Two which contains the results of an exploratory experimental investigation of the plane jet.

CHAPTER 2

AN EXPERIMENTAL STUDY

2.1 Introduction

The experimental work in this chapter should be viewed in the light of the scope and the objectives of this study. The study is essentially concerned with the development of a numerical predictive technique for jet flows. A full experimental investigation involving, for example, the measurement of the distribution of the fluctuating components of velocity, is not proposed. Established data of this nature may be found in the relevant literature[4][14][15][38]. The principal objective of this investigation was to familiarise the author with the physical characteristics of the plane jet. The experimental work was conducted in the Fluid Mechanics Laboratory at the City University employing the air jet apparatus belonging to the Department of Civil Engineering.

2.2 Experimental Apparatus

The apparatus used in the investigation was an adaptation of a standard piece of equipment designed and built by Plint and Partners Ltd.[41] to demonstrate the main air jet characteristics. It is illustrated in Figure (10) and basically consists of a nozzle mounted horizontally on a horizontal plate. The air was supplied to the nozzle by a centrifugal fan which discharged into a plenum chamber containing a smoothing gauze. The discharge velocity was controlled by a throttle valve and the pressure in the plenum chamber was indicated by a sensitive manometer. The velocity distribution in the jet was measured by a total head tube carried on a graduated slide capable of traversing across any section of the jet.

The use of a total head tube implies that the static pressure is constant throughout the jet. Whilst this is not strictly true, it may be argued that it is a valid assumption for experimental purposes[14]. The subject was investigated in some detail by Miller and Comings[22], who concluded that although a small negative static pressure field exists throughout the turbulent region, it plays a minor role in the X-Reynolds equation and may be considered negligible.

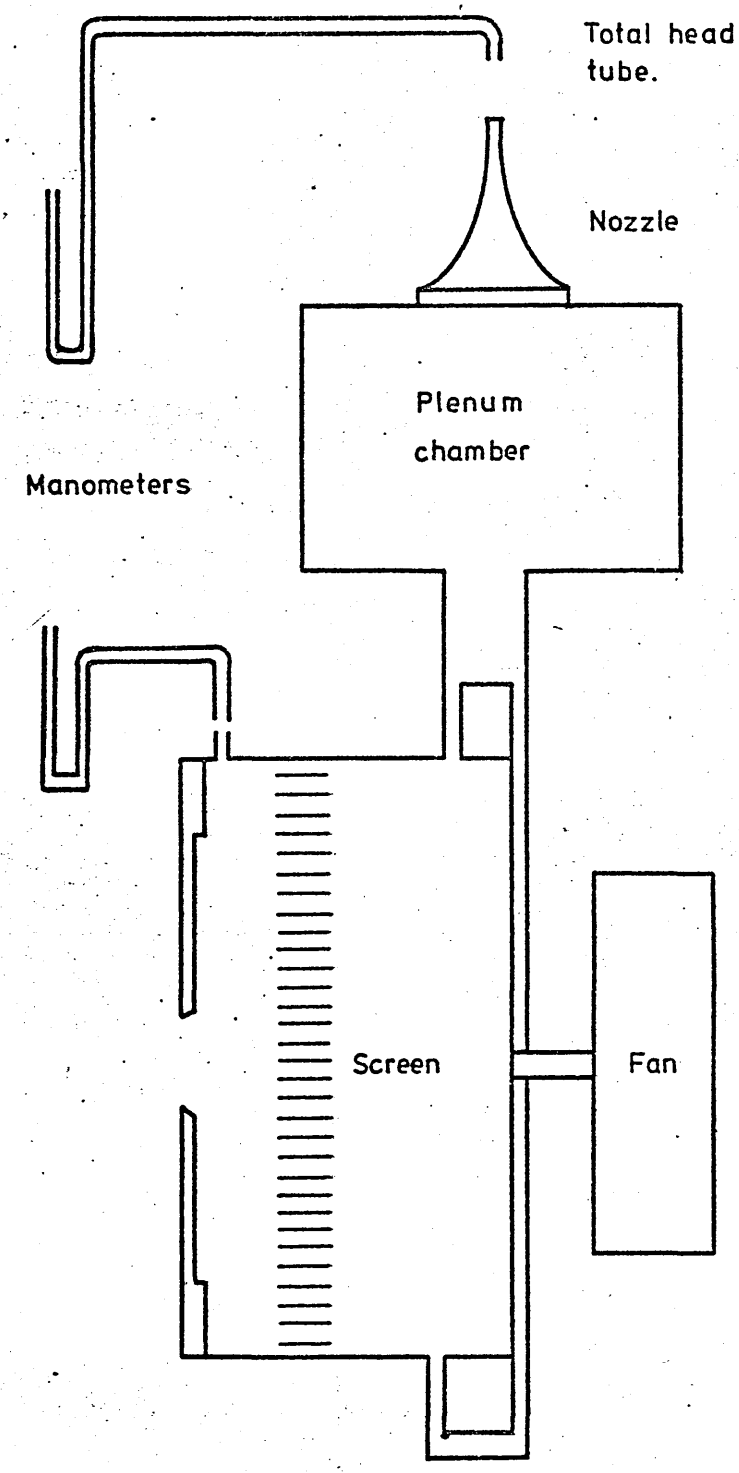

Schematic Layout Of Apparatus.

Figure 10

The nozzle was designed by the author and constructed in the Polytechnic workshop. Its purpose was to provide a smooth transition from an orifice of circular cross-section to a slot of sufficiently high length to breadth ratio to approximate the two-dimensional flow of the plane jet. The working drawing for the nozzle construction is shown in Figure (11). The nozzle dimensions had to be chosen not only to fit the existing apparatus, but also to satisfy criteria of two-dimensionality. Various length to breadth ratios have been employed in previous investigations. Fürthmann[6] states that the condition of two-dimensionality may be closely approached by a slot whose length is twenty times its breadth. The length to breadth ratio used in this study was just over twenty-eight to one. This is in excess of the ratios employed by Weinstein[12] and Van der Hegge Zijnen[14]. A preliminary traverse was carried out along the Z-axis, as shown in Figure (12), of the jet to ensure that the velocity was reasonably uniform over the middle section of the nozzle. This was found to be the case and the conditions for two-dimensional flow were assumed to exist along the X-axis of the jet.

2.3 Experimental Procedure

The transverse distribution of the mean velocity, 'U', was investigated at a Reynolds number, 'Re', of 1.2×10^4 where;

$$Re = \frac{U_0 b_0}{\nu} \qquad \ldots\ldots\ldots \quad (2.1)$$

is based on the exit velocity, 'U_0', and the slot breadth, 'b_0'. Traverses in the X-Y plane of the jet were carried out at seven different stations along its centre-line, as depicted in Figure (12). The complete set of data obtained in the experiment is given in Tables (1) to (5) and is represented graphically in Figure (13).

Corrections for the displacement of the effective centre of the total head tube, 'd', were not made. It has been found[42] that in a pure shear flow, the ratio 'd/D' (where D is the external diameter of the tube) is independant of Reynolds number and has a constant value of the order of 0.15. Corrections of this magnitude were not warranted by the accuracy of the experimental apparatus.

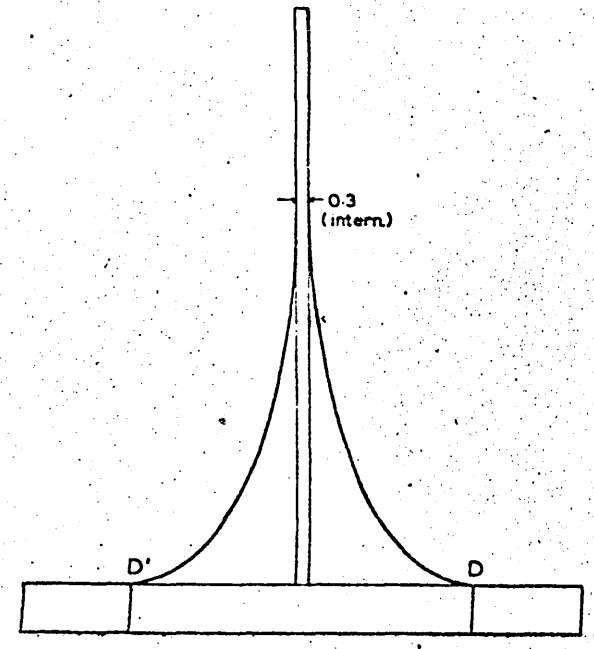

SECTION THRU BD'D

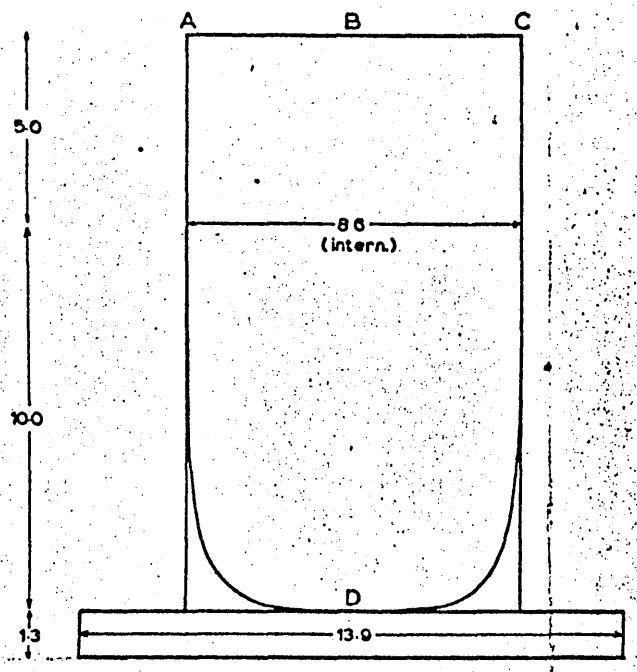

SIDE ELEVATION

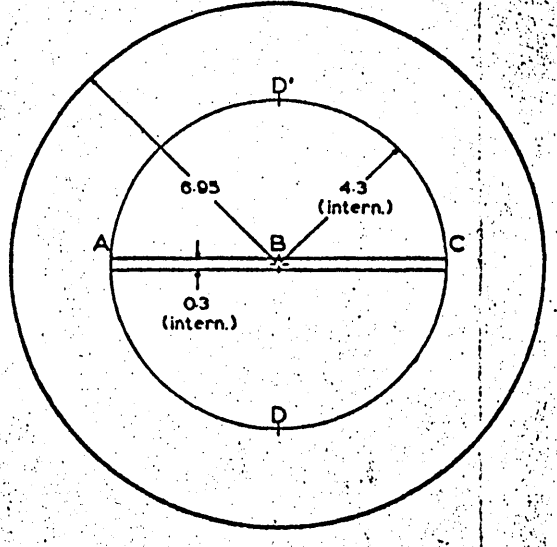

PLAN

PLANE JET NOZZLE.
SCALE 1:1

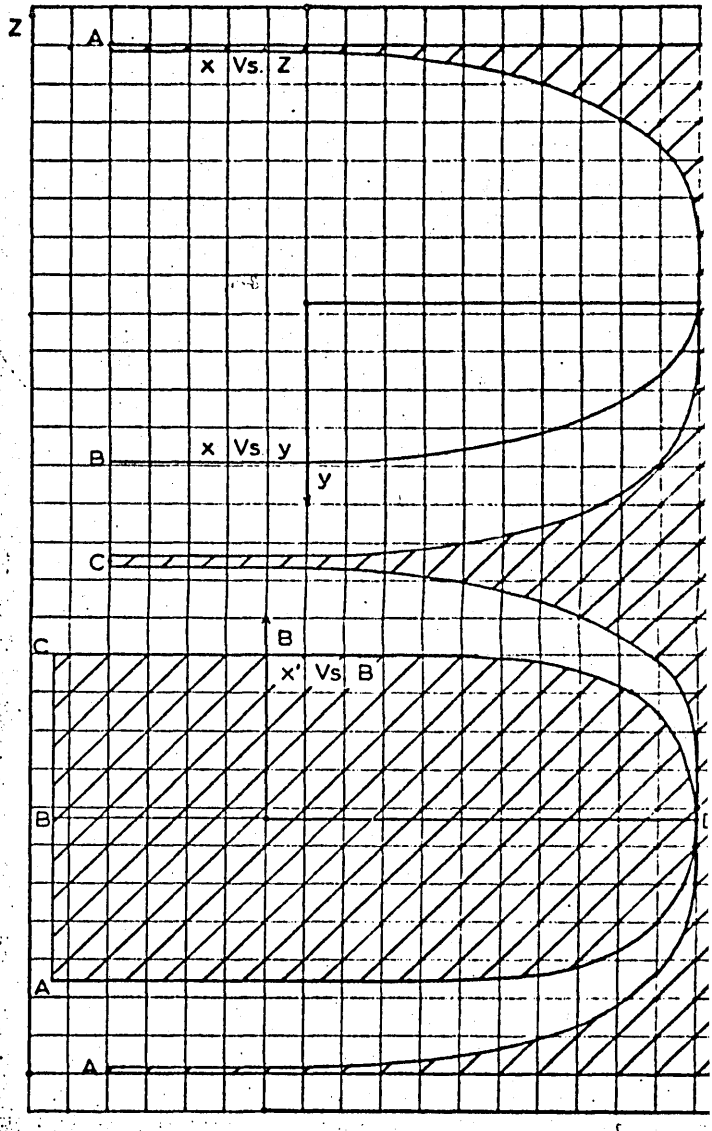

DEVELOPED SECTION ON A PLANE ADCD'

060875

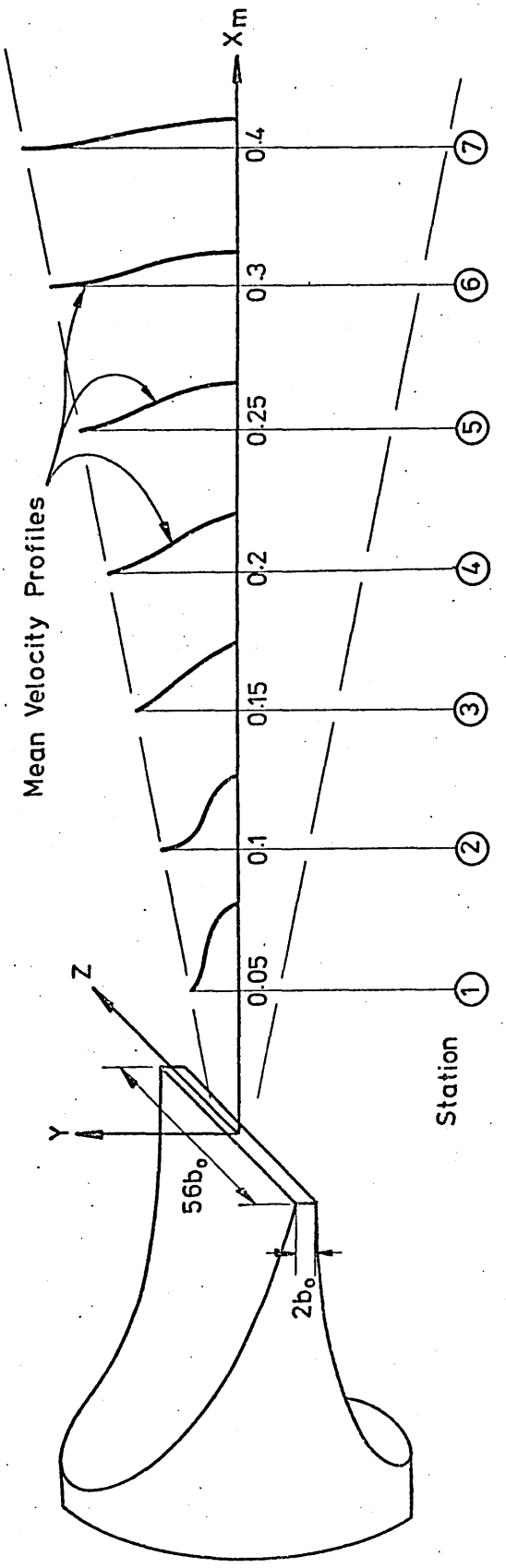

Jet Orientation & Measuring Stations

Figure 12

X (m)	Y (m)	$\frac{Y}{X}$	U (m/s)	$\frac{U}{U_m}$
0.050	0.000	0.000	33.732	1.000
	0.002	0.040	29.627	0.878
	0.004	0.080	21.712	0.644
	0.006	0.120	13.966	0.414
	0.008	0.160	6.983	0.207
	0.010	0.200	0.000	0.000
	-0.002	-0.040	32.001	0.949
	-0.004	-0.080	25.178	0.746
	-0.006	-0.120	16.623	0.493
	-0.008	-0.160	9.876	0.293
	-0.010	-0.200	4.032	0.119
	-0.012	-0.240	0.000	0.000
0.100	0.000	0.000	24.854	1.000
	0.002	0.020	23.853	0.960
	0.004	0.040	21.712	0.874
	0.006	0.060	19.336	0.778
	0.008	0.080	16.624	0.669
	0.010	0.100	14.537	0.585
	0.012	0.120	11.404	0.459
	0.014	0.140	9.016	0.363
	0.016	0.160	6.983	0.281
	0.018	0.180	4.032	0.162
	0.020	0.200	0.000	0.000
	-0.002	-0.020	24.525	0.987
	-0.004	-0.040	23.162	0.932
	-0.006	-0.060	20.950	0.843
	-0.008	-0.080	18.031	0.726
	-0.010	-0.100	15.086	0.607
	-0.012	-0.120	12.750	0.513

MEAN VELOCITY MEASUREMENTS

TABLE 1

X (m)	Y (m)	$\frac{Y}{X}$	U (m/s)	$\frac{U}{U_m}$
0.100	-0.014	-0.140	10.667	0.429
	-0.016	-0.160	8.064	0.324
	-0.018	-0.180	5.702	0.229
	-0.020	-0.200	4.032	0.162
	-0.022	-0.220	0.000	0.000
0.150	0.000	0.000	20.950	1.000
	0.002	0.013	20.559	0.981
	0.004	0.026	19.752	0.943
	0.006	0.040	19.336	0.923
	0.008	0.053	18.031	0.861
	0.010	0.067	16.624	0.794
	0.012	0.080	15.086	0.720
	0.014	0.093	13.967	0.667
	0.016	0.107	12.096	0.577
	0.018	0.120	10.667	0.509
	0.020	0.133	9.876	0.471
	0.022	0.147	9.016	0.430
	0.024	0.160	8.064	0.385
	0.026	0.173	6.983	0.333
	0.028	0.187	5.702	0.272
	0.030	0.200	4.032	0.193
	0.032	0.213	4.032	0.193
	0.034	0.227	0.000	0.000
	-0.004	-0.027	20.160	0.962
	-0.008	-0.053	18.477	0.882
	-0.012	-0.080	15.615	0.745
	-0.016	-0.107	12.750	0.609
	-0.020	-0.133	9.876	0.472
	-0.024	-0.160	8.064	0.385

MEAN VELOCITY MEASUREMENTS

TABLE 2

X (m)	Y (m)	$\frac{Y}{X}$	U (m/s)	$\frac{U}{U_m}$
0.150	-0.028	-0.187	5.702	0.272
	-0.032	-0.213	4.032	0.192
	-0.034	-0.227	0.000	0.000
0.200	0.000	0.000	18.477	1.000
	0.004	0.020	18.447	1.000
	0.008	0.040	17.106	0.926
	0.012	0.060	16.128	0.873
	0.016	0.080	13.967	0.756
	0.020	0.100	12.096	0.655
	0.024	0.120	10.667	0.577
	0.028	0.140	6.983	0.378
	0.032	0.160	6.983	0.378
	0.036	0.180	5.702	0.309
	0.038	0.190	4.032	0.218
	0.040	0.200	0.000	0.000
	-0.004	-0.020	18.031	0.976
	-0.008	-0.040	17.575	0.951
	-0.012	-0.060	16.128	0.873
	-0.016	-0.080	13.967	0.756
	-0.020	-0.100	12.096	0.655
	-0.024	-0.120	9.876	0.535
	-0.028	-0.140	8.064	0.436
	-0.032	-0.160	6.983	0.378
	-0.036	-0.180	5.702	0.309
	-0.040	-0.200	4.032	0.218
	-0.044	-0.220	0.000	0.000
0.250	0.000	0.000	17.106	1.000
	0.004	0.016	16.624	0.972

MEAN VELOCITY MEASUREMENTS

TABLE 3

X (m)	Y (m)	$\frac{Y}{X}$	U (m/s)	$\frac{U}{\bar{U}_m}$
0.250	0.008	0.032	16.128	0.943
	0.012	0.048	15.086	0.882
	0.016	0.064	13.967	0.816
	0.020	0.080	12.096	0.707
	0.024	0.096	11.404	0.667
	0.028	0.112	9.876	0.577
	0.032	0.128	8.064	0.471
	0.036	0.144	6.983	0.408
	0.040	0.160	5.702	0.333
	0.044	0.176	5.702	0.333
	0.048	0.192	4.032	0.236
	0.052	0.208	0.000	0.000
0.300	0.000	0.000	15.086	1.000
	0.005	0.017	15.086	1.000
	0.010	0.033	14.537	0.964
	0.015	0.050	13.372	0.886
	0.020	0.067	12.096	0.802
	0.025	0.083	10.667	0.707
	0.030	0.100	9.876	0.655
	0.035	0.117	8.064	0.535
	0.040	0.133	6.983	0.463
	0.045	0.150	5.702	0.378
	0.050	0.167	4.032	0.267
	0.055	0.183	4.032	0.267
	0.060	0.200	0.000	0.000
0.400	0.000	0.000	12.750	1.000
	0.010	0.025	12.096	0.949
	0.020	0.050	11.404	0.894

MEAN VELOCITY MEASUREMENTS

TABLE 4

X (m)	Y (m)	$\frac{Y}{X}$	U (m/s)	$\frac{U}{U_m}$
0.400	0.030	0.075	9.876	0.775
	0.040	0.100	8.064	0.633
	0.050	0.125	5.702	0.447
	0.060	0.150	4.032	0.316
	0.070	0.175	4.032	0.316
	0.080	0.200	0.000	0.000

MEAN VELOCITY MEASUREMENTS

TABLE 5

X (m)	U_m (m/s)	$\frac{10^4}{U_m^2}$ ($m^{-2}s^2$)	$Y\|_{0.5}$ (m)
0.050	33.70	8.81	0.0038
0.100	24.90	16.13	0.0079
0.150	21.00	22.68	0.0128
0.200	18.50	29.22	0.0180
0.250	17.10	34.20	0.0210
0.300	15.10	43.86	0.0260
0.400	12.80	61.04	0.0350

THE DECAY OF THE CENTRE-LINE VELOCITY AND THE JET SPREAD.

TABLE 6

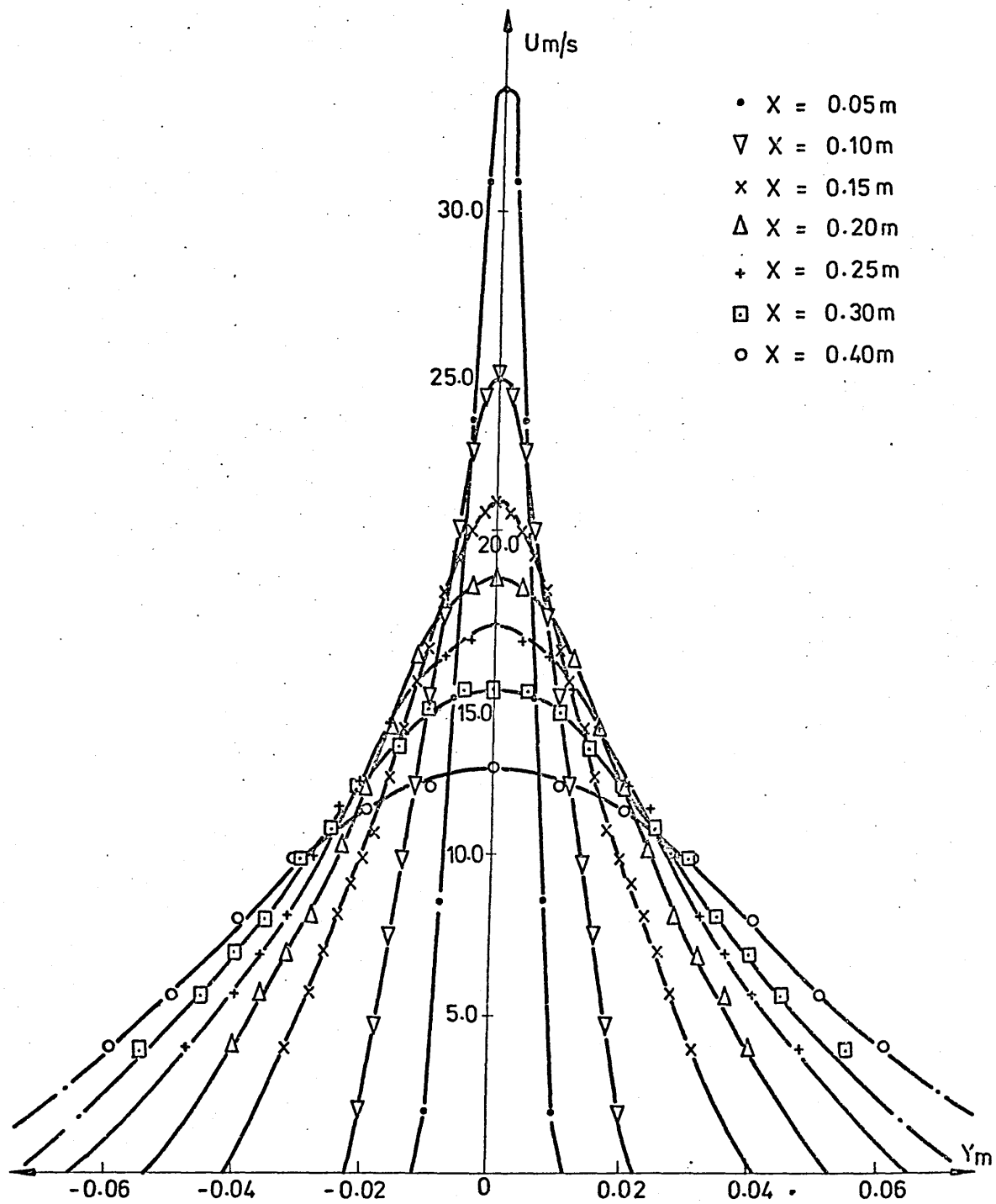

Mean Velocity Profiles

Figure 13

2.4 Laser Study

The feasibility of measuring the fluctuating components of velocity, by a method commensurate with the scope of this study, was also investigated. To this end some exploratory work was carried out using a Laser Doppler anemometer in a pipe flow experiment. Details of the technique and the results obtained have been included in Appendix (I). The implications of this work was that the problems likely to be encountered in the application of this method to the measurement of turbulent quantities in the plane jet were such as to render it unsuitable for the purposes of this study. The main reasons for this conclusion were as follows. Whilst water was the most convenient fluid medium to use from the point of view of laser measurements, it was inpracticable with regard to achieving the desired flow conditions with the apparatus available. Also, the seeding of the flow of a jet of air, a prerequisite of measurements in air with a laser, made this approach equally inpractable. A further objection to the use of an air jet was the necessity of designing, constructing and tuning a new wind tunnel, there not being a suitable existing one available. The use of a hot-wire anemometer was also discounted on these grounds.

2.5 Experimental Results

The non-dimensionalised profiles are plotted in Figure (14). They may be seen to conform closely to those produced by Heskastad[4]. The values of the mean velocities, 'U_m', and the reciprocals of their squares at different stations along the X-axis of the jet, are given in Table (6). The decay of 'U_m' as 'X' increases is illustrated in Figure (15). The relationship between 'U_m^{-2}' and 'X' may be seen to be linear (the correlation coefficient is equal to 0.99), demonstrating that the decay of the centre-line velocity is proportional to the square root of the distance from the efflux section, or,

$$U_m^2 = \text{constant}.X^{-1} \qquad \ldots\ldots\ldots \quad (2.2)$$

Also given in Table (6) is the value of $Y|_{0.5}$ at different values of 'X'. The variation of '$Y|_{0.5}$' is shown in Figure (16) and it may be seen to be linear with 'X', the correlation coefficient

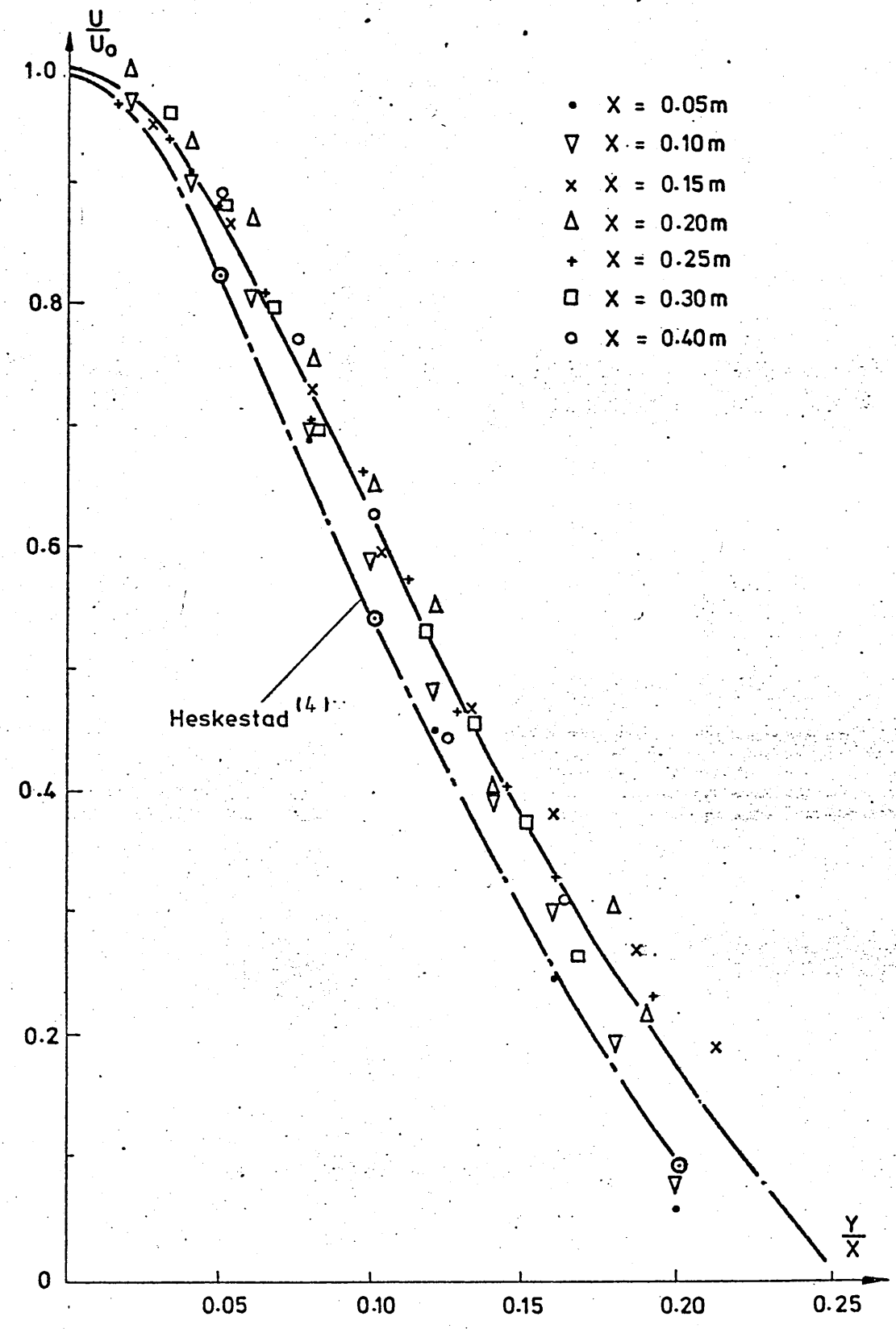

Non-dimensionalised Mean Velocities

Figure 14

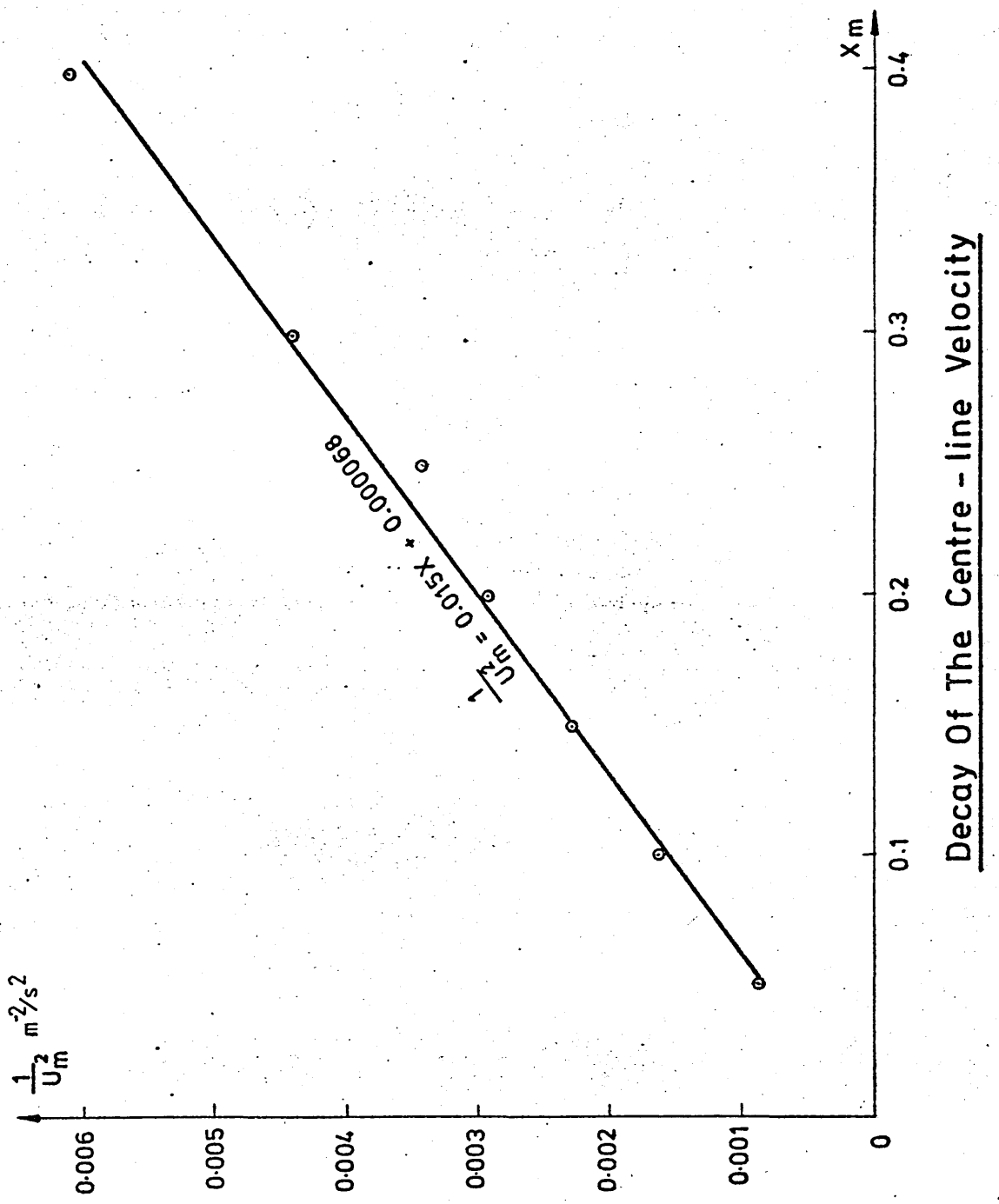
Decay Of The Centre - line Velocity
$\frac{1}{U_m^2}$ m^{-2}/s^2
x m
0·001
0·002
0·003
0·004
0·005
0·006
0
0.1
0.2
0.3
0.4
$\frac{1}{U_m^2} = 0.015x + 0.000068$

Figure 15

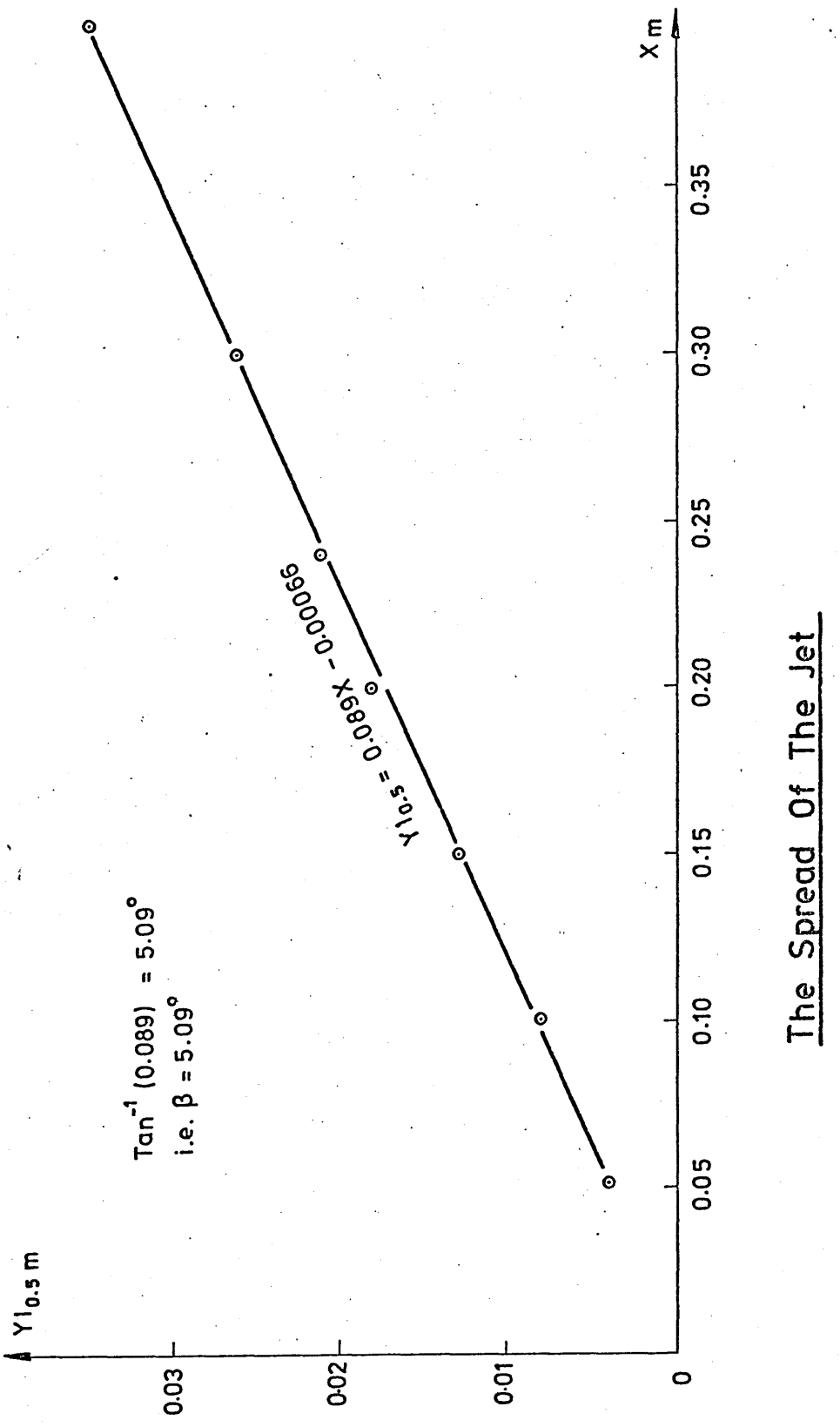

The Spread Of The Jet

Figure 16

being equal to 0.99. Thus, the spread of the jet may also be seen to be linear, that is ;

$$\frac{db}{dX} = \text{constant} \qquad \ldots\ldots\ldots \quad (2.3)$$

The gradient of the line, 'm', has a value of 8.906×10^{-2}. The half-angle 'β' is given by the relationship ;

$$\beta = \tan^{-1}(m) \qquad \ldots\ldots\ldots \quad (2.4)$$

and has a value of 5.09° which falls within the range quoted in section 1.2.

2.6 Summary

The chapter deals with the exploratory investigation of the plane turbulent jet. The design and construction of an adaptor nozzle, for the purpose of producing a plane jet using existing apparatus, was described. The jet produced by the nozzle exhibited the 'mean' characteristics of the required flow. The mean velocity profiles, the decay of the centre-line velocity and the spread of the jet were consistant with the results of previous investigations. The detailed investigation of the jet (ie; of turbulent quantities) was found to be beyond the scope of this study.

The remaining chapters of this study are concerned with an account of turbulence models designed to describe the physical properties as previousely delineated, and the development of an appropriate discrete numerical method for their solution.

CHAPTER 3

THE TURBULENCE MODEL

2.1 Introduction

Prior to the application of a Finite Difference/Finite Element technique to the jet problem, the governing continuum field equations must be delineated. The essential feature of turbulent flows is that the velocity and the pressure at any point in the fluid contain components that are random functions of time[19]. Although these flows may be expressed by the Navier-Stokes equations[18], the small-scale nature of the detailed turbulent motion denies the possibility of a general time-dependant solution[25]. Faced with this problem, it is customary to split the velocities and the pressures into their mean and fluctuating parts and develop equations based on the time averaged properties of turbulence only[37].

The Navier-Stokes equation for the acceleration of a fluid element in the X-direction of an iso-thermal, incompressible flow in three dimensions may be written[18] ;

$$\frac{\partial U}{\partial t} + U\frac{\partial U}{\partial X} + V\frac{\partial U}{\partial Y} + W\frac{\partial U}{\partial Z} = -\frac{1}{\rho}\cdot\frac{\partial P}{\partial X} + \nu\nabla^2 U \qquad \ldots\ldots\ldots \quad (3.1)$$

Decomposing the components of instantaneous velocity and pressure into time-averaged and fluctuating components, that is;

$$U = U + u \quad ; \qquad P = P + p \qquad \ldots\ldots\ldots \quad (3.2)$$

respectively, and time-averaging, gives ;

$$\frac{\partial U}{\partial t} + U\frac{\partial U}{\partial X} + V\frac{\partial U}{\partial Y} + W\frac{\partial U}{\partial Z} + \overline{u\frac{\partial u}{\partial X}} + \overline{v\frac{\partial u}{\partial Y}} + \overline{w\frac{\partial u}{\partial Z}}$$

$$= -\frac{1}{\rho}\cdot\frac{\partial P}{\partial X} + \nu\nabla^2 U \qquad \ldots \quad (3.3)$$

where ;

$$\overline{U + u} = \bar{U} + \bar{u} = \bar{U} \qquad \ldots\ldots\ldots \quad (3.4)$$

The absence of solid boundaries to the flow, and consequently a laminar sublayer, means that the viscosity term may be neglected[43]. The pressure gradient, as mentioned in Chapter 1, may be considered to be negligible. If the flow is considered to be stationary with respect to the mean velocities, the acceleration term disappears and the equation may be re-written for two-dimensional flow as;

$$U\frac{\partial U}{\partial X} + V\frac{\partial U}{\partial Y} + \overline{u\frac{\partial u}{\partial X}} + \overline{v\frac{\partial u}{\partial Y}} = 0 \qquad \ldots\ldots\ldots (3.5)$$

The equation of continuity for the two-dimensional flow of an incompressible fluid may be written[27];

$$\frac{\partial U}{\partial X} + \frac{\partial V}{\partial Y} = 0 \qquad \ldots\ldots\ldots (3.6)$$

Whereupon ;

$$\frac{\partial U}{\partial X} + \frac{\partial V}{\partial Y} + \overline{\frac{\partial u}{\partial X}} + \overline{\frac{\partial v}{\partial Y}} = 0 \qquad \ldots\ldots\ldots (3.7)$$

and ; $$\frac{\partial U}{\partial X} + \frac{\partial V}{\partial Y} = 0 \qquad \ldots\ldots\ldots (3.8)$$

since ; $$\overline{\frac{\partial u}{\partial X}} + \overline{\frac{\partial v}{\partial Y}} = 0 \qquad \ldots\ldots\ldots (3.9)$$

thus ; $$\frac{\partial u}{\partial X} + \frac{\partial v}{\partial Y} = 0 \qquad \ldots\ldots\ldots (3.10)$$

since ; $$\frac{\partial U}{\partial X} + \frac{\partial V}{\partial Y} + \frac{\partial u}{\partial X} + \frac{\partial v}{\partial Y} = 0 \qquad \ldots\ldots\ldots (3.11)$$

Therefore ;

$$\overline{u\frac{\partial u}{\partial X}} + \overline{u\frac{\partial v}{\partial Y}} = 0 \qquad \ldots\ldots\ldots (3.12)$$

Since ; $$\overline{\frac{\partial u^2}{\partial X}} = \overline{u\frac{\partial u}{\partial X}} + \overline{u\frac{\partial u}{\partial X}} \qquad \ldots\ldots\ldots (3.13)$$

and ; $$\overline{\frac{\partial uv}{\partial Y}} = \overline{u\frac{\partial v}{\partial Y}} + \overline{v\frac{\partial u}{\partial Y}} \qquad \ldots\ldots\ldots (3.14)$$

then ; $$\overline{\frac{\partial u^2}{\partial X}} + \overline{\frac{\partial uv}{\partial Y}} = \overline{u\frac{\partial u}{\partial X}} + \overline{v\frac{\partial u}{\partial Y}} \qquad \ldots\ldots\ldots (3.15)$$

Substituting equation (3.15) into equation (3.5) gives ;

$$U\frac{\partial U}{\partial X} + V\frac{\partial U}{\partial Y} + \frac{\partial \overline{u^2}}{\partial X} + \frac{\partial \overline{uv}}{\partial Y} = 0 \qquad \ldots\ldots\ldots \quad (3.16)$$

Since the velocities and their fluctuations change much more slowly along the axis of the flow than in the transverse direction[44], the third term of the equation may be neglected. Since the magnitudes of 'u' and 'v' are of the same order, however, the last term must be retained. The equation becomes, therefore ;

$$U\frac{\partial U}{\partial X} + V\frac{\partial U}{\partial Y} + \frac{\partial \overline{uv}}{\partial Y} = 0 \qquad \ldots\ldots\ldots \quad (3.17)$$

and is known as the momentum equation.

A natural consequence of time-averaging the equations is the presence of more unknowns than equations. The terms introduced into the equations by this method include statistical correlations whose magnitude are difficult, if not impossible, to determine directly[40]. Further equations may be generated from the Navier-Stokes equations, but no matter how large the set becomes, the number of equations is always less than the number of dependent variables. Consequently, any theory based on mean equations must, at some stage, truncate the set. This objective may be achieved by approximating to, or modelling, the effects of the quantities that are unknown in terms of those which can be determined. Different approaches to modelling these quantities are discussed in the following section.

3.2 Turbulence Models

Perhaps a first move towards a model of turbulence can be attributed to Boussinesq[45]. In the last century he suggested that the stress-strain law for time-averaged turbulent flows could be represented in the same form as that for a Newtonian fluid in laminar motion. In this manner the effective turbulent shear-stress, arising from the cross-correlation of fluctuating velocities, may be replaced by the product of the mean velocity gradient and a quantity termed the 'turbulent viscosity', 'μ_t', ie;

$$-\rho\overline{uv} = \mu_t\frac{\partial U}{\partial Y} \qquad \ldots\ldots\ldots \quad (3.18)$$

This suggestion in itself is not a turbulence model, but by expressing the turbulent viscosity in terms which are known, or quantities that may be calculated, this end may be attained.

Models based on this approach may be divided into two groups. Firstly there is a group in which the turbulent viscosity is modelled by an algebraic formula whose unknowns represent properties of the mean velocity profile only. Secondly, there is a group in which the turbulent viscosity is determined by the solution of differential equations for one property, or more, of the turbulent motion. Examples of the first group include Prandtl's well-known mixing-length hypothysis[18] (proposed in 1925), von Karman's similarity hypothesis[19], and various models of the 'Eddy-Viscosity' type. In 1945 Prandtl proposed another model, on this occasion of the type represented by the second group. He proposed that the turbulent viscosity should be defined by the expression ;

$$\mu_t = \rho k^{\frac{1}{2}} L \qquad \ldots\ldots\ldots (3.19)$$

where 'k' is the kinetic energy of turbulence, determined from the solution of a differential equation expressing the processes by which it is transported, and 'L' is an algebraically prescribed length scale. Various other models of the type represented by the second group have been developed and may be found described in standard texts[40].

There is a further group of turbulence models in which, in the mean momentum equation at least (ie; equation (3.17)), the notion of effective turbulence transport properties is dispensed with and differential transport equations for the turbulent fluxes themselves are provided. One of the earlier models of this type was proposed and developed by Bradshaw, Ferris and Atwell[46]. Deterred from simulating the τ-equation itself by the lack of experimental data, they solved a differential equation for 'k' and then determined the shear-stress from the assumption of its proportionality to 'k'. The length scale of this model was prescribed algebraically. A later model, developed by Hanjalic in 1970[47], consisted of three differential equations of transport, the first for the shear-stress itself and the other two for 'k' and 'L' which appear as unknowns

in this equation. Even more recently, Rotta proposed a similar [illegible] model[48], which was essentially a simplification of a proposal of his made in 1951[43]. One of the drawbacks of his previous method was the assumption that ;

$$\text{Rate of diffusion of L} \propto \frac{dL}{dY} \qquad \ldots\ldots\ldots \quad (3.20)$$

a process that is not reflected by reality. Rotta attempted to overcome this deficiency by producing an equation for the product of the kinetic energy of turbulence and the length scale. This model was essentially adopted by Rodi and Spalding[44], who used it in the investigation of a number of free turbulent flows. It is also the [illegible] model that has been adopted in this study and its derivation is now considered.

3.3 Transport Equations for Turbulent Quantities

The turbulence model employed in this study consists of the momentum equation (equation (3.17)) and three differential transport equations for the turbulent quantities '$\overline{uv}$', '$\bar{k}$' and 'kL' respectively. For homogeneous turbulence at high Reynolds Numbers, the transport equation for '$\overline{uv}$' can be taken as ;

$$\overline{uv} = -C_\mu k^{\frac{1}{2}} L \frac{\partial U}{\partial Y} \qquad \ldots\ldots\ldots \quad (3.21)$$

where C_μ is a constant. It may be noted that equation (3.21) is analagous to the combination of equations (3.18) and (3.19). This model, therefore, may be considered to be one of the group in which 'μ_t' is determined by the solution of a differential equation, that is the second group.

The transport equations for 'k' and 'kL' may be derived by the appropriate manipulation of the Navier-Stokes equations. The Navier-Stokes equations, expressed in terms of the mean and the fluctuating components of velocity and pressure, may be written in standard tensor notation as[43];

$$\frac{\partial}{\partial t}(U_i + u_i) + \sum_{k=1}^{3} (U_k + u_k)\frac{\partial}{\partial X_k}(U_i + u_i)$$

$$= -\frac{1}{\rho}\frac{\partial}{\partial X_i}(P + p) - \nu\nabla^2(U_i + u_i) \qquad \ldots\ldots\ldots \quad (3.22)$$

multiplying through by u_j and time averaging gives;

$$\overline{u_j\frac{\partial u_i}{\partial t}} + \sum_{k=1}^{3}\overline{u_j U_k\frac{\partial u_i}{\partial X_k}} + \sum_{k=1}^{3}\overline{u_j u_k\frac{\partial U_i}{\partial X_k}} + \sum_{k=1}^{3}\overline{u_j u_k\frac{\partial u_i}{\partial X_k}}$$

$$= -\frac{1}{\rho}\overline{u_j\frac{\partial p}{\partial X_i}} + \nu\overline{u_j\nabla^2 u_i} \qquad \ldots\ldots\ldots (3.23)$$

Interchanging 'i' and 'j' and adding the resulting equation to equation (3.23) gives;

$$G_1 + G_2 + G_3 + G_4 = G_5 + G_6 \qquad \ldots\ldots\ldots (3.24)$$

where; $$G_1 = \overline{u_j\frac{\partial u_i}{\partial t}} + \overline{u_i\frac{\partial u_j}{\partial t}} \qquad \ldots\ldots\ldots (3.25)$$

$$= \frac{\partial\overline{u_i u_j}}{\partial t} \qquad \ldots\ldots\ldots (3.26)$$

$$G_2 = \sum_{k=1}^{3}\overline{u_j U_k\frac{\partial u_i}{\partial X_k}} + \sum_{k=1}^{3}\overline{u_i U_k\frac{\partial u_j}{\partial X_k}} \qquad \ldots\ldots\ldots (3.27)$$

$$= \sum_{k=1}^{3} U_k\frac{\partial\overline{u_i u_j}}{\partial X_k} \qquad \ldots\ldots\ldots (3.28)$$

$$G_3 = \sum_{k=1}^{3}\overline{u_j u_k\frac{\partial U_i}{\partial X_k}} + \sum_{k=1}^{3}\overline{u_i u_k\frac{\partial U_j}{\partial X_k}} \qquad \ldots\ldots\ldots (3.29)$$

$$G_4 = \sum_{k=1}^{3}\overline{u_j u_k\frac{\partial u_i}{\partial X_k}} + \sum_{k=1}^{3}\overline{u_i u_k\frac{\partial u_j}{\partial X_k}} \qquad \ldots\ldots\ldots (3.30)$$

$$= \sum_{k=1}^{3}\frac{\partial\overline{u_i u_j u_k}}{\partial X_k} \qquad \ldots\ldots\ldots (3.31)$$

and; $$G_5 = -\frac{1}{\rho}\overline{u_j\frac{\partial p}{\partial X_i}} - \frac{1}{\rho}\overline{u_i\frac{\partial p}{\partial X_i}} \qquad \ldots\ldots\ldots (3.32)$$

where ; $G_5 = \overline{\frac{p}{\rho}\left(\frac{\partial u_i}{\partial x_j} + \frac{\partial u_j}{\partial x_i}\right)}$ ..... (3.33)

'δ_{ik}' is the Kronecker-delta, where ;

$$\delta_{ik} = 1, \quad i = k \qquad \ldots\ldots\ldots (3.34)$$

$$\delta_{ik} = 0, \quad i \neq k \qquad \ldots\ldots\ldots (3.35)$$

Finally, $G_6 = \nu \overline{u_j \nabla^2 u_i} + \nu \overline{u_i \nabla^2 u_j}$ ..... (3.36)

$$= \nu \left[\nabla^2 \overline{u_i u_j} - 2 \sum_{k=1}^{3} \overline{\frac{\partial u_i}{\partial x_k} \frac{\partial u_j}{\partial x_k}} \right] \qquad \ldots\ldots\ldots (3.37)$$

Thus equation (3.24) may now be written in the form ;

$$\overline{\frac{\partial u_i u_j}{\partial t}} + \sum_{k=1}^{3} U_k \overline{\frac{\partial u_i u_j}{\partial x_k}} + \sum_{k=1}^{3} \overline{u_k u_j} \frac{\partial U_i}{\partial x_k} + \sum_{k=1}^{3} \overline{u_k u_i} \frac{\partial U_j}{\partial x_k} -$$

$$\overline{\frac{p}{\rho}\left(\frac{\partial u_j}{\partial x_i} + \frac{\partial u_i}{\partial x_j}\right)} + \sum_{k=1}^{3} \frac{\partial}{\partial x_k} \left[-\nu \overline{\frac{\partial u_i \partial u_j}{\partial x_k}} - \overline{u_i u_j u_k} + \right.$$

$$\left. \overline{(\delta_{ik} u_j + \delta_{jk} u_i) \frac{p}{\rho}} + 2\nu \sum_{k=1}^{3} \overline{\frac{\partial u_i}{\partial x_k} \frac{\partial u_j}{\partial x_k}} \right] = 0 \qquad \ldots\ldots (3.38)$$

Rotta's equation (2.11)[43] in his derivation of the transport equation for 'k' may now be obtained by considering the case when 'i = j' in equation (3.38) and multiplying by '$\rho/2$';

$$\underbrace{\frac{\rho}{2} \overline{\frac{\partial u_i^2}{\partial t}} + \frac{\rho}{2} \sum_{k=1}^{3} U_k \overline{\frac{\partial u_i^2}{\partial x_k}}}_{\text{Total change of kinetic energy}} + \underbrace{\rho \sum_{k=1}^{3} \overline{u_k u_i} \frac{\partial U_i}{\partial x_k}}_{\text{Work of Reynold's stresses}} - \underbrace{\overline{p \frac{\partial u_i}{\partial x_i}} +}_{\text{Energy exchange with other fluctuating components}}$$

(continued)

$$\underbrace{\sum_{k=1}^{3} \frac{\partial}{\partial X_k}\left[-\frac{1}{2}\overline{\rho u_i^2 u_k} + u_k\left(\tau_{ik} - \delta_{ik}\overline{p}\right)\right]}_{\text{Diffusion of } \rho\overline{u_i^2}/2} +$$

$$\underbrace{\sum_{k=1}^{3}\left(\frac{\partial \overline{u}_i^2}{\partial X_k}\right)}_{\text{Dissipation}} = 0 \qquad \ldots\ldots\ldots (3.39)$$

By substituting 'k' for $1/2\sum_{k=1}^{3}\overline{u}_i^{2\prime}$, and adding the three equations (ie; for i = 1,3), a total energy balance for the the turbulent motion is obtained. Rewriting this equation for two-dimensional time-steady flow gives ;

$$\rho\left[U\frac{\partial k}{\partial X} + V\frac{\partial k}{\partial Y}\right] + \left[\rho\,\overline{u}^2\frac{\partial U}{\partial X} + \rho\,\overline{uv}\frac{\partial V}{\partial X} + \rho\,\overline{uv}\frac{\partial U}{\partial Y} + \rho\,\overline{v}^2\frac{\partial V}{\partial Y}\right] +$$

$$\underbrace{\left[\frac{\partial}{\partial X}\left(-\rho\nu\frac{\partial k}{\partial X}\right) - \frac{\partial}{\partial Y}\left(-\rho\nu\frac{\partial k}{\partial Y}\right)\right]}_{\text{Viscous diffusion}} + \left[\frac{\partial}{\partial X}\left(\rho\,\overline{uk} + \overline{up}\right) +\right.$$

$$\left.\frac{\partial}{\partial Y}\left[\rho\,\overline{vk} + \overline{pv}\right] + \rho\nu\sum_{i=1}^{3}\sum_{k=1}^{3}\left(\frac{\partial \overline{u}_i}{\partial X_k}\right)^2\right] = 0 \qquad \ldots\ldots\ldots (3.40)$$

Also ; $\rho\,\overline{v}^2\frac{\partial V}{\partial Y} = -\rho\,\overline{v}^2\frac{\partial U}{\partial X}$ $\qquad \ldots\ldots\ldots (3.41)$

from continuity considerations. As before, the viscous diffusion terms may be neglected and the terms containing transverse gradients disappear. The result may be seen to be equivalent to equation (1.22) in Chapter One and is in fact identical to the 'k-equation' of Rodi and Spalding[44] when boundary layer assumptions are adopted and the fourth term is neglected. That is ;

$$U\frac{\partial k}{\partial X} + V\frac{\partial k}{\partial Y} + \overline{uv}\frac{\partial U}{\partial Y} + \left(\overline{u}^2 - \overline{v}^2\right)\frac{\partial U}{\partial X} + \frac{\partial}{\partial Y}\left(\overline{kv} + \frac{1}{\rho}\overline{pv}\right) + \epsilon = 0 \qquad (3.42)$$

where ϵ is the dissipation term. 'The diffusive action of turbulence is presumed similar to molecular diffusion processes. Thus the rate of transport of turbulent energy is taken as the product of the

spatial gradient of 'k' and the turbulent viscosity divided by the effective Prandtl number for the diffusion of turbulent energy[40] ;

$$(\rho\overline{vk} + \overline{pv}) = \text{constant.}\ k^{1/2} L \frac{\partial k}{\partial Y} \qquad \ldots\ldots\ (3.43)$$

$$= \frac{\mu_t}{\sigma_k} \cdot \frac{\partial k}{\partial Y} \qquad \ldots\ldots\ (3.44)$$

The production term is replaced by the product of 'ν_t' and the mean velocity gradient. The dissipation of the turbulent kinetic energy occurs by way of the cascade process described in Chapter One. Thus, since the dissipation is controlled, not by dissipative motions themselves, but by the processes which transfer energy from larger to successively smaller eddies, this process may be supposed to depend only on 'ρ', 'k' and 'L'. For dimensional consistency, it follows that the dissipative rate is of the form ;

$$\sum_{i=1}^{3}\sum_{k=1}^{3}\left(\frac{\partial \overline{u}_i^2}{\partial X_k}\right)^2 \equiv C_D k^{3/2}/L \qquad \ldots\ldots\ (3.45)$$

whereupon the 'k-equation' may be written[40],

$$\rho \frac{Dk}{Dt} = \frac{\partial}{\partial Y}\left(\frac{\mu_t}{\sigma_k}\frac{\partial k}{\partial Y}\right) + \mu_t\left(\frac{\partial U}{\partial Y}\right)^2 - C_D\, k^{3/2}/L \qquad \ldots\ldots\ (3.46)$$

where 'D' is a differential operator and the effective Prandtl number, 'σ_k', and 'C_D' are constants. The equation is suitable for numerical treatment with the appropriate values assigned to 'σ_k' and 'C_D'.

The derivation of the 'k-equation' was lengthy and rather involved. The same end result could have been more easily achieved by suitable manipulation of the 'z-equation' of Launder and Spalding[40]. This equation is a length-scale-determining generalisation in which 'z' represents some product of 'k' and 'L'. It is derived using a similar technique to that used for the 'k-equation'. As before, the Navier-Stokes equations require manipulation such that the chosen variable is brought into prominence. Approximations for the various correlations may then be made by calculable flow properties. A consistency with the previous assumptions may be maintained by representing the diffusive flux of 'z' as being proportional to the spatial gradient of the variable in question times the local turbulent viscosity[40]. That is ;

The 'z equation' may then be written,

$$\frac{Dz}{Dt} = \frac{\partial}{\partial Y}\left(\frac{\mu_t}{\sigma_z}\frac{\partial z}{\partial Y}\right) + z\left[C_1\frac{\mu_t}{k}\left(\frac{\partial U}{\partial Y}\right)^2 - C_2\frac{\rho^2 k}{\mu_t}\right] + s_z \quad \ldots \quad (3.48)$$

where 'σ_z', 'C_1', and 'C_2' represent appropriate constants, as before, and 's_z' represents secondary source terms. It may be noted that by replacing 'z' with 'k', equation (3.46) is obtained. If 'z' is now replaced with the product 'kL' and approximations consistent with the previous assumptions are made, the equation for the transport of the term 'kL' is obtained, ie;

$$\rho\frac{DkL}{Dt} = \frac{\partial}{\partial Y}\left[\frac{\mu_t}{\sigma_{kL}}\left(\frac{\partial kL}{\partial Y} + C_{kL}L\frac{\partial k}{\partial Y}\right)\right]$$

$$+ C_B\mu_t L\left(\frac{\partial U}{\partial Y}\right)^2 - C_s\rho k^{3/2} \quad \ldots\ldots\ldots \quad (3.49)$$

where 'σ_{kL}', 'C_{kL}', 'C_B' and 'C_s' are appropriate constants. This is a reasonable approach towards constructing an equation for the determination of the length scale since the 'z-equation' simply expresses the processes whereby the change in 'z' along a streamline is brought about by the influence of diffusive transport, the inter-action of turbulence and the mean flow and through the self-inter-action of the turbulence[40]. The momentum equation and the differential transport equations for '$\overline{uv}$', 'k' and 'kL' constitute a turbulence model only requiring further the assignation of values to the constants to be fully defined and suitable for numerical treatment.

3.4 Evaluation of the Constants Appearing in the Transport Equations

Since the model is equally valid for a range of flow configurations, information concerning the magnitude of some of the constants may be gained from the consideration of some simpler flows. The magnitude of the constant effective Prandtl numbers (σ_k, σ_{kL}), by virtue of their very nature, may be expected to be of the order of unity[40]. Rotta's[43] length scale was chosen to represent a measure of the time-averaged diameter of the energy-containing eddies and may be defined as;

$$L = \frac{1}{k}\int_0^{\infty} F(\bar{n})\,\frac{dn}{n} \qquad \ldots\ldots\ (3.50)$$

where 'n' is the wave number of the turbulence spectrum and 'F(n)' is the spectral distribution of the turbulent kinetic energy[44]. The value assigned to 'C_μ' depends upon the definition of 'L', noting equation (3.21). Since 'L' cannot as yet be determined experimentally, its absolute magnitude is of academic interest only and 'C_μ' may be put equal to unity with no loss of generality.

Having established a value for 'C_μ', an estimate of the magnitude of 'C_D' may be made by considering the behaviour of flows in the vicinity of solid boundaries. It is characteristic of flows such as these, that convection and diffusion of energy are negligible with the consequence that the production of 'k' is balanced by the dissipation[44]. That is ;

$$\mu_t\left(\frac{\partial U}{\partial Y}\right)^2 = C_D\rho\frac{k^{3/2}}{L} \qquad \ldots\ldots\ (3.51)$$

Incorporation of equation (3.21) and multiplication by 'μ_t' gives ;

$$\left(\mu_t\frac{\partial U}{\partial Y}\right)^2 = C_D\rho^2 C_\mu k^{1/2} L\frac{k^{3/2}}{L} \qquad \ldots\ldots\ (3.52)$$

Re-arranging the equation and incorporating equation (3.18) gives ;

$$\rho^2\overline{uv}^2 = C_D C_\mu \rho^2 k^2 \qquad \ldots\ldots\ (3.53)$$

thus ; $$\left(\frac{\overline{uv}}{k}\right) = (C_D C_\mu)^{1/2} \qquad \ldots\ldots\ (3.54)$$

In an experimental investigation into pipe flow, Laufer[49] found the same ratio to have a magnitude of approximately 0.3. Since a value of unity has been assigned to 'C_μ', it is reasonable to expect 'C_D' to have a value of about 0.09. The value of C_s in equation (3.49) may be found by consideration of the decay of turbulence behind a grid. Experimental data indicates that the ratio of 'C_s' to 'C_D' has a value lying somewhere between 0.5 and 0.8, depending on the turbulence intensity. Thus it is reasonable to expect the value of 'C_s' to be in the range 0.045 - 0.072[40].

It should be strongly emphasised that the values obtained

in this manner only represent an estimate of the magnitude of the constants. In the final analysis, the overiding criterion in selecting the constants to be adopted by the model must be that its predictions conform closely with established experimental data. Rodi and Spalding[40] carried out many calculations, systematically varying the constants. They found that the rate of spread and the level of turbulence was strongly influenced by 'C_D', 'C_s' and 'C_B' and that the profiles of 'U', 'k', '$\overline{uv}$' and 'L' were influenced by 'σ_k', 'σ_{kL}', and 'C_{kL}'. They determined the final values by a computer-optimisation technique, in which the weighting was biased towards the rate of spread, the velocity profile and the profile for 'k' and '$\overline{uv}$', in that order. The same values were initially adopted in this study.

3.5 Summary

The underlying principles of turbulence models in general, and their historical background, have been discussed. The model of turbulence to be adopted in this study has been introduced and the more important steps in the derivation of the equations have been detailed. Complete definition of the classical/phenomenological equations now allows for their numerical treatment. This is the primary concern of the present study. The basic principles of the numerical technique to be employed are described in the following chapter.

CHAPTER 4

GENERALISED COLLOCATION

4.1 The Discrete Methods

The turbulence model described in the previous chapter is constructed of a set of partial differential equations of a parabolic nature with the initial conditions and the boundary conditions for an 'open' domain of solution being known[50]. For equations of this type, for which no classical solution can be found, approximation methods, whether algebraic or numerical in character, provide the only means of solution apart from the use of analogue devices[51]. Perhaps the most important group of approximate numerical methods in the field of engineering science is the 'Discrete Methods'[52][53].

Classically, the domain of solution is regarded as being a macro-continuum. The implication of this is that there exists an infinite number of degrees of freedom, an infinite series relating to these, and an infinite number of points adjacent to each point within the continuum. The Discrete Methods exist primarily due to the inability of classical mathematics to solve the classical expressions of continuum mechanics except in relatively simple cases. In these methods the macro-continuum is idealised as a set of generalised co-ordinates which are prominent variables dependent upon the space-time co-ordinates, interconnected by a series of curve functions[52]. Thus, the number of degrees of freedom is represented as being finite, the infinite series is truncated, and there is a finite distance between co-ordinate points. Such approximate models, by their very nature, pre-suppose inherent errors. Solution by these methods entails the minimisation of such errors according to some valid method criterion.

4.2 Historical Development of the Discrete Methods

By the end of the nineteenth century only the simplest of problems of continuum mechanics were capable of solution. There were, however, due to the problems posed by technological advances brought about by the industrial revolution, increasing pressures to obtain practical results. These pressures were particularly significant in

the field of structural mechanics and it was in this area that the first steps towards the development of present-day discrete techniques were made.

The first two decades of the twentieth century saw the introduction firstly of the Ritz method, in 1908, and then the Galerkin method in 1915[52]. The nineteen-twenties and early nineteen-thirties saw the introduction of variants of these methods; that is, the methods of Polhausen (1921), Bienzeno-koch (1926), Kravchuk (1932), and Kantorovich (1933). Also during this period, an an approach based on the theory of statistics, the Least Squares method, was developed by Picone[54].

The year 1937 was a significant one in the development of the Discrete Methods. The Collocation method was postulated by Frazer, Jones and Scan. The same authors also attempted the first assessment of the relative merits of the Discrete Methods seen as a unified group, although the study was limited to the Galerkin, Collocation and Least Squares methods[55]. Concurrently the method of Finite Differences was introduced[54]. This represented a major improvement over the previous methods and it quickly became the most widely used numerical method in field mechanics. The Finite Difference method was the first practical localised technique; that is, shape functions are set up locally and solution over the problem domain is obtained through co-ordinate transformation of the local field analogue. Previously, laborious overall functions had been employed.

It was not until the mid-nineteen-fifties that the newly-developed technologies were provided with a method suited to their requirements, namely the Ritz Finite Element method[56]. It was initially derived from a standard stiffness method of structural analysis and, for this reason perhaps, the mathematical implications of the method were not immediately appreciated[52]. The introduction of this method, coupled with the accelerating development of the electronic digital computer, provided a powerful tool for structural analysis which rapidly supplanted all rivals. Again, local functions were employed and the organisation and solution of the resulting set of equations, which had hitherto presented such difficulties, was greatly facilitated by the computer. For some considerable time the other Discrete Methods were largely ignored, although the Finite Difference method was still widely used in other fields of engineering.

It took until the mid-nineteen-sixties for it to be finally appreciated that the Direct Stiffness Finite Element method was in fact a generalisation of the original Ritz method. Thus, the Ritz Finite Element method is a more rigorous description of the technique[52][57]. Similarly, it was realised that the Finite Difference method was a degenerate generalisation of the Collocation method[58].

Generalisation is implied by the employment of localised functions, as opposed to overall functions, global definition being obtained by the requisite co-ordinate transformation. These 'discoveries' brought about a drastic re-appraisal of the Discrete Methods, particularly in the field of advanced structural analysis where well-defined potential functions are readily available. An appreciation of the wider implications of the Ritz Finite Element method led not only to increasing interest in the mathematical aspects of the method, but also its application to other branches of science and engineering[53].

Another comparative investigation of the Discrete Methods as a group was carried out in 1966, this time by Finlayson and Scriven[54]. A study of the localised, or generalised, forms of these methods was made by Taylor[52], who was principally concerned with the concept of localisation and its application to the generalisation of the remaining Discrete Methods, which had been largely ignored. This enlightened trend is reflected by Croll's use of the Generalised Collocation (or Hypar Finite Difference) method[58][59]. This method could be described as the Collocation Finite Element method and is the technique to be adopted in this study.

4.3 The Discrete Methods and Fluid Flows

Since their introduction to the field of fluid dynamics, there has been a scarcity of solutions of the Navier-Stokes equations, mainly because of their degree of high order and their non-linearity[60]. Some solutions of the limiting cases of zero and infinitely large Reynolds numbers were obtained, but it took the advent of the electronic digital computer to bring about significant progress[25]. Prior to this, solutions of the full

Navier-Stokes equations required such an immense ammount of computation as to be impossible for practical purposes.

Probably the first attempt to integrate the Navier-Stokes equations was made by Thom[61]. As early as 1933, he managed to obtain a numerical solution for the wake behind a cylinder in a uniform stream. The exhaustive computation, which he performed by hand, proved to be the forerunner of a number of later studies conducted along the same lines. These were made by such authors as Kawaguti and Allen and Southwell[62]. They did not appear until the mid-nineteen-fifties, when the Finite Difference method coupled with the use of the elecronic digital computer were becoming established.

The Finite Difference method has been the most widely used numerical technique employed for the treatment of the Navier-Stokes equations since its introduction into the field of fluid mechanics[63]. A wide variety of flow configurations have been tackled by a number of different authors, prominent amongst these being Kawaguti (1961), Sinuni (1964) and Burggraf (1966)[64].

The obstacle of numerical divergence, which had previousely prevented the solution of high Reynolds number flows, was overcome by Runchal and Wolfstein in 1966[60]. Since that time a number of authors associated with Imperial College have contributed towards the development of this approach regarding a number of associated problems. The development of a group of solution schemes, based on the Patankar-Spalding Finite Difference routine enabled the investigation of a number of flow configurations[65].

The replacement of the Finite Difference method by the Finite Element as the most widely used numerical technique has not yet occurred in the field of fluid mechanics, as it did in the field of structural mechanics. A contributory factor to this situation is that the method of adaptation of a technique principally developed for the solution of problems in the field of structural analysis (essentially a Langrangian method) to the solution of problems in fluid mechanics (naturally described by a Eulerian approach) is not immediately obvious[66]. More important, however, is the fact that for the Navier-Stokes equations for viscous flow there is no simple variational principle. The Ritz Finite Element method was employed in the solution of problems for

for which there were potential functions available (ie; the variational formulation was possible) notably by Zienkiewicz[55], Martin[67] and de Vries and Norrie[68].

Recently, with the continuing development of alternative Discrete methods, a growing number of problems in fluid mechanics have been treated with Finite Element type methods. A Least Squares Finite Element technique was employed by Hutton[69] in 1974. Galerkin Finite Element techniques were employed by Oden[66] in 1974 and Cooke and Blanchard[70], Murphy[71] and Luchi[72] in 1977. The method to be adopted in this study is the Generalised Collocation method, which may be regarde as a Hypar Finite Difference method in which certain Finite Element type concepts are included.

4.4 The Generalised Collocation Method

The Discrete Methods provide a means of obtaining approximate solutions to the partial differential equations which govern a given physical problem. Any approximate discrete technique for the solution of partial equations consists of the determination of the unknown functions at a finite number of discrete points distributed throughout the domain of the problem. The values of the functions at these points are obtained from the solution of a system of algebraic equations determined from a discrete representation of the governing differential equations.

The manner in which this is accomplished by the Generalised Collocation method may be broadly outlined in the following stages First, a topological idealisation of the domain of the problem is obtained by defining a number of discrete points, or nodes, in a global mesh. Each node has a set of generalised co-ordinates associated with it relating to the unknown parameters of the problem. Second, the nodal mesh is considered to consist of sets of locally related nodes. Each set has an independent approximate local function, or functions, appertaining to the elementary nodal set and the associated generalised co-ordinates. These sets and their immediate environs are termed finite elements, the elements being interconnected as required by the particular problem definition. Third, the approximating functions, in terms of the local generalised co-ordinates, are subjected to the Collocation method criterion,

which incorporates the governing field equations and the discrete principle, to produce an algebraic local field analogue or analogues. Finally; the set of global algebraic equations is obtained by the appropriate co-ordinate transformation and the application of boundary conditions.

The mathematics of the process may be delineated by considering the governing field equation, or equations, to be of the form ;

$$Lu = f \qquad \ldots\ldots\ldots \quad (4.1)$$

together with the kinematic boundary conditions ;

$$D_g u = 0 \qquad \ldots\ldots\ldots \quad (4.2)$$

and the stress boundary conditions, which may or may not exist ;

$$D_n u = g_n \qquad \ldots\ldots\ldots \quad (4.3)$$

where 'L' and 'D' are differential operators and 'f_n' and 'g_n' are prescribed spatial functions with 'n' and 'e' as set subscripts.

An approximate discrete function, in the form of a truncated series, may be postulated for the generalised co-ordinates ;

$$\bar{u} = \sum_{j=0}^{m} a_j x^{j-k} y^{k} \qquad \ldots\ldots\ldots \quad (4.4)$$

with respect to two-dimensional problems, where 'a_j' are 'm+1' unknown co-efficients, '$x^{j-k}y^{k}$' is one of the 'm+1' linearly independant terms in 'x' and 'y' with '$0 \leqslant k \leqslant j$' and 'm' finite. Initially, 'x' and 'y' can be taken as valid through the entire field (ie; overall functions).

The transformed version of equation (4.4) may be written ;

$$\bar{u} = \sum_{i=1}^{m+1} u_i f_i(x,y) \qquad \ldots\ldots\ldots \quad (4.5)$$

where 'u_i' is the 'i^{th}' generalised co-ordinate, and '$f_i(x,y)$' is

the corresponding 'shape function'[52]. The object of the Discrete Methods is to approximate the solution of 'u' by means of the substitution of equation (4.5) into the respective method criterion, the latter involving the classical definition and the discrete principle. The method criterion adopted by Collocation is that the inherent error is set to zero at a finite number of points throughout the domain, as opposed to being zero over the whole domain as in the classical approach. That is ;

$$Lu|_i = f \qquad (\text{for } u_i) \qquad \ldots\ldots\ldots \quad (4.6)$$

$$D_n u|_j = g_n \qquad (\text{for } u_j) \qquad \ldots\ldots\ldots \quad (4.7)$$

where 'i' and 'j' typify internal and boundary nodes respectively.

Generalisation, or localisation, takes the form ;

$$Lu|_{i_k} = f \qquad (\text{for } u_i) \qquad \ldots\ldots\ldots \quad (4.8)$$

$$D_n u|_{j_h} = g_n \qquad (\text{for } u_j) \qquad \ldots\ldots\ldots \quad (4.9)$$

where set notational subscripts imply that 'i' and 'j' are in sub-regions 'k' and 'h' respectively. The terms 'x' and 'y' which appear in the associated expressions (represented by equations (4.4) and (4.5)) now relates to the appropriate element sub-field. Global definition is now achieved by the co-ordinate transformation of the local elements with respect to the domain of the solution.

Although the pointwise manner of dealing with the inherent error is somewhat crude, the method has the dual advantage of relatively straight forward formulation and the obviation of non-nodal piecewise inter-element continuity requirements as such[52]. The technique may be further refined by incorporating Hermitian, as opposed to Lagrangian, functions within the Generalised Collocation method[58].

4.5 Summary

The proposed numerical treatment of the field equations and appropriate boundary conditions have been described. It may be noted that expressions of the form (4.2) are generally classically

defined when this approach is adopted.

Having described the numerical technique to be employed and delineated the physical problem to be treated, consider now the application of the Generalised Collocation Method to the problem of the turbulent plane jet.

THE DISCRETE MODELLING OF THE TURBULENT PLANE JET

5.1 The Generalised Co-ordinates

In order to employ a Finite Element type model, the essential continuum parameters must first be identified in a convenient form. These parameters will then be subject to the respective discretisation procedure. First, the momentum equation and the transport equations for '$\overline{\overline{uv}}$', 'k' and 'kL' (equations (3.17), (3.18), (3.46) and (3.49) respectively) may be written as ;

$$UU_{,X} + VV_{,Y} + (\overline{\overline{uv}})_{,Y} = 0 \qquad \ldots\ldots\ldots (5.1)$$

$$\overline{\overline{uv}} + \nu_t U_{,Y} = 0 \qquad \ldots\ldots\ldots (5.2)$$

$$Uk_{,X} + Vk_{,Y} - \left(\frac{\nu_t}{K_1} k_{,Y}\right)_{,Y} - \nu_t (U_{,Y})^2 + K_2 \frac{k^{3/2}}{L} = 0 . \qquad (5.3)$$

$$U(kL)_{,X} + V(kL)_{,Y} - \left(\frac{\nu_t}{K_3}((kL)_{,Y} + K_4 Lk_{,Y})\right)_{,Y} -$$

$$K_5 \nu_t L (U_{,Y})^2 + K_6 k^{3/2} = 0 \qquad \ldots\ldots\ldots (5.4)$$

where the differential notation employed is typified by ;

$$U_{,X} = \partial U / \partial X \qquad \ldots\ldots\ldots (5.5)$$

and the constants K_i $(i = 1,6)$ represent 'σ_k', 'C_D', 'σ_{kL}', 'C_{kL}', 'C_B' and 'C_s' respectively.

Introduction of the stream function 'ψ' where ;

$$\psi_{,Y} = U \qquad \ldots\ldots\ldots (5.6)$$

$$\psi_{,X} = -V \qquad \ldots\ldots\ldots (5.7)$$

and the relationship from equation (3.19)

$$\nu_t = K_7 k^{1/2} L \qquad \ldots\ldots\ldots (5.8)$$

where K_7 represents C_μ, allows the momentum equation to be written ;

$$\Psi_{,Y}\Psi_{,YX} - \Psi_{,X}\Psi_{,YY} - K_7(\phi_{,Y}L\Psi_{,YY} + \phi L_{,Y}\Psi_{,YY} + \phi L\Psi_{,YYY}) = 0 \quad \ldots\ldots\ldots (5.9)$$

and the k-equation (the transport equation for 'k') as ;

$$\Psi_{,Y}(\phi^2)_{,X} - \Psi_{,X}(\phi^2)_{,Y} - D_1(\phi_{,Y}L(\phi^2)_{,Y} + \phi L_{,Y}(\phi^2)_{,Y} + \phi L(\phi^2)_{,YY}) - K_7\phi L(\Psi_{,YY})^2 + K_2\phi^3/L = 0 \quad \ldots\ldots\ldots (5.10)$$

and the kL-equation (the transport equation for 'kL') as ;

$$\Psi_{,Y}(\phi^2)_{,X}L + \Psi_{,Y}\phi^2L_{,X} - \Psi_{,X}(\phi^2)_{,Y}L - \Psi_{,X}\phi^2L_{,Y} - D_4(\phi_{,Y}(\phi^2)_{,Y}L^2 + \phi(\phi^2)_{,YY}L^2 + \phi(\phi^2)_{,Y}(L^2)_{,Y}) - D_2((\phi^3)_{,Y}LL_{,Y} + \phi^3L_{,Y}L_{,Y} + \phi^3LL_{,YY}) - D_3\phi L^2(\Psi_{,YY})^2 + K_6\phi^3 = 0 \quad \ldots\ldots\ldots (5.11)$$

The kinetic energy of turbulence, 'k', has been written as ;

$$k = \phi^2 \quad \ldots\ldots\ldots (5.12)$$

and

$$D_1 = K_7/K_1 \quad \ldots\ldots\ldots (5.13)$$

$$D_2 = K_7/K_3 \quad \ldots\ldots\ldots (5.14)$$

$$D_3 = K_5K_7 \quad \ldots\ldots\ldots (5.15)$$

$$D_4 = D_2(1 + K_4) \quad \ldots\ldots\ldots (5.16)$$

The turbulence model developed in Chapter Three may now be expressed in the form of the three equations (5.9), (5.10) and (5.11). There are three basic unknown quantities, 'ψ', 'k' and 'L'. These

three continuous parametric functions are to be represented by discrete generalised co-ordinates associated with with each nodal point throughout the domain of the problem. Having identified the basic continuum parameters and their field relationship, it remains to define the boundary conditions appertaining to the Turbulent Plane Jet case. The domain of the problem is illustrated in Figure (17). A suitable global discrete mesh is superimposed for clarity. The depicted nodes give a balanced topology through the field and on the boundaries.

The boundary conditions should be chosen so as to be consistent with the known distribution of the relevant quantities. The form of the profiles of the quantities 'U', 'k', and '$\overline{uv}$' have been established experimentally[4][14]; note Figures (18.a) to (18.c). The form of the 'Ψ-profile' and the '$U_{,Y}$-profile' may be deduced from the 'U-profile'; note Figures (18.d) and (18.e). The 'L-profile' may be determined qualitatively from the consideration of the profiles of the quantities 'k', 'uv' and '$U_{,Y}$' employing the relationship ;

$$\overline{uv} = C_\mu \phi L U_{,Y} \qquad \ldots\ldots\ldots (5.17)$$

In order to be consistent with these factors, it is necessary for the 'L-profile' to be both symmetric and positive; note Figure (18.f). A further property possessed by the 'L-profile' is that its derivative with respect to Y is zero at the free boundary[44]. Consideration of the profiles demonstrates that the boundary conditions, relating to the basic parameters, that must be observed are as follows ;

$$\Psi_{,Y}\big|_{fb} = U = 0 \qquad \ldots\ldots\ldots (5.18)$$

$$\phi\big|_{fb} = 0 \qquad \ldots\ldots\ldots (5.19)$$

$$L_{,Y}\big|_{fb} = 0 \qquad \ldots\ldots\ldots (5.20)$$

$$\Psi_{,X}\big|_{sb} = 0 \qquad \ldots\ldots\ldots (5.21)$$

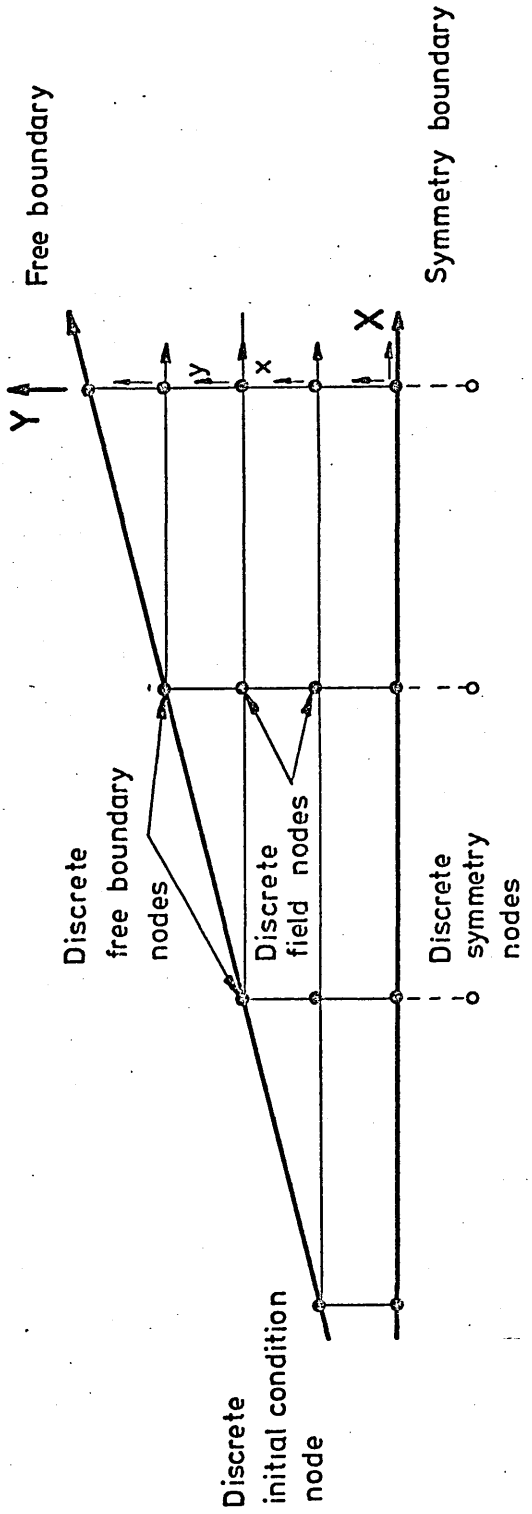

The Global Domain.

Figure 17.

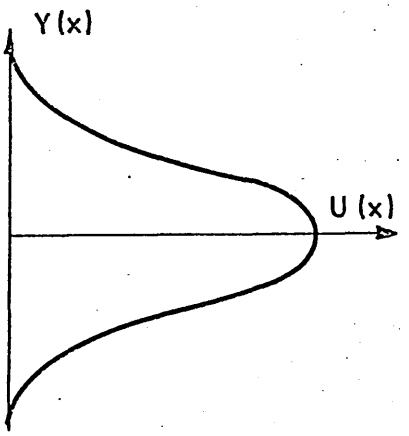

a) U-profile

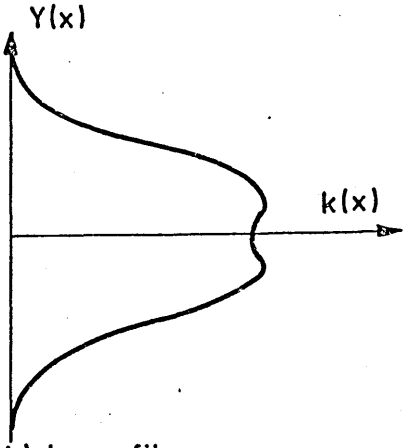

b) k-profile

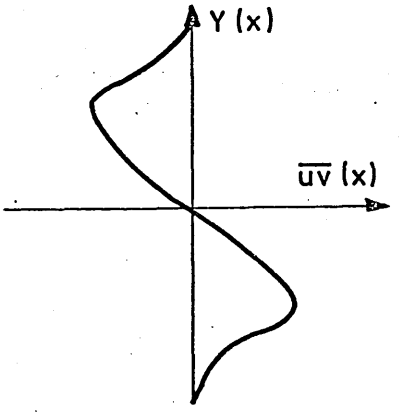

c) $\overline{uv}$-profile

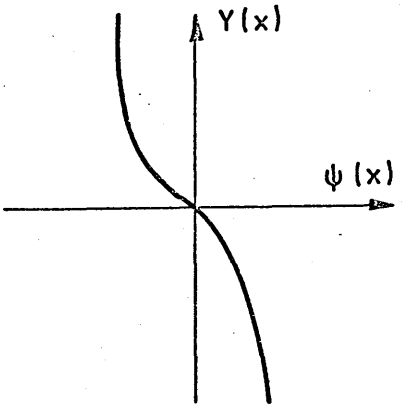

d) ψ-profile

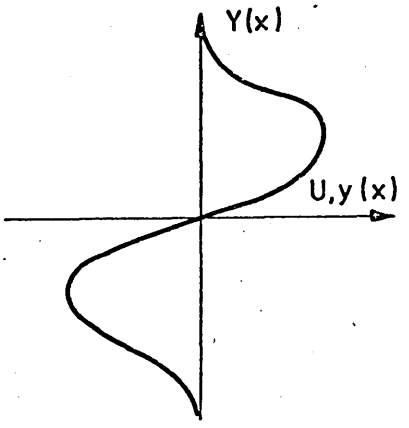

e) U,y-profile

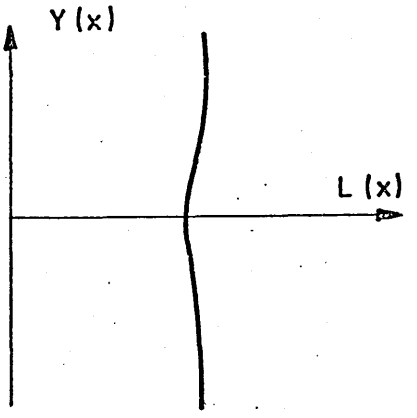

f) L-profile

Figure 18

$$(\phi^2)_{,Y}\big|_{sb} = 0 \qquad \ldots\ldots\ (5.22)$$

where the subscripts 'fb' and 'sb' refer to the free and the symmetry (ie; the centre line) boundaries respectively. It should be noted further that the 'U', 'k' and 'L' profiles are symmetrical and the 'ψ', '$\overline{uv}$' and '$U_{,Y}$' profiles anti-symmetrical about the centre line of the jet.

Having set up the classical-phenomenological equations and delineated the boundary conditions in terms of the basic parameters, consider now the development of a suitable local Generalised Collocation Finite Element.

5.2 The Local Model Topology

The topology and the approximating functions of any Finite Element are intimately connected, as discussed previously. In the interest of clarity, however, consider initially the former aspect. The most suitable scheme is that shown in Figure (19.a), with Figure (19.b) demonstrating how it should be employed in the global sense, having been subjected to the appropriate co-ordinate transformation.

The element possesses two definite attributes. First, the necessary linear translational transformation is of a regular form. Second, no external nodes should be required, noting of course, the symmetry limitation, since the element is chosen to fit the field and boundaries from the outset. This is most important and is one of the advantages of the Generalised Collocation Finite Element approach to the localised discretisation procedure over that generally associated with the (Lagrangian) Finite Difference technique[52].

At each node there are to be discrete generalised co-ordinates. These are denoted in Figure (19.a) by the symbols 'Π_i' ($i = 1,4$) and will be considered in further detail in the following section. The geometric parameter is denoted by 'h'.

5.3 The Postulated Approximating Functions and Generalised Co-ordinates

The choice of the approximating functions is dictated by a number of considerations. It is beyond the scope of this study to

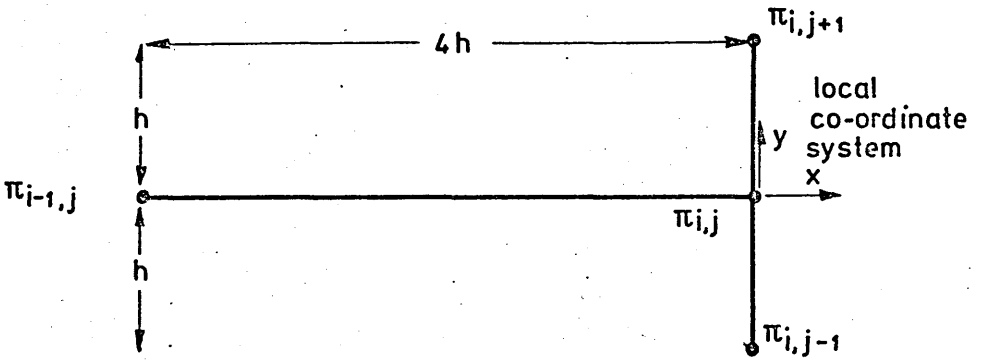

a) The Local Element.

Elements depicted in two-stage
and three-stage transformed mode.

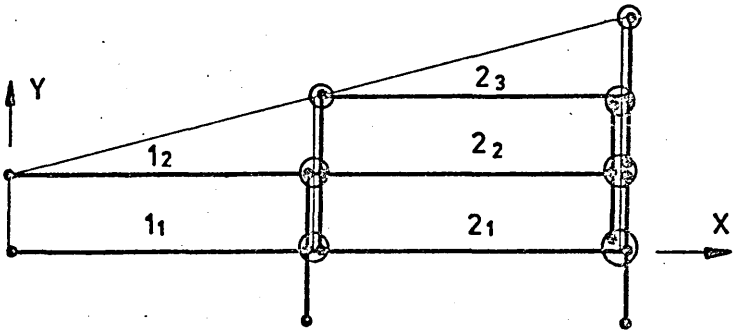

b) The Global Mesh.

Figure 19.

enter into a detailed examination of so complex a subject. However, in view of the emphasis on the numerical aspects of this study, it is appropriate to indicate the importance of achieving a suitable function and to consider some of the more significant factors which influence its selection[52][53].

There are three basic considerations of fundemental importance involved in the selection of the approximating elementary or localised functions inherent in the Discrete Methods. First, the number of terms in the polynomial must be commensurate with the number of local unknowns or generalised co-ordinates involved. Second, the resulting coefficient matrix must be capable of inversion in order to obtain the local interpolatory function. Mathematical singularities must be avoided. Third, the polynomial must be suited to any required co-ordinate transformation. The number of unknowns involved is dependent upon the topology of the local model. Thus a choice of the approximating function is generally made in conjunction with the choice of the element geometry as a result of their close inter-relationship.

The choice of the approximating function is often made with reference to Pascal's triangle; note Figure (20.a). A series that gives a multi-apex pattern is generally suitable for problems whose co-ordinate transformation only involves linear translation[52]. Further if the problem is such that there is no spatial bias in the parameters, a symmetrical polynomial is generally chosen. In the case of the jet there is a distinct spatial orientation and this is reflected in the choice of the approximating function or series. The same general function is employed for all three parameters, as depicted in Figure (20.b), and takes the form;

$$\Pi = \lambda_0 + \lambda_1 x + \lambda_2 y + \lambda_3 y^2 \qquad \ldots\ldots\ (5.23)$$

where 'Π' represents each of the three parametric generalised co-ordinates 'ψ', 'ϕ' and 'L' in turn and 'λ_i' represents the corresponding polynomial coefficients 'a_i', 'b_i' and 'c_i' respectively. Lagrangian functions were therefore employed.

It is important to note that the production of this twelve degree-of-freedom model took considerable effort. Various alternative configurations were attempted in order to optimise the problem -

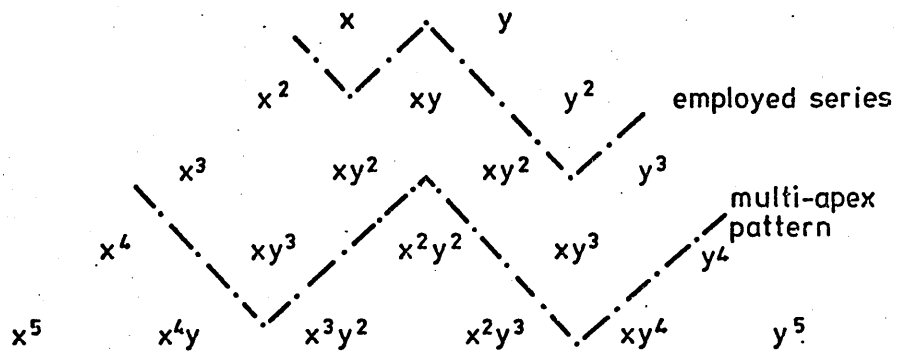

a) Pascals Triangle To The Fifth Degree.

$$\psi = a_0 + a_1x + a_2y + a_3y^2$$

$$\varphi = b_0 + b_1x + b_2y + b_3y^2$$

$$L = c_0 + c_1x + c_2y + c_3y^2$$

b) Local Lagrangian Functions.

Figure 20.

orientation characteristics of the element; note Figure (21).

5.4 Elementary Interpolatory Functions

The 'λ_i' terms are initially convenient general polynomial unknown coefficients which are to be related to the appropriate 'λ_i' discrete generalised co-ordinates. Consider now the derivation of the elementary interpolating function. The general approximating polynomial, equation (5.23), may be written as ;

$$\Pi = xy\,\lambda \qquad \ldots\ldots\ldots (5.24)$$

where ; $xy = |1 \;\; x \;\; y \;\; y^2|$ $\ldots\ldots\ldots (5.25)$

and ; $\lambda^T = |\lambda_0 \;\; \lambda_1 \;\; \lambda_2 \;\; \lambda_3|$ $\ldots\ldots\ldots (5.26)$

Re-writing the approximating functions in terms of the localised generalised co-ordinates, that is with respect to the local element, gives the following set of equations, expressed in matrix format;

$$\begin{vmatrix} \Pi_{i-1,j} \\ \Pi_{i,j-1} \\ \Pi_{i,j} \\ \Pi_{i,j+1} \end{vmatrix} = \begin{vmatrix} 1 & -4h & 0 & 0 \\ 1 & 0 & -h & h^2 \\ 1 & 0 & 0 & 0 \\ 1 & 0 & h & h^2 \end{vmatrix} \begin{vmatrix} \lambda_0 \\ \lambda_1 \\ \lambda_2 \\ \lambda_3 \end{vmatrix} \quad \ldots (5.27)$$

ie; $\Pi_e = C\lambda$ $\ldots\ldots\ldots (5.28)$

The polynomial coefficients may be expressed in terms of the local generalised co-ordinates by the inversion of the 'C-matrix';

$$\begin{vmatrix} \lambda_0 \\ \lambda_1 \\ \lambda_2 \\ \lambda_3 \end{vmatrix} = \begin{vmatrix} 0 & 0 & 1 & 0 \\ -\frac{1}{4h} & 0 & \frac{1}{4h} & 0 \\ 0 & -\frac{1}{2h} & 0 & \frac{1}{2h} \\ 0 & \frac{1}{2h^2} & -\frac{1}{h^2} & \frac{1}{2h^2} \end{vmatrix} \begin{vmatrix} \Pi_{i-1,j} \\ \Pi_{i,j-1} \\ \Pi_{i,j} \\ \Pi_{i,j+1} \end{vmatrix} . \quad (5.29)$$

$$\binom{1}{1\text{-}8}$$

$$\binom{x}{1\text{-}8} \quad \binom{y}{1\text{-}8}$$

$$\binom{x^2}{6\text{-}8} \quad \binom{xy}{1,3,5\text{-}8} \quad \binom{y^2}{2\text{-}8}$$

$$\binom{x^3}{5\text{-}8} \quad \binom{xy^2}{5\text{-}8} \quad \binom{y^2}{5\text{-}8} \quad \binom{y^3}{4\text{-}8}$$

$$\binom{x^4}{6,8} \quad \binom{xy^3}{5\text{-}8} \quad \binom{x^2y^2}{6,8} \quad \binom{xy^3}{5\text{-}8} \quad \binom{y^4}{6,8}$$

$$\binom{x^3y^2}{8} \quad \binom{x^2y^3}{8}$$

$$\binom{x^3y^3}{8}$$

a) Pascals 2-D Triangle With Superposed Trial Element Functions.

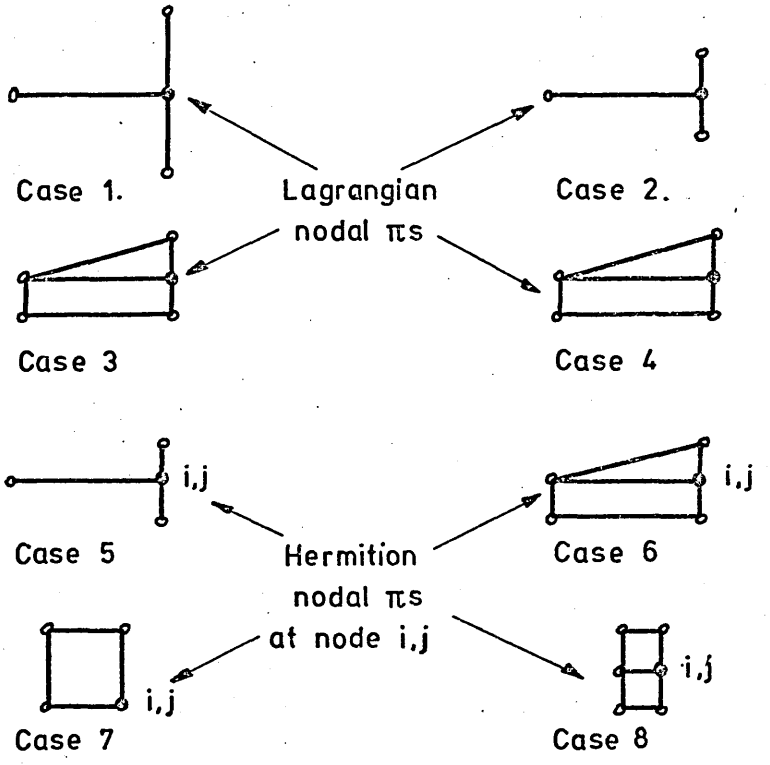

b) Alternative Element Topologies

Postulated Finite Elements.

Figure 21.

or, $$\lambda = c^{-1} \Pi_e \qquad \ldots\ldots\ldots (5.30)$$

This elucidates the essential inversion and numerical term equivalence requirements noted in section 5.3. Equation (5.24) may now be written ;

$$\Pi = xy\, c^{-1} \Pi_e \qquad \ldots\ldots\ldots (5.31)$$

ie; $$\Pi = (-\frac{1}{4h}x)\Pi_{i-1,j} + (-\frac{1}{2h}y + \frac{1}{2h^2}y^2)\Pi_{i,j-1} +$$

$$(1 + \frac{1}{4h}x - \frac{1}{h^2}y^2)\Pi_{i,j} + (\frac{1}{2h}y + \frac{1}{2h^2}y^2)\Pi_{i,j+1} \quad . \qquad (5.32)$$

As 'Π' represents 'Ψ', 'ϕ' and 'L' in turn equation (5.32) relates to their assumed local nature.

Consider now the formulation of the local field analogues in terms of the the discrete generalised co-ordinates as represented in the above. For convenience the following notation is adopted ;

$$\begin{vmatrix} \Pi_{i-1,j} \\ \Pi_{i,j-1} \\ \Pi_{i,j} \\ \Pi_{i,j-1} \end{vmatrix} = \begin{vmatrix} \Pi_1 \\ \Pi_2 \\ \Pi_3 \\ \Pi_4 \end{vmatrix} \qquad \ldots\ldots\ldots (5.33)$$

5.5 The Local Field Analogues

The discretised or localised field equations or analogues are obtained by subjecting the elementary interpolatary functions to the appropriate Discrete Method Criterion. Noting the element topology and the form of the general approximating function, it follows that;

$$\Psi_{,x} = a_1 \qquad \ldots\ldots\ldots (5.34)$$

$$\Psi_{,y} = a_2 + 2a_3 y \qquad \ldots\ldots\ldots (5.35)$$

$$\psi_{,xy} = 0 \quad \ldots\ldots \quad (5.36)$$

$$\psi_{,yy} = 2a_3 \quad \ldots\ldots \quad (5.37)$$

$$\psi_{,yyy} = 0 \quad \ldots\ldots \quad (5.38)$$

$$\phi_{,y} = b_2 + 2b_3y \quad \ldots\ldots \quad (5.39)$$

$$(\phi^2)_{,x} = 2(b_0 + b_1x + b_2y + by^2)b_1 \quad \ldots\ldots \quad (5.40)$$

$$(\phi^2)_{,y} = 2(b_0 + b_1x + b_2y + b_3y^2)(b_2 + 2b_3y) \quad \ldots \quad (5.41)$$

$$(\phi^2)_{,yy} = 2((b_0 + b_1x + b_2y + b_3y^2) + (b_2 + 2b_3y)(b_2 + 2b_3y)) \quad \ldots\ldots \quad (5.42)$$

$$(\phi^3) = (b_0 + b_1x + b_2y + b_3y^2)^3 \quad \ldots\ldots \quad (5.43)$$

$$(\phi^3)_{,y} = 3(b_0 + b_1x + b_2y + b_3y^2)^2(b_2 + 2b_3y) \quad \ldots \quad (5.44)$$

$$L_{,x} = c_1 \quad \ldots\ldots \quad (5.45)$$

$$L_{,y} = c_2 + 2c_3y \quad \ldots\ldots \quad (5.46)$$

$$L_{,yy} = 2c_3 \quad \ldots\ldots \quad (5.47)$$

$$L^2 = (c_0 + c_1x + c_2y + c_3y^2)^2 \quad \ldots\ldots \quad (5.48)$$

and ; $$(L^2)_{,y} = 2(c_0 + c_1x + c_2y + c_3y^2)(c_2 + 2c_3y) \quad \ldots \quad (5.49)$$

Substitution of these terms into equation (5.9) gives;

$$(a_2 + 2a_3y)(0) - (a_1)(2a_3) - K_7((b_2 + 2b_3y)$$

$$(c_0 + c_1x + c_2y + c_3y^2)(2a_3) + (b_0 + b_1x + b_2y + b_3y^2)$$

$$(c_2 + 2c_3y)(2a_3) + (b_0 + b_1x + b_2y + b_3y^2)$$

$$(c_0 + c_1x + c_2y + c_3y^2)(0)) = \text{residual error} \quad \ldots \quad (5.50)$$

Collocation is made at each field and boundary node. In local terms, generalised field collocation is made at node (i,j) and boundary collocation at nodes (i-1,j), (i,j-1) and (i,j+1) respectively. Thus, collocating at node (i,j), when 'x' and 'y' are zero, the residual error becomes equal to zero and equation (5.50) becomes;

$$(a_1)(2a_3) + K_7((b_2)(c_0)(2a_3) + (b_0)(c_2)(2a_3)) = 0 \quad . \quad (5.51)$$

ie; $$2a_1 + K_7(2b_2c_0 + 2b_0c_2) = 0 \quad \ldots\ldots\ldots \quad (5.52)$$

Substituting into equation (5.10) and collocating at node (i,j) gives ;

$$(a_2)(2b_0b_1) - (a_1)(2b_0b_1) - D_1((b_2)(c_0)(2b_0b_2) +$$

$$(b_0)(c_2)(2b_0b_2) + (b_0)(c_0)(4b_0b_3 + 2b_2^2)) -$$

$$K_7(b_0)(c_0)(2a_3)^2 + K_2b_0^3/c_0 = 0 \quad \ldots\ldots\ldots \quad (5.53)$$

ie; $$2a_2b_0b_1 - 2a_1b_0b_2 - D_1(2b_0b_2b_2c_0 + 2b_0b_0b_2c_3 +$$

$$4b_0b_0b_3 + 2b_0b_2b_2c_0) - K_7(4a_3a_3b_0c_0) + K_2b_0^3/c_0 = 0 \quad (5.54)$$

As 'b_0' and 'c_0' are both non-zero quantities, equation (5.54) may be divided by 'b_0' and multiplied by 'c_0' to give;

$$2a_2b_1c_0 - 2a_1b_2c_0 - D_1(2b_0b_2c_0c_2 + 4b_0b_3c_0c_0 +$$

$$4b_2b_2c_0c_0) - K_7(4a_3a_3c_0c_0) + K_2b_0b_0 = 0 \quad \ldots\ldots\ldots \quad (5.55)$$

Substituting into equation (5.11) and collocating at node (i,j) gives ;

$$(a_2)(2b_0b_1)(c_0) + (a_2)(b_0)(b_0)(c_1) - (a_1)(2b_0b_2)(c_0) -$$

$$(a_1)(b_0b_0)(c_2) - D_4((b_2)(2b_0b_2)(c_0c_0) +$$

$$(b_0)(4b_0b_3 + 2b_2^2)(c_0)(c_0) + (b_0)(2b_0b_2)(2c_0c_2)) -$$

(continued)

$$D_2((3b_0^2b_2)(c_0)(c_2) + (b_0b_0b_0)(c_2)(c_2) + (b_0b_0b_0)(c_0)(2c_3)) -$$

$$D_3(b_0)(c_0)(c_0)(2a_3)^2 + K_6b_0^3 = 0 \qquad \ldots\ldots\ldots (5.56)$$

ie;
$$2a_2b_0b_1c_0 + a_2b_0b_0c_1 - 2a_1b_0b_2c_0 - a_1b_0b_0c_2 -$$

$$D_4(2b_0b_2b_2c_0c_0 + 4b_0b_0b_3c_0c_0 + 2b_0b_2b_2c_0c_0 +$$

$$4b_0b_0b_2c_0c_2) - D_2(3b_0b_0b_2c_0c_2 + b_0b_0b_0c_2c_2 + 2b_0b_0b_0c_0c_3) -$$

$$D_3(4a_3a_3b_0c_0c_0) + K_6b_0b_0b_0 = 0 \qquad \ldots\ldots\ldots (5.57)$$

Dividing equation (5.57) by 'b_0', a non-zero quantity, gives ;

$$2a_2b_1c_0 + a_2b_0c_1 - 2a_1b_2c_0 - a_1b_0c_2 -$$

$$D_4(4b_0b_3c_0c_0 + 4b_2b_2c_0c_0 + 4b_0b_2c_0c_2) -$$

$$D_2(3b_0b_2c_0c_2 + b_0b_0c_2c_2 + 2b_0b_0c_0c_3) -$$

$$D_3(4a_3a_3c_0c_0) + K_6b_0b_0 = 0 \qquad \ldots\ldots\ldots (5.58)$$

Equations (5.52), (5.55) and (5.58) represent the local field analogue for the momentum, the 'k' and the 'kL' equations respectively, expressed in terms of the coefficients of the (Langrangian) interpolatory functions. Re-writing the coefficients in terms of the generalised co-ordinates (nb; equation (5.29)) and substituting into equation (5.52) gives;

$$(-\tfrac{1}{2h}\psi_1 + \tfrac{1}{2h}\psi_3) + K_7((-\tfrac{1}{h}\phi_2L_3 + \tfrac{1}{h}\phi_4L_3) +$$

$$(-\tfrac{1}{h}\phi_3L_2 + \tfrac{1}{h}\phi_3L_4)) = 0 \qquad \ldots\ldots\ldots (5.59)$$

For convenience in the manipulation a second notational transformation is made as expressed by ;

$$
\begin{vmatrix} \psi_1 \\ \phi_1 \\ L_1 \\ \psi_2 \\ \phi_2 \\ L_2 \\ \psi_3 \\ \phi_3 \\ L_3 \\ \psi_4 \\ \phi_4 \\ L_4 \end{vmatrix} = \begin{vmatrix} u_1 \\ u_2 \\ u_3 \\ u_4 \\ u_5 \\ u_6 \\ u_7 \\ u_8 \\ u_9 \\ u_{10} \\ u_{11} \\ u_{12} \end{vmatrix} \qquad \ldots\ldots\ldots (5.60)
$$

Re-writing equation (5.59) in this notation gives;

$$
(-\tfrac{1}{2h}u_1 + \tfrac{1}{2h}u_7) + K_7((-\tfrac{1}{h}u_5u_9 + \tfrac{1}{h}u_9u_{11}) +
$$

$$
(-\tfrac{1}{h}u_6u_8 + \tfrac{1}{h}u_8u_{12})) = 0 \qquad \ldots\ldots\ldots (5.61)
$$

Re-writing equation (5.55) in terms of the generalised co-ordinates gives;

$$
(\tfrac{1}{4h^2}u_2u_4u_9 - \tfrac{1}{4h^2}u_4u_8u_9 - \tfrac{1}{4h^2}u_2u_9u_{10} + \tfrac{1}{4h^2}u_8u_9u_{10}) -
$$

$$
(\tfrac{1}{4h^2}u_1u_5u_9 - \tfrac{1}{4h^2}u_5u_7u_9 - \tfrac{1}{4h^2}u_1u_9u_{11} + \tfrac{1}{4h^2}u_7u_9u_{11}) -
$$

$$D_1\left(\left(\frac{1}{2h^2}u_5u_5u_9u_9 - \frac{1}{h^2}u_5u_9u_9u_{11} + \frac{1}{2h^2}u_9u_9u_{11}u_{11}\right) + \left(\frac{1}{2h^2}u_5u_6u_8u_9 - \frac{1}{2h^2}u_5u_8u_9u_{12} - \frac{1}{2h^2}u_6u_8u_9u_{11} + \frac{1}{2h^2}u_8u_9u_{11}u_{12}\right) + \left(\frac{2}{h^2}u_5u_8u_9u_9 - \frac{4}{h^2}u_8u_8u_9u_9 + \frac{2}{h^2}u_8u_9u_9u_{11}\right) + \left(\frac{1}{2h^2}u_5u_5u_9u_9 - \frac{1}{h^2}u_5u_9u_9u_{11} + \frac{1}{2h^2}u_9u_9u_{11}u_{11}\right)\right) -$$

$$K_7\left(\left(\frac{1}{h^4}u_4u_4u_9u_9 + \frac{4}{h^4}u_7u_7u_9u_9 + \frac{1}{h^4}u_9u_9u_{10}u_{10} - \frac{4}{h^4}u_4u_7u_9u_9 + \frac{2}{h^4}u_4u_9u_9u_{10} - \frac{4}{h^4}u_7u_9u_9u_{10}\right)\right) + K_2(u_8u_8) = 0 \quad \ldots\ldots (5.62)$$

Re-writing equation (5.58) in terms of the generalised co-ordinates gives;

$$\left(\frac{1}{4h^2}u_2u_4u_9 - \frac{1}{4h^2}u_4u_8u_9 - \frac{1}{4h^2}u_2u_9u_{10} + \frac{1}{4h^2}u_8u_9u_{10}\right) + \left(\frac{1}{8h^2}u_3u_4u_8 - \frac{1}{8h^2}u_4u_8u_9 - \frac{1}{8h^2}u_3u_8u_{10} + \frac{1}{8h^2}u_8u_9u_{10}\right) - \left(\frac{1}{4h^2}u_1u_5u_9 - \frac{1}{4h^2}u_1u_9u_{11} - \frac{1}{4h^2}u_5u_7u_9 + \frac{1}{4h^2}u_7u_9u_{11}\right) - \left(\frac{1}{8h^2}u_1u_6u_8 - \frac{1}{8h^2}u_1u_8u_{12} - \frac{1}{8h^2}u_6u_7u_8 + \frac{1}{8h^2}u_7u_8u_{12}\right) -$$

$$D_4\left(\left(\frac{1}{2h^2}u_5u_5u_9u_9 - \frac{1}{h^2}u_5u_9u_9u_{11} + \frac{1}{2h^2}u_9u_9u_{11}u_{11}\right) + \left(\frac{2}{h^2}u_5u_8u_9u_9 - \frac{4}{h^2}u_8u_8u_9u_9 + \frac{2}{h^2}u_8u_9u_9u_{11}\right) + \left(\frac{1}{2h^2}u_5u_5u_9u_9 - \frac{1}{h^2}u_5u_9u_9u_{11} + \frac{1}{2h^2}u_9u_9u_{11}u_{11}\right) + \left(\frac{1}{h^2}u_5u_6u_8u_9 - \frac{1}{h^2}u_5u_8u_9u_{12} - \frac{1}{h^2}u_6u_8u_9u_{11} + \frac{1}{h^2}u_8u_9u_{11}u_{12}\right)\right) -$$

$$D_2\left(\left(\frac{3}{4h^2}u_5u_6u_8u_9 - \frac{3}{4h^2}u_5u_8u_9u_{12} - \frac{3}{4h^2}u_6u_8u_9u_{11} + \frac{3}{4h^2}u_8u_9u_{11}u_{12}\right) + \left(\frac{1}{4h^2}u_6u_6u_8u_8 - \frac{1}{2h^2}u_6u_8u_8u_{12} + \frac{1}{4h^2}u_8u_8u_{12}u_{12}\right) + \left(\frac{1}{h^2}u_6u_8u_8u_9 - \frac{2}{h^2}u_8u_8u_9u_9 + \frac{1}{h^2}u_8u_8u_9u_{12}\right)\right) -$$

(continued)

$$D_3((\frac{1}{h^4}u_4u_4u_9u_9 + \frac{4}{h^4}u_7u_7u_9u_9 + \frac{1}{h^4}u_9u_9u_{10}u_{10} -$$

$$\frac{4}{h^4}u_4u_7u_9u_9 + \frac{2}{h^4}u_4u_9u_9u_{10} - \frac{4}{h^4}u_7u_9u_9u_{10})) +$$

$$K_6u_8u_8 = 0 \qquad \ldots\ldots\ldots (5.63)$$

The equations (5.61), (5.62) and (5.63) may be expressed more conveniently in matrix form. The respective matrices are depicted in Figures (22) to (25). The extra constants appearing in the equations arise through the grouping of like terms ; that is ;

$$D_5 = -3D_2 - 4D_4 \qquad \ldots\ldots\ldots (5.64)$$

$$D_6 = 2D_2 + 4D_4 \qquad \ldots\ldots\ldots (5.65)$$

5.6 The Local Boundary Analogues

The solution of field problems requires not only the delineation of field equations but also of the appropriate boundary conditions. Having considered the discretised form of the former, consider now the local boundary conditions. The topological relationship between the local element and the global field is illustrated in Figure (26). The global conditions appertaining to the centre-line have been discussed in section (5.1). The 'ψ-profile' exhibits skew-symmetry and the 'ϕ-profile' and the 'L-profile' exhibit symmetry on the centre-line. The value of 'ψ' is constant along the centre-line. The corresponding boundary conditions may be expressed mathematically, in localised terms, as follows ;

$$\begin{vmatrix} \psi_{i-1,j} \\ \psi_{i,j-1} \\ \phi_{i,j-1} \\ L_{i,j-1} \end{vmatrix} = \begin{vmatrix} \psi_{i,j} \\ -\psi_{i,j+1} \\ \phi_{i,j+1} \\ L_{i,j+1} \end{vmatrix} \qquad \ldots\ldots\ldots (5.66)$$

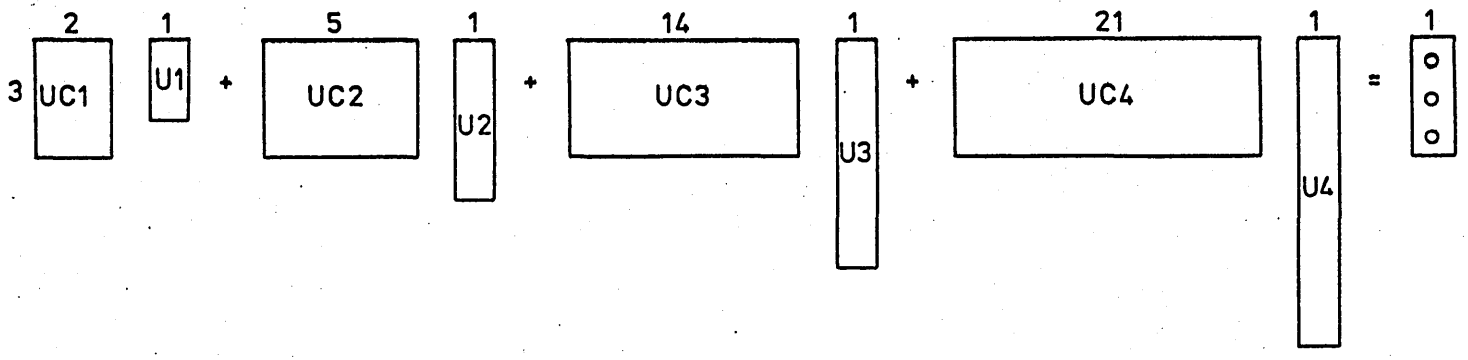

U1 – Matrix in linear terms in U

UC1 – Associated matrix of coefficients

U2 – Matrix of quadratic terms in U

UC2 - Associated matrix of coefficients

U3 - Matrix of cubic terms in U

UC3 - Associated matrix of coefficients

U4 - Matrix of quartic terms in U

UC4 - Associated matrix of coefficients

N.B. Matrices contain only the terms in U appearing in the equations, there are no zero columns in the coefficient matrices.

Figure 22

The Local Field Analogue In Schematic Form

$$ucl = \begin{vmatrix} -\frac{1}{2h} & \frac{1}{2h} \\ 0 & 0 \\ 0 & 0 \end{vmatrix}$$

$$ul = \begin{vmatrix} u_1 \\ u_7 \end{vmatrix}$$

$$uc2 = \begin{vmatrix} -\frac{K_7}{h} & -\frac{K_7}{h} & 0 & \frac{K_7}{h} & \frac{K_7}{h} \\ 0 & 0 & K_2 & 0 & 0 \\ 0 & 0 & K_6 & 0 & 0 \end{vmatrix}$$

$$u2 = \begin{vmatrix} u_5u_9 \\ u_6u_8 \\ u_8u_8 \\ u_8u_{12} \\ u_9u_{11} \end{vmatrix}$$

The Matrices ucl, ul, uc2 and u2

Figure 23

$$[\,u3\,] = \begin{vmatrix} u_1u_5u_9 \\ u_1u_6u_8 \\ u_1u_8u_{12} \\ u_1u_9u_{11} \\ u_2u_4u_9 \\ u_2u_9u_{10} \\ u_3u_4u_8 \\ u_3u_8u_{10} \\ u_4u_8u_9 \\ u_5u_7u_9 \\ u_6u_7u_8 \\ u_7u_8u_{12} \\ u_7u_9u_{11} \\ u_8u_9u_{10} \end{vmatrix}$$

$$[\,u4\,] = \begin{vmatrix} u_4u_4u_9u_9 \\ u_4u_7u_9u_9 \\ u_4u_9u_9u_{10} \\ u_5u_5u_9u_9 \\ u_5u_6u_8u_9 \\ u_5u_8u_9u_9 \\ u_5u_8u_9u_{12} \\ u_5u_9u_9u_{11} \\ u_6u_6u_8u_8 \\ u_6u_8u_8u_9 \\ u_6u_8u_8u_{12} \\ u_6u_8u_9u_{11} \\ u_7u_7u_9u_9 \\ u_7u_9u_9u_{10} \\ u_8u_8u_9u_9 \\ u_8u_8u_9u_{12} \\ u_8u_8u_{12}u_{12} \\ u_8u_9u_9u_{11} \\ u_8u_9u_{11}u_{12} \\ u_9u_9u_{10}u_{10} \\ u_9u_9u_{11}u_{11} \end{vmatrix}$$

The Matrices u3 and u4

Figure 24

$$[UC3] \equiv \begin{vmatrix}
0 & 0 & 0 & 0 & 0 & 0 & 0 & 0 & 0 & 0 & 0 & 0 \\
-\frac{1}{4h^2} & 0 & 0 & 0 & \frac{1}{4h^2} & -\frac{1}{4h^2} & 0 & 0 & 0 & 0 & 0 & 0 \\
-\frac{1}{4h^2} & -\frac{1}{8h^2} & 0 & \frac{1}{8h^2} & \frac{1}{4h^2} & -\frac{1}{4h^2} & \frac{1}{8h^2} & -\frac{1}{8h^2} & 0 & 0 & 0 & 0 \\
0 & 0 & 0 & 0 & 0 & 0 & 0 & 0 & -\frac{1}{4h^2} & \frac{1}{4h^2} & -\frac{1}{4h^2} & \frac{1}{4h^2} \\
0 & 0 & 0 & 0 & 0 & 0 & 0 & 0 & \frac{1}{4h^2} & 0 & \frac{1}{8h^2} & -\frac{1}{8h^2} \\
0 & 0 & 0 & 0 & 0 & 0 & 0 & 0 & \frac{1}{4h^2} & \frac{1}{4h^2} & \frac{3}{8h^2} & -\frac{1}{8h^2} \\
0 & 0 & 0 & 0 & 0 & 0 & 0 & 0 & 0 & \frac{1}{4h^2} & \frac{1}{8h^2} & \frac{3}{8h^2}
\end{vmatrix}$$

$$[UC4] \equiv \begin{vmatrix}
0 & 0 & 0 & 0 & 0 & 0 & 0 & 0 & 0 & 0 & 0 & 0 \\
-\frac{K_7}{h^4} & \frac{4K_7}{h^4} & -\frac{2K_7}{h^4} & -\frac{D_1}{h^2} & -\frac{D_1}{2h^2} & -\frac{2D_1}{h^2} & \frac{D_1}{2h^2} & \frac{2D_1}{h^2} & 0 & 0 & 0 & 0 \\
-\frac{D_3}{h^4} & \frac{4D_3}{h^4} & -\frac{2D_3}{h^4} & -\frac{D_4}{h^2} & \frac{D_5}{h^2} & \frac{2D_4}{h^2} & -\frac{D_5}{h^2} & \frac{2D_4}{h^2} & -\frac{D_2}{h^2} & -\frac{D_2}{h^2} & -\frac{D_2}{h^2} & -\frac{D_2}{h^2} \\
0 & 0 & 0 & 0 & 0 & 0 & 0 & 0 & \frac{D_4}{h^2} & \frac{D_4}{h^2} & 0 & 0 \\
0 & 0 & 0 & 0 & 0 & 0 & 0 & 0 & \frac{D_1}{2h^2} & -\frac{D_5}{h^2} & -\frac{4K_7}{h^4} & \frac{4K_7}{h^4} \\
0 & 0 & 0 & 0 & 0 & 0 & 0 & 0 & 0 & -\frac{4D_3}{h^4} & \frac{4D_3}{h^4} & \frac{4D_1}{h^2} \\
0 & 0 & 0 & 0 & 0 & 0 & 0 & 0 & 0 & 0 & -\frac{D_2}{h^2} & -\frac{D_2}{h^2} \\
0 & 0 & 0 & 0 & 0 & 0 & 0 & 0 & 0 & 0 & 0 & -\frac{2D_1}{h^2} \\
0 & 0 & 0 & 0 & 0 & 0 & 0 & 0 & 0 & 0 & -\frac{D_2}{h^2} & -\frac{2D_4}{h^2} \\
0 & 0 & 0 & 0 & 0 & 0 & 0 & 0 & 0 & 0 & 0 & -\frac{D_1}{2h^2} \\
0 & 0 & 0 & 0 & 0 & 0 & 0 & 0 & 0 & 0 & 0 & -\frac{K_7}{h^4} \\
0 & 0 & 0 & 0 & 0 & 0 & 0 & 0 & 0 & 0 & 0 & -\frac{D_5}{h^4} \\
0 & 0 & 0 & 0 & 0 & 0 & 0 & 0 & 0 & 0 & 0 & -\frac{D_4}{h^2}
\end{vmatrix}$$

The Matrices UC3 And UC4.

Figure 25.

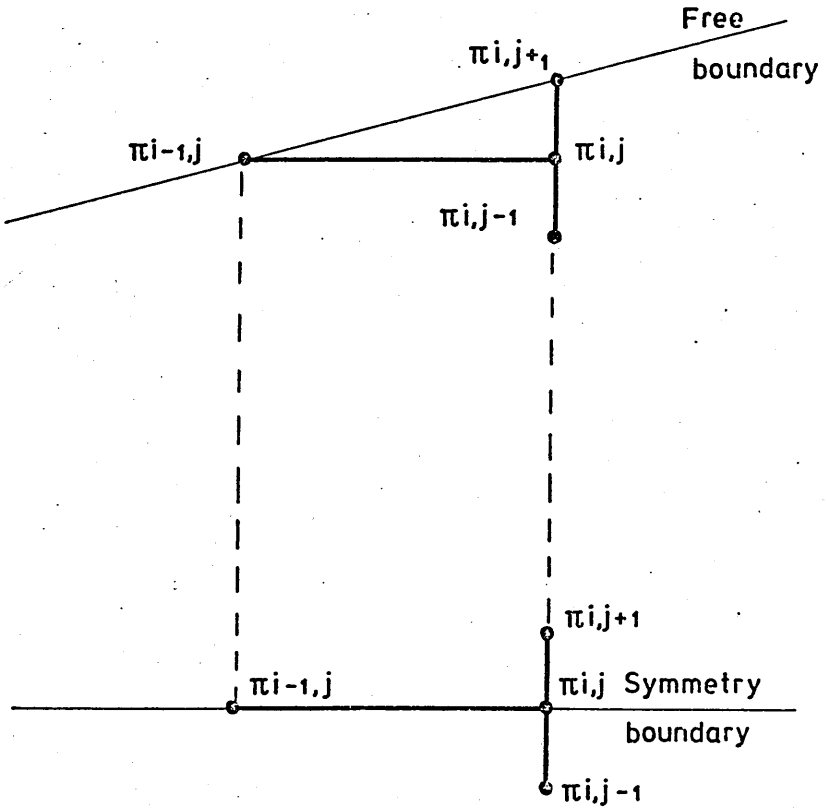

Boundary Elements

Figure 26.

The quantities 'ϕ' and 'L' on the centre-line appear as unknowns in the final equations.

The global conditions to be satisfied on the free boundary are given by equations (5.18), (5.19) and (5.20). Substituting equation (5.35) into equation (5.18) and collocating at node (i,j+1) (where 'x' is zero and 'y' is equal to 'h' with respect to the local co-ordinate system) gives;

$$\psi_{,y} = a_2 + 2a_3 h = 0 \qquad \ldots\ldots\ (5.67)$$

Re-writing equation (5.67) in terms of the generalised co-ordinates,

$$\left(-\frac{1}{2h}\psi_{i,j-1} + \frac{1}{2h}\psi_{i,j+1}\right) +$$

$$2\left(\frac{1}{2h^2}\psi_{i,j-1} - \frac{1}{h^2}\psi_{i,j} + \frac{1}{2h^2}\psi_{i,j+1}\right) = 0 \qquad \ldots\ldots\ (5.68)$$

ie; $$\frac{1}{2h}\psi_{i,j-1} - \frac{2}{h}\psi_{i,j} + \frac{3}{2h}\psi_{i,j+1} = 0 \qquad \ldots\ldots\ (5.69)$$

thus; $$\psi_{i,j+1} = \frac{4}{3}\psi_{i,j} - \frac{1}{3}\psi_{i,j-1} \qquad \ldots\ldots\ (5.70)$$

The derivative of 'L' with respect to 'y' is similarly equal to zero on the free boundary. It follows, therefore, that since the interpolatory function is of the same form for both 'ψ' and 'L',

$$L_{i,j+1} = \frac{4}{3}L_{i,j} - \frac{1}{3}L_{i,j-1} \qquad \ldots\ldots\ (5.71)$$

The local boundary conditions on the free boundary may now be written as;

$$\begin{vmatrix} \psi_{i,j+1} \\ \phi_{i,j+1} \\ L_{i,j+1} \end{vmatrix} = \begin{vmatrix} \frac{4}{3} & -\frac{1}{3} & 0 & 0 \\ 0 & 0 & 0 & 0 \\ 0 & 0 & \frac{4}{3} & -\frac{1}{3} \end{vmatrix} \begin{vmatrix} \psi_{i,j} \\ \psi_{i,j-1} \\ L_{i,j} \\ L_{i,j-1} \end{vmatrix} \qquad (5.72)$$

The co-ordinate transformation is such that the initial boundary conditions have to be satisfied locally at only two nodes, one occurring at the free boundary and the other on the symmetry boundary. The value of 'ϕ' is zero on the free boundary. The remaining parameters associated with the two nodes falling on the initial boundary must have values assigned to them. The initial conditions may be of an arbitary choice. 'Owing to the tendency to similarity, the initial conditions have no influence on the final solution'[44]. In the event, the values assigned to the parameters were chosen so that their relationship to one another reflected the physical reality of the flow configuration.

5.7 Global Transformation of the Local Analogues

As previously stated in Chapter Four, the macro-continuum enclosed by the domain of the problem may be idealised into a finite number of discrete points located at the nodes of a mesh generated with respect to a global co-ordinate system. The proposed global mesh is illustrated in Figure (27.a). A global field analogue of the governing equations may be constructed by the incorporation of the appropriate repetitive application of the local field analogue throughout the domain of the problem, together with the application of the requisite boundary conditions. The local generalised co-ordinates are therefore transformed with respect to the global mesh system, with the local functions inherently linearly translated. The local function is of the neccessary form to permit this as it satisfies the transformation requirements as discussed previously in section 5.3.

The requirements of the transformation routine itself may be more clearly appreciated by consideration of the overall method of solution. Due to the parabolic nature of the problem, the global field extends to infinity in the 'X-direction'. Solution of the problem over the whole field, however, is rendered unnecessary by the phenomenon of similarity[44]. Therefore the solution must necessarily be of a step-wise nature.

The first translation step is shown in Figure (27.b). Two elements, with their associated field analogues and initial, free and symmetrical boundary conditions, span the breadth of the jet,

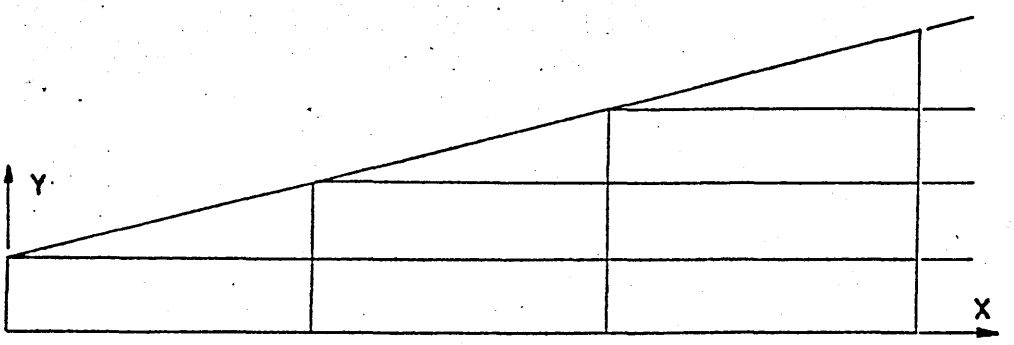

a) Proposed Global Mesh

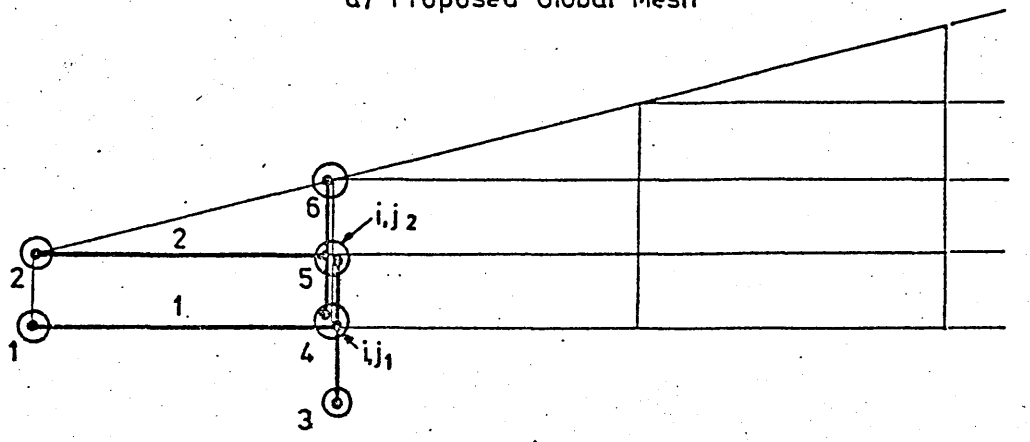

b) Transformation : Step 1.

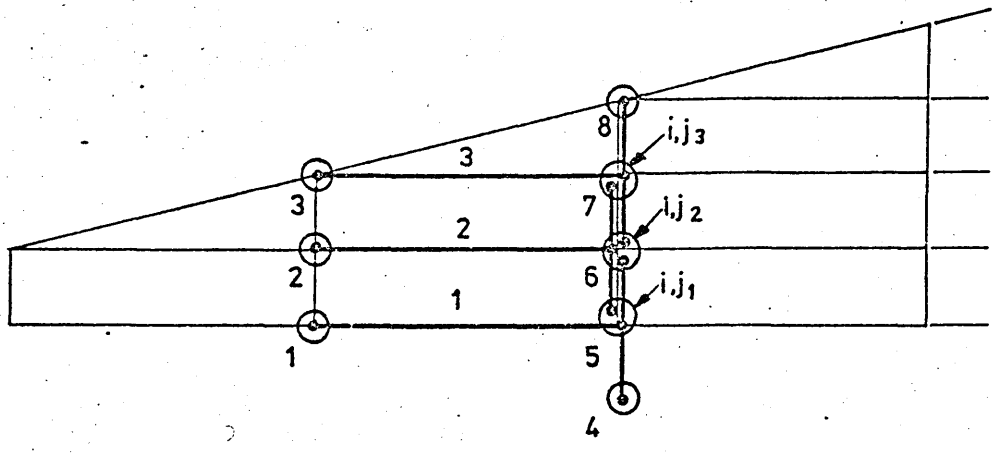

c) Transformation : Step 2.

Co-ordinate Transformation

Figure 27.

producing a set of 'n' non-linear algebraic discrete equations in 'n' unknowns. In further transformations, the initial conditions for the next step downstream are obtained from the solution of the previous equations. Full solution is achieved when similarity profiles are obtained[44]. The overall solution of the problem, therefore, entails a step-wise procedure in which co-ordinate translation of the element across the jet and the intermediate solution of the resulting equations occur at each step.

The co-ordinate transformation procedure involves considerable computational effort, due to the high degree of non-linearity in the equations, and requires the employment of an electronic digital computer. In order to facilitate the computer programming as far as possible, emphasis was placed on specific applicability rather than considerations of algebraic generality. Thus, the transformation routine, listed in Appendix II, was written specifically with regard to the element employed and the rectangular global topology illustrated in Figure (19). In general terms however, a two-dimensional linear translation for quartic functions, or matrices, was derived. The program language was Fortran IV and an IBM 370/135 electronic digital computer was employed.

If the global field analogue component at any step in the solution is constructed of the equations formed by a co-ordinate transformation entailing 'n' translations, there are '(n-1)' overlaps with two nodes being duplicated at each one. This is denoted in Figure (28). Since the element has four nodes, the number of global nodal points, 'P', is '4n' less the number of duplications. That is;

$$P = 4n - 2(n-1) \qquad \ldots\ldots\ldots (5.73)$$

Further, since there are three generalised co-ordinates associated with each node of the element, the number of global unknowns, 'N', is '3P'. That is;

$$N = 3(4n - 2(n-1)) \qquad \ldots\ldots\ldots (5.74)$$

$$= 6(n+1) \qquad \ldots\ldots\ldots (5.75)$$

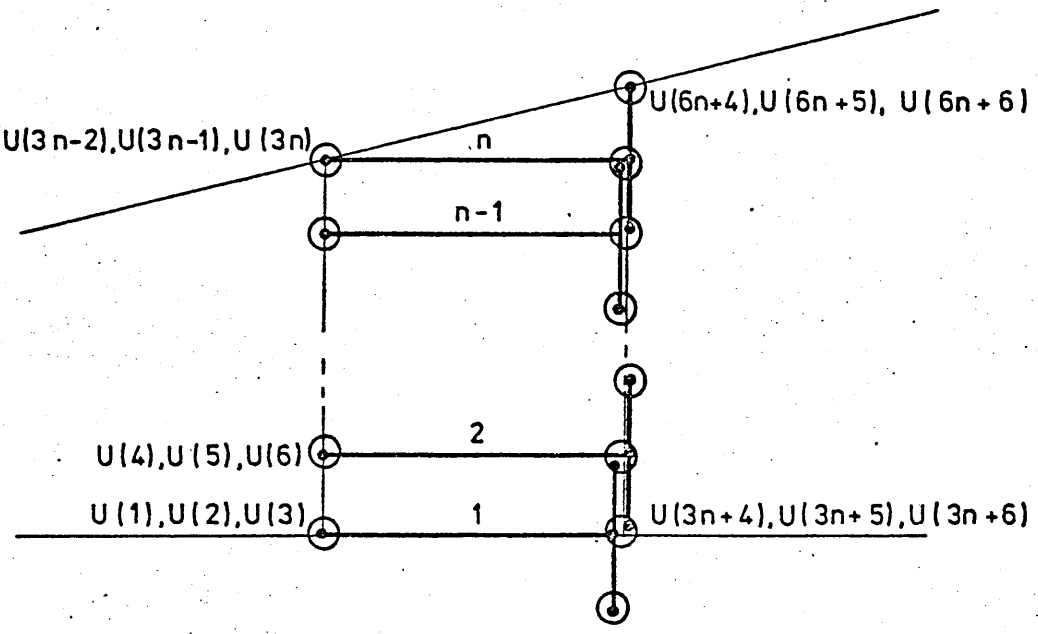

a) Global Generalised Co-ordinates

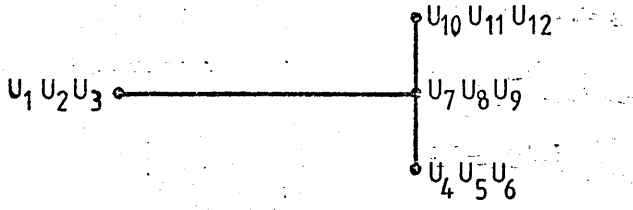

b) Local Generalised Co-ordinates

Figure 28

Any given generalised co-ordinate appearing in the local field analogue will appear 'n' times in the global field analogue, that is, once for each translation. For example, the co-ordinate 'u_{12}' clearly corresponds to the term 'U(6n - 6)' generated by the final translation. Each local generalised co-ordinate may be treated in a like manner. Global co-ordinates are denoted by 'U(i)' (i = 1, N).

The procedure may be explicitly demonstrated with reference to the transformation of the generalised co-ordinates represented by the first equation of the matrices 'ul' and 'ucl' of Figure (23). On transformation, 'u_1' will appear in the global analogue in 'n' locations, that is;

$$u_1 \rightarrow U(1),\ U(4),\ \ldots\ldots\ U(3n-2) \qquad \ldots\ldots \quad (5.76)$$

and similarly, 'u_7' will appear in 'n' locations corresponding to

$$u_7 \rightarrow U(3n+4),\ U(3n+7)\ \ldots\ldots\ U(6n+1) \quad \ldots \quad (5.77)$$

occuring in the first, second and 'n^{th}' equations respectively. For example, if 'n' is equal to two,

$$\left|\begin{matrix} -\frac{1}{2h} & \frac{1}{2h} \end{matrix}\right| \left\|\begin{matrix} u_1 \\ u_7 \end{matrix}\right| \rightarrow \left|\begin{matrix} -\frac{1}{2h} & 0 & \frac{1}{2h} & 0 \\ 0 & -\frac{1}{2h} & 0 & \frac{1}{2h} \end{matrix}\right| \left\|\begin{matrix} U(1) \\ U(4) \\ U(10) \\ U(18) \end{matrix}\right| \qquad (5.78)$$

The procedure may equally well be carried out on the higher order terms although it is complicated slightly by the occurrence of overlaps from equation to equation. Suppose, for the sake of simplicity, that the matrices 'u2' and 'uc2' were ;

$$\left|\begin{matrix} 1 & 1 \end{matrix}\right| \left\|\begin{matrix} u_5 u_9 \\ u_9 u_{11} \end{matrix}\right|$$

On transformation the first term will correspond to the terms

$$U(3n-2)U(3n-6), U(3n-5)U(3n-9), \ldots\ U(6n-1)U(6n-3)$$

and the second to ;

$$U(3n-5)U(3n-9), U(3n-8)U(3n-12), \ldots\ U(6n-2)U(6n-6)$$

in the global field analogue. Therefore, if;

$$n = 2$$

$$\begin{vmatrix} 1 & 1 \end{vmatrix} \begin{vmatrix} u_5 u_9 \\ u_9 u_{11} \end{vmatrix} \longrightarrow \begin{vmatrix} 1 & 1 & 0 \\ 0 & 1 & 1 \end{vmatrix} \begin{vmatrix} U(8)U(12) \\ U(11)U(15) \\ U(14)U(18) \end{vmatrix} \qquad (5.79)$$

A final illustration of the procedure, including terms of up to the fourth order, is given by the transformation of an example of a simple local field analogue with ;

$$n = 2 \qquad \ldots\ldots\ (5.80)$$

and is shown in Figure (29).

Thus, on transformation each term in the local field analogue corresponds to a specific global unknown which is defined by the local and global topologies and the number of translations involved. Since the relationship between the global unknowns and the local generalised co-ordinates is not only specific but also systematic, a general transformation routine may be written.

Comparison of the local field analogues in Figures (22) and (29) shows clearly that the transformation of the former is considerably more complex than that of the latter. Not only does the analogue consists of three equations, as compared with one, but each one contains many more terms. Further, in order to provide enough information to be useful, co-ordinate transformations in which 'n'

$$\begin{bmatrix}1 & 1\end{bmatrix}\begin{bmatrix}U_{1(a)}\\U_{2(b)}\end{bmatrix}+\begin{bmatrix}1 & 1\end{bmatrix}\begin{bmatrix}U_5\,U_{9(c)}\\U_9\,U_{11(d)}\end{bmatrix}+\begin{bmatrix}1 & 1\end{bmatrix}\begin{bmatrix}U_1\,U_5\,U_9\\U_1\,U_6\,U_8\end{bmatrix}+\begin{bmatrix}U_4\,U_4\,U_9\,U_9\end{bmatrix}=0$$

a) Local Field Analogue.

$$\begin{bmatrix}1 & 0 & 1 & 0\\0 & 1 & 0 & 1\end{bmatrix}\begin{bmatrix}U(1)_a\\U(4)_a\\U(10)_b\\U(13)\end{bmatrix}+\begin{bmatrix}1 & 1 & 0\\0 & 1 & 1\end{bmatrix}\begin{bmatrix}U(8)\;U(12)_c\\U(11)\;U(15)_{cd}\\U(14)\;U(18)_d\end{bmatrix}+\begin{bmatrix}1 & 0 & 1 & 0\\0 & 1 & 0 & 1\end{bmatrix}\begin{bmatrix}U(1)\;U(8)\;U(12)\\U(1)\;U(9)\;U(11)\\U(4)\;U(11)\;U(15)\\U(4)\;U(12)\;U(14)\end{bmatrix}$$

$$+\begin{bmatrix}1 & 0\\0 & 1\end{bmatrix}\begin{bmatrix}U(7)\;U(12)\;U(12)\;U(12)\\U(10)\;U(10)\;U(15)\;U(15)\end{bmatrix}=\begin{bmatrix}0\\0\end{bmatrix}$$

N.B. Subscripts a,b,c and denotes transformation of local generalised co-ordinates to global locations.

b) Global Equations.

Figure 29.

Example Co-ordinate Transformation.

is at least three are required. The situation is complicated still further by the restrictions on the presentation of the equations imposed by the non-linear solution routine. Thus it was found to be expeditous to write the transformation program so as to achieve the dual purpose of producing the final system of equations and at the same time to set them up in the requisite format for solution.

The program may be considered to proceed in four main stages. The first stage is concerned with the formulation of the global matrices of coefficients (labelled LINT, QUDT, CUBT and QURT) built up through the transformation of the local matrices of coefficients 'uc1', 'uc2', 'uc3' and 'uc4' respectively (depicted in Figures (22) and (30)). As a consequence of the ordered and systematic arrangement of the equations generated by the co-ordinate transformation, the matrices of coefficients may be composed by employing a routine which defines the 'pattern' of coefficients, appropriate to each particular global matrix, in general terms.

Each matrix in the local field analogue may be divided into blocks as shown in Figure (30). The global matrices of coefficients were constructed by allocating each block of local coefficients to its appropriate position within the global matrices. The locations of the blocks in the global matrices arising from a transformation for which ;

$$n = 3 \qquad \ldots\ldots\ldots \quad (5.81)$$

is shown in Figures (31) to (33), which also show the dimensions of the matrices involved. It may be seen that for the intermediate equations the location of the blocks relative to each other are repetitive, the first and last three equations being special cases. The programming of this part of the routine, then, consists of determining the 'starting positions' of the blocks and then proceeding with a standard sequence.

The second stage of the program involves the generation of the appropriate 'subscripts' of the global parameters from the transformation of the local generalised co-ordinates in the manner previously discussed. The arrays of global parameters associated with the matrices of Figures (31) to (33) are illustrated in Figures (35) and (36), Figure (34) being a general diagnostic

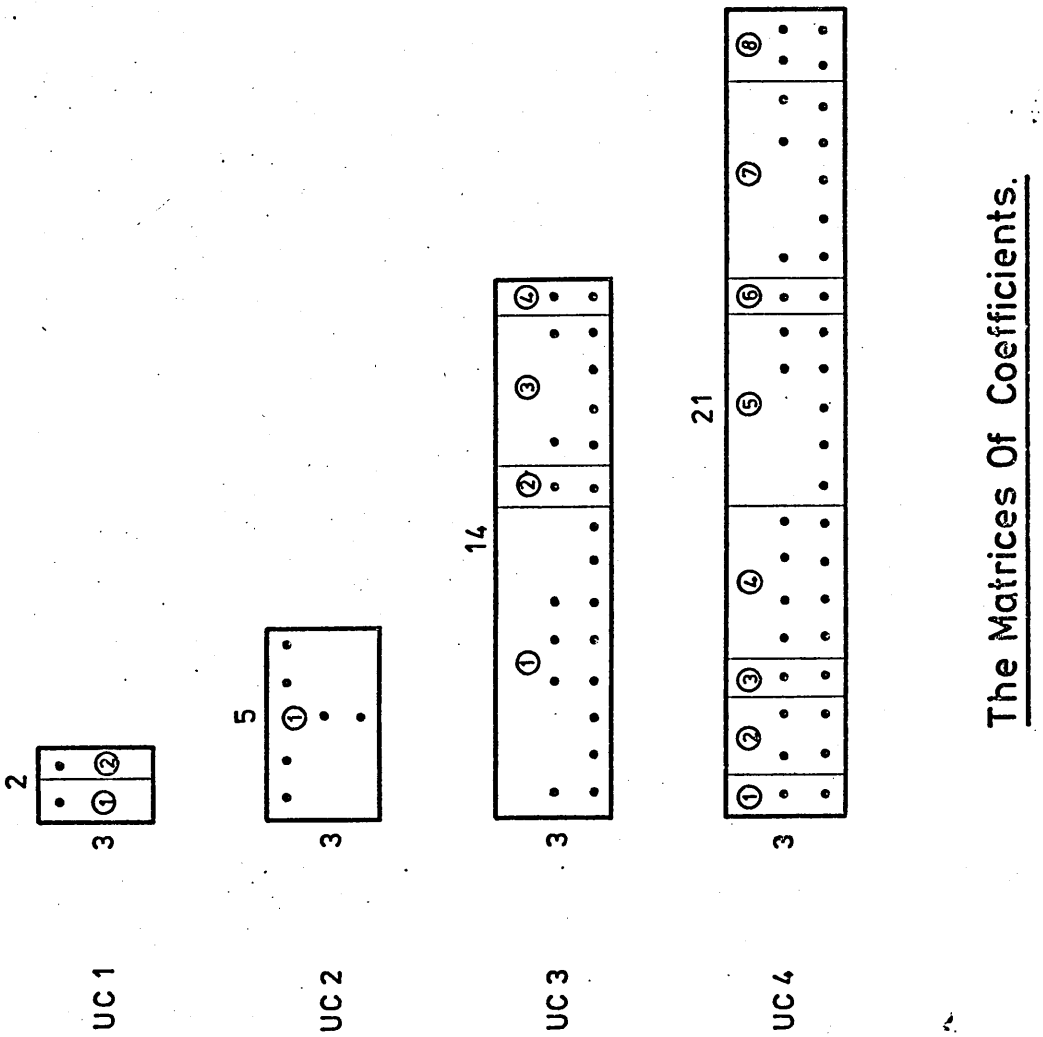

Figure 30

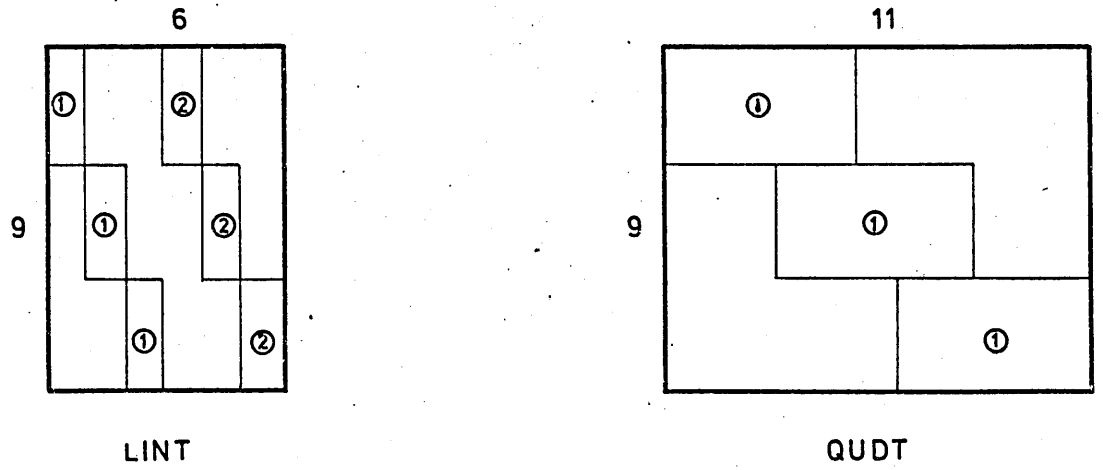

Figure 31

Transformation Of The Matrices UC1 And UC2, n=3.

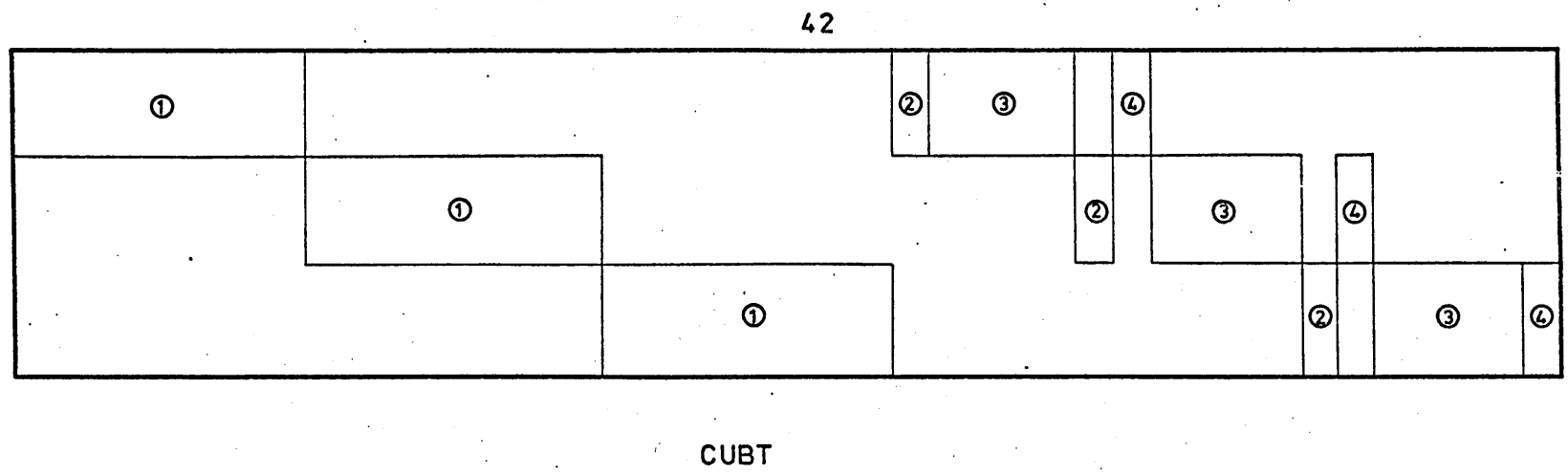

Figure 32

Transformation Of The Matrix UC3, n=3.

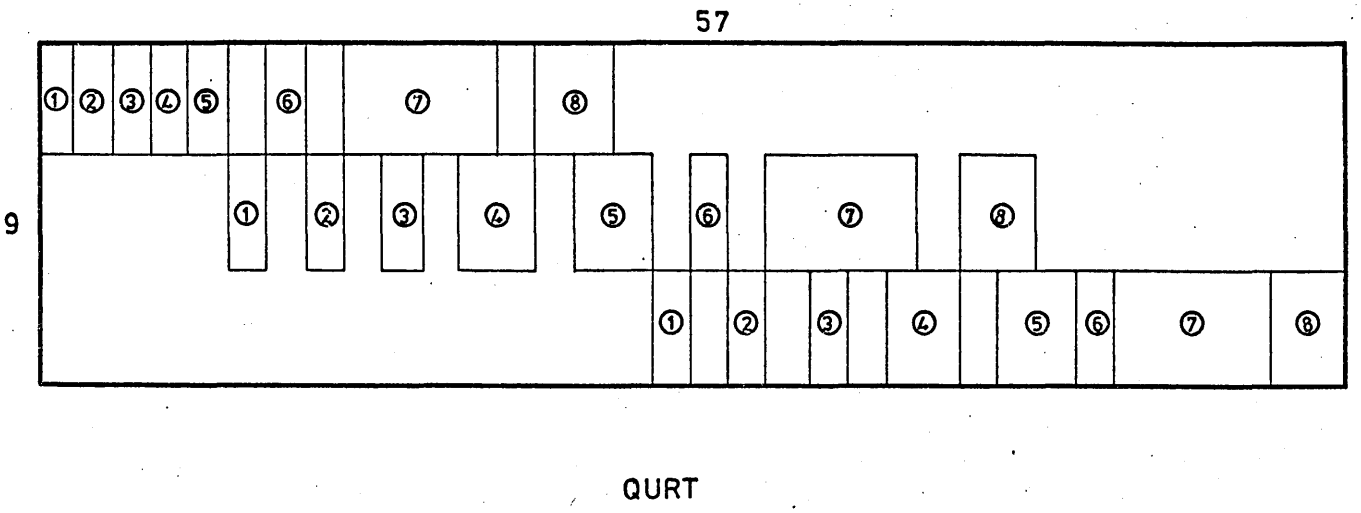

Figure 33

Transformation Of The Matrix UC4, n=3.

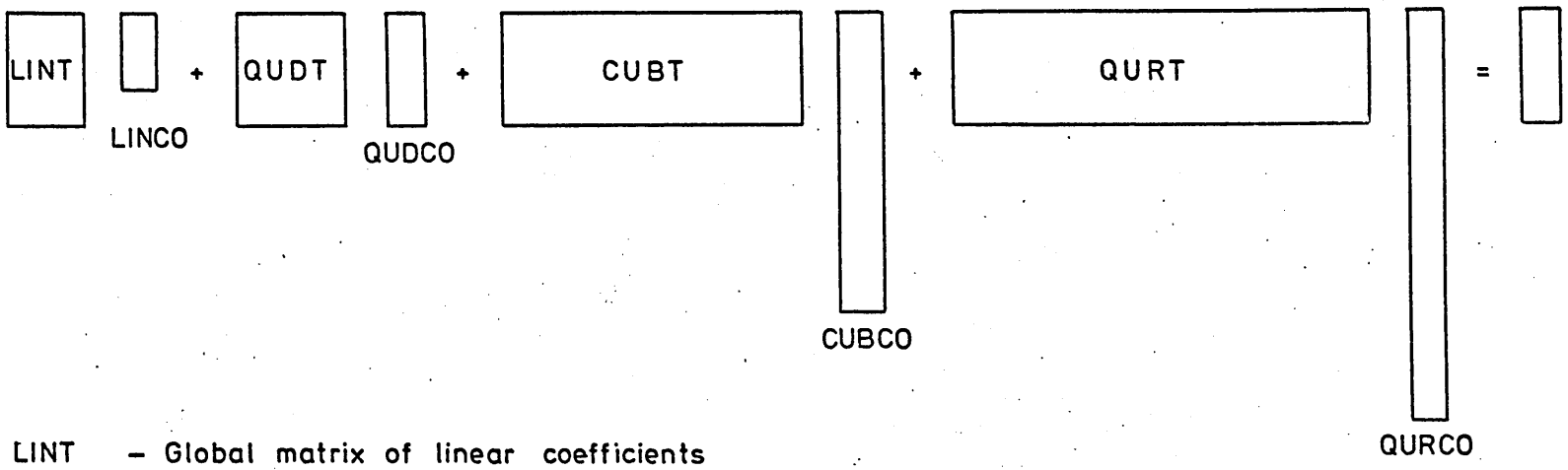

LINT - Global matrix of linear coefficients

LINCO - Matrix of linear terms in U

QUDT - Global matrix of quadratic coefficients

QUDCO - Matrix of quadratic terms in U

CUBT - Global matrix of cubic coefficients

CUBCO - Matrix of cubic terms in U

QURT - Global matrix of quartic coefficients

QURCO - Matrix of quartic terms in U

Figure 34

The Discrete Global Field Equations In Schematic Form

$$|\text{LINCO}| = \begin{vmatrix} U(1) \\ U(4) \\ U(7) \\ U(13) \\ U(16) \\ U(19) \end{vmatrix} \qquad |\text{QUDCO}| = \begin{vmatrix} U(11)U(15) \\ U(12)U(14) \\ U(14)U(14) \\ U(14)U(18) \\ U(15)U(17) \\ U(17)U(17) \\ U(17)U(21) \\ U(18)U(20) \\ U(20)U(20) \\ U(20)U(24) \\ U(21)U(23) \end{vmatrix}$$

THE MATRICES LINCO AND QUDCO

FIGURE 35

$$[CUBCO] = \begin{vmatrix} U(1)U(11)U(15) \\ U(1)U(12)U(14) \\ U(1)U(14)U(18) \\ U(1)U(15)U(17) \\ U(2)U(10)U(15) \\ U(2)U(15)U(16) \\ U(3)U(10)U(14) \\ U(3)U(14)U(16) \\ U(4)U(14)U(18) \\ U(4)U(15)U(17) \\ U(4)U(17)U(21) \\ U(4)U(18)U(20) \\ U(5)U(13)U(18) \\ U(5)U(18)U(19) \\ U(6)U(13)U(17) \\ U(6)U(17)U(19) \\ U(7)U(17)U(21) \\ U(7)U(18)U(20) \\ U(7)U(20)U(24) \\ U(7)U(21)U(23) \\ U(8)U(16)U(21) \\ U(8)U(21)U(22) \\ U(9)U(16)U(20) \\ U(9)U(20)U(22) \\ U(10)U(14)U(15) \\ U(11)U(13)U(15) \\ U(12)U(13)U(14) \\ U(13)U(14)U(18) \\ U(13)U(15)U(17) \\ U(13)U(17)U(18) \\ U(14)U(15)U(16) \\ U(14)U(16)U(18) \\ U(15)U(16)U(17) \\ U(16)U(17)U(21) \\ U(16)U(18)U(20) \\ U(16)U(20)U(21) \\ U(17)U(18)U(19) \\ U(17)U(19)U(21) \\ U(18)U(19)U(20) \\ U(19)U(20)U(24) \\ U(19)U(21)U(23) \\ U(20)U(21)U(22) \end{vmatrix}$$

$$[QURCO] = \begin{vmatrix} U(10)U(10)U(15)U(15) \\ U(10)U(13)U(15)U(15) \\ U(10)U(15)U(15)U(16) \\ U(11)U(11)U(15)U(15) \\ U(11)U(12)U(14)U(15) \\ U(11)U(14)U(15)U(15) \\ U(11)U(14)U(15)U(18) \\ U(11)U(15)U(15)U(17) \\ U(12)U(12)U(14)U(14) \\ U(12)U(14)U(14)U(15) \\ U(12)U(14)U(14)U(18) \\ U(12)U(14)U(15)U(17) \\ U(13)U(13)U(15)U(15) \\ U(13)U(13)U(18)U(18) \\ U(13)U(13)U(15)U(16) \\ U(13)U(16)U(16)U(18) \\ U(13)U(18)U(18)U(19) \\ U(14)U(14)U(15)U(15) \\ U(14)U(14)U(15)U(18) \\ U(14)U(14)U(18)U(18) \\ U(14)U(15)U(15)U(17) \\ U(14)U(15)U(17)U(18) \\ U(14)U(17)U(18)U(18) \\ U(14)U(17)U(18)U(21) \\ U(14)U(18)U(18)U(20) \\ U(15)U(15)U(16)U(16) \\ U(15)U(15)U(17)U(17) \\ U(15)U(17)U(17)U(18) \\ U(15)U(17)U(17)U(21) \\ U(15)U(17)U(18)U(20) \\ U(16)U(16)U(18)U(18) \\ U(16)U(16)U(21)U(21) \\ U(16)U(18)U(18)U(19) \\ U(16)U(19)U(21)U(21) \\ U(16)U(21)U(21)U(22) \\ U(17)U(17)U(18)U(18) \\ U(17)U(17)U(18)U(21) \\ U(17)U(17)U(21)U(21) \\ U(17)U(18)U(18)U(20) \\ U(17)U(18)U(20)U(21) \\ U(17)U(20)U(21)U(21) \\ U(17)U(20)U(21)U(24) \\ U(17)U(21)U(21)U(23) \\ U(18)U(18)U(19)U(19) \\ U(18)U(18)U(20)U(20) \\ U(18)U(20)U(20)U(21) \\ U(18)U(20)U(20)U(24) \\ U(18)U(20)U(21)U(23) \\ U(19)U(19)U(21)U(21) \\ U(19)U(21)U(21)U(22) \\ U(20)U(20)U(21)U(21) \\ U(20)U(20)U(21)U(24) \\ U(20)U(20)U(24)U(24) \\ U(20)U(21)U(21)U(23) \\ U(20)U(21)U(23)U(24) \\ U(21)U(21)U(22)U(22) \\ U(21)U(21)U(23)U(23) \end{vmatrix}$$

THE MATRICES CUBCO AND QURCO

FIGURE 36

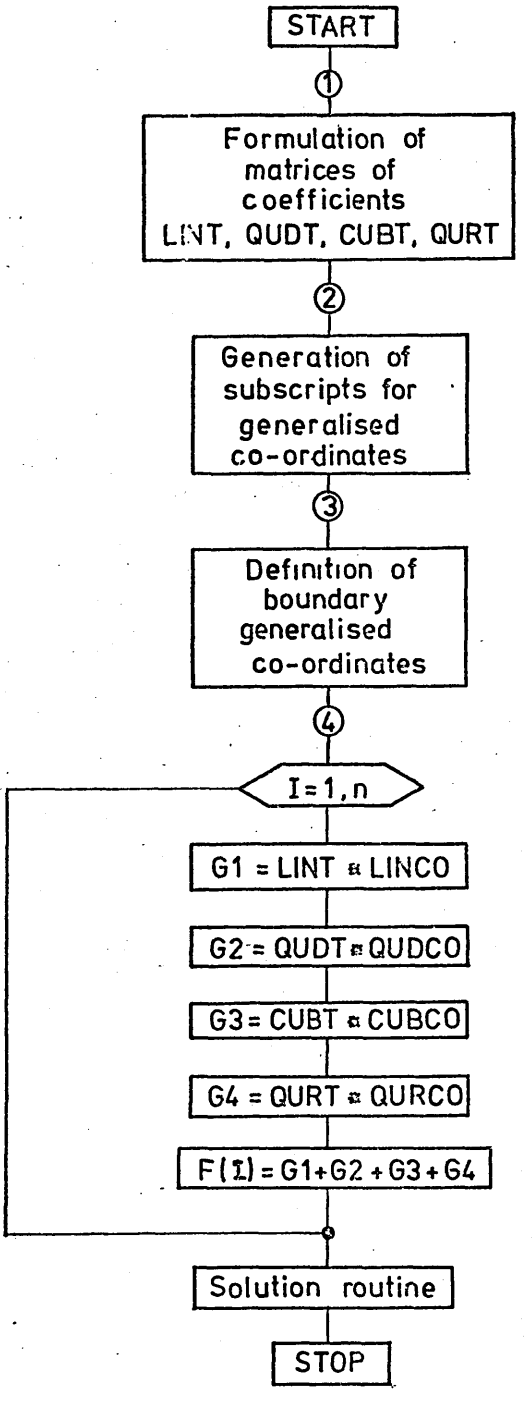

Flow Chart Elucidating The Definition Of The Global Functions

Figure 37

diagram relating the various matrices.

The third stage is concerned with satisfying the boundary conditions of equations (5.66) and (5.72) and defining the initial conditions. A consequence of fully satisfying the boundary conditions in the manner described is that the first of the '3n' equations is rendered trivial. However, there remain only '3n-1' global unknowns and these may be determined from the simultaneous solution of the remaining set of '3n-1' non-linear algebraic equations. Thus in this stage of the program values are assigned to the known global parameters through the application of equations (5.56) and (5.72) and the initial conditions are set.

The fourth stage of the program entails the presentation of the global equations in the manner required by the solution routine. To this end, the remaining global unknowns are made equivalent to 'x_i' where

$$i = 1,3n-1 \qquad \ldots\ldots\ldots (5.82)$$

Thus the parameter 'x_i' appearing in the non-linear solution routine described in the following chapter, represents the global unknowns, 'U(i)', which are not eliminated through the application of boundary conditions.

The equations are defined as the functions '$f_i(x)$' through the multiplication of the matrices of coefficients by the appropriate column vectors of generalised co-ordinates. The basic principle of the operation is illustrated in the flow diagram in Figure (37). The actual programming employed is rather more complex. Further details of the method are provided by the 'comment' statements included in the program listing given in Appendix II.

5.8 Summary

In this chapter the classical differential continuous field and boundary expressions have been converted into a global set of discrete algebraic functions by the application of the Collocation Finite Element, or Hypar Finite Difference, method[59]. Consider now the solution of these equations.

CHAPTER 6

SOLUTION OF DISCRETE GLOBAL SYSTEM

6.1 Introduction

The global equations provided by the co-ordinate transformation of the local field and boundary analogues consist of a set of non-linear simultaneous algebraic equations including terms of up to the fourth order. The algorithm chosen for their solution is a hybrid of the Newton-Raphson and the Steepest Descent methods, developed by Powell[73][74]. Software details being available[74], the present study will content itself with a broad outline of the method and a description of some of its more important features.

6.2 The Newton-Raphson Method.

The underlying principles of the Newton-Raphson method may be appreciated most easily by considering its application to a single variable function, 'f(x)'. This is a special case of the method which is equivalent to Newton's technique for finding the root of 'f(x)'.

The relationship ;

$$f'(x^{(k)}) = \frac{f(x^{(k)})}{x^{(k)} - x^{(k+1)}} \qquad \ldots\ldots\ldots \quad (6.1)$$

is self-evident from Figure (38). Re-arranging the terms gives the well known Newton-Raphson formula[75] ;

$$x^{(k+1)} = x^{(k)} - \frac{f(x^{(k)})}{f'(x^{(k)})} \qquad \ldots\ldots\ldots \quad (6.2)$$

A solution may be gained by an iteration procedure in which the estimate, '$x^{(k)}$', of the solution is replaced by ;

$$x^{(k+1)} = x^{(k)} + \delta^{(k)} \qquad \ldots\ldots\ldots \quad (6.3)$$

where ; $$f(x^{(k)}) + f'(x^{(k)})\,\delta^{(k)} = 0 \qquad \ldots\ldots\ldots \quad (6.4)$$

The procecure converges to the root of the equation and the solution is obtained when the updated estimate agrees with the previous estimate within an acceptable degree of accuracy.

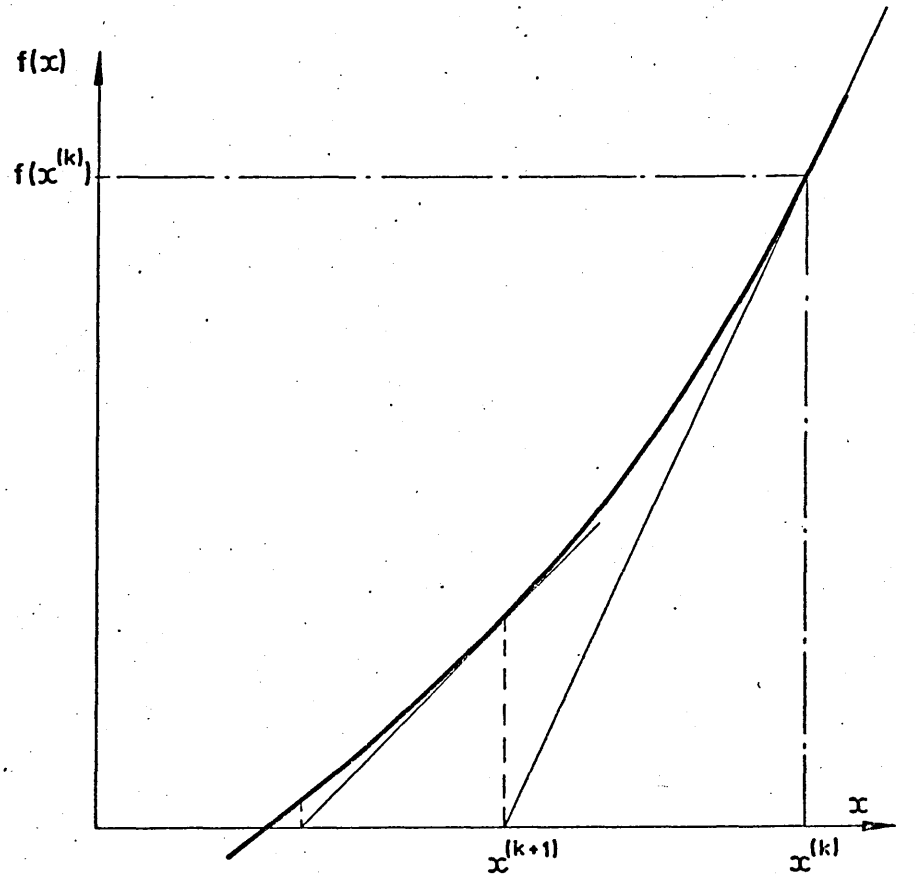

The Newton - Raphson Iteration
For A Function In One Variable

Figure 38

For the general case of a system of non-linear algebraic equations[13];

$$f_i(X) = f_i(x_1, x_2, \ldots, x_n) = 0 \quad (i = 1,n) \quad \ldots \quad (6.5)$$

the estimate '$X^{(k)}$' of the solution is replaced by the estimate ;

$$X^{(k+1)} = X^{(k)} + \delta^{(k)} \quad \ldots\ldots\ldots \quad (6.6)$$

where '$\delta^{(k)}$' solves the linear system ;

$$f_i(X^{(k)}) + \sum_{j=1}^{n} J_{ij}^{(k)} \delta_j^{(k)} = 0 \quad (i = 1,n) \quad \ldots \quad (6.7)$$

The Jacobian matrix, '$|J|$' is composed of first derivatives, that is ;

$$J_{ij}^{(k)} = \left[\frac{\partial f_i}{\partial x_j}\right]_{X=X^{(k)}} \quad \ldots\ldots\ldots \quad (6.8)$$

As before, an iterative process for the solution of '$f(X)$' is achieved.

6.3 The Steepest Descent Method

An alternative approach to the problem is the implementation of a minimisation technique. The roots of the system (6.5) may clearly be obtained by minimisation of the function '$F(X)$' with respect to 'X', where ;

$$F(X) = \sum_{i=1}^{n} [f_i(X)]^2 \quad \ldots\ldots\ldots \quad (6.9)$$

since '$F(X)$' is non-negative and so has the least possable value of zero. Thus the solution of the equations is provided by the particular value of 'X' for which the function is zero.

The Steepest Descent method is one of the step-by-step multivariate minimisation procedures in which a univariate search along a line from the current best point to a new point (which is a minimum on that line) is carried out at each step. Thus if the current point is '$X^{(k)}$', then ;

$$Z = X^{(k)} + \alpha^{(k)} p^{(k)} \quad \ldots\ldots\ldots \quad (6.10)$$

defines a line through '$X^{(k)}$' in the direction '$p^{(k)}$', where '$\alpha^{(k)}$' is an undetermined scalar. Minimisation of '$f(Z)$' with respect to '$\alpha^{(k)}$', may be carried out by a univariate minimisation technique. Assuming that ;

$$\alpha = \alpha^{*} \qquad \ldots\ldots\ldots (6.11)$$

at the minimum, the new point is taken as ;

$$X^{(k+1)} = X^{(k)} + \alpha^{*} p^{(k)} \qquad \ldots\ldots\ldots (6.12)$$

A new direction is then determined and the procedure is repeated until an overall minimum is found. The procedure applied to a function in two variables is illustrated in Figure (39).

The manner in which the direction is determined depends on the particular method used. The Steepest Descent method, as its name would imply, entails the determination of the steepest downhill direction at some point '$X^{(i)}$'. The difference, 'Δ', between the function at this point, '$f(X^{(i)})$', and a neighbouring point, '$f(X^{(i)}+p^{(i)})$', where '$|p|$' is constant, is a maximum along the line of steepest descent, as shown in Figure (39). The first term in the Taylor expansion[76] gives ;

$$\Delta = -\sum_{j} p_j \frac{\partial f}{\partial x_j} \qquad \ldots\ldots\ldots (6.13)$$

$$= -pg \qquad \ldots\ldots\ldots (6.14)$$

where 'g' is the gradient. Thus 'Δ' is the scalar product ;

$$\Delta = -\|p\|\|g\|\cos\theta \qquad \ldots\ldots\ldots (6.15)$$

where 'θ' is the angle between the vectors 'p' and 'g'. The difference 'Δ' is clearly a maximum when 'p' and 'g' are anti-parallel. Thus the direction of the steepest descent is given by '$-g$' and the estimate, '$X^{(k)}$', of the solution is replaced by

$$X^{(k+1)} = X^{(k)} - \alpha^{*} g^{(k)} \qquad \ldots\ldots\ldots (6.16)$$

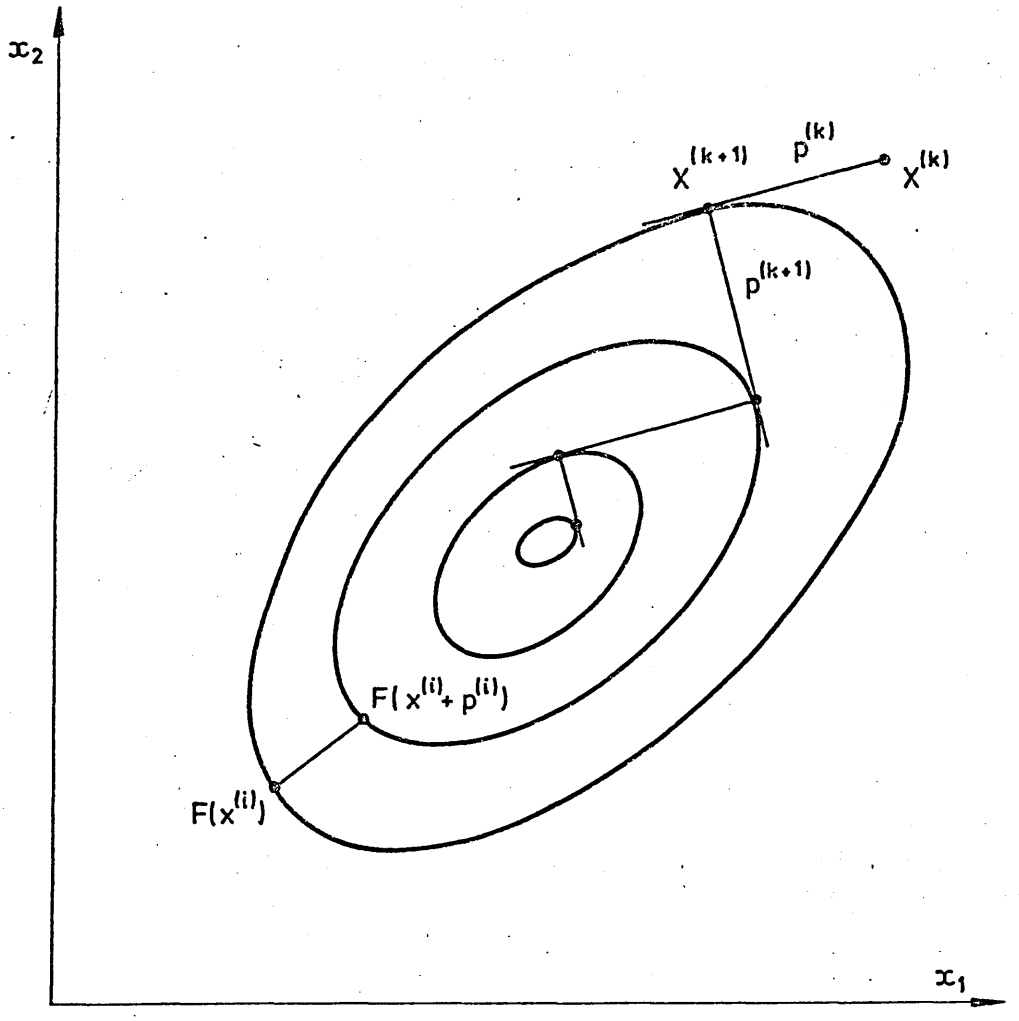

The Steepest Descent Method For A Function In Two Variables

Figure 39

As in the previous case, the iteration procedure is continued until it converges to an estimate of the solution with an acceptable degree of accuracy.

6.4 Powell's Algorithm

The classical Newton-Raphson iteration often fails to converge if '$X^{(k)}$' is not a good estimate of the solution of the system (6.5). A number of algorithms have been developed to try and provide reliable convergence even when a close initial estimate of the solution is not available. One common strategy is to retain the direction but to restrict the length of the step predicted by the classical method. Thus equation (6.6) is replaced by the expression ;

$$X^{(k+1)} = X^{(k)} + \lambda^{(k)} \delta^{(k)} \qquad \ldots\ldots\ldots \quad (6.17)$$

where the number '$\lambda^{(k)}$' is calculated to prevent the estimate '$X^{(k+1)}$' from being worse than '$X^{(k)}$'. This condition may be tested by evaluating the sum of the squares of the residuals (that is the function of equation (6.9)) and ensuring that ;

$$F(X^{(k+1)}) < F(X^{(k)}) \qquad \ldots\ldots\ldots \quad (6.18)$$

The approach is not altogether satisfactory as it will fail in certain situations, one of them being when the Jacobian matrix becomes singular.

A method for modifying the Newton-Raphson iteration still further may be derived by introducing the parameter 'λ^*' into the 'normal least squares' formulation of the equation (6.7), that is ;

$$\sum_{j=1}^{n} \left\{ \sum_{k=1}^{n} J_{ki} J_{kj} \right\} \delta_j = -\sum_{k=1}^{n} J_{ki} f_k(X) \qquad (i = 1,n) \quad (6.19)$$

A correction vector, 'δ^*', is obtained by solving the set of linear equations ;

$$\sum_{j=1}^{n} \left\{ \lambda^* I_{ij} + \sum_{k=1}^{n} J_{ki} J_{kj} \right\} \delta_j^* = -\sum_{k=1}^{n} J_{ki} f_k(X) \quad \ldots \quad (6.20)$$

where 'I' is a unit matrix. When 'λ^*' is zero, the system (6.20) is

equivalent to the classical iteration itself. When ' λ ' becomes large, the solution of the linear equations yields ;

$$\delta_j^* \longrightarrow -\sum_{k=1}^{n} J_{ki} f_k(X)/\lambda^* \qquad \ldots\ldots\ldots (6.21)$$

$$= -\tfrac{1}{2}\left[\frac{\partial}{\partial x_i} F(X)\right]_{X=X^{(k)}}/\lambda^* \qquad \ldots\ldots\ldots (6.22)$$

which shows that ' $\delta^{*(k)}$ ' tends to a small negative multiple of the gradient of 'F(X)' at ' $X^{(k)}$ '. Therefore, the large values of ' λ^* ' tend to make the iteration similar to the classical Steepest Descent method applied to the function 'F(X)' and, unless ' $X^{(k)}$ ' is a stationary point of 'F(X)', a value of ' λ^* ' can be calculated so as to satisfy the inequality (6.20).

Powell's method[73] is very similar to this approach, although it differs from previous algorithms of this type in a number of ways. The classical iteration is modified in such a manner that it is unnecessary to solve a linear system, such as (6.20), on every iteration. Nor are explicit expressions for the derivatives required as the Jacobian matrix is revised by a numerical approximation technique. In this way, economies are made in computational effort whilst retaining the main features of this type of method, namely that if the full Newton-Raphson correction is too large, the displacement from ' $X^{(k)}$ ' is biased towards the steepest descent direction of 'F(X)'.

A general outline of one iteration of the method is illustrated by the flow diagram of Figure (40). The algorithm has several initial requirements which are illustrated in the block diagram of Figure (41). The iterative process begins by evaluating the full Newton-Raphson correction, ' $\delta^{(k)}$ ', by solving the system ;

$$f_i(X^{(k)}) + \sum_{j=1}^{n} J_{ij}^{(k)} \delta_j^{(k)} = 0 \qquad (i = 1,n) \ldots (6.23)$$

The gradient is then found from the calculation ;

$$g_j^{(k)} = \left[\frac{\partial}{\partial x_j} F(X)\right] \qquad \ldots\ldots\ldots (6.24)$$

$$= 2\sum_{i=1}^{n}\left[f_i(X)\frac{\partial}{\partial x_j} f_i(X)\right]_{X=X^{(k)}} \qquad \ldots\ldots\ldots (6.25)$$

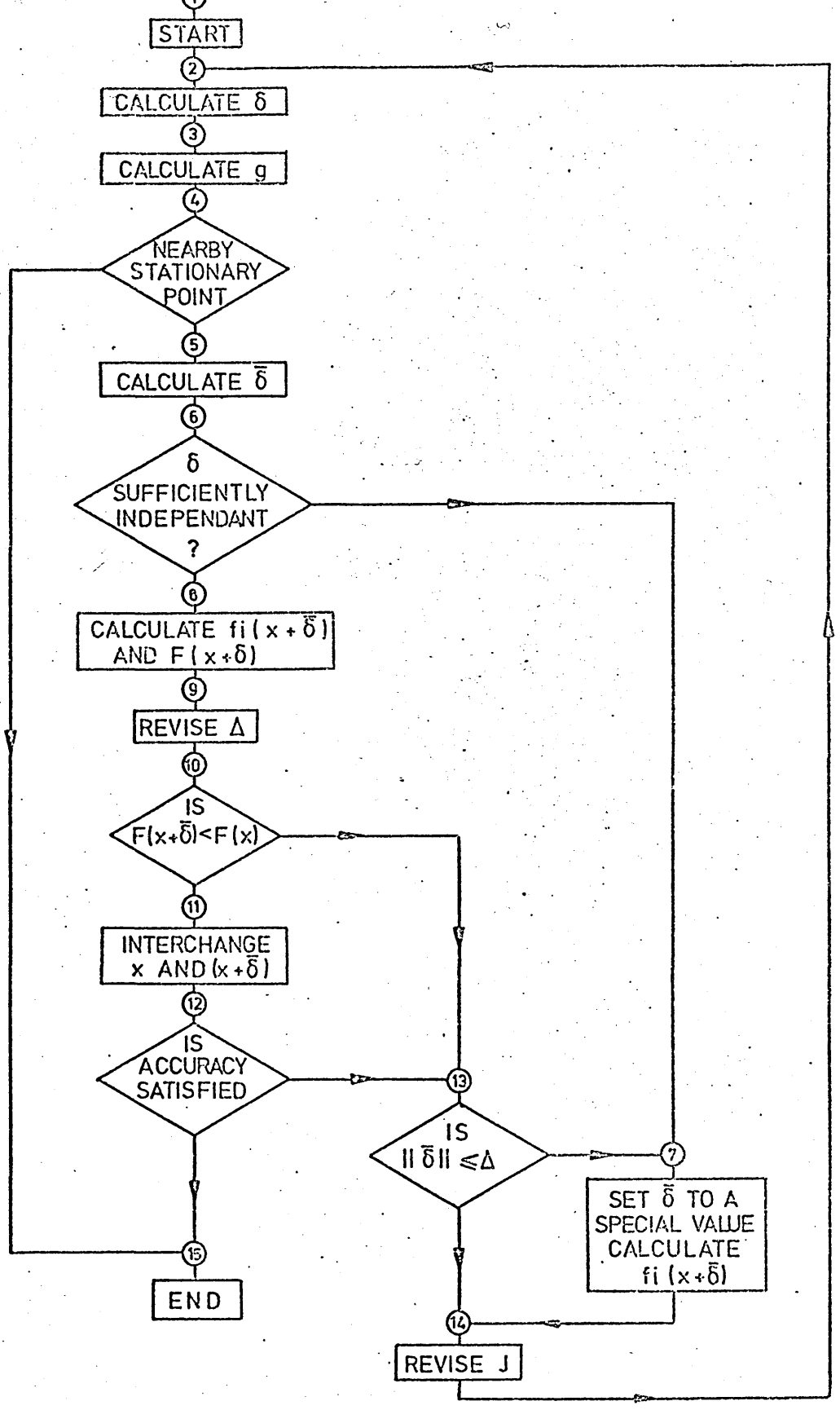

Solution Flow Diagram

Figure 40

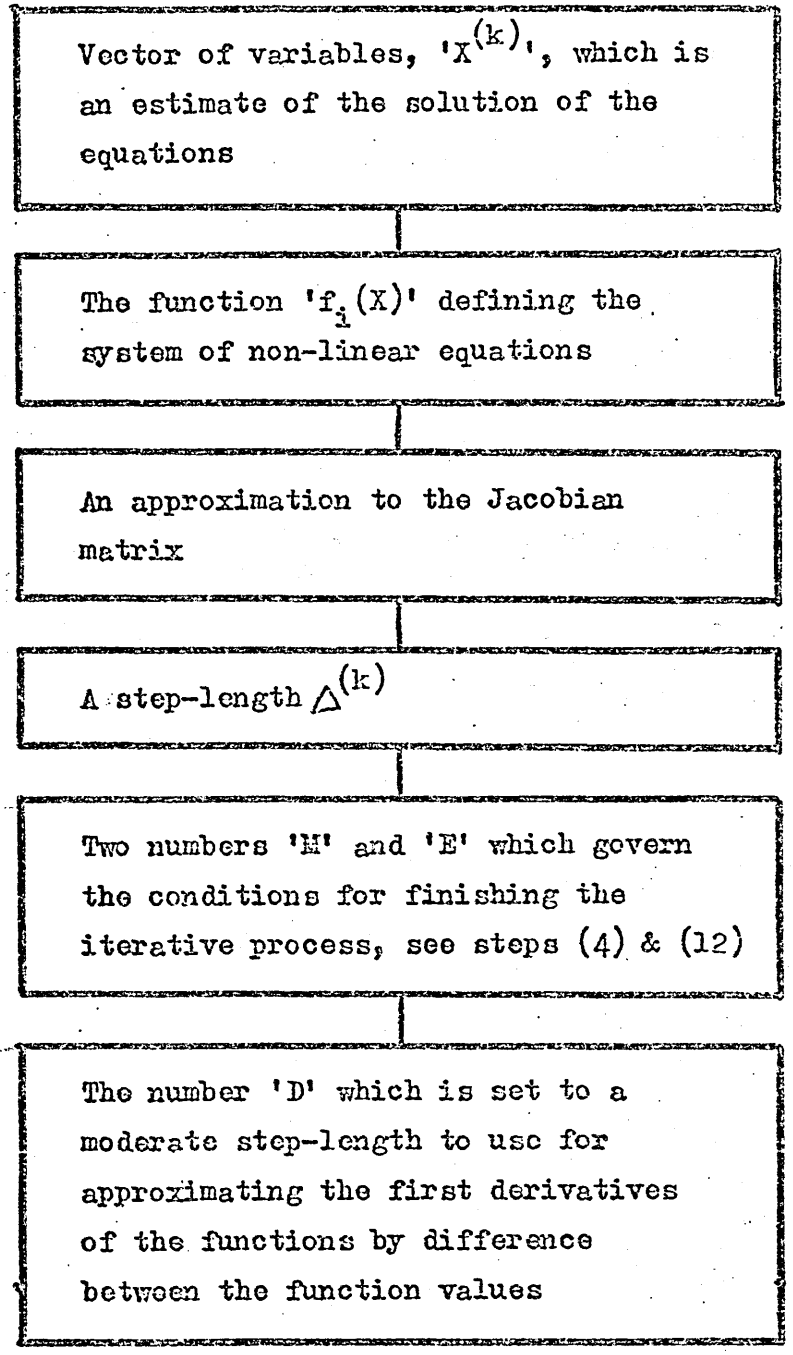

THE INITIAL ALGORITHM REQUIREMENTS

Figure 41

The number 'M' represents an over-estimate of the distance from '$X^{(1)}$' to the solution. If the gradient of 'F(X)' is so small that the distance from '$X^{(k)}$' to a solution is predicted to exceed 'M', the presence of a nearby stationary point, usually a local minimum, is indicated. The fourth step of the algorithm institutes the test ;

$$F(X^{(k)}) \geqslant M \|g^{(k)}\|_2 \qquad \ldots\ldots\ldots \quad (6.26)$$

If the inequality holds, the iteration is complete.

The next stage of the algorithm is the calculation of the displacement, '$\bar{\delta}^{(k)}$', to add to the vector '$X^{(k)}$'. Providing the inequality ;

$$\Delta^{(k)} \geqslant \|\delta^{(k)}\|_2 \qquad \ldots\ldots\ldots \quad (6.27)$$

holds, the displacement, '$\bar{\delta}^{(k)}$', is taken to be the classical Newton-Raphson displacement, '$\delta^{(k)}$'. If the inequality (6.27) does not hold, '$\bar{\delta}^{(k)}$' is taken as the step-length, '$\Delta^{(k)}$', along the direction of steepest descent. That is ;

$$\bar{\delta}^{(k)} = -\Delta \frac{g^{(k)}}{\|g^{(k)}\|_2} \qquad \ldots\ldots\ldots \quad (6.28)$$

The step-length, '$\Delta^{(k)}$', can be changed on each iteration, its purpose being to restrict the length of the displacement between the previous and the updated estimates so that the iteration decreases the value of 'F(X)'. This displacement is only adopted if it does not exceed the predicted minimum along the path of steepest descent, which occurs at the point ;

$$X^{(k)} - \frac{\frac{1}{2}\|g^{(k)}\|_2^2}{\|J^{(k)} g^{(k)}\|_2^2} g^{(k)} \qquad \ldots\ldots\ldots \quad (6.29)$$

Equation (6.16) should be noted. Thus the inequality ;

$$\Delta^{(k)} \frac{g^{(k)}}{\|g^{(k)}\|_2} \leqslant \left[\frac{\frac{1}{2}\|g^{(k)}\|_2^2}{\|J^{(k)} g^{(k)}\|_2^2}\right] g^{(k)} \qquad \ldots\ldots\ldots \quad (6.30)$$

ie; $$\Delta^{(k)} \leqslant \frac{\|F^{(k)}\|_2^2}{\|J^{(k)}g^{(k)}\|_2^2} \qquad \ldots\ldots\ldots (6.31)$$

is tested. If neither the inequality (6.27) nor (6.31) holds, the new estimate is taken to lie on the straight line joining the points predicted by the Steepest Descent and the full Newton-Raphson methods respectively. The actual components of the displacement are determined from the condition ;

$$\|\bar{\delta}^{(k)}\|_2 = \Delta^{(k)} \qquad \ldots\ldots\ldots (6.32)$$

Thus the algorithm calculates a displacement ' $\delta^{(k)}$ ' which is of the form;

$$\bar{\delta}^{(k)} = \beta\delta^{(k)} + \gamma g^{(k)} \qquad \ldots\ldots\ldots (6.33)$$

where ' β ' and ' γ ' are scalars, such that it interpolates between the Steepest Descent and the classical Newton-Raphson corrections.

The method for revising the Jacobian approximation, step (14) in Figure (40), is such that linear dependence in the directions ' δ ' that are generated by successive iterations, should be avoided. The calculations of the previous step often tend to provide dependant directions. This condition is tested and, if necessary, extra directions are introduced to ensure that independence is maintained.

If the condition of linear independance is satisfied, the values of the functions (based on the updated estimate) and the sum of the squares of the residuals are calculated.

The revision of ' Δ ' is aimed at making the step-length as large as possible, subject to the condition that each Jacobian approximation provides a good prediction of the differences of the function values calculated at the previous and the updated estimates of the solution. This is carried out in order to decrease the sum of squares, 'F(X)', on every iteration without taking extravagantly small steps. If this condition, tested at step (10) of Figure (40), does not hold, the step-length is reduced. The magnitude of the step-length always lies between the upper and the lower bounds of the values of 'M' and 'D' respectively.

to the solution of the equations for the next iteration has been achieved and '(X)' and '(X-$\bar{\delta}$)' are interchanged. Furthermore, if the inequality ;

$$\sum_{i=1}^{n} [f_i(X)]^2 < E \qquad \ldots\ldots\ldots (6.34)$$

holds, the estimate '$X^{(k)}$' is acceptably close to the solution of the equations and the algorithm finishes.

If either of the last two inequalities does not hold, control is switched to step (13) of the flow diagram in Figure (40) where the inequality ;

$$\|\bar{\delta}\| \leqslant \Delta \qquad \ldots\ldots\ldots (6.35)$$

is tested. If it fails, control is switched consecutively to steps (7) and (14) in the flow diagram. If it holds, the algorithm proceeds straight to step (14) and the Jacobian is revised.

The method for revising the Jacobian approximation depends on the vector '$\bar{\delta}$' and on the differences ;

$$\epsilon_i = f_i(X + \bar{\delta}) - f_i(X) \qquad (i = 1,n) \qquad \ldots\ldots\ldots (6.36)$$

the revised matrix being defined by the equation ;

$$J^{(k+1)} = J^{(k)} + \frac{(\epsilon^{(k)} - J^{(k)}\bar{\delta}^{(k)})\bar{\delta}^{(k)T}}{\|\bar{\delta}^{(k)}\|_2^2} \qquad \ldots\ldots\ldots (6.37)$$

If '$\bar{\delta}$' is too small, the differences are liable to be dominated by computer rounding errors. The introduction of the inequality ;

$$\delta < D \qquad \ldots\ldots\ldots (6.38)$$

and the consequent transfer of control to step (7) of the flow diagram is designed to circumvent this situation. The revision of the Jacobian matrix completes one cycle of the iteration.

6.5 Trial Runs with the Algorithm

The algorithm developed by Powell[73] was modified for the purposes of this study only in so far as was necessary to accomodate the sub-routine defining the equations. Two other minor modifications were made ; the introduction of a standard package for matrix inversion, and a modification to the output procedure to facilitate program monitoring.

The constituent parts of the program (that is the co-ordinate transformation routine, described in the previous chapter, and the non-linear solution routine based on Powell's algorithm) were thoroughly tested. The solution routine was checked against standard problems[73]. Further, a series of equations of very similar form to those generated by the co-ordinate trandformation of the local field analogue, but whose solution was known, were solved. The program was found to operate correctly and was used for the solution of the equations formulated in Chapter Five.

6.6 Summary

This chapter has been concerned with a description of the algorithm employed for the solution of the global set of algebraic non-linear equations generated by the co-ordinate transformation routine. Particular attention has been paid to the structure of the solution routine due to its complex nature. The results obtained from the application of the solution routine to the global equations formulated for the plane jet problem, are considered in the following chapter.

7.1 The Calculation Procedure

It was originally envisaged that the procedure would take the form of a step-wise calculation designed to terminate on the attainment of the condition of similarity. It was hoped that calculations involving a large number of steps would be unnecessary, or at least only required for clearer definition of results after similarity had been established. However, in order to minimise the number of unknowns it was decided to adopt an alternative approach in which, as the first stage, the step-wise procedure was continued only for as long as was necessary to produce profiles of an acceptable form. The second stage of the procedure then involved a similarity check on the profiles. This was achieved by shifting the whole mesh bodily downstream and repeating stage one of the procedure from a different starting position. The final profiles obtained at each stage were examined for similarity.

The main attraction of this scheme is that, for a small amount of additional manipulative effort, a solution involving a relatively small amount of equations may be obtained. The advantages gained in this manner are discussed further in the next chapter. The two-stage procedure is illustrated in Figures (42.a) and (42.b). In order to gain results for a more complete similarity check, and also to gain a fuller definition of the downstream development of the flow, the procedure was carried on for an extra two stages for the purposes of this study. The extra stages are illustrated in the remainder of Figure (42). The dimension 'B', which defines the location of the local mesh within the global domain, was assigned a nominal value and the mesh was moved downstream at each stage by increasing the value of 'h' relative to 'B'.

It should be noted that the equations making up the local analogue, and hence the global set, were not derived in terms of fully non-dimensionalised parameters. Thus the units of 'h' have a dimensional significance which is reflected in the final results.

Stage 1.

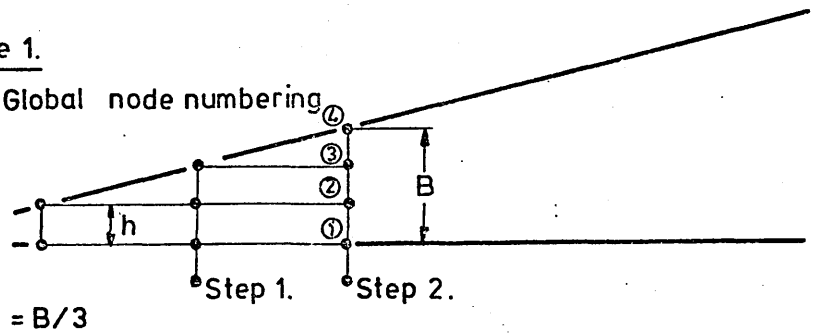

a) h = B/3

Stage 2.

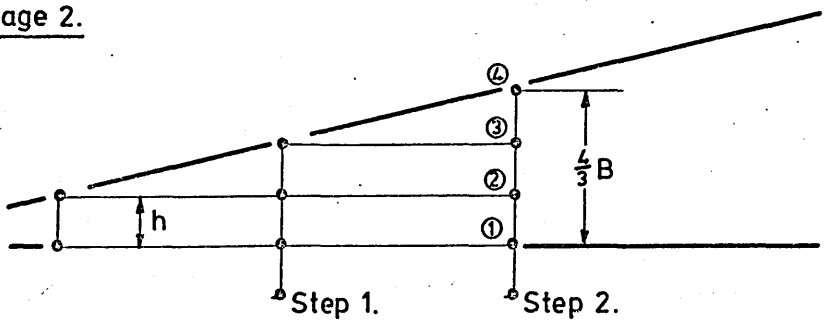

b) h = 4B/9

Stage 3.

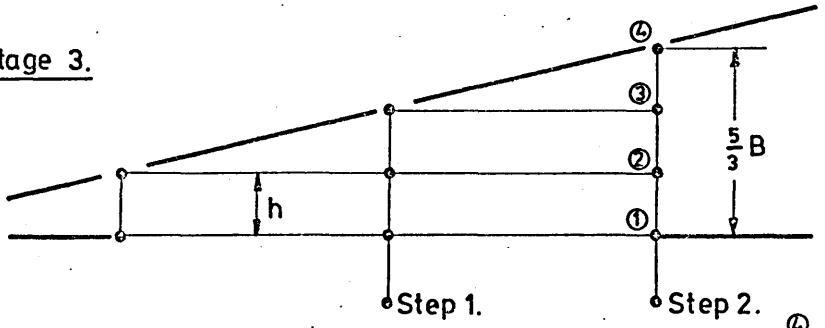

c) h = 5B/9

Stage 4.

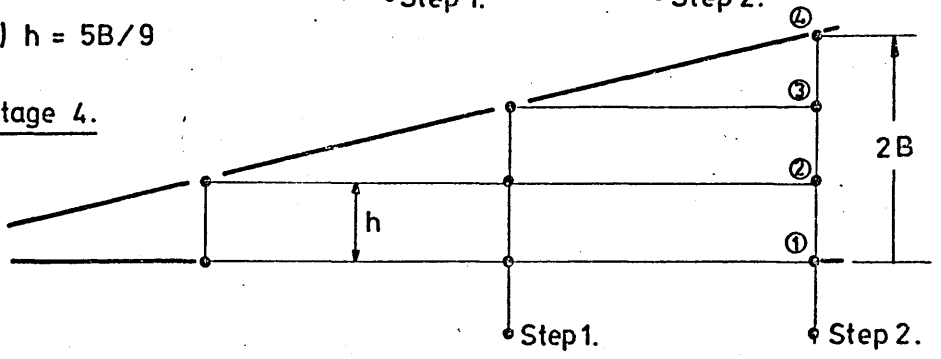

d) h = 2B/3

The Stages Of Solution.

Figure 42

7.2 Computational Results

The computational results for the runs representing the stages (1) to (4), as illustrated in Figure (42), are given in the Tables (7) and (8). The runs were carried out on the basis that ;

$$B = 0.15 \qquad \ldots\ldots\ldots (7.1)$$

The manner in which the parameters 'ψ', 'ϕ' and 'L' developed along the mesh at stage (1) is illustrated in Figures (43) to (45). The streamwise development of the parameters as calculated at step (2) for stages (1) to (4) is illustrated in Figures (46) to (48). These results, and specified derivatives, are listed in Tables (9) to (12). The numbered columns in the Tables refer to the corresponding nodal numbering in the Figures.

7.3 Non-dimensionalised Profiles

The standard velocity and length scales adopted for non-dimensionalising the parameters are 'U_m' and '$Y|_{0.5}$' respectively[44]. The velocity profiles were derived from the ψ-profiles by discrete numerical approximation, that is ;

$$U|_{n,Y} = \frac{\partial \psi}{\delta Y}_{n,Y} \simeq \frac{\psi|_{(n+1),Y} - \psi|_{(n-1),Y}}{2h} \qquad \ldots\ldots\ldots (7.2)$$

The nature of the curve was found to be such that the approximation agreed very closely with the results from a graphical check. The streamwise development of the velocity profiles is illustrated in Figure (49). The values of 'U_m' and '$Y|_{0.5}$' at each stage were obtained from the profiles. It was noted that the conditions for self-preservation, as defined by equations (1.13) and (1.14), were satisfied. The jet spread and the centre-line velocity are shown in Figures (50.a) and (50.b). The jet spread was found to agree with the value obtained by Spalding[44]. The results for the jet spread and the centre-line velocity decay are listed in Table (13).

The evaluation of the transverse velocity profile required the following assumptions;

(1) similarity of ψ-profiles,

(2) jet spread linearity, and

(3) characteristic decay of centre-line velocity (ie; $X \alpha U^{-2}$).

all of which have been shown to be valid.

	INITIAL CONDITIONS	STEP 1	STEP 2
STAGE 1 : h = 0.05			
X	0.200	0.400	0.600
$b_{(x)}$	0.050	0.100	0.150
$\psi 1$	0	0	0
$\phi 1$	0.800×10^{1}	0.551×10^{1}	0.443×10^{1}
L1	0.250×10^{-2}	0.362×10^{-2}	0.460×10^{-2}
$\psi 2$	0.165×10^{1}	0.169×10^{1}	0.172×10^{1}
$\phi 2$	0	0.313×10^{1}	0.492×10^{1}
L2	0.300×10^{-2}	0.375×10^{-2}	0.499×10^{-2}
$\psi 3$		0.225×10^{1}	0.230×10^{1}
$\phi 3$		0	0.151×10^{1}
L3		0.379×10^{-2}	0.503×10^{-2}
$\psi 4$			0.250×10^{1}
$\phi 4$			0
L4			0.504×10^{-2}
STAGE 2 : h = 0.0667			
X	0.267	0.533	0.800
$b_{(X)}$	0.067	0.133	0.200
$\psi 1$	0	0	0
$\phi 1$	0.700×10^{1}	0.519×10^{1}	0.367×10^{1}
L1	0.333×10^{-2}	0.663×10^{-2}	0.589×10^{-2}
$\psi 2$	0.175×10^{1}	0.151×10^{1}	0.181×10^{1}
$\phi 2$	0	0.346×10^{1}	0.362×10^{1}
L2	0.333×10^{-2}	0.920×10^{-2}	0.609×10^{-2}
$\psi 3$		0.201×10^{1}	0.241×10^{1}
$\phi 3$		0	0.101×10^{1}
L3		0.101×10^{-2}	0.591×10^{-2}
$\psi 4$			0.261×10^{1}
$\phi 4$			0
L4			0.585×10^{-2}

TABLE 7 : COMPUTATIONAL RESULTS

	INITIAL CONDITIONS	STEP 1	STEP 2
STAGE 3 : h = 0.0833			
X	0.333	0.667	1.000
$b_{(x)}$	0.083	0.167	0.250
$\psi 1$	0	0	0
$\phi 1$	0.550×10^{1}	0.373×10^{1}	0.298×10^{1}
L1	0.400×10^{-2}	0.578×10^{-2}	0.720×10^{-2}
$\psi 2$	0.195×10^{1}	0.199×10^{1}	0.202×10^{1}
$\phi 2$	0	0.167×10^{1}	0.314×10^{1}
L2	0.400×10^{-2}	0.542×10^{-2}	0.745×10^{-2}
$\psi 3$		0.265×10^{1}	0.270×10^{1}
$\phi 3$		0	0.883×10^{0}
L3		0.529×10^{-2}	0.725×10^{-2}
$\psi 4$			0.292×10^{1}
$\phi 4$			0
L4			0.719×10^{-2}
STAGE 4 : h = 0.1			
X	0.400	0.800	1.200
$b_{(X)}$	0.100	0.200	0.300
$\psi 1$	0	0	0
$\phi 1$	0.600×10^{1}	0.390×10^{1}	0.305×10^{1}
L1	0.500×10^{-2}	0.763×10^{-2}	0.985×10^{-2}
$\psi 2$	0.190×10^{1}	0.196×10^{1}	0.200×10^{1}
$\phi 2$	0	0.163×10^{1}	0.302×10^{1}
L2	0.600×10^{-2}	0.764×10^{-2}	0.104×10^{-1}
$\psi 3$		0.261×10^{1}	0.267×10^{1}
$\phi 3$		0	0.916×10^{0}
L3		0.765×10^{-2}	0.104×10^{-1}
$\psi 4$			0.290×10^{1}
$\phi 4$			0
L4			0.104×10^{-1}

TABLE 8 : COMPUTATIONAL RESULTS

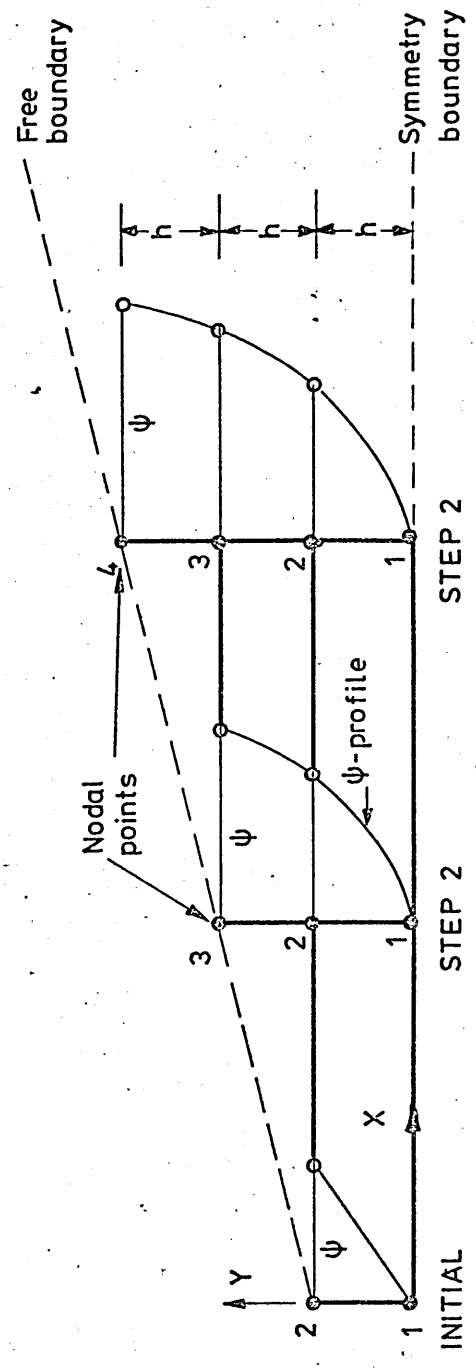

The Streamwise Development Of Ψ.

Figure 43

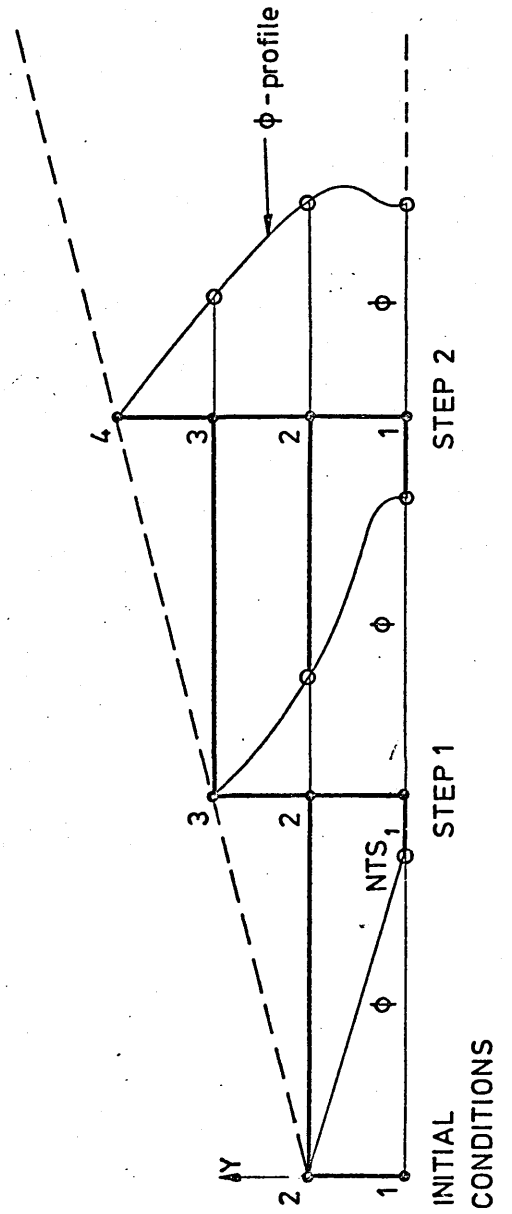
Streamwise Development Of ϕ.
ϕ-profile
4
3
2
1
STEP 2
STEP 1
INITIAL CONDITIONS
NTS1
ϕ
Y

Figure 44

Streamwise Development Of L

Figure 45

	1	2	3	4
ψ	0	0.172×10^{1}	0.230×10^{1}	0.250×10^{1}
$\frac{\partial\psi}{\partial X}$	0	-0.518×10^{0}	0.108×10^{1}	0.422×10^{1}
$\frac{\partial\psi}{\partial Y}$	0.343×10^{2}	0.230×10^{2}	0.783×10^{1}	0
$\frac{\partial^2\psi}{\partial Y^2}$	0	-0.85×10^{3}	-0.330×10^{3}	0
$(\frac{\partial^2\psi}{\partial Y^2})^2$	0	0.148×10^{6}	0.109×10^{6}	0
ϕ	0.443×10^{1}	0.492×10^{1}	0.151×10^{1}	0
$\frac{\partial\phi}{\partial Y}$	0	-0.200×10^{2}	-0.520×10^{2}	-0.233×10^{2}
ϕ^2	0.196×10^{2}	0.242×10^{2}	0.229×10^{1}	0
$\frac{\partial(\phi^2)}{\partial X}$	-0.327×10^{2}	-0.310×10^{2}	0.220×10^{2}	0.600×10^{1}
$\frac{\partial(\phi^2)}{\partial Y}$	0	-0.192×10^{3}	-0.193×10^{3}	0
$\frac{\partial^2(\phi^2)}{\partial Y^2}$	0.300×10^{5}	-0.148×10^{5}	0.224×10^{5}	0.660×10^{3}
ϕ^3	0.870×10^{2}	0.119×10^{3}	0.346×10^{1}	0
L	0.460×10^{-2}	0.499×10^{-2}	0.503×10^{-2}	0.504×10^{-2}
$\frac{\partial L}{\partial Y}$	0	0.432×10^{-2}	0.438×10^{-3}	0

STAGE 1 : DERIVED RESULTS

TABLE 9

	1	2	3	4
Ψ	0	0.181×10^{1}	0.241×10^{1}	0.261×10^{1}
$\frac{\partial\Psi}{\partial X}$	0	-0.457×10^{0}	0.715×10^{0}	0.283×10^{1}
$\frac{\partial\Psi}{\partial Y}$	0.271×10^{2}	0.181×10^{2}	0.602×10^{1}	0
$\frac{\partial^2\Psi}{\partial Y^2}$	0	-0.194×10^{3}	-0.146×10^{3}	0
$(\frac{\partial^2\Psi}{\partial Y^2})^2$	0	0.376×10^{5}	0.214×10^{5}	0
ϕ	0.367×10^{1}	0.362×10^{1}	0.101×10^{1}	0
$\frac{\partial\phi}{\partial Y}$	0	-0.168×10^{2}	-0.321×10^{2}	-0.100×10^{2}
ϕ^2	0.134×10^{2}	0.131×10^{2}	0.102×10^{1}	0
$\frac{\partial(\phi^2)}{\partial X}$	-0.168×10^{2}	-0.600×10^{1}	0.110×10^{2}	0.150×10^{1}
$\frac{\partial(\phi^2)}{\partial Y}$	0	-0.125×10^{3}	-0.660×10^{2}	0
$\frac{\partial^2(\phi^2)}{\partial Y^2}$	0.360×10^{4}	-0.450×10^{4}	0.570×10^{4}	0.600×10^{1}
ϕ^3	0.492×10^{1}	0.474×10^{2}	0.103×10^{1}	0
L	0.589×10^{-2}	0.609×10^{-2}	0.591×10^{-2}	0.585×10^{-2}
$\frac{\partial L}{\partial Y}$	0	-0.525×10^{-3}	-0.182×10^{-2}	0

STAGE 2 : DERIVED RESULTS

TABLE 10

	1	2	3	4
Ψ	0	0.202×10^{1}	0.270×10^{1}	0.292×10^{1}
$\frac{\partial\Psi}{\partial X}$	0	-0.326×10^{0}	0.571×10^{0}	0.133×10^{1}
$\frac{\partial\Psi}{\partial Y}$	0.242×10^{2}	0.162×10^{2}	0.542×10^{1}	0
$\frac{\partial^2\Psi}{\partial Y^2}$	0	-0.133×10^{3}	-0.109×10^{3}	0
$(\frac{\partial^2\Psi}{\partial Y^2})^2$	0	0.177×10^{5}	0.119×10^{5}	0
ϕ	0.298×10^{1}	0.314×10^{1}	0.883×10^{0}	0
$\frac{\partial\phi}{\partial Y}$	0	-0.900×10^{1}	-0.220×10^{2}	-0.600×10^{1}
ϕ^2	0.886×10^{1}	0.987×10^{1}	0.779×10^{0}	0
$\frac{\partial(\phi^2)}{\partial X}$	-0.886×10^{1}	-0.600×10^{1}	0.500×10^{1}	0.700×10^{0}
$\frac{\partial(\phi^2)}{\partial Y}$	0	-0.428×10^{2}	-0.280×10^{2}	0
$\frac{\partial^2(\phi^2)}{\partial Y^2}$	0.288×10^{4}	-0.249×10^{4}	0.144×10^{4}	0.100×10^{3}
ϕ^3	0.264×10^{2}	0.310×10^{2}	0.688×10^{0}	0
L	0.720×10^{-2}	0.745×10^{-2}	0.725×10^{-2}	0.719×10^{-2}
$\frac{\partial L}{\partial Y}$	0	0.309×10^{-3}	-0.154×10^{-2}	0

STAGE 3 : DERIVED RESULTS

TABLE 11

	1	2	3	4
ψ	0	0.200×10^{1}	0.268×10^{1}	0.290×10^{1}
$\frac{\partial\psi}{\partial X}$	0	-0.271×10^{0}	0.603×10^{0}	0.110×10^{1}
$\frac{\partial\psi}{\partial Y}$	0.200×10^{2}	0.134×10^{2}	0.450×10^{1}	0
$\frac{\partial^2\psi}{\partial Y^2}$	0	-0.103×10^{3}	-0.700×10^{2}	0
$(\frac{\partial^2\psi}{\partial Y^2})^2$	0	0.106×10^{5}	0.490×10^{4}	0
ϕ	0.305×10^{1}	0.302×10^{1}	0.916×10^{0}	0
$\frac{\partial\phi}{\partial Y}$	0	-0.155×10^{2}	-0.143×10^{2}	-0.667×10^{1}
ϕ^2	0.928×10^{1}	0.910×10^{1}	0.839×10^{0}	0
$\frac{\partial(\phi^2)}{\partial X}$	-0.773×10^{1}	-0.200×10^{1}	0.350×10^{1}	0.100×10^{1}
$\frac{\partial(\phi^2)}{\partial Y}$	0	-0.109×10^{3}	-0.290×10^{2}	0
$\frac{\partial^2(\phi^2)}{\partial Y^2}$	0.160×10^{4}	-0.280×10^{4}	0.800×10^{3}	0.500×10^{2}
ϕ^3	0.283×10^{2}	0.274×10^{2}	0.768×10^{0}	0
L	0.985×10^{-2}	0.104×10^{-1}	0.104×10^{-1}	0.104×10^{-1}
$\frac{\partial L}{\partial Y}$	0	0.252×10^{-2}	-0.900×10^{-4}	0

STAGE 1 : DERIVED RESULTS

TABLE 12

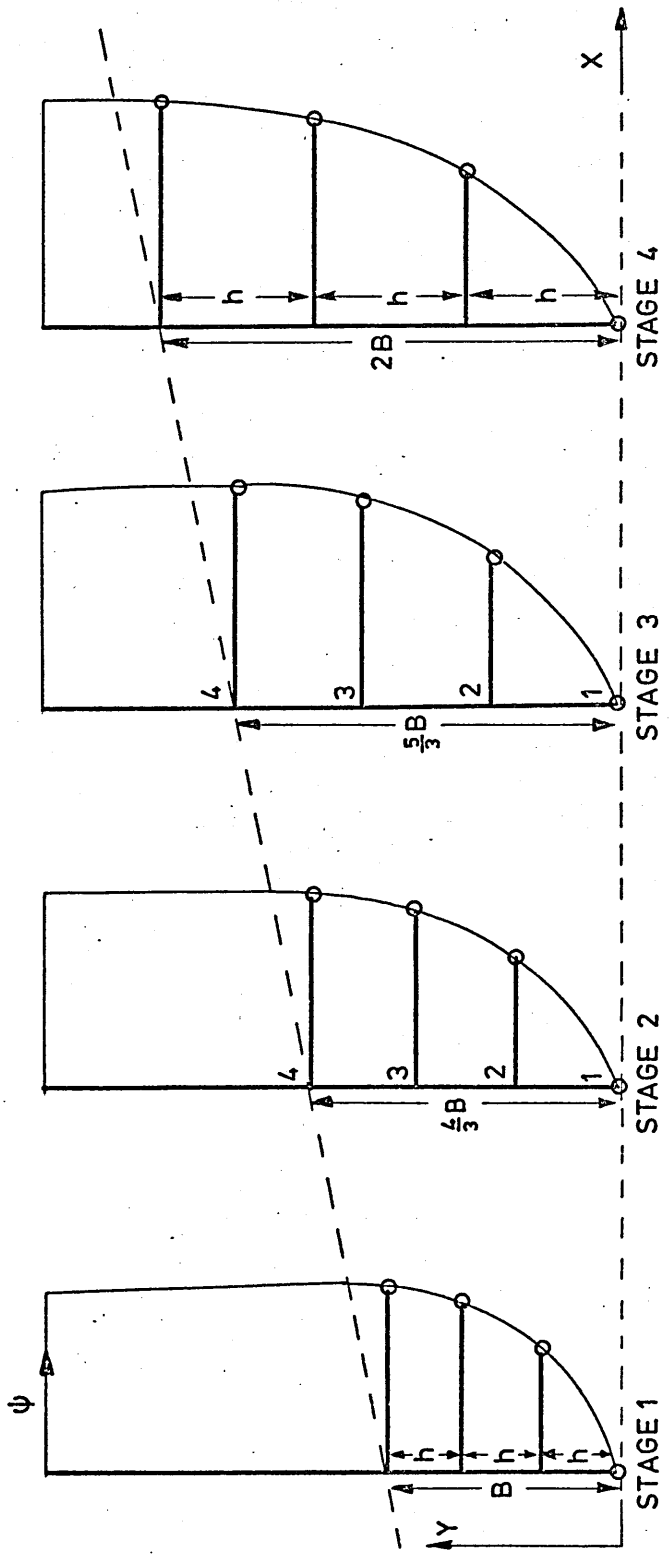

The Streamwise Development Of The Ψ-profile.

Figure 46

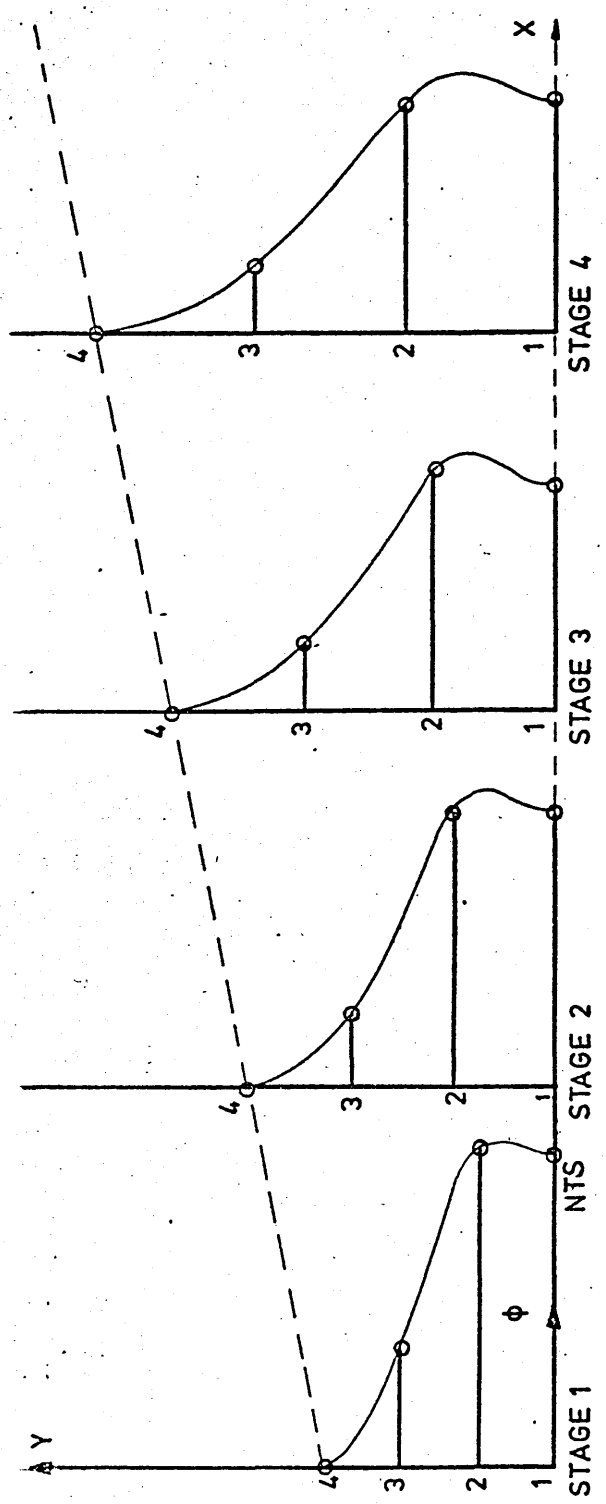

The Streamwise Development Of The φ-profiles.

Figure 47

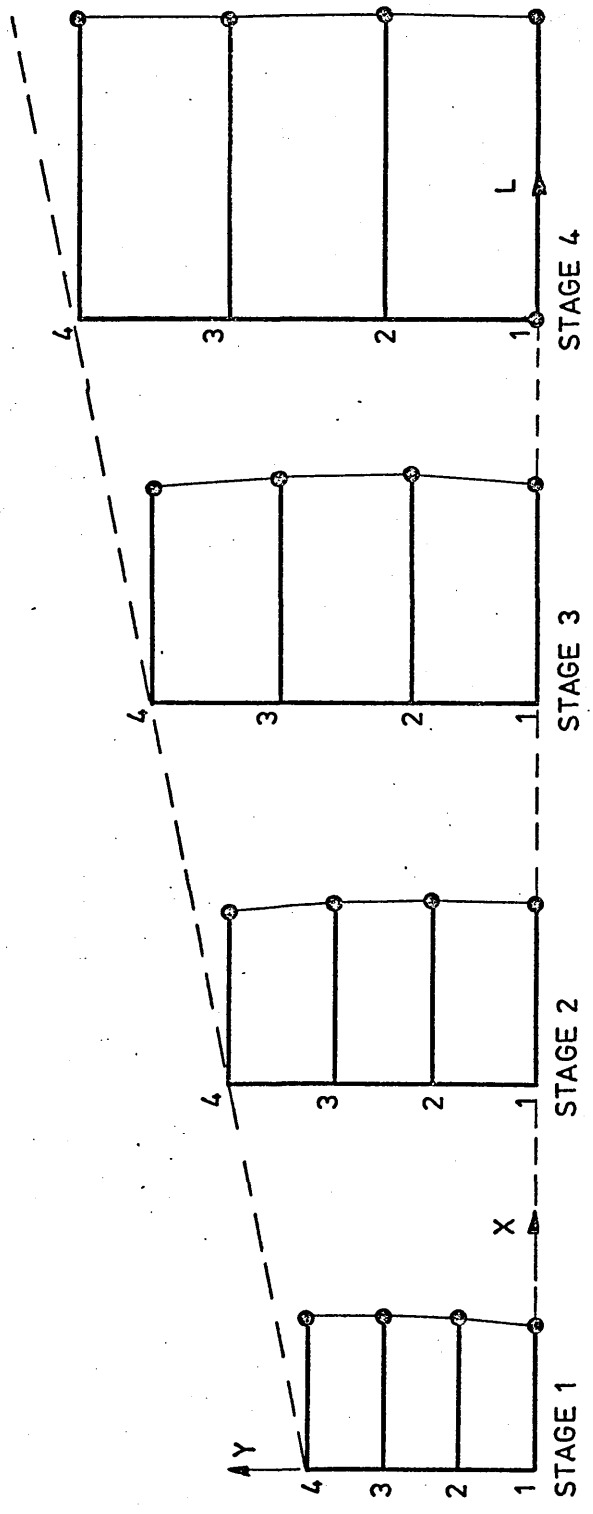

Figure 48

The Streamwise Development Of The L-profiles.

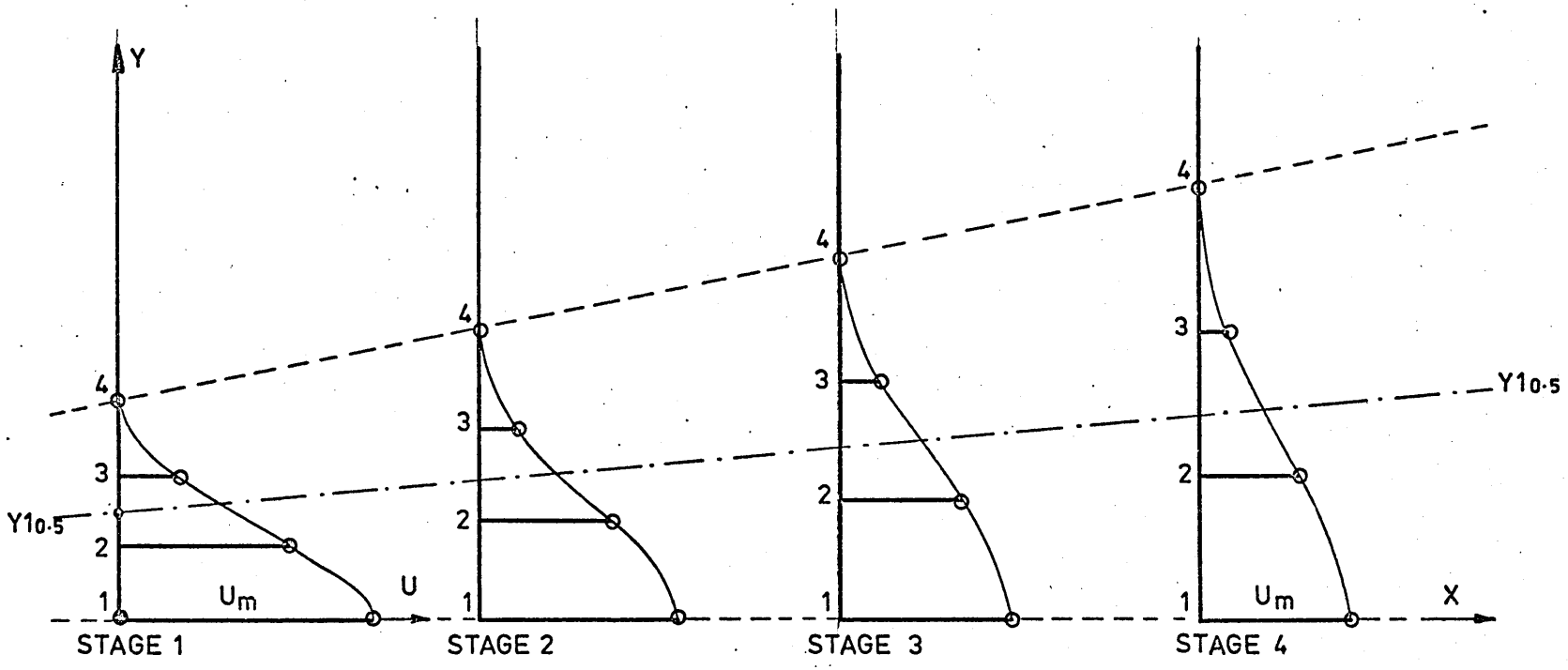

Figure 49

The Streamwise Development Of The U-profiles.

X	U_m	$Y_{0.5}$	$\frac{10^4}{U_m^2}$
0.0	34.304	0.069	8.498
0.8	27.133	0.090	13.585
1.0	24.207	0.113	17.065
1.2	20.006	0.133	24.985

RESULTS FOR THE JET SPREAD AND THE DECAY OF THE CENTRE-LINE VELOCITY

TABLE 13

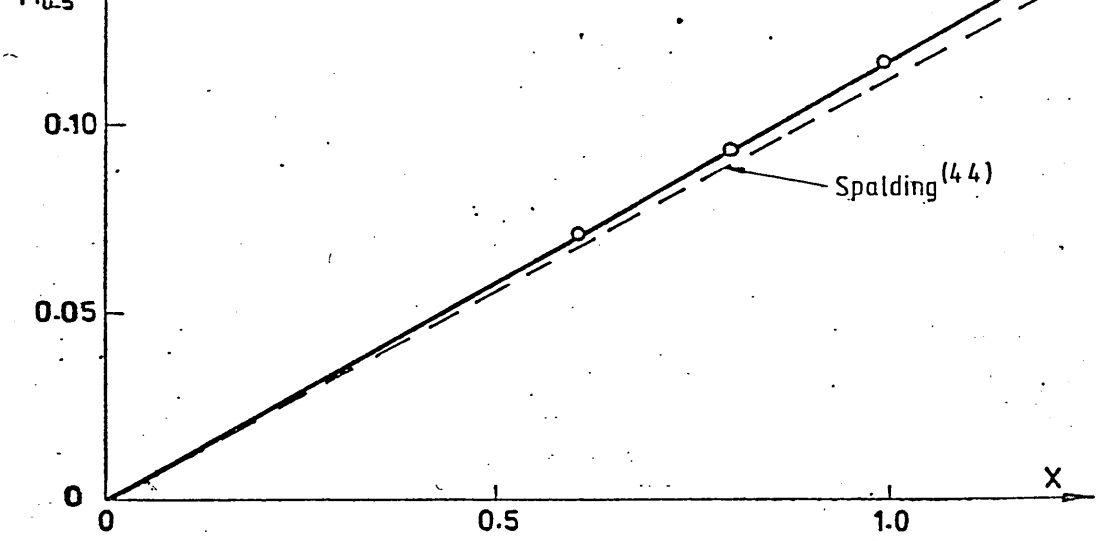

a) $y_{0.5}$ vs X : The Jet Spread

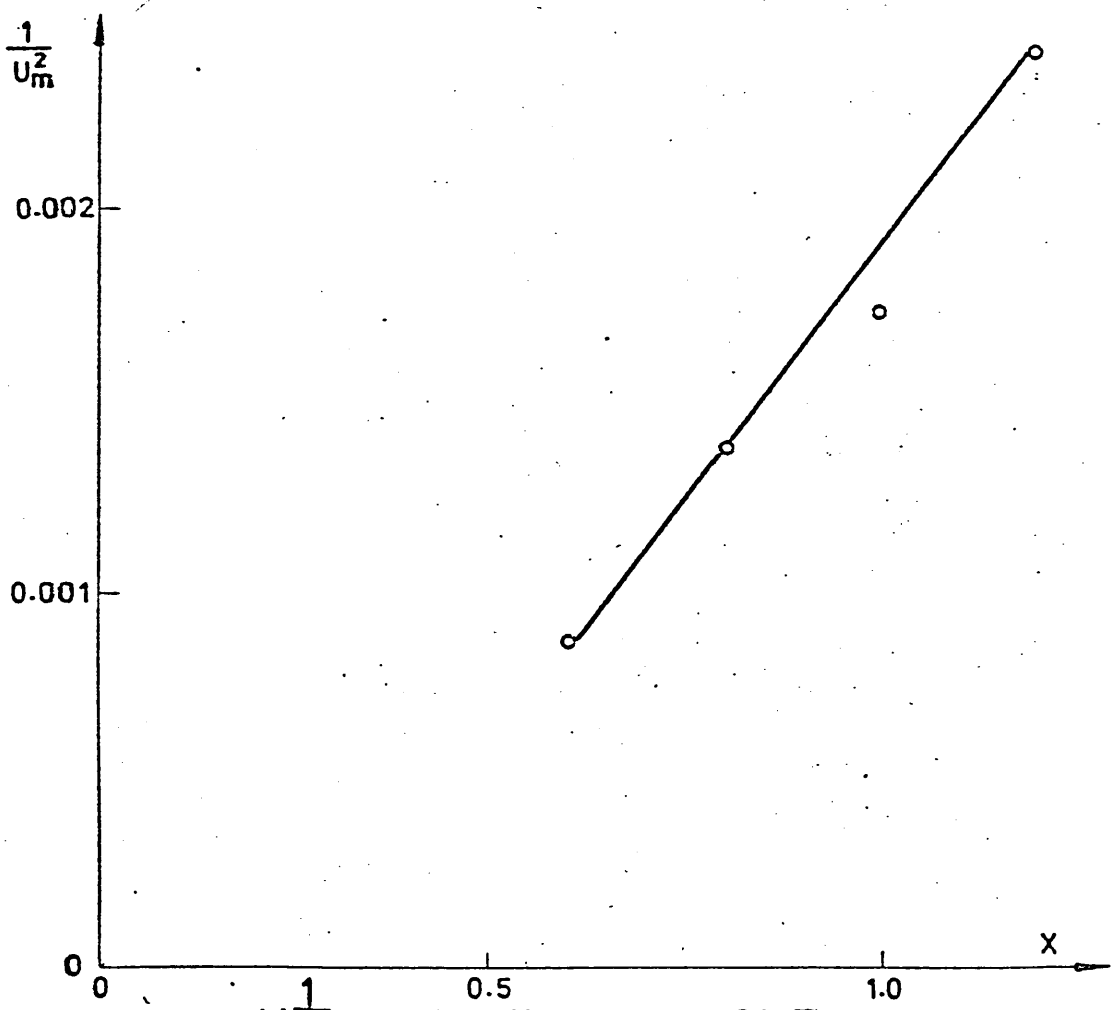

b) $\frac{1}{U_m^2}$ vs X : The Decay Of The Centre-line Velocity

Figure 50

With reference to the notational system denoted in Figure (51.a), if;

$$\frac{Y_3}{b_I} = \frac{Y_1}{b_{II}} \qquad \ldots\ldots\ldots (7.3)$$

then; $$\frac{\Psi_I}{U_{mI} b_I} = \frac{\Psi_{III}}{U_{mII} b_{II}} \qquad \ldots\ldots\ldots (7.4)$$

If; $$\frac{Y_3}{b_3} = \frac{Y_2}{b_2} \qquad \ldots\ldots\ldots (7.5)$$

then; $$\frac{\Psi_{II}}{U_{mII} b_{II}} - \frac{\Psi_{II2}}{U_{mII} b_{II}} \qquad \ldots\ldots\ldots (7.6)$$

Since; $$b \propto X \qquad \ldots\ldots\ldots (7.7)$$

and $$\bar{U}_m^2 \propto X \qquad \ldots\ldots\ldots (7.8)$$

then; $$\left(\frac{b_{II}}{b_I}\right)^{\frac{1}{2}} = \frac{U_{mI}}{U_{mII}} \qquad \ldots\ldots\ldots (7.9)$$

and $$\left(\frac{b_{II}}{b_{III}}\right)^{\frac{1}{2}} = \frac{U_{mIII}}{U_{mII}} \qquad \ldots\ldots\ldots (7.10)$$

Thus; $$\Psi_I = \left(\frac{b_{II}}{b_I}\right)^{\frac{1}{2}} \left(\frac{b_I}{b_{II}}\right) \Psi_{III} \qquad \ldots\ldots\ldots (7.11)$$

$$= \left(\frac{b_I}{b_{II}}\right)^{\frac{1}{2}} \Psi_{III} \qquad \ldots\ldots\ldots (7.12)$$

$$\Psi_{II} = \left(\frac{b_{III}}{b_{II}}\right)^{\frac{1}{2}} \Psi_{II2} \qquad \ldots\ldots\ldots (7.13)$$

and $$\frac{\Psi_{III} - \Psi_I}{\delta X} = \left(\frac{b_{III}}{b_{II}}\right)^{\frac{1}{2}} \frac{\Psi_{II2}}{\delta X} - \left(\frac{b_I}{b_{II}}\right)^{\frac{1}{2}} \frac{\Psi_{III}}{\delta X} \qquad \ldots\ldots\ldots (7.14)$$

Since; $$b_I = b_{II} - \frac{\delta Y}{2} \qquad \ldots\ldots\ldots (7.15)$$

$$b_{III} = b_{II} + \frac{\delta Y}{2} \qquad \ldots\ldots\ldots (7.16)$$

and $$\delta X = M \delta Y \qquad \ldots\ldots\ldots (7.17)$$

then; $$\frac{\Psi_{III} - \Psi_I}{\delta X} = \left(\frac{Y_3}{Y_2}\right)^{\frac{1}{2}} \frac{\Psi_{II2}}{M \delta Y} - \left(\frac{Y_3}{Y_1}\right)^{\frac{1}{2}} \frac{\Psi_{III}}{M \delta Y} \qquad \ldots\ldots\ldots (7.18)$$

where, $$Y_1 = \frac{b_{II}}{(b_{II} - \delta Y/2)} \cdot Y_3 \qquad \ldots\ldots\ldots (7.19)$$

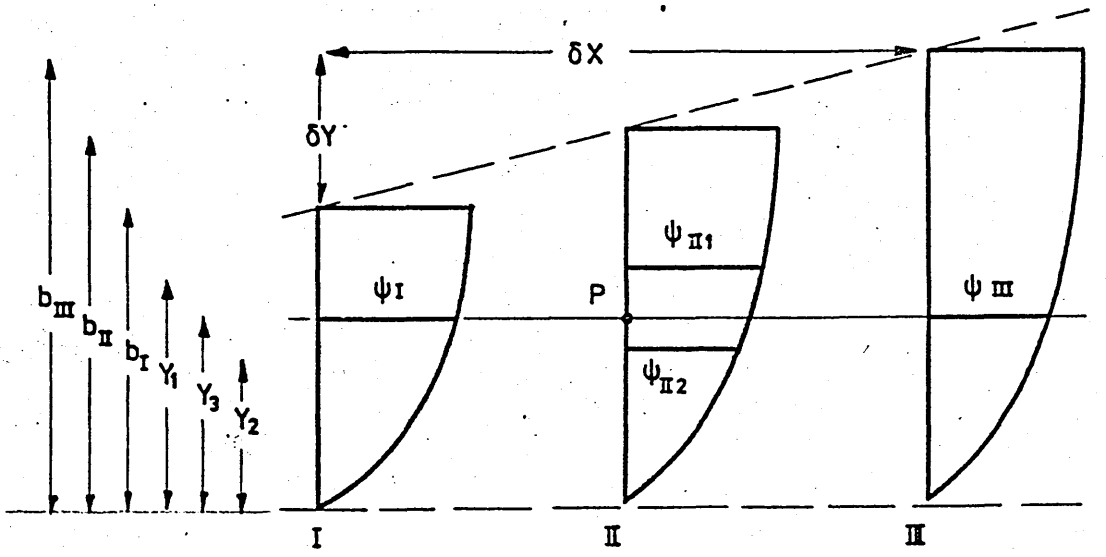

a) Discrete Representation Of $\psi_{,x}$

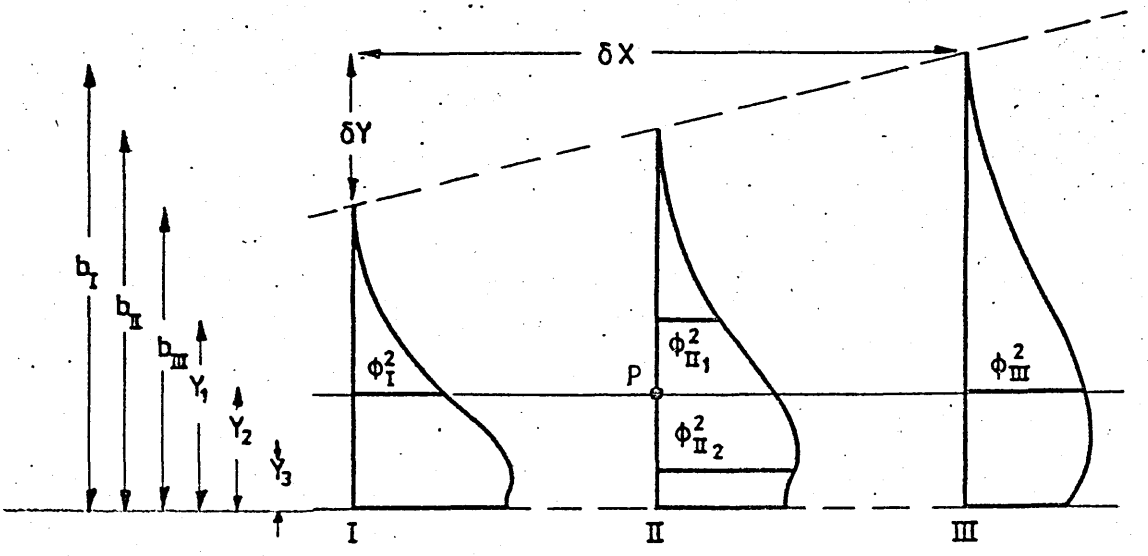

b) Discrete Representation Of $(\phi^2)_{,x}$

Figure 51

and $$Y_2 = \frac{}{(b_{II} + \delta Y/2)} \cdot Y_3 \qquad \ldots\ldots\ldots (7.20)$$

and 'Y_3' is the co-ordinate of 'p', the point on the section at which the gradient with respect to 'X' is being measured. The partial derivative was obtained by fitting a curve to the ψ-profile to obtain values of 'ψ' corresponding to 'Y_1' and 'Y_2', and substituting into equation (7.18). The value of 'δY' was decreased until the partial derivative converged to a constant. The curve was of the standard-error-type, this being chosen because of the close correlation between the normal distribution curve and the velocity profile[2]. The curve was accurate over the portion of the profile being considered. A similar approach was used to obtain the partial derivative of 'ϕ^2' with respect to 'X', a quantity required in the calculations for the energy balance. The final equation, using the notation of Figure (51.b), took the form ;

$$\frac{\partial(\phi^2)}{\partial X} \simeq \frac{\phi^2_{III} - \phi^2_{I}}{\delta X} \qquad \ldots\ldots\ldots (7.21)$$

$$= \frac{Y_2}{Y_3}\frac{\phi^2_{II2}}{M\delta Y} - \frac{Y_1}{Y_3}\frac{\phi^2_{III}}{M\delta X} \qquad \ldots\ldots\ldots (7.22)$$

The values of 'ϕ^2_{II2}' and 'ϕ^2_{III}' were found graphically.

The Reynolds stresses and the components of the energy balance were calculated on the following basis ;

$$\overline{uv} \quad : -C_\mu \phi L \frac{\partial^2 \psi}{\partial Y^2} \qquad \ldots\ldots\ldots (7.23)$$

$$\text{convection} \quad : -\left(\frac{\partial \psi}{\partial Y}\frac{\partial(\phi^2)}{\partial X} - \frac{\partial \psi}{\partial X}\frac{\partial(\phi^2)}{\partial Y}\right) \qquad \ldots\ldots\ldots (7.24)$$

$$\text{production} \quad : C_\mu \phi L \left(\frac{\partial^2 \psi}{\partial Y^2}\right)^2 \qquad \ldots\ldots\ldots (7.25)$$

$$\text{diffusion} \quad : \frac{C_\mu}{\sigma_k}\left(\frac{\partial \phi}{\partial Y} L \frac{\partial(\phi^2)}{\partial Y} + \phi \frac{\partial L}{\partial Y}\frac{(\phi^2)}{\partial Y} + \phi L \frac{\partial^2(\phi^2)}{\partial Y^2}\right) \qquad (7.26)$$

$$\text{dissipation} \quad : -C_D \frac{\phi^3}{L} \qquad \ldots\ldots\ldots (7.27)$$

Partial derivatives were determined graphically from the 'ψ', 'ϕ' and 'L' profiles where necessary. The overall results are listed in Tables (14) to (17) and are illustrated in Figures (52) to (55).

	1	2	3	4
$\frac{Y}{b}$	0	0.333	0.667	1
$\frac{Y}{Y\|_{0.5}}$	0	0.727	0.146×10^{1}	0.218×10^{1}
$\frac{\psi}{Y\|_{0.5}U_m}$	0	0.333	0.448	0.486
$\frac{U}{U_m}$	1	0.671	0.228	0
$\frac{V}{U_m}$	0	0.151×10^{-1}	0.315×10^{-1}	-0.636×10^{-1}
$\frac{\phi}{U_m}$	0.129	0.143	0.440×10^{-1}	0
$\frac{L}{b}$	0.306×10^{-1}	0.333×10^{-1}	0.335×10^{-1}	0.336×10^{-1}
$\frac{\overline{uv}}{U_m^2}$	0	0.803×10^{-2}	0.213×10^{-2}	0
$\frac{Y\|_{0.5}Pn}{U_m^3}$	0	0.622×10^{-2}	0.142×10^{-2}	0
$\frac{Y\|_{0.5}Cn}{U_m^3}$	0.192×10^{-2}	0.139×10^{-2}	-0.650×10^{-3}	0
$\frac{Y\|_{0.5}Df}{U_m^3}$	0.105×10^{-2}	-0.600×10^{-3}	0.380×10^{-3}	0
$\frac{Y\|_{0.5}Dp}{U_m^3}$	-0.291×10^{-2}	-0.367×10^{-2}	-0.110×10^{-3}	0

Pn :- production
Cn - convection
Df - diffusion
Dp - dissipation

STAGE 1 : NON-DIMENSIONALISED RESULTS

TABLE 14

	1	2	3	4
$\frac{Y}{b}$	0	0.333	0.667	1
$\frac{Y}{Y\|_{0.5}}$	0	0.741	0.148×10^{1}	0.222×10^{1}
$\frac{\psi}{Y\|_{0.5}U_m}$	0	0.333	0.444	0.481
$\frac{U}{U_m}$	1	0.667	0.222	0
$\frac{V}{U_m}$	0	0.168	-0.210×10^{-1}	-0.819×10^{-1}
$\frac{\phi}{U_m}$	0.135	0.133	0.037	0
$\frac{L}{b}$	0.299×10^{-1}	0.304×10^{-1}	0.295×10^{-1}	0.292×10^{-1}
$\frac{\overline{uv}}{U_m^2}$	0	0.581×10^{-2}	0.118×10^{-2}	0
$\frac{Y\|_{0.5}Pn}{U_m^3}$	0	0.374×10^{-2}	0.580×10^{-3}	0
$\frac{Y\|_{0.5}Cn}{U_m^3}$	0.205×10^{-2}	0.750×10^{-3}	-0.510×10^{-3}	0
$\frac{Y\|_{0.5}Df}{U_m^3}$	0.360×10^{-3}	-0.390×10^{-3}	0.210×10^{-3}	0
$\frac{Y\|_{0.5}Dp}{U_m^3}$	-0.334×10^{-2}	-0.316×10^{-2}	-0.700×10^{-4}	0

Pn – production
Cn – convection
Df – diffusion
Dp – dissipation

STAGE 2 : NON-DIMENSIONALISED RESULTS

TABLE 15

	1	2	3	4
$\frac{Y}{b}$	0	0.333	0.667	1
$\frac{Y}{Y\|_{0.5}}$	0	0.741	0.148×10^{1}	0.222×10^{1}
$\frac{\Psi}{Y_{0.5}U_m}$	0	0.333	0.445	0.483
$\frac{U}{U_m}$	1	0.668	0.224	0
$\frac{V}{U_m}$	0	0.136×10^{-1}	-0.236×10^{-1}	-0.547×10^{-1}
$\frac{\phi}{U_m}$	0.123	0.130	0.360×10^{-1}	0
$\frac{L}{b}$	0.288×10^{-1}	0.298×10^{-1}	0.290×10^{-1}	0.288×10^{-1}
$\frac{\overline{uv}}{U_m^2}$	0	0.531×10^{-2}	0.119×10^{-2}	0
$\frac{Y\|_{0.5}Pn}{U_m^3}$	0	0.330×10^{-2}	0.610×10^{-3}	0
$\frac{Y\|_{0.5}Cn}{U_m^3}$	0.171×10^{-2}	0.880×10^{-3}	-0.340×10^{-3}	0
$\frac{Y\|_{0.5}Df}{U_m^3}$	0.490×10^{-3}	-0.440×10^{-3}	0.110×10^{-3}	0
$\frac{Y\|_{0.5}Dp}{U_m^3}$	-0.263×10^{-2}	-0.298×10^{-2}	-0.700×10^{-4}	0

Pn - production
Cn - convection
Df - diffusion
Dp - dissipation

STAGE 3 : NON-DIMENSIONALISED RESULTS

TABLE 16

	1	2	3	4
$\frac{Y}{b}$	0	0.333	0.667	1
$\frac{Y}{Y\|_{0.5}}$	0	0.755	0.151×10^{1}	0.226×10^{1}
$\frac{\psi}{Y_{0.5}U_m}$	0	0.333	0.446	0.483
$\frac{U}{U_m}$	1	0.669	0.225	0
$\frac{V}{U_m}$	0	0.135×10^{-1}	-0.754×10^{-1}	-0.113
$\frac{\phi}{U_m}$	0.152	0.151	0.460×10^{-1}	0
$\frac{L}{b}$	0.328×10^{-1}	0.345×10^{-1}	0.345×10^{-1}	0.345×10^{-1}
$\frac{\overline{uv}}{U_m^2}$	0	0.800×10^{-2}	0.170×10^{-2}	0
$\frac{Y\|_{0.5}Pn}{U_m^3}$	0	0.550×10^{-2}	0.770×10^{-3}	0
$\frac{Y\|_{0.5}Cn}{U_m^3}$	0.257×10^{-2}	0.950×10^{-3}	0.550×10^{-3}	0
$\frac{Y\|_{0.5}Df}{U_m^3}$	0.800×10^{-3}	-0.112×10^{-2}	0.200×10^{-3}	0
$\frac{Y\|_{0.5}Dp}{U_m^3}$	-0.429×10^{-2}	-0.396×10^{-2}	-0.110×10^{-3}	0

Pn - production
Cn - convection
Df - diffusion
Dp - dissipation

STAGE 4 : NON-DIMENSIONALISED RESULTS

TABLE 17

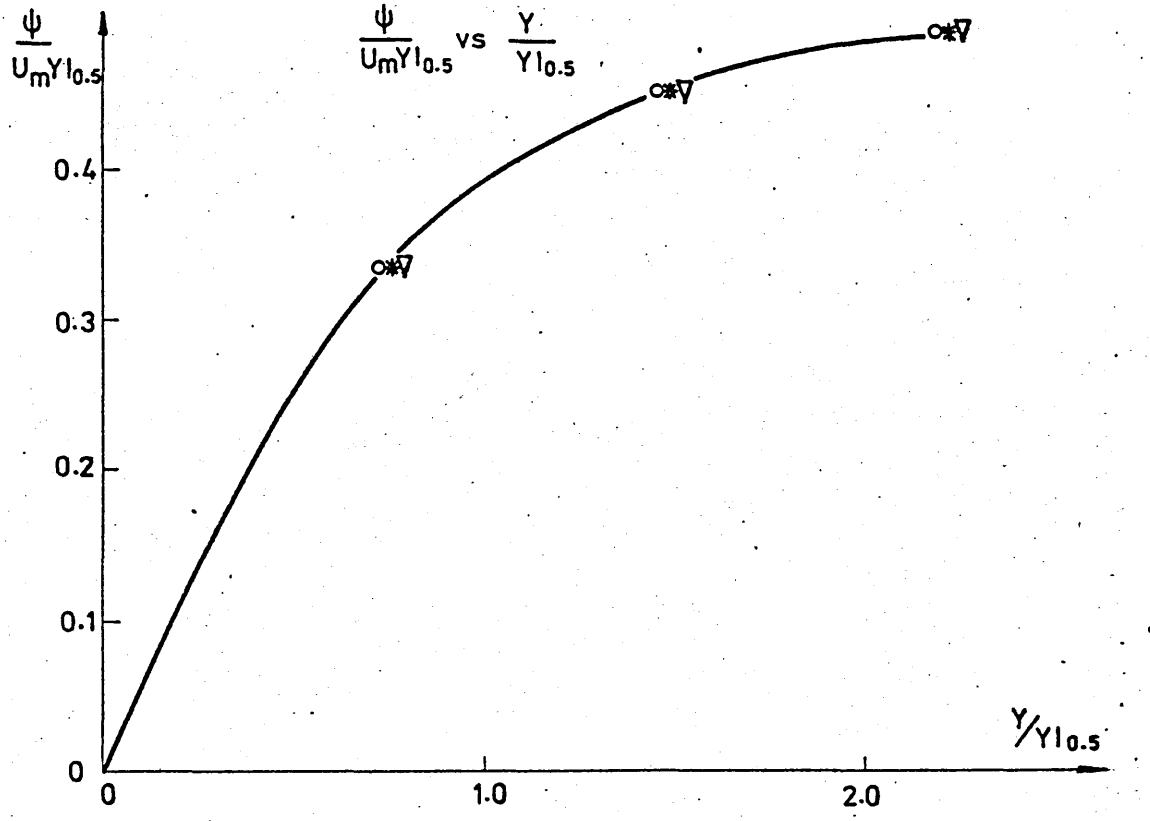

a) ψ - profiles

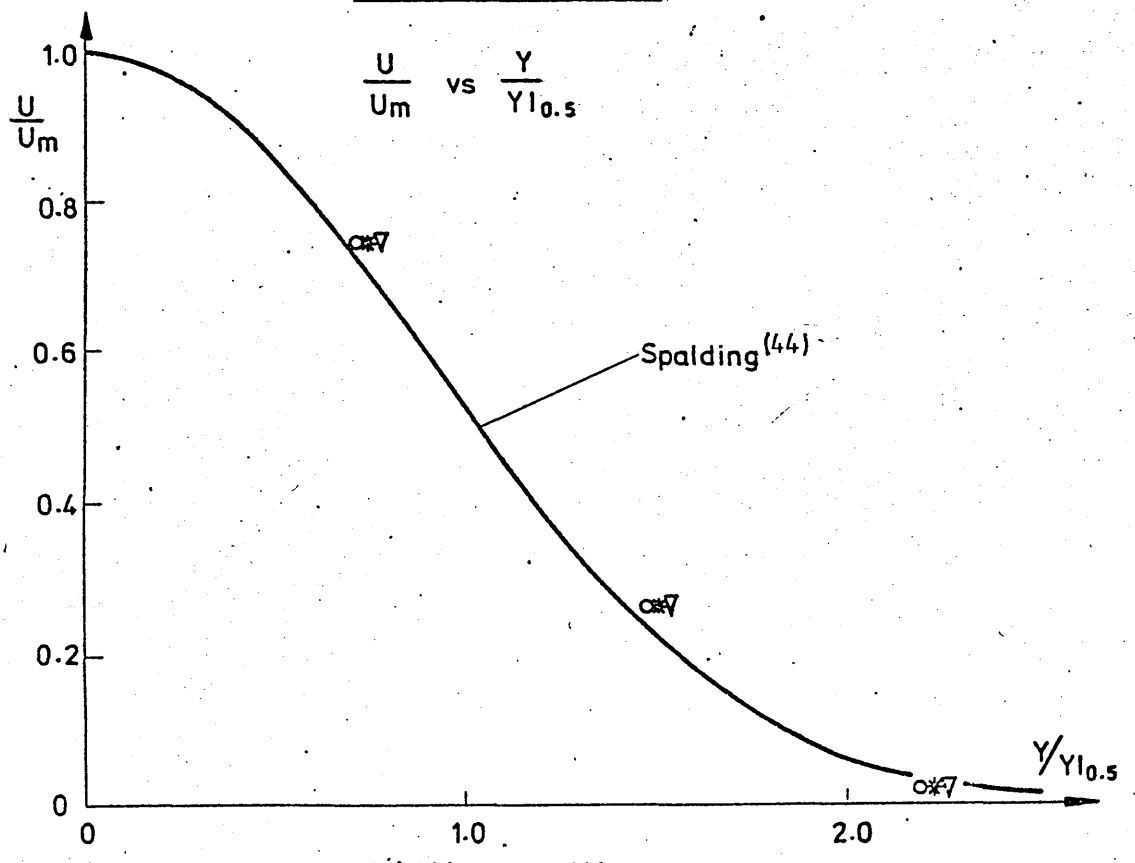

b) U - profiles

Figure 52

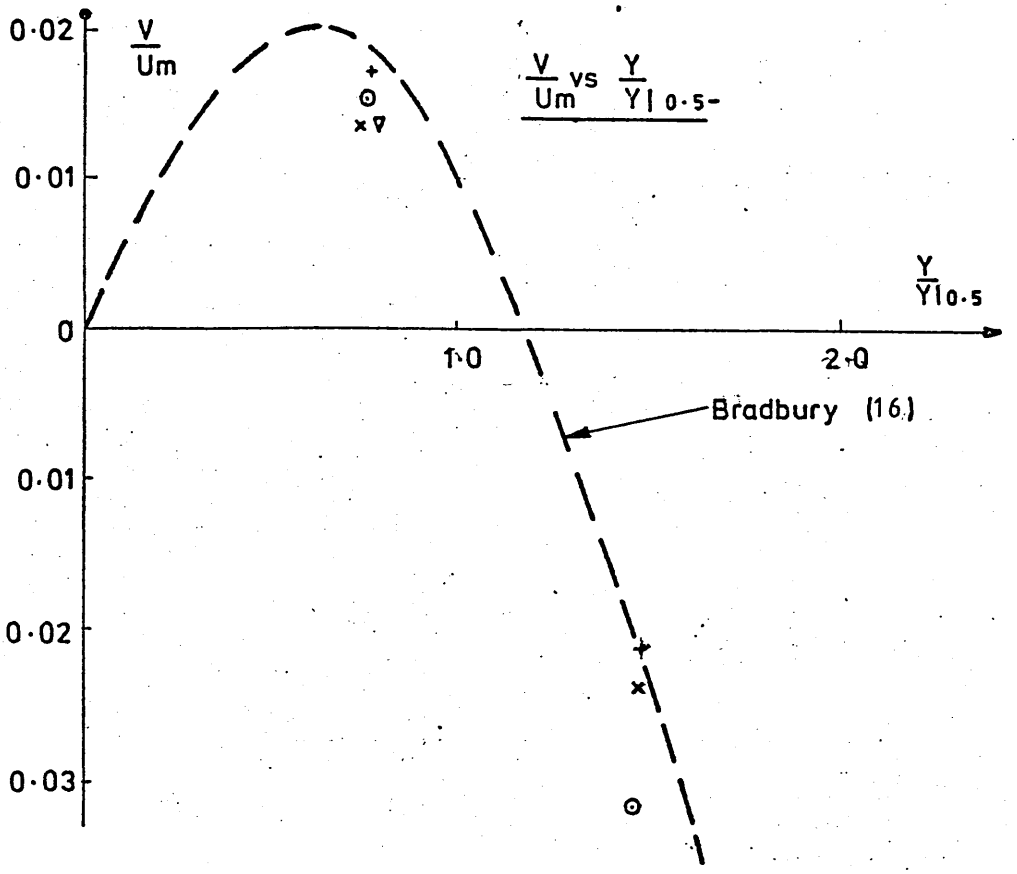

a) Transverse Velocity Profile.

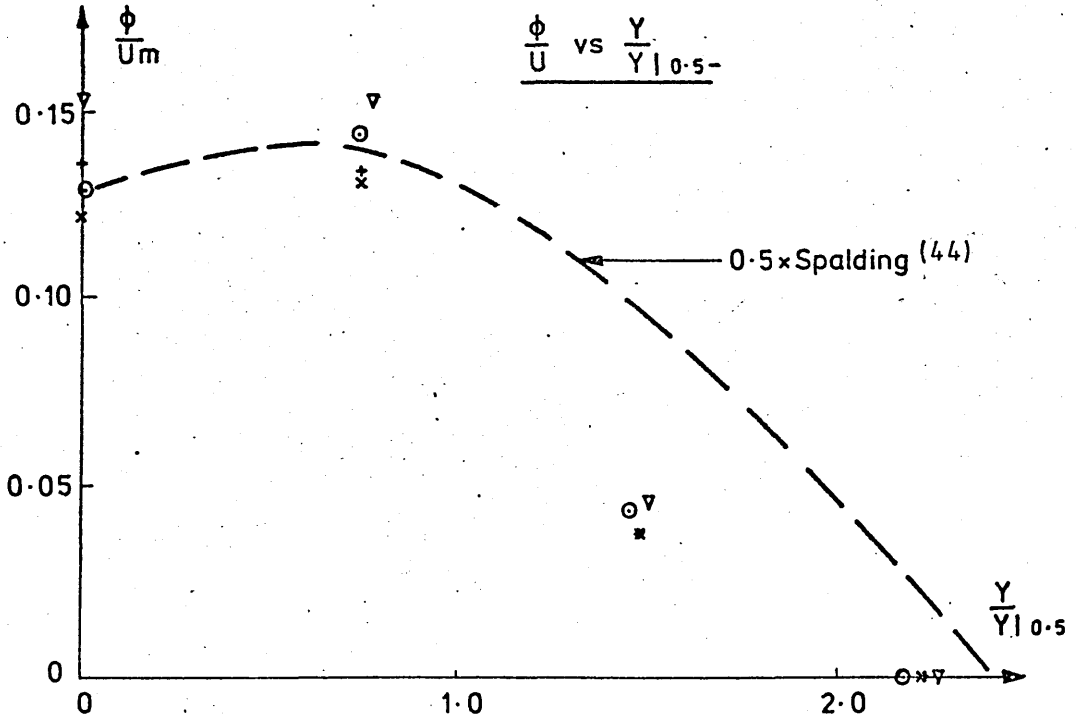

b) φ - profile.

Figure 53

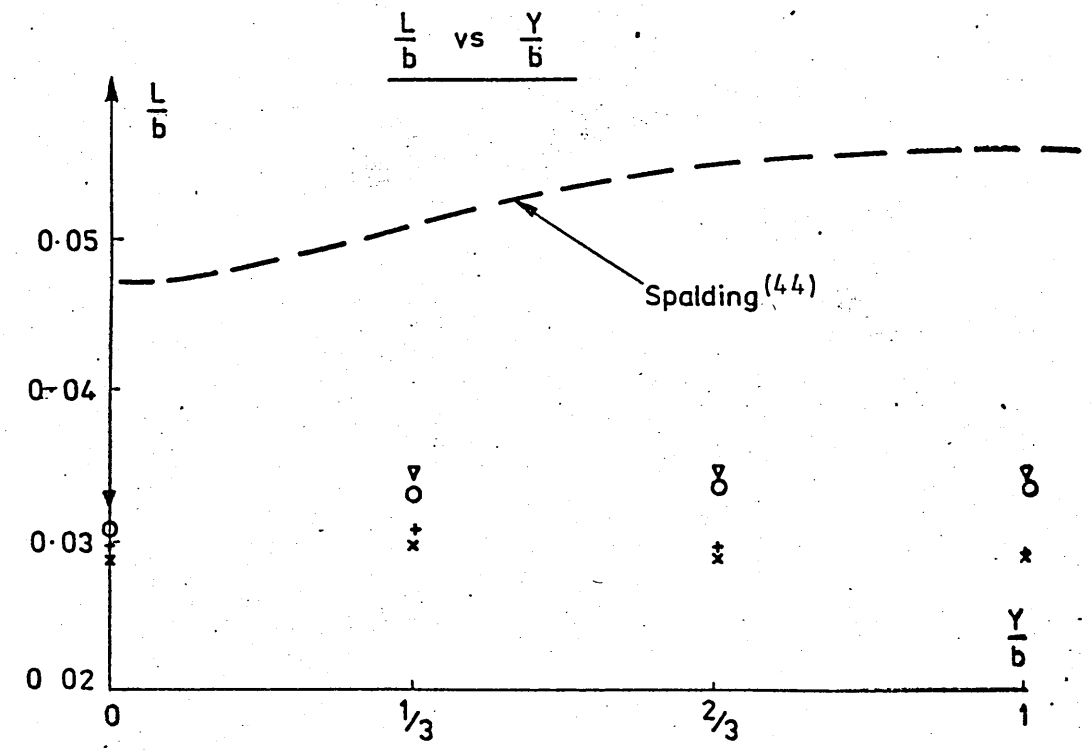

a) L-profile.

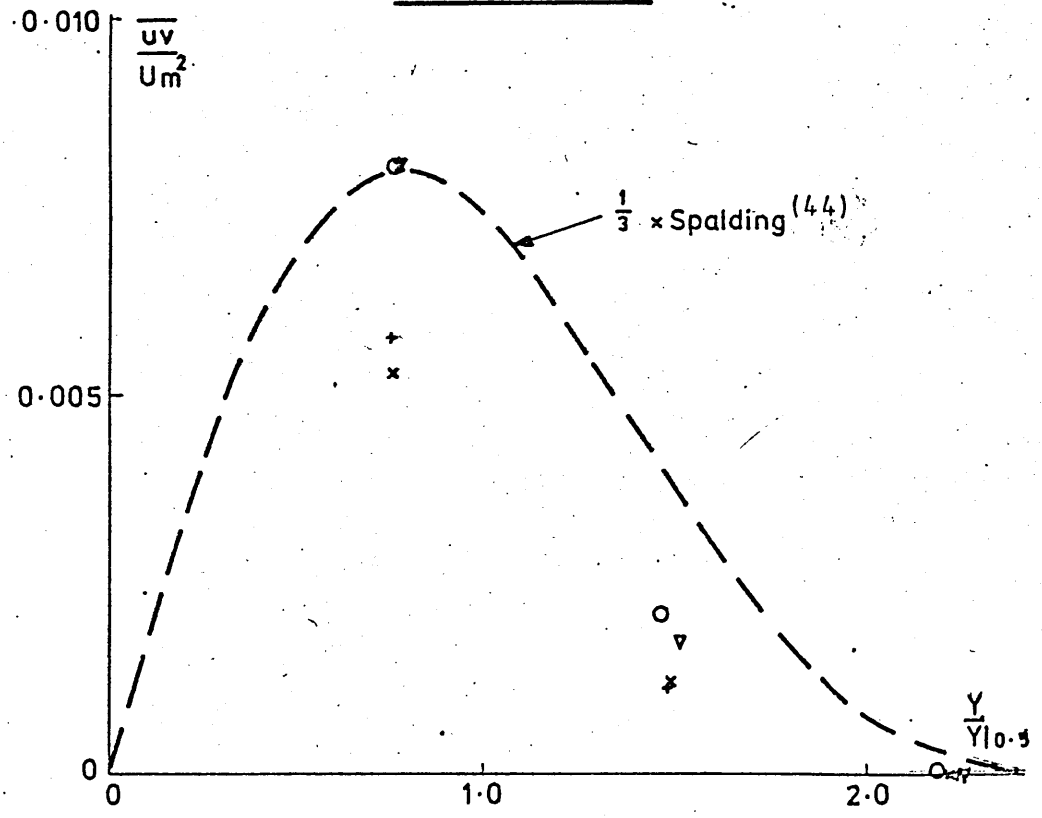

b) $\overline{uv}$ -profile.

Figure 54.

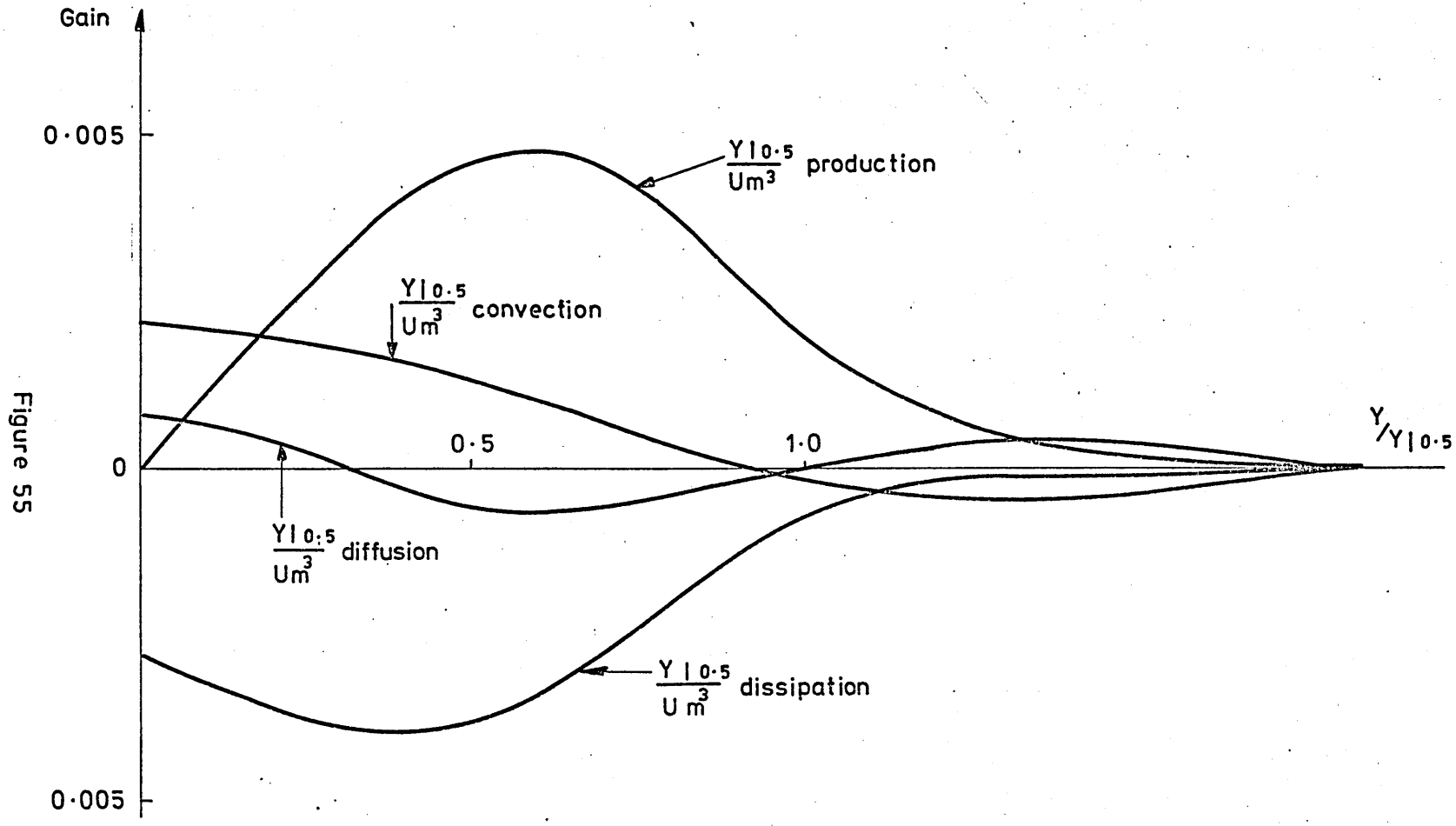

Figure 55

The Energy Balance

7.4 Résumé of Results

In the early calculations, prior to the adoption of the two-stage procedure, it became evident that as the number of equations increased, there was a growing tendency towards instability in the results. The results obtained from the solution of a small number of equations (eg; eight equations obtained through the final co-ordinate transformation of the two-stage procedure), however, were not found to exhibit this phenomenon.

The profiles of 'ψ', 'ϕ' and 'L' at various locations in the flow obtained by the latter approach are all of an acceptable form. Furthermore, their development downstream displays the trends that one would expect them to follow, in that the maximum value of the stream function, 'ψ_m' increases, '$\psi_{m,Y}$' decreases, 'ϕ' decreases and 'L' increases. In magnitude the values of 'ψ', 'U' and 'V' agree closely with results from other studies[16][44], as do the spread of the jet and the decay of the centre-line velocity. Those for both 'ϕ' and 'L' are about half the corresponding values obtained in other studies. Since these parameters have a considerable influence on, and in some cases dominate, the terms making up the Reynolds stresses and the components of the energy balance, their values are accordingly much lower than those with which they were compared.

Numerical integration of the various terms yields the results ;

$$(Y|_{0.5}/U_m^2)_0\int^{\infty} \text{production} = 3.63\times10^{-3} \quad \ldots\ldots \quad (7.28)$$

$$(Y|_{0.5}/U_m^2)_0\int^{\infty} \text{dissipation} = -3.05\times10^{-3} \quad \ldots\ldots \quad (7.29)$$

$$(Y|_{0.5}/U_m^2)_0\int^{\infty} \text{convection} = 0.96\times10^{-3} \quad \ldots\ldots \quad (7.30)$$

$$(Y|_{0.5}/U_m^2)_0\int^{\infty} \text{diffusion} = 0.13\times10^{-3} \quad \ldots\ldots \quad (7.31)$$

The production and dissipation terms may be seen to be the most significant terms in the energy balance. Although the production and the convection terms are not balanced by the dissipation, (a consequence of its too rapid approach towards zero at the outer

regions of the jet) nor is there a zero net diffusion of turbulent energy across the flow, the integral value of the convection term is about 26% of that of the production term (which compares well with Bradbury's 22%) and the diffusion is relatively small.

7.5 Discussion of Results

The results of the preceding section raise two questions. First, is the cause of the trend towards instability in the results as the number of equations increases, the result of an inherent instability in the method of setting up the equations, or is it due to the inability of the non-linear solution routine to solve them as they become increasingly complex. Secondly, for what reason are the results, which clearly demonstrate qualitatively the main features of the flow, not altogether satisfactory in some respects from a quantitative point of view. Before coming to a conclusion concerning the first question the following factors should be considered.

First, the procedure starts with initial conditions which are represented by linear profiles. The profiles develop through successive downstream translations brought about by the co-ordinate transformation routine. The trend reflected by the results of the two-stage procedure is towards increasingly realistic profiles as illustrated in Figures (43) to (45). This trend would be contradicted by the existence of numerical instability due to a progressive error, or as a result of an accumulation of errors.

Second, even when the grid size is altered, a process which often reveals numerical instability in a method, the results are of a consistent form.

Third, the equations become increasingly complex, a fact that may be appreciated from a consideration of the size of the matrices of coefficients involved at the third downstream step. The dimensions of the linear, quadratic, cubic and quartic matrices are (12,8), (12,14), (12,56) and (12,75) respectively. One equation is discarded to leave the routine to solve for eleven variables.

Finally, Powell[73] describes an example of a non-linear system for which the classical iteration scheme converges to a point which is not the solution of the equations. The example is the system;

$$f_1(X) = x_1 = 0 \qquad \ldots\ldots\ (7.32)$$

$$f_2(X) = 10x_1/(x_1 + 0.1) + 2x_2^2 \qquad \ldots\ldots\ (7.33)$$

The classical iteration converges to the point (1.8016, 0.0000). Since the system is two-dimensional, $F(x_1, x_2)$ may be visualised as the surface ;

$$x_3 = F(x_1, x_2) \qquad \ldots\ldots\ (7.34)$$

The shape of the surface in the rectangle ;

$$1 \leqslant x_1 \leqslant 3 \qquad \ldots\ldots\ (7.35)$$

$$|x_2| \leqslant 1 \qquad \ldots\ldots\ (7.36)$$

is that of a trough which slopes very gradually towards the solution of the equations. Powell has shown that the solution proceeds along a direction which tends to be across the trough, so that the total displacement down the trough is limited to such a small value that the process converges prematurely. Although Powell's routine represents a considerable improvement over the classical iteration, when applied to this problem (with the initial estimate (3,1)) it required sixty evaluations of the functions to reduce the sum of the squares of the residuals to the value of 1.45×10^{-8}, the corresponding values of the variables being (-0.000072, 0.060228). The sequence of points '$X^{(k)}$' leading to this solution was very erratic. It may be argued that even if this example is not directly analagous to the present situation, it does at least demonstrate that there are certain situations in which the solution routine will converge to a point other than the solution of the equations.

Given these factors it would seem not unreasonable to argue that the method of setting up the equations is, in itself, valid but that in their present form the equations are not suitable to solution by the routine. One criticism of the solution routine made by Powell[73] was the desirability of choosing the scale of the components of 'X' so that their magnitudes are similar, since the

algorithm makes frequent use of the Euclidean lengths of vectors. The equations were scaled accordingly, but although the iteration was found to converge more rapidly, similar results were obtained. However, it might reasonably be inferred that the equations are in fact of the correct form but as they become increasingly complex, require a more sophisticated mathematical treatment for their solution.

The point concerning the magnitude of the results, which are qualitatively convincing, should be considered with reference to a more detailed appraisal of the constants appearing in the equations. The constants are not inherent in the equations (as may be seen from the momentum equation (3.17) and the k-equation (3.42), for example) but are introduced through the modelling of various terms in the equations. It is desirable to justify the values adopted for the constants in terms of the physical realities of the flow. However, it should be borne in mind that they are only of an empirical nature.

The constants may be divided into two groups, the first of which is comprised of the constant effective Prandtl numbers. This group appear in the equations as a consequence of the assumption of gradient type diffusion, which may be expressed by the Flux Law[40];

$$J_\phi = -\Gamma_\phi \text{ grad } \phi \qquad \ldots\ldots\ldots (7.37)$$

where 'J_ϕ' is the diffusive flux and 'Γ_ϕ' is the diffusivity of 'ϕ'. Thus, the transfer of momentum is given by ;

$$\tau = \rho \nu \frac{\partial U}{\partial Y} \qquad \ldots\ldots\ldots (7.38)$$

and the transfer of heat by[77];

$$Q = -\rho C_p \alpha \frac{\partial T}{\partial Y} \qquad \ldots\ldots\ldots (7.39)$$

where 'Q' is the heat flux, 'T' is the temperature, 'C_p' is the specific heat and ;

$$\alpha = \frac{K}{\rho C_p} \qquad \ldots\ldots\ldots (7.40)$$

The parameter 'K' is the thermal conductivity. The Prandtl number, 'N_{PR}', is the ratio of the momentum and the thermal diffusivity[27];

$$N_{PR} = \frac{\nu}{\alpha} \qquad \ldots\ldots\ldots (7.41)$$

$$= \frac{\rho \nu C_p}{K} \qquad \ldots\ldots\ldots (7.42)$$

$$= \frac{\mu}{\Gamma_T} \qquad \ldots\ldots\ldots (7.43)$$

The Prandtl number is composed only of physical properties of the fluid and is a constant.

The effective Prandtl number, $\sigma_{\phi,t}$, is the turbulent analogue of its molecular equivalent[27]. Thus, re-writing the Flux Law for the turbulent diffusion of 'ϕ', which may be the temperature, or any other turbulent quantity ;

$$J_\phi = -\Gamma_{\phi,t} \text{ grad } \phi \qquad \ldots\ldots\ldots (7.44)$$

The effective Prandtl number may thus be written ;

$$\sigma_{\phi,t} = \frac{\mu_t}{\Gamma_{\phi,t}} \qquad \ldots\ldots\ldots (7.45)$$

As has been previousely discussed, 'μ_t' is proportional to the length scale 'L' and varies through the flow. The diffusivity of 'ϕ' is also proportional to some length scale 'L_ϕ' and varies through the flow. The effective Prandtl number, then, is not a constant but represents the ratio of the length scales at any one point in the flow. For the present model the effective Prandtl numbers have been assumed to be constant and have been introduced into the equations so that the diffusion of 'k' and 'kL' may be described in terms of one length scale.

Measured values of Prandtl numbers are scarce in any flow configurations[78]. The length scales of the turbulent properties at any point in the flow may be supposed to be of the same order of magnitude and it is therefore reasonable to expect the effective Prandtl numbers to be approximately unity[40]. Reported values for free shear flows are given as approximately 0.5 [40][78].

discussed in section 3.4, for evaluating the remaining constants. The various methods are summarised in Table 18. It should be noted that all of them require some assumption as to the value of 'C_μ'; that is, none of them is evaluated independently from 'C_μ'. The table also gives the values of the constants assuming that 'C_μ' is unity and the values adopted by Rodi and Spalding[40]. The equation for finding 'C_B' is more appropriate for a turbulence model in which the parameter 'z' in the z-equation is replaced by '$(k^{3/2})/L$'.

Thus, when considering the constants to be adopted in the turbulence model it should be appreciated that there is insufficient data to enable precise values to be assigned to them. An informed guess as to their order of magnitude, deduced from available related evidence, may be made. In the final analysis, however, the overriding criterion for their selection must be that the predictions of the model conform as closely as possible to experimental evidence[44].

With these points in mind, the consequences of revising the values of the constants was investigated. A rather simplistic calculation was carried out with the objective of determining a new set of constants commensurate with the attainment of results for 'ϕ' of twice their previous value. The constants obtained in this manner are not intended to represent the optimum set but only to demonstrate the consequences of their revision. The revised constants are given in Table 18. The procedure, as previously described, was carried out with the revised constants. The results are listed in Tables 19 to 21 and shown graphically in Figures (56) to (58). Also shown are the results with the initial set of constants. The integral values of the terms in the energy balance were found to be ;

$$(Y|_{0.5}/U_m^2) \int_0^\infty \text{production} = 0.0097 \quad \ldots\ldots\ldots (7.46)$$

$$(Y|_{0.5}/U_m^2) \int_0^\infty \text{dissipation} = -0.0074 \quad \ldots\ldots\ldots (7.47)$$

$$(Y|_{0.5}/U_m^2) \int_0^\infty \text{convection} = 0.0028 \quad \ldots\ldots\ldots (7.48)$$

$$(Y|_{0.5}/U_m^2) \int_0^\infty \text{diffusion} = 0.0000 \quad \ldots\ldots\ldots (7.48)$$

	Possible methods of evaluating constants	Values assuming that C_μ is unity	Values adopted by Rodi & Spalding	Revised Constants
C_μ		1	1	2
C_D	(1) Integration of energy balance (2) $\overline{uv}/k = (C_\mu C_D)^{\frac{1}{2}} = 0.3$ (3) $0.06 \leqslant C_D \leqslant 0.11$	0.09 0.09 $0.06 \leqslant C_D \leqslant 0.11$	0.090	0.045
C_s	(1) $C_\mu C_s = C_D(1 - \frac{1}{2})$ (40) (2) $0.5 \leqslant C_s/C_D \leqslant 0.8$	0.045 $0.045 \leqslant C_s \leqslant 0.092$	0.057	0.0285
C_B	$C_B = C_\mu C_s/C_D - (0.4^2)/\sigma_{kL} C_D^{\frac{1}{2}}$ (40)	-0.03	1	1
σ_k σ_{kL} C_{kL}	Effective Prandtl numbers for free shear flows given as ; 0.5 ± 0.2 (40)(78)		1 0.300 -0.700	4 1.200 -0.700

COMPARISON OF EMPIRICAL CONSTANTS

TABLE 18

	INITIAL CONDITIONS	STEP 1	STEP 2
STAGE 1 : h = 0.0833			
X	0.333	0.667	1.000
$b_{(x)}$	0.083	0.167	0.250
ψ_1	0	0	0
ϕ_1	0.550×10^{1}	0.427×10^{1}	0.368×10^{1}
L1	0.400×10^{-2}	0.514×10^{-2}	0.605×10^{-2}
ψ_2	0.195×10^{1}	0.203×10^{1}	0.209×10^{1}
ϕ_2	0	0.310×10^{1}	0.553×10^{1}
L2	0.400×10^{-2}	0.521×10^{-2}	0.678×10^{-2}
ψ_3		0.271×10^{1}	0.286×10^{1}
ϕ_3		0	0.131×10^{1}
L3		0.523×10^{-2}	0.652×10^{-2}
ψ_4			0.311×10^{1}
ϕ_4			0
L4			0.643×10^{-2}

REVISED COMPUTATIONAL RESULTS

TABLE 19

	1	2	3	4
ψ	0	0.209×10^{1}	0.286×10^{1}	0.311×10^{1}
$\frac{\partial\psi}{\partial X}$	0	-0.400×10^{0}	0.708×10^{0}	0.133×10^{1}
$\frac{\partial\psi}{\partial Y}$	0.250×10^{2}	0.171×10^{2}	0.615×10^{1}	0
$\frac{\partial^2\psi}{\partial Y^2}$	0	-0.137×10^{3}	-0.119×10^{3}	0
$(\frac{\partial^2\psi}{\partial Y^2})^2$	0	0.189×10^{5}	0.143×10^{5}	0
ϕ	0.368×10^{1}	0.553×10^{1}	0.131×10^{1}	0
$\frac{\partial\phi}{\partial Y}$	0	-0.147×10^{2}	-0.369×10^{2}	-0.390×10^{1}
ϕ^2	0.136×10^{2}	0.306×10^{2}	0.171×10^{1}	0
$\frac{\partial(\phi^2)}{\partial X}$	-0.136×10^{2}	-0.255×10^{2}	0.132×10^{2}	0.786×10^{0}
$\frac{\partial(\phi^2)}{\partial Y}$	0	-0.151×10^{3}	-0.756×10^{2}	0
$\frac{\partial^2(\phi^2)}{\partial Y^2}$	0.281×10^{5}	-0.144×10^{5}	0.360×10^{4}	0.300×10^{3}
ϕ^3	0.499×10^{2}	0.169×10^{3}	0.223×10^{1}	0
L	0.605×10^{-2}	0.678×10^{-2}	0.652×10^{-2}	0.643×10^{-2}
$\frac{\partial L}{\partial Y}$	0	0.960×10^{-2}	-0.300×10^{-2}	0

STAGE 1 : DERIVED RESULTS

TABLE 20

	1	2	3	4
$\frac{Y}{b}$	0	0.333	0.667	1
$\frac{Y}{Y\|_{0.5}}$	0	0.714	0.143×10^{1}	0.214×10^{1}
$\frac{\psi}{Y\|_{0.5}U_m}$	0	0.712	0.975	0.106×10^{1}
$\frac{U}{U_m}$	1	0.684	0.246	0
$\frac{V}{U_m}$	0	0.160×10^{-1}	-0.283×10^{-1}	0.856×10^{-1}
$\frac{\phi}{U_m}$	0.147	0.221	0.520×10^{-1}	0
$\frac{L}{b}$	0.242×10^{-1}	0.271×10^{-1}	0.261×10^{-1}	0.257×10^{-1}
$\frac{\overline{uv}}{U_m^2}$	0	0.164×10^{-1}	0.320×10^{-2}	0
$\frac{Y\|_{0.5}Pn}{U_m^3}$	0	0.106×10^{-1}	0.180×10^{-2}	0
$\frac{Y\|_{0.5}Cn}{U_m^3}$	0.253×10^{-2}	0.371×10^{-2}	-0.101×10^{-2}	0
$\frac{Y\|_{0.5}Df}{U_m^3}$	0.233×10^{-2}	-0.199×10^{-2}	0.183×10^{-3}	0
$\frac{Y\|_{0.5}Dp}{U_m^3}$	-0.277×10^{-2}	-0.838×10^{-2}	-0.115×10^{-3}	0

Pn - production
Cn - convection
Df - diffusion
Dp - dissipation

STAGE 1 : NON-DIMENSIONALISED RESULTS

TABLE 21

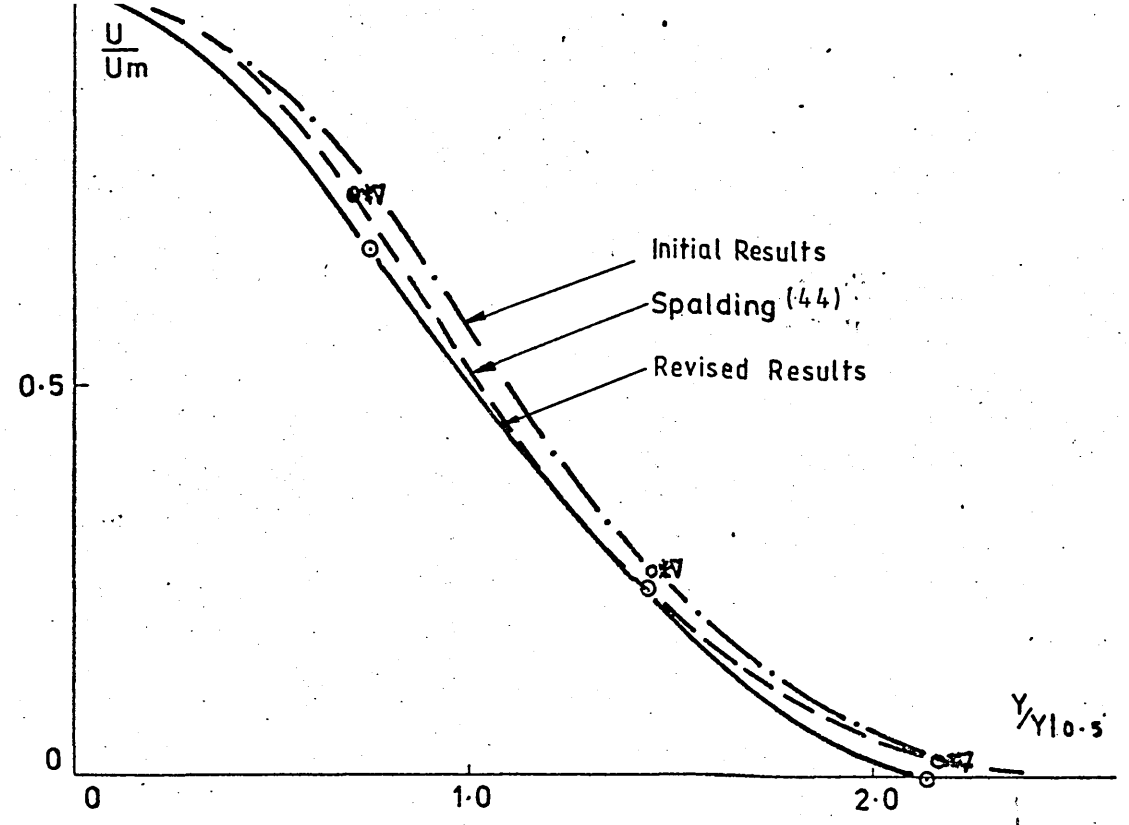

a) Revised U-profile.

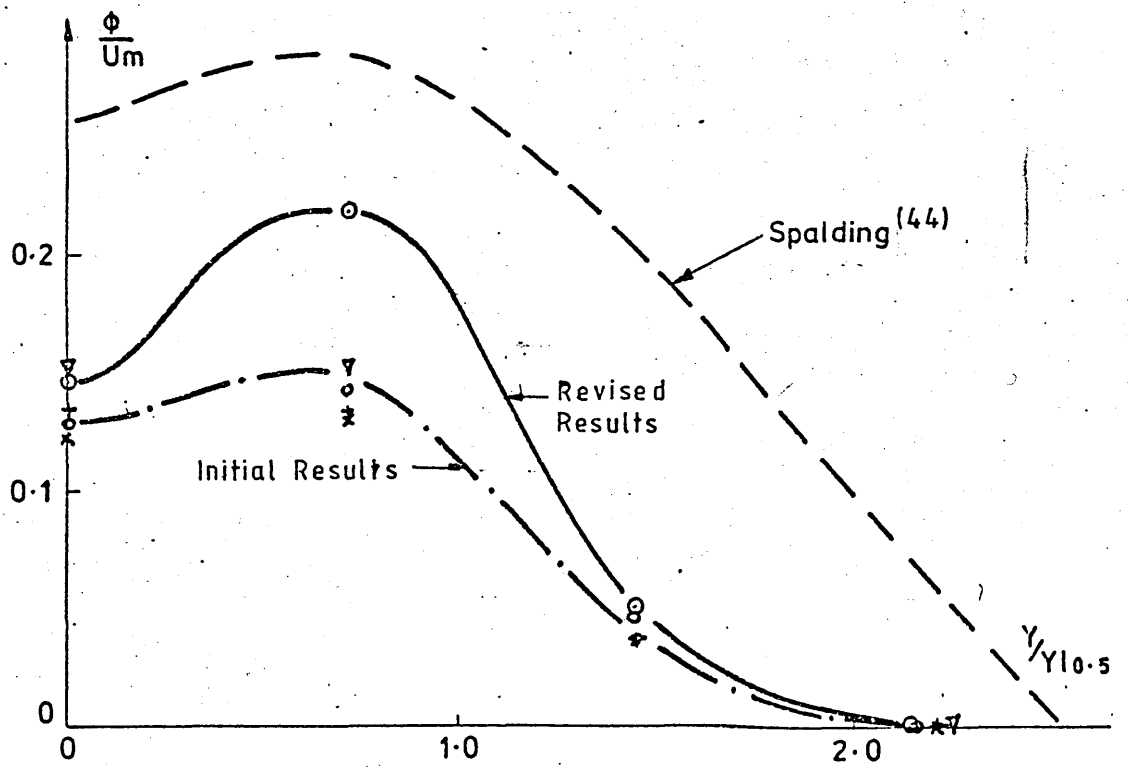

b) Revised Φ-profile.

Figure 56.

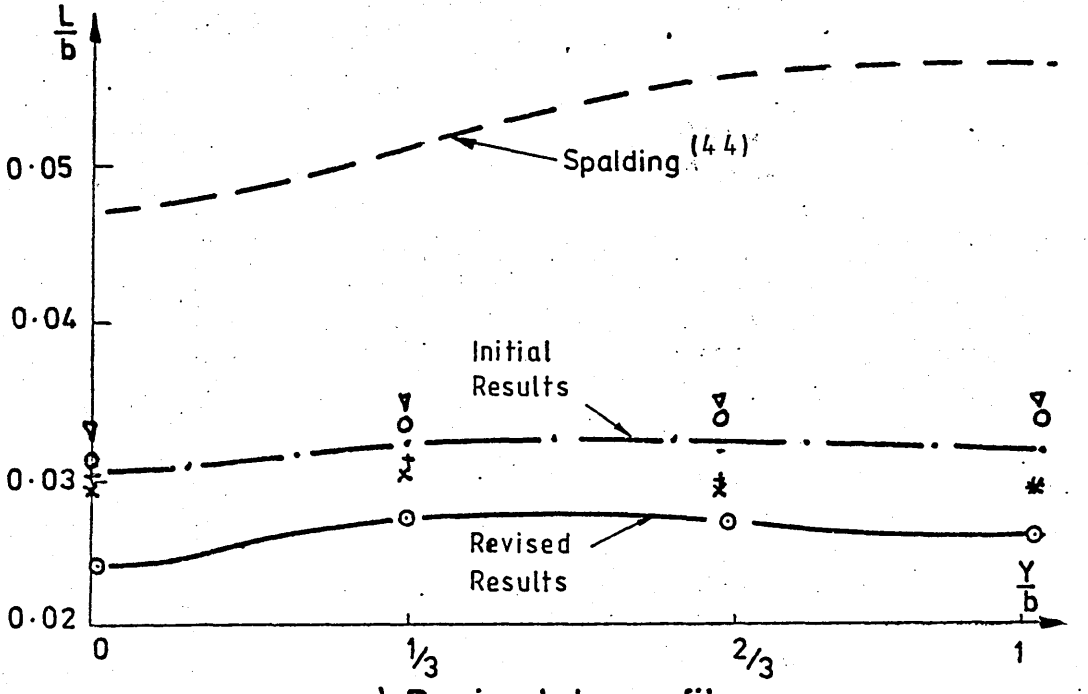

a) Revised L-profile.

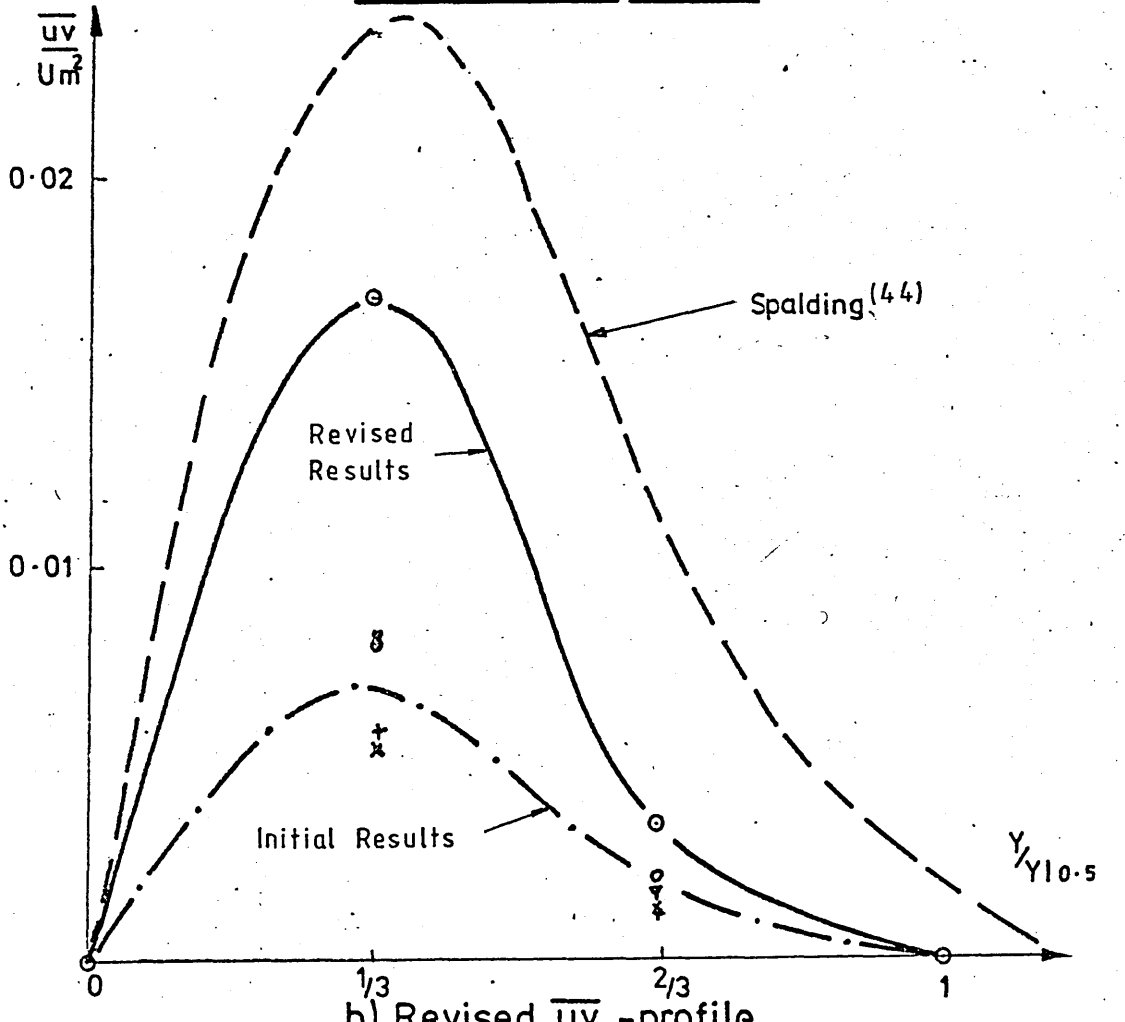

b) Revised $\overline{uv}$ -profile.

Figure 57

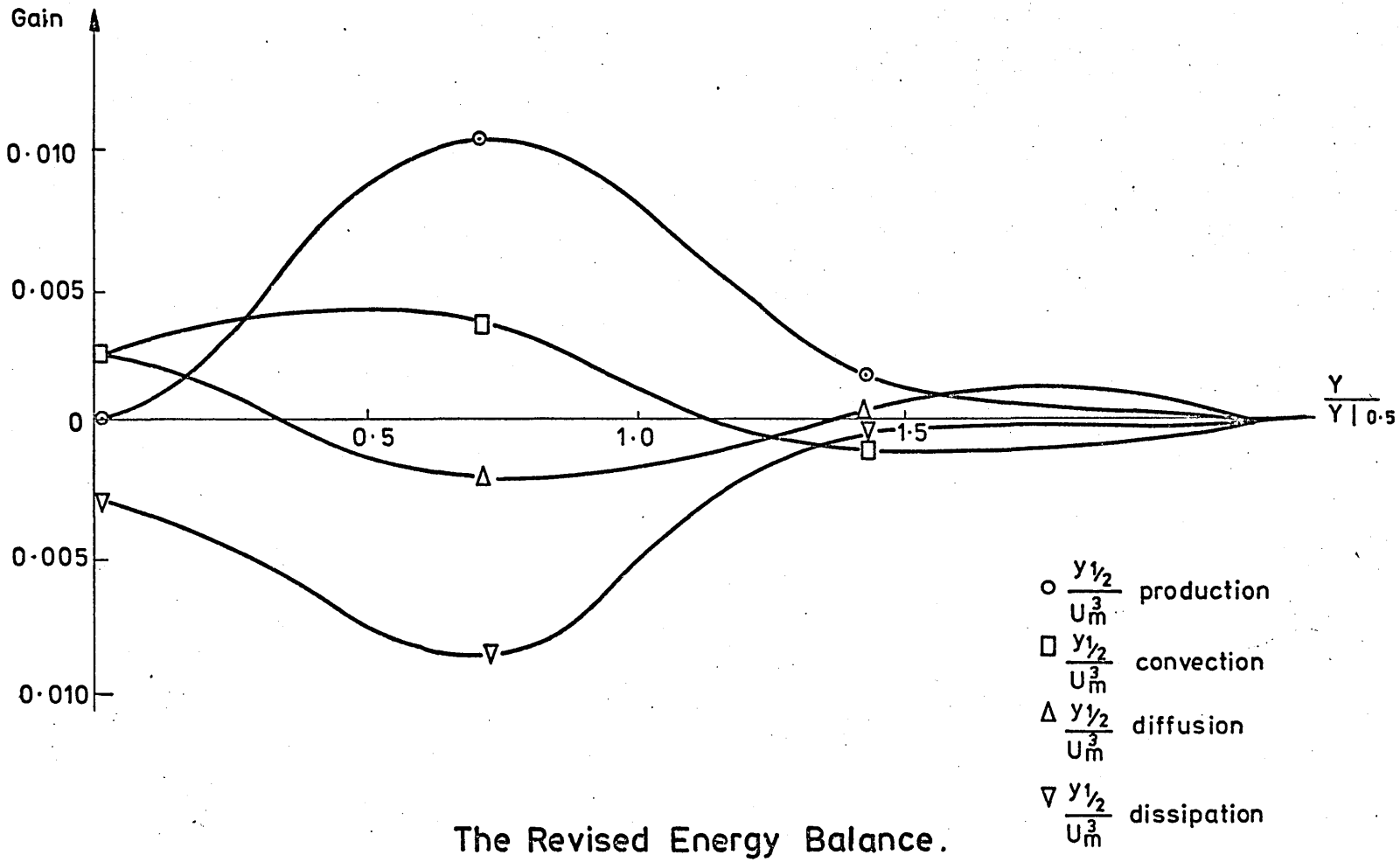

Figure 58

The Revised Energy Balance.

Although the combination of constants was not selected by sophisticated techniques, such as computer optimisation, it may be seen that in most respects the new set of results represent a a considerable improvement over the original set. The U-profile remains in good agreement with the results of Rodi and Spalding[40]. The ϕ-profile and the $\overline{uv}$-profile are also much closer to the expected results. The energy balance is improved in as much as the integral values are considerably closer to those obtained by Bradbury[16] and the net diffusion of turbulent energy across the jet is effectively zero.

7.6 Summary

The results obtained from the application of a Generalised Collocation Finite Element Method to the problem of the Turbulent Plane Jet, have been presented in this chapter. An original numerical model, embracing a two stage solution scheme, has been employed for this purpose. The results are of a qualitatively valid nature and indicate that a complete set of acceptably accurate profiles could be obtained through the choice of an appropriate combination of constants. Factors effecting the magnitude of the results have been discussed and methods for improving their accuracy have been suggested.

CHAPTER 8

CONCLUSIONS

8.1 Introduction

Accepting the original nature of the numerical model and solution routine, the qualitative nature of the results may be considered to demonstrate that a valid analysis of the Turbulent Plane Jet has been instituted. The quantitative aspect of the results should be viewed in the light of the discussion concerning the nature of the constants introduced into the equations through the turbulence modelling. The determination of the best set of constants is complex and involves carrying out many calculations in which they are systematically varied[40]. A detailed investigation of this subject is beyond the scope of the present study. The constants that were employed in this study, then, are not presented as being the optimum set. They are, however, considered to be commensurate with the production of valid data upon which an assessment of the numerical method may be based.

8.2 Appraisal of the Study

A survey of numerical studies involving problems in the field of fluid mechanics in recent years, shows a trend towards the increasing employment of various Finite Element orientated techniques[70][71][79]. The principal objective of this study was to formulate an improved Finite Difference scheme based on this type of approach. Accordingly, a mathematical model of this nature was developed and tested on a problem for which numerical and experimental data was available, namely the Turbulent Plane Jet. The Generalised Collocation approach employed (a method which has shown to some advantage in the solution of linear problems in the field of structural mechanics[58]) has not, to the best of the author's knowledge, been previousely used in the field of fluid mechanics.

The method of solution entailed the application of a two-stage technique. Whilst this method had the advantages associated with the employment of a solution routine requiring relatively few

equations, some sacrifice was made with regard to the nodal definition of the profiles. Nonetheless, the analysis did produce accurate velocity profiles, the characteristic decay of the centre-line velocity and an accurate value for the spread of the jet. The remaining results were qualitatively sound and indicated that an accuracy comparable with that attained for the parameter 'ψ' might well be achieved by further refinement of the magnitude and the inter-relationship of the constants in the field equations.

Although some aspects of the study warrant further attention, it is felt that the advantages of the technique (such as its flexibility with regard to the treatment of boundary nodes) have been demonstrated and its results are not without promise. Accepting the limited nature of the present research programme, it is felt that its main objectives have been realised.

8.3 Suggestions for Further Work

The analysis described in the preceeding chapters may be considered to resolve itself into three distinct, but inter-related, constituent parts. The first concerns the modelling of turbulence, the second, the method of converting the resulting partial differential governing equations into algebraic equations, and the third relates to their solution. There is scope for further work not only in each of these areas, but also in the application of the model to different flow configurations.

Regarding the aspect of the model concerned with the modelling of turbulence, perhaps the most important piece of work that could be carried out is the determination of the optimum set of constants appearing in the field equations. An investigation into the nature of the constants, based on appropriately balanced numerical and phenomenological considerations, would enable the further refinement of the present model and provide an insight into a subject of general interest.

The advantages of mathematical models employing Hermitian functions have been clearly demonstrated in the field of linear structural mechanics[52][58]. Thus, a logical extension of the present study would be the development of a more sophisticated local element which would allow for their incorporation.

this study must depend heavily on the nature of the solution scheme incorporated in it. Its importance in this respect warrants a more detailed investigation into the most suitable scheme to be adopted, and its manner of interfacing with the numerical model, than the scope of the present study allowed.

The objective of the preceeding analysis has been the development of a mathematical model for the prediction of two-dimensional turbulent shear flow at high Reynolds numbers. The example of shear flow used throughout the study for testing the numerical work has been the turbulent Plane Jet. However, the governing equations formulated in Chapter Three were derived from general equations equally applicable to other classes of shear flow.

Minor adaptations to the model would allow its application to a number of plane shear flow configurations; the Plane Mixing Layer and the Plane Jet in a co-flowing stream, for example. Provision for accounting for the laminar sub-layer near the wall would allow its application to be extended to Wall Jets. The requisite adjustment to the governing equations[44] (which are not extensive and could be incorporated into the programming) would allow its application to axi-symmetric shear flows; the Round Jet and the Radial Jet, for example. The main changes in the model would involve re-definition of the global field, appropriate adjustment of the boundary conditions and, in some cases, revision of the constants employed in the field equations. A final area of further work, then, is the application of the model to a wide range of two-dimensional shear flows at high Reynolds number.

To sum up, with the accelerating development of numerical prediction techniques based upon Finite Element computer orientated methods, it is desirable that their full potential should be explored. Further reliable interpretation of empirical data for incorporation into phenomenological equations is an essential pre-requisite for the success of these methods. However, the development of the mathematics required for the treatment of such complex equations is also an important subject, requiring continuing research. The present investigation represents a preliminary study in this field.

APPENDIX 1

THE LASER DOPPLER ANEMOMETER

A1 Introduction

A wave scattered or radiated from a moving object will suffer a shift in frequency proportional to the instantaneous velocity of the object. This phenomenom, first explained by Christian Doppler in 1842, has been widely used for the measurement of relative velocity. One of its oldest applications has been in the field of astronomy, in which spectrometers have long been used for the determination of large recession rates of distant light sources. Unfortunately, since the fractional frequency shift of electromagnetic waves is in the order of 10^{-9} times the velocity in m/s (80), the resolving power of optical spectrometers is quite insufficient for measuring relative velocities below approximately 10^{3} m/s. The development of heterodyning techniques enabled detection of Doppler shifts of very small fractional values. The technique, however, is restricted to coherent waves and until recently only signals in the radio-frequency portion of the electromagnetic spectrum were available to fulfil this requirement. Within these limitations radar Doppler instruments allow the measurement of objects moving with a wide range of velocities.

The introduction of lasers removed the main obstacle in the path of the 'optical' measurement of low relative velocities. A laser cavity may be considered to be a high-gain oscillator of extremely narrow band width. Only a small portion of the energy is emitted, but this is very intense compared with the emission within a comparable frequency range from a conventional source. In short, lasers are intense sources of highly monochromatic light and as such are ideally suited to the application of heterodyning techniques. Before continuing with an account of the development of laser anemometry it may be worthwhile to consider the Doppler effect in slightly more detail.

A2 The Doppler Effect

An observer on a particle moving away from a fixed source of light would see light at a lower frequency than the source

frequency and, to the stationary observer, the light scattered from the particles would also suffer an apparent frequency shift. The geometry of this situation is shown in Figure A.1; 'e_i' and 'e_s' are unit vectors in the directions of the incident and scattered light waves respectively and '$\bar{v}$' is the velocity of any specified particle. The frequency relationship between the scattered light waves and the light wave it originates from is given according to the vector equation[81];

$$f_s = f_i + \frac{1}{\lambda} \bar{v} (\hat{e}_s - \hat{e}_i) \qquad \ldots\ldots\ldots \quad (A.1)$$

where, f_s = frequency of scattered light
f_i = frequency of incident light
$\hat{e}_s$ = unit vector in scattering direction
$\hat{e}_i$ = unit vector in incident direction
λ = wavelength of incident light
and $\bar{v}$ = velocity vector

The frequency shift is equal to the Doppler frequency, f_D;

$$f_D = f_s - f_i \qquad \ldots\ldots\ldots \quad (A.2)$$

thus, $$f_D = \frac{1}{\lambda} \bar{v} (\hat{e}_s - \hat{e}_i) \qquad \ldots\ldots\ldots \quad (A.3)$$

It may be seen from this equation that the Doppler frequency is directly proportional to the particle frequency. The laser anemometer, then, measures the Doppler frequency, f_D, obtained by way of particles in the flow. The particle diameter may well be as small as the laser light wavelength and, thus, the particles have approximately the same local velocity as the flow medium even in a high frequency turbulent stream.

A3 The Development of Laser Anemometry

In the early sixties the feasibility of measuring steady fluid velocities from the Doppler shift in frequency of scattered radiation was demonstrated by Yeh and Cummins[82]. Using a laser-Doppler spectrometer they measured the velocity profile in a liquid flow and obtained results which agreed remarkably well with theoretical predictions. Foreman et al[83] are generally believed to

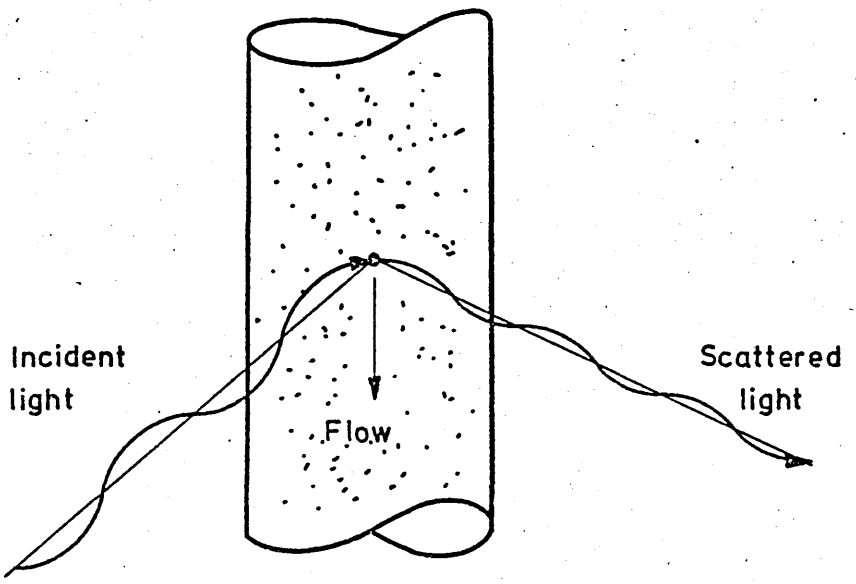

a) The Frequency Shift In Scattered Light.

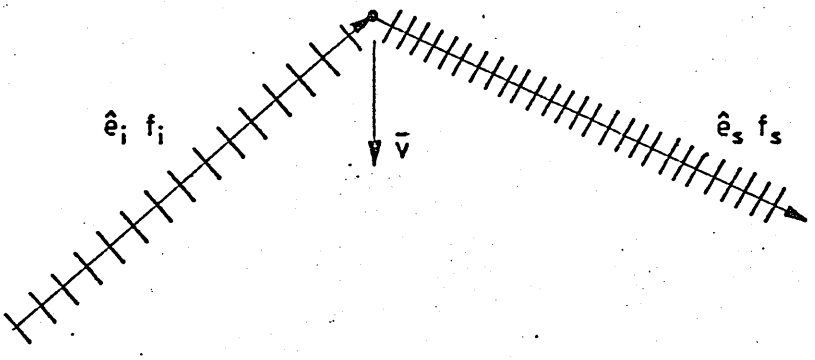

b) The Vector Representation Of The Doppler Effect.

Figure A-1.

have carried out the first Doppler measurement of local flow velocities in a gas. Scattering was achieved by introducing smoke particles into the flow. By the late sixties, the possibility of measuring time varying velocities with similar instrumentation was being investigated Goldstein and Hagen[84] and Pike et al[85]. Results comparing very favourably with the experimental data of Laufer were obtained. This period also saw a number of further innovations and improvements in instrumentation, mostly concerned with the treatment of the Doppler signal.

In 1969, Rudd[86] proposed an alternative approach to the frequency analysis then currently in use. It was based on the consideration of interference fringes in the focal region rather than on the heterodyning of reference and scattered frequencies on a photomultiplier. In fact in a number of cases these alternatives can be shown to be two interpretations of the same phenomenon. This may be most easily understood by considering the interception of the two laser beams focussed at a point illustrated in Figure A.2. Each beam will focus to a long narrow pencil shaped diffraction region which contains essentially planar phase fronts. Because the two radiations are mutually coherent and identically polarised, they will interfere constructively and destructively to establish a set of closely spaced interference fringes in the beam cross-over region. In this way plane parallel regions of maximum and minimum illuminating intensity are formed. It may also be seen from the same Figure that any two adjacent fringes are seperated by the distance ;

$$y = \frac{\lambda}{2\sin(\theta/2)} \qquad \ldots\ldots\ldots \quad (A.4)$$

where 'λ' is the wavelength and 'θ' is the angle between the illuminating beams.

As a moving scattering centre passes through the focal region, it will intercept the interference fringes and the illumination level it experiences will alternate from maximum to minimum. Thus, as it passes through the probe region it will alternately scatter and then not scatter light into the photo-multiplier and generate a current. The fluctuation frequency of the current will be proportional to the rate at which the particle

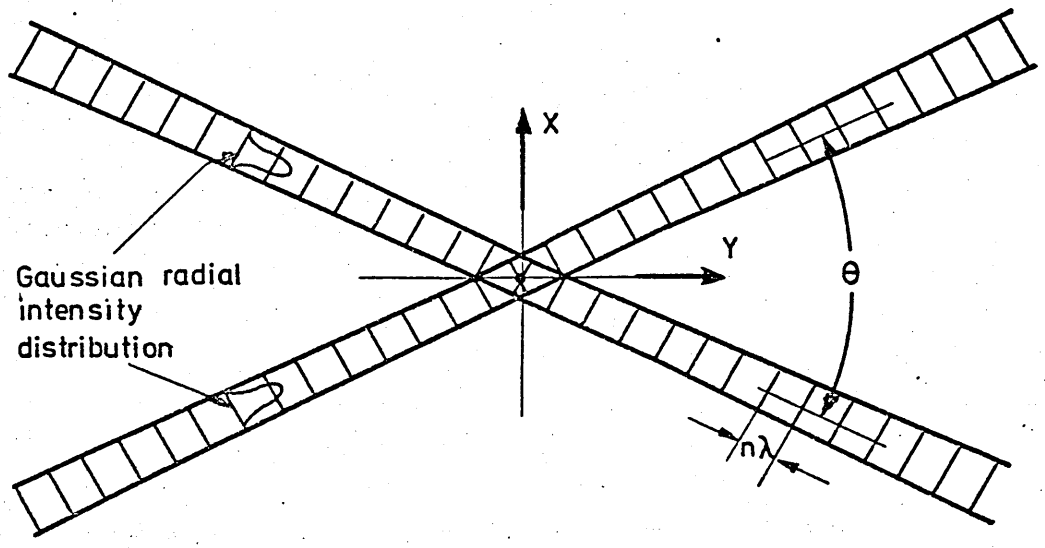

a) Measuring Volume.

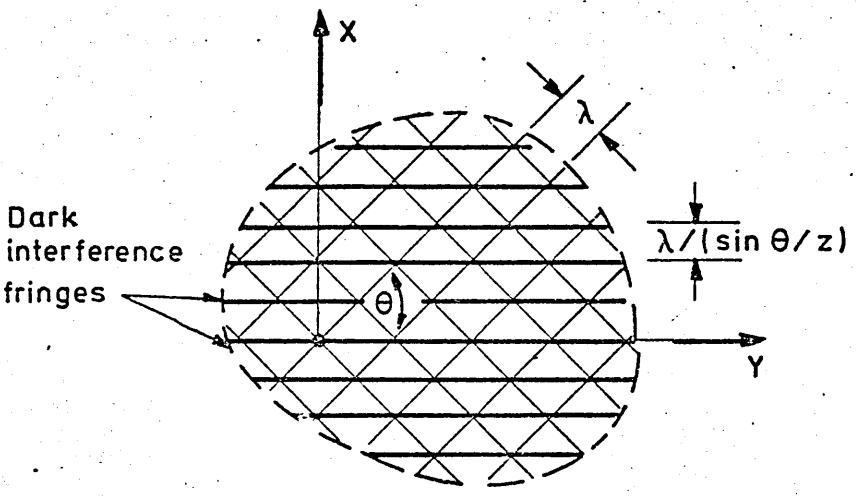

b) The Fringe Pattern.

Figure A-2

component of the particle orthogonal to the fringes, $\bar{v}$. It may be deduced from equation AII.5 that $\bar{v}$ will be given by ;

$$\bar{V} = \frac{\lambda}{2\text{SIN}(\theta/2)} \cdot f_D \qquad \ldots\ldots\ldots \quad (A.5)$$

where f_D is the frequency of the detected current. Again, it may be seen that the particle velocity is directly proportional to the frequency f_D, as in equation A.4. In certain experimental configurations the relationships are in fact identical.

There have been many papers published describing the laser anemometry instrumentation[80][87][88]. Several optical geometries have been proposed which prompted Durst and Whitelaw[88] to attempt the classification of the possible configurations of optical systems according to the light distribution in the measuring control volume. They were clasified as being one of the following three modes;-the reference beam, the fringe or the Doppler modes.

The Doppler modes are characterised by a single incident light beam at the measuring control volume. The light intensity at this point is governed by the intensity distribution of the incident light beam and the action of the focussing lens. This light intensity distribution can be calculated and has been shown to be of Gaussian form.

Fringe modes are those in which the actual light intensity distributions within the measuring control volumes show distinct fringe patterns due to the interaction of two coherent light beams. Those arrangements with intense incident light beams allow the scattered light to be measured, whereas those with less intense beams require the detector to be placed on the symmetry axis of the beam where it records the light which is not blocked off by the particles.

The reference beam modes have a light intensity distribution which is a hybrid of those of the Doppler and fringe modes. This is caused by the two beams having different intensities and resulting in the disappearance of the distinct fringe pattern and also of the smooth Gaussian light distribution. The resulting light intensity distribution is of a form indicating a weak fringe pattern superimposed on a Gaussian distribution.

Most of the early anemometer systems were based on the Doppler mode and then, later, the reference beam mode. The signal processors generally associated with these methods were either spectrum analysers, (involving the sequential analysis of frequencies), or frequency trackers, (in which the analyser frequency follows the frequency fluctuations in the signal). The systems most widely in use today are generally based on the fringe mode. The fringes are three-dimensional and suitable arrangement of the geometry of the equipment makes the measurement of all three components of the velocity feasible. The trend in signal processing in the latest anemometer systems is towards counting techniques. A typical set-up might be composed of a counting system, (counting apparatus and amplifier, filters and validation criteria circuits) and a spectrum analyser to control signal quality and to choose the correct filter bandwidth. The digital output of the counter may be connected to a mini computer in order to calculate in real time the mean velocity, turbulence intensity and also the turbulence spectra if the data aquisition rate is high enough[89].

A4 Pipe Flow Experimentation

An experimental investigation of flow through a pipe, with an R_e of approximately 4.0×10^4, using a laser anemometer was made with a view to assessing its suitability for measurement in the plane turbulent jet. The laser used was a Spectra Physics model 120 helium-neon gas laser with a nominal output of 5 milliwatts at 6328 Angstroms. Auxillary equipment included an optical unit, a photomultiplier, a signal processor, a signal conditioner, a digital voltmeter and a true RMS meter. The arrangement of the equipment is illustrated in Figure A.3.

The optical unit splits the laser beam up into two seperate beams which are then focussed so that they intersect at the point of measurement. The Doppler shifted light, scattered by particles passing through the measuring volume, is detected by the photomultiplier. The signal from the photomultiplier is directed to the signal processor, which basically consists of a preamplifier, a frequency tracker and a meter unit. Unwanted noise in the signal is minimised in the preamplifier by a high/low pass filter system. The

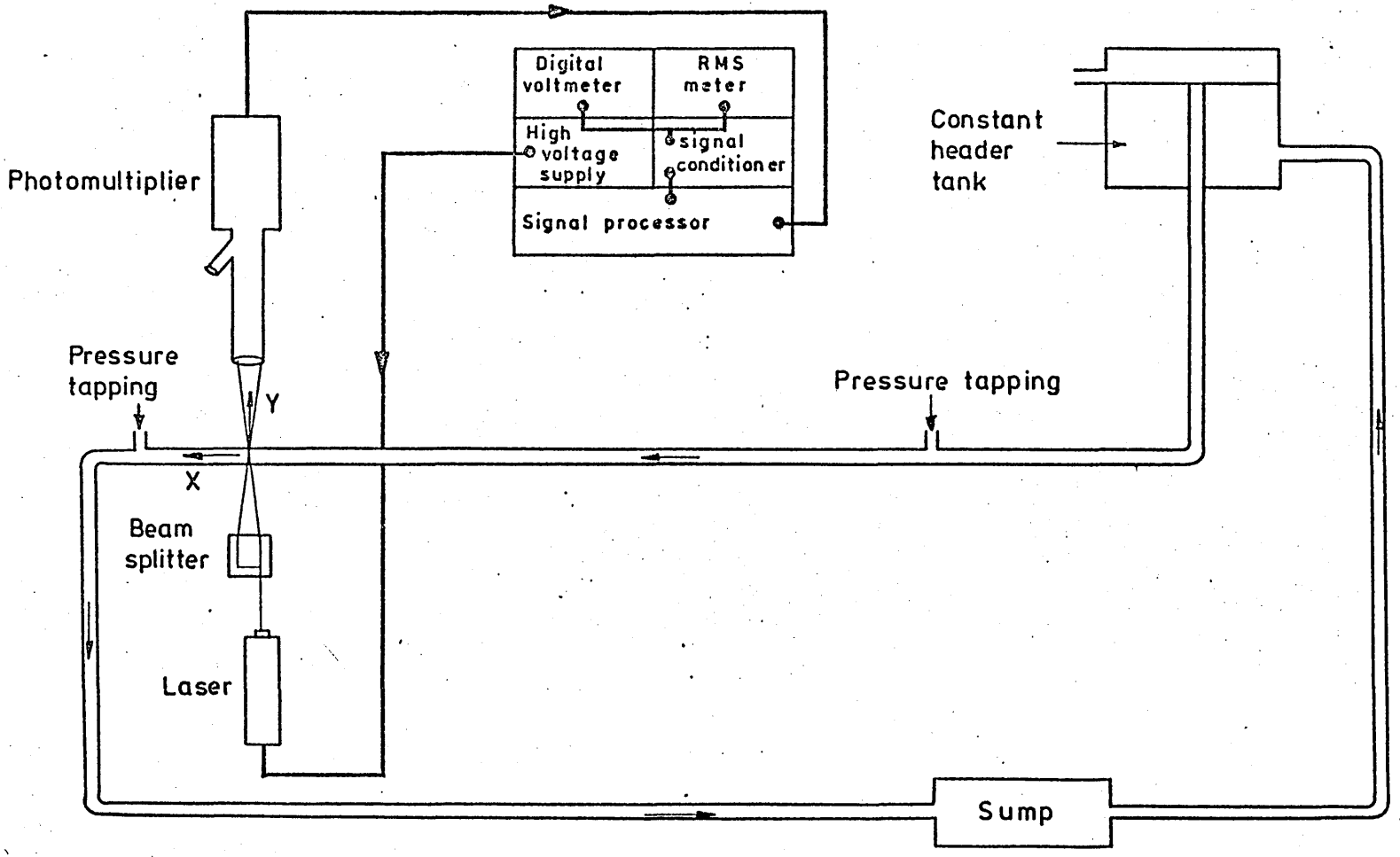

Figure A-3

Schematic Arrangement For Pipe Flow Measurement.

signal, which is time-dependant, is then fed to the frequency tracker where it is combined with the output of a voltage controlled local oscillator. The output signal, at a difference frequency, is passed to a sensitive frequency discriminator which provides a D.C. output proportional to the frequency deviation from a fixed centre value, 'f_0'. The resulting error voltage is then fed back to the oscillator. In this way the oscillator frequency tracks that of the Doppler signal, maintaining a nearly constant difference equal to 'f_0'. Thus, the error voltage provides a continuous electrical analogue of the instantaneous Doppler frequency.

The noise-like turbulence signal from the frequency tracker is passed through the signal conditioner, (which has a number of facilities for improving its quality), to the meter unit. The mean value of the voltage is registered on a digital voltmeter and the fluctuating component is computed on the true RMS meter. Having established the relationship between the voltage and the frequency, the mean velocity may be calculated from the equation
the laser anemometer is an inherently linear instrument, the ratio of the RMS meter reading to the digital voltmeter reading yields the turbulence intensity.

The water was supplied to the pipe from a constant head tank. After flowing through the pipe the water was pumped from the sump back to the tank. The pipe was 2 m long and of 0.02 m internal diameter. The measuring point was located 1.2 m from the upstream end of the pipe, that is sixty pipe diameters, at which point the flow was assumed to be fully developed. The flow rate was measured by diverting the flow into a weigh tank in which the amount of water collected over a given time interval was weighed.

A5 Results of Pipe Flow Test

A measure of the accuracy of the values of the mean velocity was obtained by comparing them with the predictions of the seventh power law and the law of the wall[18]. The experimental results, as illustrated in Figure A.4, may be seen to be in good agreement with the theoretical results. The shear velocity, 'U_*', was calculated to be 0.119 m/s. A further check was made by comparing the

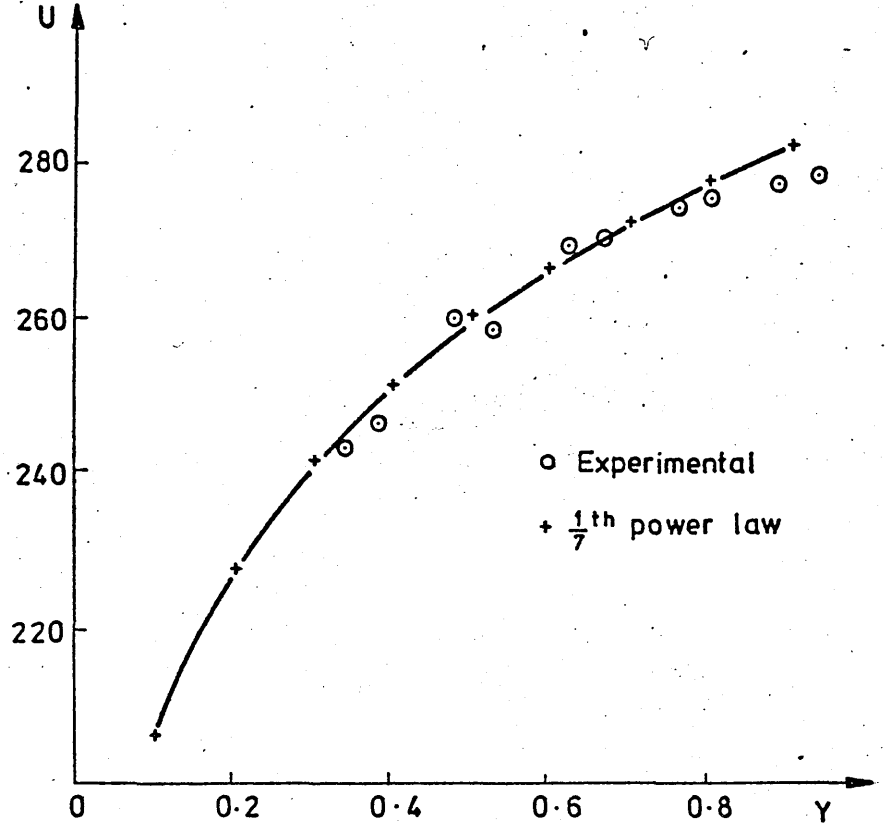

a) The Seventh Power Law.

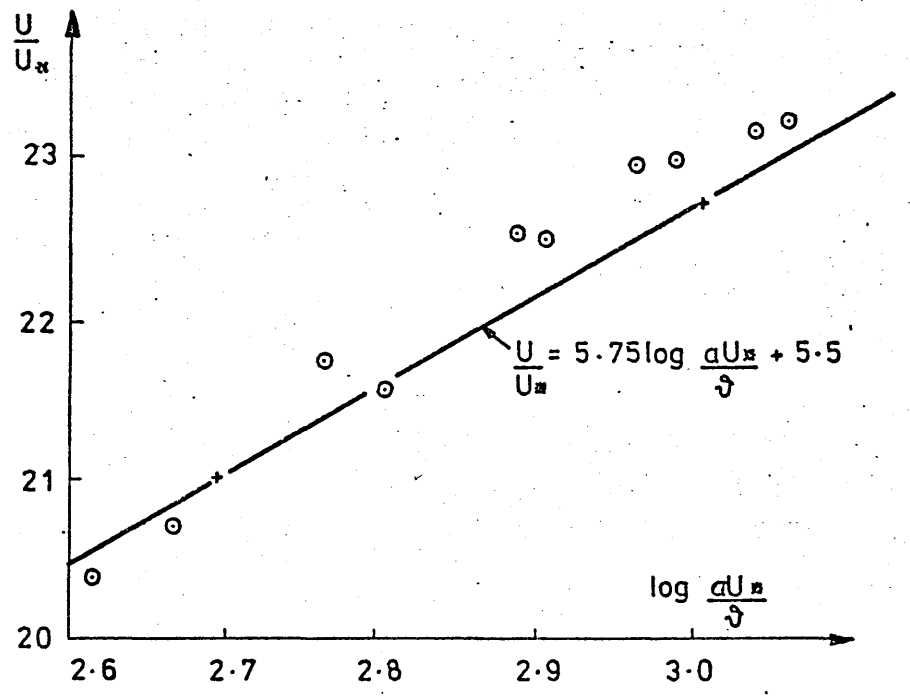

b) The Law Of The Wall.

Figure A:4

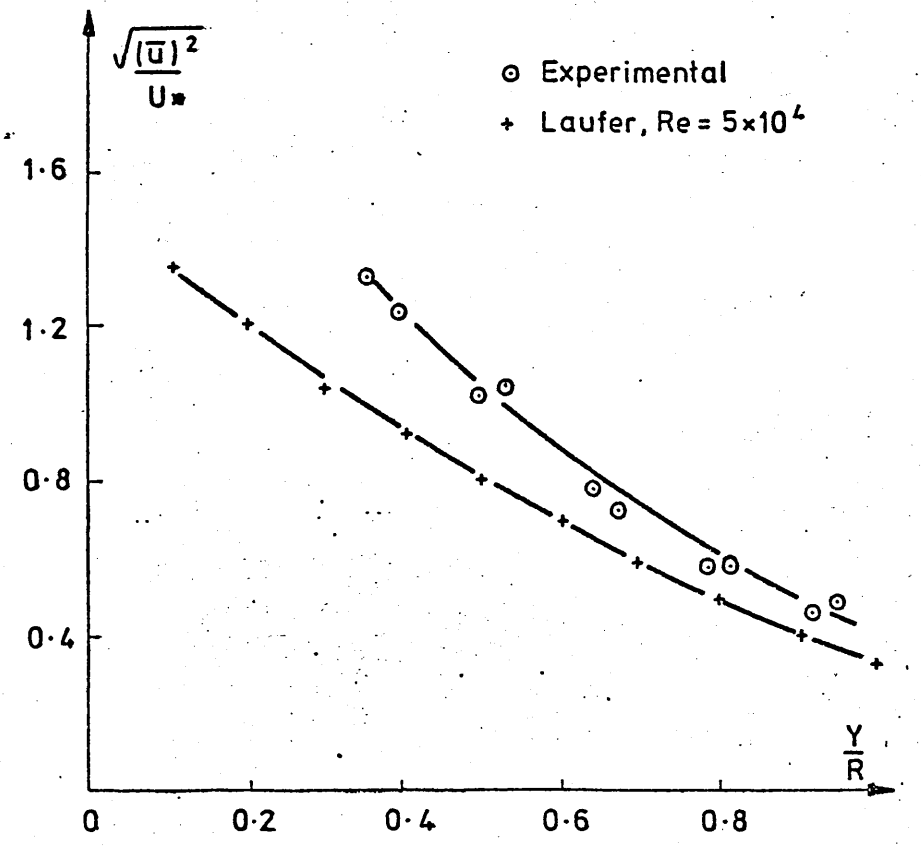

The Turbulence Intensity.

Figure A·5

flowrate obtained from the numerical integration of the measured velocity profile ;

$$Q = 2\pi \int_0^r rU\,dr \qquad \ldots\ldots \quad (A.6)$$

with the actual measured flowrate. Agreement was found to be within 2%. The turbulence intensity was non-dimensionalised with respect to the shear velocity and plotted with the results obtained by Laufer[52], at a Reynolds number of 5×10^4. The results may be seen to be of about the right order and of the correct form, as illustrated in Figure A.5.

A6 Conclusions

The laser anemometer has been described as approaching the attainment of the requirements of an ideal instrument[80]. advantages are;

(i) it presents no disturbance to the medium,

(ii) calibration is simple, very accurate, and practically invariant,

(iii) the measurement may be highly localised,

(iv) the output is linear with the input, and

(v) the dynamic range is very large and the response time is very short.

However, the instrument does also have disadvantages. Prominant amongst these is the fact that it actually measures particle velocity, not fluid velocity. Therefore, there must be particles in the flow in sufficient concentration and of suitable size to give the required signal. In many cases, flow seeding may be necessary and the case of the plane turbulent jet is a case in point. The difficulties encountered in setting up a jet with water as the fluid medium make it desirable to use air in its place. The inpracticability in the present instance of suitably adapting existing apparatus, prohibited the use of the laser in an investigation which was by nature only exploratory. The design of apparatus involving laser anemometry is of necessity complex and should only be undertaken in cases whose experimental scope really warrants it.

```
      IMPLICIT REAL*8(A-H,O-Z)
      COMMON/ACOM/LINT,QUDT,CUBT,QURT,CUCO,QRCO,U,G
      COMMON/BCOM/AJINV,W
      COMMON/CCOM/LIV,MIV
      COMMON/DCOM/X,F
      COMMON/ECOM/A
      COMMON/FCOM/SCALE
      DIMENSION LIN(3,2),LINT(12,8),QUD(3,5),QUDT(12,14),CUB(3,14),
     1 CUCO(14,3),CUBT(12,56),QUR(3,21),QRCO(21,4),QURT(12,75),B(12),
     2 G(4),F(11),X(11),AJINV(11 11),XDAT(30),W(300),U(30),A(121),
     3 LIV(11),MIV(11),SCALE(11)
      INTEGER CUCO,QRCO
      REAL*8 LIN,LINT
C
C     READ IN INITIAL DATA INCLUDING THE COEFFICIENTS
C     OF THE LOCAL FIELD ANALOGUE AND THE CONSTANTS
C     APPEARING IN THE GOVERNING EQUATIONS.
C
      ACCEPT *,CMU,CD,CS,CB,SIGK,SIGKL,CKL,IDIV
      ACCEPT *,(X(I),I=1,11)
      ACCEPT *,(SCALE(I),I=1,11)
      ACCEPT *,SCALE1,SCALE2,SCALE3
      ACCEPT *,((LIN(I,J),J=1,2),I=1,3)
      ACCEPT *,((QUD(I,J),J=1,5),I=1,3)
      ACCEPT *,((CUB(I,J),J=1,14),I=1,3)
      ACCEPT *,((QUR(I,J),J=1,21),I=1,3)
      ACCEPT *,((CUCO(I,J),J=1,3),I=1,14)
      ACCEPT *,((QRCO(I,J),J=1,4),I=1,21)
C
C     PROVISION FOR THE ALLOCATION OF REVISED
C     CONSTANTS IF REQUIRED.
C
      IF(IDIV.GT.0)GOTO 10
      D1=CMU/SIGK
      D2=CMU/SIGKL
      D3=CB*CMU
      D4=D2*(1.0+CKL)
      D5=-3.0*D2-4.0*D4
      D6=2.0*D2+4.0*D4
      QUD(1,1)=-CMU
      QUD(1,2)=-CMU
      QUD(1,4)=CMU
      QUD(1,5)=CMU
      QUD(2,3)=CD
      QUD(3,3)=CS
      QUR(2,1)=-CMU
      QUR(2,2)=4.0*CMU
      QUR(2,3)=-2.0*CMU
      QUR(2,4)=-D1
      QUR(2,5)=-D1/2.0
      QUR(2,6)=-2.0*D1
      QUR(2,7)=D1/2.0
      QUR(2,8)=2.0*D1
      QUR(2,12)=D1/2.0
      QUR(2,13)=-4.0*CMU
      QUR(2,14)=4.0*CMU
      QUR(2,15)=4.0*D1
      QUR(2,18)=-2.0*D1
      QUR(2,19)=-D1/2.0
```

```
      QUR(3,1)=-D3
      QUR(3,2)=4.0*D3
      QUR(3,3)=-2.0*D3
      QUR(3,4)=-D4
      QUR(3,5)=D5/4.0
      QUR(3,6)=-2.0*D4
      QUR(3,7)=-D5/4.0
      QUR(3,8)=2.0*D4
      QUR(3,9)=-D2/4.0
      QUR(3,10)=-D2
      QUR(3,11)=D2/2.0
      QUR(3,12)=-D5/4.0
      QUR(3,13)=-4.0*D3
      QUR(3,14)=4.0*D3
      QUR(3,15)=D6
      QUR(3,16)=-D2
      QUR(3,17)=-D2/4.0
      QUR(3,18)=-2.0*D4
      QUR(3,19)=D5/4.0
      QUR(3,20)=-D3
      QUR(3,21)=-D4
10    IWRI=0
      MESH=4
      H=1.0
      NSETZX=0
C
C     DIVIDE THE COEFFICIENTS OF THE LOCAL FIELD
C     ANALOGUE BY THE APPROPRIATE POWER OF 'H'.
C
      LIN(1,1)=LIN(1,1)/H
      LIN(1,2)=LIN(1,2)/H
      DO 20 J=1,5
20    QUD(1,J)=QUD(1,J)/H
      DO 70 I=2,3
      DO 30 J=1,14
      CUB(I,J)=CUB(I,J)/H**2
30    CONTINUE
      DO 40 J=1,3
40    QUR(I,J)=QUR(I,J)/(H**4)
      DO 50 J=4,12
50    QUR(I,J)=QUR(I,J)/(H**2)
      QUR(I,13)=QUR(I,13)/(H**4)
      QUR(I,14)=QUR(I,14)/(H**4)
      DO 60 J=15,19
60    QUR(I,J)=QUR(I,J)/(H**2)
      QUR(I,20)=QUR(I,20)/(H**4)
      QUR(I,21)=QUR(I,21)/(H**2)
70    CONTINUE
C
C     SET ZERO ELEMENTS IN THE LOCAL FIELD ANALOGUE
C
      IZOEND=3*MESH
      DO 120 IZERO=1,IZOEND
      JZEND1=2*MESH
      DO 80 JZER1=1,JZEND1
80    LINT(IZERO,JZER1)=0.0
      JZEND2=IZOEND+2
      DO 90 JZER2=1,JZEND2
```

```
100   CUBT(IZER0,JZER3)=0.0
      JZEND4=18*MESH+3
      DO 110 JZER4=1,JZEND4
110   QURT(IZER0,JZER4)=0.0
120   CONTINUE
C
C     BLOCKWISE CO-ORDINATE TRANSFORMATION OF THE
C     LOCAL FIELD ANALOGUE.
C
      J1=1
      KA=0
      LA=0
      L2=8*MESH+6
      M1=14
      NC=0
      NULOOP=3*MESH
      DO 350 I=1,NULOOP
      NC=NC+1
      LINT(I,J1)=LIN(NC,1)
      J2=J1+MESH
      LINT(I,J2)=LIN(NC,2)
      DO 130 K=1,5
      K1=K+KA
      QUDT(I,K1)=QUD(NC,K)
130   CONTINUE
      GOTO(140,140,140),I
      GOTO 190
140   DO 150 L=1,8
      CUBT(I,L)=CUB(I,L)
150   CONTINUE
      DO 160 L=9,13
      LA1=L+(8*MESH)-8
      CUBT(I,LA1)=CUB(I,L)
160   CONTINUE
      LA2=8*MESH+7
      CUBT(I,LA2)=CUB(I,14)
      DO 170 M=1,13
      QURT(I,M)=QUR(I,M)
170   CONTINUE
      QURT(I,15)=QUR(I,14)
      DO 180 M=15,19
      MA7=M+3
      QURT(I,MA7)=QUR(I,M)
180   CONTINUE
      QURT(I,26)=QUR(I,20)
      QURT(I,27)=QUR(I,21)
      IF(I.EQ.3)GOTO 310
      GOTO 340
190   DO 200 L=1,8
      L1=L+LA
      CUBT(I,L1)=CUB(NC,L)
200   CONTINUE
      CUBT(I,L2)=CUB(NC,9)
      DO 210 L=10,13
      L3=L+L2-8
      CUBT(I,L3)=CUB(NC,L)
210   CONTINUE
```

```
      M2=M+M1
      QURT(I,M2)=QUR(NC,M)
220   CONTINUE
      M3=M1+6
      QURT(I,M3)=QUR(NC,4)
      DO 230 M=5,8
      M4=M+M1+3
      QURT(I,M4)=QUR(NC,M)
230   CONTINUE
      DO 240 M=9,13
      M5=M+M1+4
      QURT(I,M5)=QUR(NC,M)
240   CONTINUE
      NEND=3*MESH-I+1
      GOTO(250,250,250),NEND
      GOTO 270
250   L4=L2+6
      CUBT(I,L4)=CUB(NC,14)
      DO 260 M=14,21
      M6=M+M1+4
      QURT(I,M6)=QUR(NC,M)
260   CONTINUE
      GOTO 330
270   L4=L2+7
      CUBT(I,L4)=CUB(NC,14)
      M6=M1+19
      QURT(I,M6)=QUR(NC,14)
      DO 280 M=15,19
      M7=M+M1+7
      QURT(I,M7)=QUR(NC,M)
280   CONTINUE
      DO 290 M=20,21
      M8=M+M1+10
      QURT(I,M8)=QUR(NC,M)
290   CONTINUE
      IF(NC.EQ.3)GOTO 300
      GOTO 320
300   L2=L2+6
      M1=M1+18
310   J1=J1+1
      KA=KA+3
      LA=LA+8
      NC=0
320   CONTINUE
330   CONTINUE
340   CONTINUE
350   CONTINUE
C
C     SET PARAMETERS FOR NON-LINEAR SOLUTION ROUTINE
C
      N=11
      DSTEP=1.0D-5
      DMAX=20.0D0
      ACC=1.0D-15
      MAXFUN=1500
      IPRINT=1
      NINV=11
      CALL NS01A(N,DSTEP,DMAX,ACC,MAXFUN,IPRINT,MESH,IWRI,NINV,SCALE1,
```

```
      STOP
      END
      SUBROUTINE CALFUN(MESH,SCALE1,SCALE2,SCALE3)
      IMPLICIT REAL*8(A-H,O-Z)
C
C     DEFINITION OF FUNCTIONS AS REQUIRED BY THE
C     NON-LINEAR SOLUTION ROUTINE.
C
      COMMON/ACOM/LINT,QUDT,CUBT,QURT,CUCO,QRCO,U,G
      COMMON/DCOM/X,F
      COMMON/FCOM/SCALE
      DIMENSION LINT(12,8),QUDT(12,14),CUCO(14,3),CUBT(12,56),QRCO(21,
     1 4),QURT(12,75),G(4),F(11),X(11),U(30),B(12),SCALE(11)
      INTEGER CUCO,QRCO
      REAL*8 LINT
      IF(NSETZX.GT.0)GOTO 10
10    IEND=3*MESH
      NMESH=IEND-3
      IQR1=1
      IQR2=14
      IQR3=5
      IQR4=19
      IQR5=9
      NQR1=0
      NQR2=13
      NQR3=0
      NQR4=0
      NQR5=0
      NQR6=0
      NQR7=0
      NQR8=0
      NQR9=0
C
C     ALLOWANCE MADE FOR SCALING THE EQUATIONS
C     IF REQUIRED.
C
      SCALE1=1.0
      SCALE2=1.0
      SCALE3=1.0
C
C     SET INITIAL CONDITIONS.
C
      U(1)=0.0
      U(2)=0.44178686D+02
      U(3)=0.72632190D-01
      U(4)=0.30046676D+03
      U(5)=0.66386309D+02
      U(6)=0.81412984D-01
      U(7)=0.41123918D+03
      U(8)=0.15671412D+02
      U(9)=0.78179938D-01
C
C     SET INITIAL FREE BOUNDARY CONDITIONS.
C
      U(10)=4.0*U(7)/3.0-U(4)/3.0
      U(11)=0.0
      U(12)=4.0*U(9)*3.0-U(7)/3.0
C
C     SET SYMMETRY BOUNDARY CONDITIONS.
```

```
      U(14)=X(4)*SCALE2
      U(15)=X(5)*SCALE3
      U(16)=0.0
      U(17)=X(1)*SCALE2
      U(18)=X(2)*SCALE3
      U(19)=X(3)*SCALE1
      U(20)=X(4)*SCALE2
      U(21)=X(5)*SCALE3
      U(22)=X(6)*SCALE1
      U(23)=X(7)*SCALE2
      U(24)=X(8)*SCALE3
      U(25)=X(9)*SCALE1
      U(26)=X(10)*SCALE2
      U(27)=X(11)/SCALE3
C
C     SET FREE BOUNDARY CONDITIONS.
C
      U(28)=(4.0*U(25)/3.0-U(22)/3.0)
      U(29)=0.0
      U(30)=(4.0*U(27)/3.0-U(24)/3.0)
C
C     DEFINITION OF FUNCTIONS AS ILLUSTRATED IN
C     FLOW DIAGRAM OF FIGURE 37.
C
      DO 370 I=1,IEND
      G(1)=0.0
      JEND1=2.0*MESH
      DO 40 J1=1,JEND1
      IF(J1.GT.MESH)GOTO 20
      I1=3*J1-2
      GOTO 30
20    I1=3*J1+1
30    G(1)=G(1)+LINT(I,J1)*U(I1)
      IF(NSETZX.GT.0)GOTO 40
40    CONTINUE
      G(2)=0.0
      JEND2=3*MESH+2
      DO 90 J2=1,JEND2
      IF(J2.EQ.1)GOTO 50
      GOTO(60,70),NUM
      I3=I3+4
      NUM=1
      GOTO 80
50    I2=3*MESH+2
      I3=I2+4
      NUM=1
      GOTO 80
60    I2=I2+1
      I3=I3-1
      NUM=2
      GOTO 80
70    I2=I2+2
      NUM=3
80    G(2)=G(2)+QUDT(I,J2)*U(I2)*U(I3)
      IF(NSETZX.GT.0)GOTO 90
90    CONTINUE
      G(3)=0.0
      ICU1=0
```

```
      NCU2=0
      NCU3=1
      NCU4=0
      JEND3=14*MESH
      DO 190 J3=1,JEND3
      IF(J3.EQ.1)NSET=4
      IF(J3.EQ.8*MESH+1)NSET=1
      GOTO(120,140,170,100),NSET
      IF(NCU1.EQ.MESH)GOTO 120
  100 CONTINUE
      ICU1=ICU1+1
      IADD1=3*MESH+3*NCU1-3
      I4=CUCO(ICU1,1)+3*NCU1
      I5=CUCO(ICU1,2)+IADD1
      I6=CUCO(ICU1,3)+IADD1
      IF(ICU1.EQ.8)GOTO 110
      GOTO 180
  110 ICU1=0
      NCU1=NCU1+1
      GOTO 180
  120 NCU2=NCU2+1
      I4=CUCO(9,1)+3*MESH+3*NCU2-6
      I5=I4+4
      I6=I4+5
      IF(J3.EQ.8*MESH+1)GOTO 130
      NSET=3
      GOTO 180
  130 NSET=2
      GOTO 180
  140 ICU3=ICU3+1
      IADD2=3*NCU3+3*MESH-6
      I4=CUCO(ICU3,1)+IADD2
      I5=CUCO(ICU3,2)+IADD2
      I6=CUCO(ICU3,3)+IADD2
      IF(ICU3.EQ.13)GOTO 150
      GOTO 180
  150 ICU3=9
      NCU3=NCU3+1
      IF(J3.EQ.14*MESH-1)GOTO 160
      NSET=1
      GOTO 180
  160 NSET=3
      GOTO 180
  170 NCU4=NCU4+1
      I4=CUCO(14,1)+3*MESH+3*NCU4-6
      I5=I4+1
      I6=I4+2
      NSET=2
      IF(J3.EQ.JEND3)NSET=4
  180 G(3)=G(3)+CUBT(I,J3)*U(I4)*U(I5)*U(I6)
      IF(NSETZX.GT.0)GOTO 190
  190 CONTINUE
      G(4)=0.0
      JEND4=18*MESH+3
      DO 360 J4=1,JEND4
      IF(J4.LT.14)GOTO 210
      IF(J4.GT.18*MESH-5)GOTO 230
      GOTO(200,250,200,290,330,240,270,310),NSET
```

```
      I7=QRCO(1,1)+INCR3
      I8=I7
      I9=I7+5
      I10=I7+5
      NSET=6
      IF(NQR3.EQ.MESH-1)NQR3=0
      GOTO 350
210   NQR1=NQR1+1
      I7=QRCO(NQR1,1)+NMESH
      I8=QRCO(NQR1,2)+NMESH
      I9=QRCO(NQR1,3)+NMESH
      I10=QRCO(NQR1,4)+NMESH
      IF(J4.EQ.13)GOTO 220
      GOTO 350
220   NSET=1
      NQR1=0
      GOTO 350
230   NQR2=NQR2+1
      INCR2=2*NMESH
      I7=QRCO(NQR2,1)+INCR2
      I8=QRCO(NQR2,2)+INCR2
      I9=QRCO(NQR2,3)+INCR2
      I10=QRCO(NQR2,4)+INCR2
      IF(J4.EQ.18*MESH+3)NQR2=13
      GOTO 350
240   NQR4=NQR4+1
      INCR4=NMESH+3*NQR4-3
      I7=QRCO(14,1)+INCR4
      I8=I7+2
      I9=I8
      I10=I8+1
      NSET=2
      IF(NQR4.EQ.MESH-1)NQR4=0
      GOTO 350
250   IQR1=IQR1+1
      INCR5=NMESH+3*NQR5+3
      I7=QRCO(IQR1,1)+INCR5
      I8=QRCO(IQR1,2)+INCR5
      I9=QRCO(IQR1,3)+INCR5
      I10=QRCO(IQR1,4)+INCR5
      IF(IQR1.EQ.3)GOTO 260
      GOTO 350
260   IQR1=1
      NQR5=NQR5+1
      NSET=7
      IF(NQR5.EQ.MESH-1)NQR5=0
      GOTO 350
270   IQR2=IQR2+1
      INCR6=NMESH+3*NQR6
      I7=QRCO(IQR2,1)+INCR6
      I8=QRCO(IQR2,2)+INCR6
      I9=QRCO(IQR2,3)+INCR6
      I10=QRCO(IQR2,4)+INCR6
      IF(IQR2.EQ.19)GOTO 280
      GOTO 350
280   IQR2=14
      NQR6=NQR6+1
      NSET=4
```

```
290   IQR3=IQR3+1
      INCR7=NMESH+3*NQR7+3
      I7=QRCO(IQR3,1)+INCR7
      I8=QRCO(IQR3,2)+INCR7
      I9=QRCO(IQR3,3)+INCR7
      I10=QRCO(IQR3,4)+INCR7
      IF(IQR3.EQ.8)GOTO 300
      GOTO 350
300   IQR3=5
      NQR7=NQR7+1
      NSET=8
      IF(NQR7.EQ.MESH-1)NQR7=0
      GOTO 350
310   IQR4=IQR4+1
      INCR8=NMESH+3*NQR8
      I7=QRCO(IQR4,1)+INCR8
      I8=QRCO(IQR4,2)+INCR8
      I9=QRCO(IQR4,3)+INCR8
      I10=QRCO(IQR4,4)+INCR8
      IF(IQR4.EQ.21)GOTO 320
      GOTO 350
320   IQR4=19
      NQR8=NQR8+1
      NSET=5
      IF(NQR8.EQ.MESH-1)NQR8=0
      GOTO 350
330   IQR5=IQR5+1
      INCR9=NMESH+3*NQR9+3
      I7=QRCO(IQR5,1)+INCR9
      I8=QRCO(IQR5,2)+INCR9
      I9=QRCO(IQR5,3)+INCR9
      I10=QRCO(IQR5,4)+INCR9
      IF(IQR5.EQ.13)GOTO 340
      GOTO 350
340   IQR5=9
      NQR9=NQR9+1
      NSET=1
      IF(J4.EQ.JEND4)NSET=4
      IF(NQR9.EQ.MESH-1)NQR9=0
350   G(4)=G(4)+QURT(I,J4)*U(I7)*U(I8)*U(I9)*U(I10)
      IF(NSETZX.GT.0)GOTO 360
360   CONTINUE
      NSETZX=1
      IF(I.EQ.1)GOTO 370
      IFUNC=I-1
      F(IFUNC)=(G(1)+G(2)+G(3)+G(4)-B(I))/SCALE(IFUNC)
370   CONTINUE
      RETURN
      END
      SUBROUTINE NS01A(N,DSTEP,DMAX,ACC,MAXFUN,IPRINT,MESH,IWRI,NINV,
     1 SCALE1,SCALE2,SCALE3)
C
C     POWELL'S SOLUTION ROUTINE FOR ALGEBRAIC
C     NON-LINEAR SIMULTANEOUS EQUATIONS.
C     (NB; FLOW CHART ILLUSTRATED IN FIGURE 40).
C
      IMPLICIT REAL*8(A-H,O-Z)
      COMMON/BCOM/AJINV,W
```

```
      DIMENSION X(11),F(11),AJINV(11,11),W(300),A(121)
C
C     SET VARIOUS PAREMETERS
C
      MAXC=0
      IMAXC=0
C
C     MAXC COUNTS THE NUMBER OF CALLS OF CALFUN
C
      NT=N+4
      NTEST=NT
C
C     NT AND NTEST CAUSE AN ERROR RETURN IF F(X) DOES NOT DECREASE
C
      DTEST=DFLOTI(N+N)-5.0D-1
C     DTEST IS USED TO MAINTAIN LINEAR INDEPENDENCE
      NX=N*N
      NF=NX+N
      NW=NF+N
      MW=NW+N
      NDC=MW+N
      ND=NDC+N
C
C     THESE PARAMETERS SEPERATE THE WORKING SPACE W
C
      FMIN=0.0
C
C     USUALLY FMIN IS THE LEAST CALCULATED VALUE OF F(X),
C     THE BEST X IS IN W(NX+1) TO W(NX+N)
C
      DD=0.0
C
C     USUALLY DD IS THE SQUARE OF THE CURRENT STEPLENGTH
C
      DSS=DSTEP*DSTEP
      DM=DMAX*DMAX
      DMM=4.0D0*DM
      IS=5
C
C     IS CONTROLS A GO TO STATEMENT FOLLOWING ACALL OF CALFUN
C
      TINC=1.0
C
C     TINC IS USED IN THE CRITERION TO INCREASE THE STEPLENGTH
C
      IF(IPRINT)20,20,10
10    PRINT 1000
C
C     CALL THE SUBROUTINE CALFUN
C
20    MAXC=MAXC+1
      CALL CALFUN(MESH,SCALE1,SCALE2,SCALE3)
C
C     TEST FOR CONVERGENCE
C
      FSQ=0.0
      DO 30 I=1,N
      FSQ=FSQ+F(I)*F(I)
```

```
C
C     PROVIDE PRINTING OF FINAL SOLUTION IF REQUESTED
C
40    CONTINUE
50    PRINT 2000,MAXC
      PRINT 3000,(I,X(I),F(I),I=1,N)
      PRINT 4000,FSQ
60    RETURN
C
C     TEST FOR ERROR RETURN BECAUSE F(X) DOES NOT DECREASE
C
70    GOTO(80,160,160,80,160),IS
80    IF(FSQ-FMIN)150,90,90
90    IF(DD-DSS)100,100,160
100   NTEST=NTEST-1
      IF(NTEST)140,110,160
110   PRINT 5000,NT
120   DO 130 I=1,N
      X(I)=W(NX+I)
      F(I)=W(NF+I)
130   CONTINUE
      FSQ=FMIN
      GOTO 40
C
C     ERROR RETURN BECAUSE NEW JACOBIAN IS UNSUCCESSFUL
C
140   PRINT 6000
      GOTO 120
150   NTEST=NT
C
C     TEST WHETHER THERE HAVE BEEN MAXFUN CALLS OF CALFUN
C
160   IF(MAXFUN-MAXC)170,170,180
170   PRINT 7000,MAXC
      IF(FSQ-FMIN)40,120,120
C
C     PROVIDE PRINTING IF REQUESTED
C
180   IF(IPRINT)220,220,190
190   IMAXC=IMAXC+1
      IF(MAXC.EQ.1)GOTO 200
      IF(IMAXC.NE.20)GOTO 220
200   CONTINUE
      IMAXC=0
210   PRINT 8000,MAXC
      PRINT 3000,(I,X(I),F(I),I=1,N)
      PRINT 4000,FSQ
220   GOTO(770,840,270,810,230),IS
C
C     STORE THE RESULT OF THE INITIAL CALL OF CALFUN
C
230   FMIN=FSQ
      DO 240 I=1,N
      W(NX+I)=X(I)
      W(NF+I)=F(I)
240   CONTINUE
C
C     CALCULATE A NEW JACOBIAN APPROXIMATION
```

```
260   IC=IC+1
      X(IC)=X(IC)+DSTEP
      GOTO 20
270   K=IC
      DO 280 I=1,N
      W(K)=(F(I)-W(NF+I))/DSTEP
      K=K+N
280   CONTINUE
      X(IC)=W(NX+IC)
      IF(IC-N)260,290,290
C
C     CALCULATE THE INVERSE OF THE JACOBIAN AND SET
C     THE DIRECTION MATRIX
C
290   K=0
      DO 310 I=1,N
      DO 300 J=1,N
      K=K+1
      AJINV(I,J)=W(K)
      W(ND+K)=0.0
300   CONTINUE
      W(NDC+K+I)=1.0
      W(NDC+I)=1.0D0+DFLOTI(N-I)
310   CONTINUE
      DO 320 J=1,N
      DO 320 I=1,N
      KADD=(J-1)*N+I
320   A(KADD)=AJINV(I,J)
      CALL INVERT(NINV,IWRI)
      DO 330 J=1,N
      DO 330 I=1,N
      LADD=(J-1)*N+I
330   AJINV(I,J)=A(LADD)
C
C     START ITERATION BY PREDICTING THE DESCENT
C     AND NEWTON MINIMA
C
340   DS=0.0
      DN=0.0
      SP=0.0
      DO 360 I=1,N
      X(I)=0.0
      F(I)=0.0
      K=I
      DO 350 J=1,N
      X(I)=X(I)-W(K)*W(NF+J)
      F(I)=F(I)-AJINV(I,J)*W(NF+J)
      K=K+N
350   CONTINUE
      DS=DS+X(I)*X(I)
      DN=DN+F(I)*F(I)
      SP=SP+X(I)*F(I)
360   CONTINUE
C
C     TEST WHETHER A NEARBY STATIONARY POINT IS PREDICTED
C
      IF(FMIN*FMIN-DMM*DS)410,410,370
```

```
C
370   GOTO(390,390,380),IS
380   PRINT 9000
      GOTO 120
390   NTEST=0
      DO 400 I=1,N
      X(I)=W(NX+I)
400   CONTINUE
      GOTO 250
C
C     TEST WHETHER TO APPLY FULL NEWTON CORRECTION
C
410   IS=2
      IF(DN-DD)420,420,440
420   DD=DMAX1(DN,DSS)
      DS=2.5D-1*DN
      TINC=1.0
      IF(DN-DSS)430,590,590
430   IS=4
      GOTO 740
C
C     CALCULATE THE LENGTH OF THE STEEPEST DESCENT STEP
C
440   K=0
      DMULT=0.0
      DO 460 I=1,N
      DW=0.0
      DO 450 J=1,N
      K=K+1
      DW=DW+W(K)*X(J)
450   CONTINUE
      DMULT=DMULT+DW*DW
460   CONTINUE
      DMULT=DS/DMULT
      DS=DS*DMULT*DMULT
C
C     TEST WHETHER TO USE THE STEEPEST DESCENT DIRECTION
C
      IF(DS-DD)500,470,470
C
C     TEST WHETHER THE INITIAL VALUE OF DD HAS BEEN SET
C
470   IF(DD)480,480,490
480   DD=DMAX1(DSS,DMIN1(DM,DS))
      DS=DS/(DMULT*DMULT)
      GOTO 410
C
C     SET THE MULTIPLYER OF THE STEEPEST DESCENT DIRECTION
C
490   ANMULT=0.0
      DMULT=DMULT*DSQRT(DD/DS)
      GOTO 510
C
C     INTERPOLATE BETWEEN THE STEEPEST DESCENT
C     AND THE NEWTON DIRECTIONS
C
500   SP=SP*DMULT
      ANMULT=(DD-DS)/((SP-DS)+DSQRT((SP-DD)**2+(DN-DD)*(DD-DS)))
```

```
C     CALCULATE THE CHANGE IN X AND ITS ANGLE
C     WITH THE FIRST DIRECTION
C
510   DN=0.0
      SP=0.0
      DO 520 I=1,N
      F(I)=DMULT*X(I)+ANMULT*F(I)
      DN=DN+F(I)*F(I)
      SP=SP+F(I)*W(ND+I)
520   CONTINUE
      DS=2.5D-1*DN
C
C     TEST WHETHER AN EXTRA STEP IS NEEDED FOR INDEPENDENCE
C
      IF(W(NDC+1)-DTEST)590,590,530
530   IF(SP*SP-DS)550,590,590
C
C     TAKE THE EXTRA STEP AND UPDATE THE DIRECTION MATRIX.
C
540   IS=2
550   DO 560 I=1,N
      X(I)=W(NX+I)+DSTEP*W(ND+I)
      W(NDC+I)=W(NDC+I+1)+1.0D0
560   CONTINUE
      W(ND)=1.0
      DO 580 I=1,N
      K=ND+I
      SP=W(K)
      DO 570 J=2,N
      W(K)=W(K+N)
      K=K+N
570   CONTINUE
      W(K)=SP
580   CONTINUE
      GOTO 20
C
C     EXPRESS THE NEW DIRECTION IN TERMS OF THOSE OF THE
C     DIRECTION MATRIX,AND UPDATE THE COUNTS IN W(NDC+1) ETC
C
590   SP=0.0
      K=ND
      DO 650 I=1,N
      X(I)=DW
      DW=0.0
      DO 600 J=1,N
      K=K+1
      DW=DW+F(J)*W(K)
600   CONTINUE
      GOTO(630,610),IS
610   W(NDC+I)=W(NDC+I)+1.0D0
      SP=SP+DW*DW
      IF(SP-DS)650,650,620
620   IS=1
      KK=I
      X(1)=DW
      GOTO 640
630   X(I)=DW
640   W(NDC+I)=W(NDC+I+1)+1.0D0
```

```
C     REORDER THE DIRECTIONS SO THAT KKIS FIRST
C
      IF(KK-1)690,690,660
660   KS=NDC+KK*N
      DO 680 I=1,N
      K=KS+I
      SP=W(K)
      DO 670 J=2,KK
      W(K)=W(K-N)
      K=K-N
670   CONTINUE
      W(K)=SP
680   CONTINUE
C
C     GENERATE THE NEW ORTHOGONAL DIRECTION MATRIX
C
690   DO 700 I=1,N
      W(NW+I)=0.0
700   CONTINUE
      SP=X(1)*X(1)
      K=ND
      DO 720 I=2,N
      DS=DSQRT(SP*(SP+X(I)*X(I)))
      DW=SP/DS
      DS=X(I)/DS
      SP=SP+X(I)*X(I)
      DO 710 J=1,N
      K=K+1
      W(NW+J)=W(NW+J)+X(I-1)*W(K)
      W(K)=DW*W(K+N)-DS*W(NW+J)
710   CONTINUE
720   CONTINUE
      SP=1.0D0/DSQRT(DN)
      DO 730 I=1,N
      K=K+1
      W(K)=SP*F(I)
730   CONTINUE
C
C     CALCULATE THE NEXT VECTOR X AND
C     PREDICT THE RIGHT HAND SIDES
C
740   FNP=0.0
      K=0
      DO 760 I=1,N
      X(I)=W(NX+I)+F(I)
      W(NW+I)=W(NF+I)
      DO 750 J=1,N
      K=K+1
      W(NW+I)=W(NW+I)+W(K)*F(J)
750   CONTINUE
      FNP=FNP+W(NW+I)**2
760   CONTINUE
C
C     CALL CALFUN USING THE NEW VECTOR OF VARIABLES
C
      GOTO 20
C
```

```
      IF(DMULT)780,790,790
  780 DD=DMAX1(DSS,2.5D-15*DD)
      TINC=1.0
      IF(FSQ-FMIN)820,840,840
C
C     TRY THE TEST TO DECIDE WHETHER TO INCREASE
C     THE STEP LENGTH
C
  790 SP=0.0
      SS=0.0
      DO 800 I=1,N
      SP=SP+DABS(F(I)*(F(I)-W(NW+I)))
      SS=SS+(F(I)-W(NW+I))**2
  800 CONTINUE
      PJ=1.0D0+DMULT/(SP+DSQRT(SP*SP+DMULT*SS))
      SP=DMIN1(4.0D0,TINC,PJ)
      TINC=PJ/SP
      DD=DMIN1(DM,SP*DD)
      GOTO 820
C
C     IF F(X) IMPROVES STORE THE NEW VALUE OF X
C
  810 IF(FSQ-FMIN)820,540,540
  820 FMIN=FSQ
      DO 830 I=1,N
      SP=X(I)
      X(I)=W(NX+I)
      W(NX+I)=SP
      SP=F(I)
      F(I)=W(NF+I)
      W(NF+I)=SP
      W(NW+I)=-W(NW+I)
  830 CONTINUE
      IF(IS-1)840,840,540
C
C     CALCULATE THE CHANGE IN F AND IN X
C
  840 DO 850 I=1,N
      X(I)=X(I)-W(NX+I)
      F(I)=F(I)-W(NF+I)
  850 CONTINUE
C
C     UPDATE THE APPROXIMATIONS TO J AND AJINV
C
      K=0
      DO 870 I=1,N
      W(MW+I)=X(I)
      W(NW+I)=F(I)
      DO 860 J=1,N
      W(MW+I)=W(MW+I)-AJINV(I,J)*F(J)
      K=K+1
      W(NW+I)=W(NW+I)-W(K)*X(J)
  860 CONTINUE
  870 CONTINUE
      SP=0.0
      SS=0.0
      DO 890 I=1,N
```

```
      DS=DS+AJINV(J,I)*A(J)
  880 CONTINUE
      SP=SP+DS*F(I)
      SS=SS+X(I)*X(I)
      F(I)=DS
  890 CONTINUE
      DMULT=1.0
      IF(DABS(SP)-1.0D-1*SS)900,910,910
  900 DMULT=0.8
  910 PJ=DMULT/SS
      PA=DMULT/(DMULT*SP+(1.0D0-DMULT)*SS)
      K=0
      DO 930 I=1,N
      SP=PJ*W(NW+I)
      SS=PA*W(MW+I)
      DO 920 J=1,N
      K=K+1
      W(K)=W(K)+SP*X(J)
      AJINV(I,J)=AJINV(I,J)+SS*F(J)
  920 CONTINUE
  930 CONTINUE
      GOTO 340
 1000 FORMAT('1')
 2000 FORMAT(///5X,'THE FINAL SOLUTION CALCULATED BY NS01A','REQUIRED',
     1 I5,'CALLS OF CALFUN AND IS',/)
 3000 FORMAT(/4X,'I',7X,'X(I)',12X,'F(I)',//(I5,2E17.8))
 4000 FORMAT(/5X,'THE SUM OF SQUARES IS',E17.8)
 5000 FORMAT(///5X,'ERROR RETURN FROM NS01A BECAUSE',I5,'CALLS OF
     1 CALFUN FAILED TO IMPROVE THE RESIDUALS')
 6000 FORMAT(///5X,'ERROR RETURN FROM NS01A BECAUSE F(X)','FAILED TO
     1 DECREASE USING A NEW JACOBIAN')
 7000 FORMAT(///5X,'ERROR RETURN FROM NS01A BECAUSE','THERE HAVE BEEN',
     1 I5,'CALLS OF CALFUN')
 8000 FORMAT(///5X,'AT THE',I5,'TH CALL OF CALFUN WE HAVE')
 9000 FORMAT(///5X,'ERROR RETURN FROM NS01A BECAUSE',' A NEARBY
     1 STATIONARY POINT IS PREDICTED')
      END
      SUBROUTINE INVERT(NINV,IWRI)
C
C      GAUSS-JORDAN METHOD
C
      IMPLICIT REAL*8(A-H,O-Z)
      COMMON/CCOM/LIV,MIV
      COMMON/ECOM/A
      DIMENSION A(121),LIV(11),MIV(11)
C     SEARCH FOR LARGEST ELEMENT
      IWRI=IWRI+1
      IF(IWR.LE.10)TYPE 1000,NINV,IWRI
      D=1.0
      NK=-NINV
      DO 190 K=1,NINV
      NK=NK+NINV
      LIV(K)=K
      MIV(K)=K
      KK=NK+K
      BIGA=A(KK)
      DO 30 J=K,NINV
      IZ=NINV*(J-1)
```

```
20    BIGA=A(IJ)
      LIV(K)=I
      MIV(K)=J
30    CONTINUE
C     INTERCHANGE ROWS
      J=LIV(K)
      IF(J-K)60,60,40
40    KI=K-NINV
      DO 50 I=1,NINV
      KI=KI+NINV
      HOLD=-A(KI)
      JI=KI-K+J
      A(KI)=A(JI)
50    A(JI)=HOLD
C     INTERCHANGE COLUMNS
60    I=MIV(K)
      IF(I-K)90,90,70
70    JP=NINV*(I-1)
      DO 80 J=1,NINV
      JK=NK+J
      JI=JP+J
      HOLD=-A(JK)
      A(JK)=A(JI)
80    A(JI)=HOLD
C     DIVIDE COLUMN BY MINUS PIVOT (VALUE OF PIVOT
C      ELEMENT IS CONTAINED IN BIGA)
90    IF(DABS(BIGA)-1.0D-20)100,100,110
100   D=0.0
      TYPE 2000
      RETURN
110   DO 130 I=1,NINV
      IF(I-K)120,130,120
120   IK=NK+I
      A(IK)=A(IK)/(-BIGA)
130   CONTINUE
C     REDUCE MATRIX
      DO 160 I=1,NINV
      IK=NK+I
      HOLD=A(IK)
      IJ=I-NINV
      DO 160 J=1,NINV
      IJ=IJ+NINV
      IF(I-K)140,160,140
140   IF(J-K)150,160,150
150   KJ=IJ-I+K
      A(IJ)=HOLD*A(KJ)+A(IJ)
160   CONTINUE
C     DIVIDE ROW BY PIVOT
      KJ=K-NINV
      DO 180 J=1,NINV
      KJ=KJ+NINV
      IF(J-K)170,180,170
170   A(KJ)=A(KJ)/BIGA
180   CONTINUE
C     PRODUCT OF PIVOTS
      D=D*BIGA
C     REPLACE PIVOT BY RECIPROCAL
```

```
C     FINAL ROW AND COLUMN INTERCHANGE
      K=NINV
200   K=(K-1)
      IF(K)270,270,210
210   I=LIV(K)
      IF(I-K)240,240,220
220   JQ=NINV*(K-1)
      JR=NINV*(I-1)
      DO 230 J=1,NINV
      JK=JQ+J
      HOLD=A(JK)
      JI=JR+J
      A(JK)=-A(JI)
230   A(JI)=HOLD
240   J=MIV(K)
      IF(J-K)200,200,250
250   KI=K-NINV
      DO 260 I=1,NINV
      KI=KI+NINV
      HOLD=A(KI)
      JI=KI-K+J
      A(KI)=-A(JI)
260   A(JI)=HOLD
      GOTO 200
270   RETURN
1000  FORMAT(5X,'NINV=',I3,I3)
2000  FORMAT('0','SINGULAR')
      END
```

APPENDIX III

A GLOSSARY OF MAJOR TERMS

a	- Coefficient of the ψ-approximating Function
b	- Coefficient of the ϕ-approximating Function
$b_{(x)}$	- The Jet Breadth at X
c	- Coefficient of the L-approximating Function
C	- Matrix of Parametric Coefficients
C , C_D, C_B, C_s	- Constants Appearing in the Governing Equations
d	- Displacement of Effective Centre of Total Head Tube
$f(x)$	- Function of x
$f(X)$	- $f_i(x_1, x_2, \ldots, x_n)$ $(i = 1,n)$
$F(X)$	- Sum of the Squares of the Residuals, $\sum_{i=1}^{n}(f_i(X))^2$
g	- Gradient
h	- Element Geometry Parameter
I	- The Unit Matrix
J	- The Jacobian Matrix
k	- The Kinetic Energy of Turbulence
L	- Length Scale
n	- Number of Translations in Co-ordinate Transformation
N	- Number of Global Unknowns
P, P, p	- Total, Mean and Fluctuating Pressures, respectively
Re	- Reynolds Number
t	- Time
U,V,W	- Total Velocities in respective X, Y and Z Directions
U, V, W	- Corrosponding Mean Velocities
u, v, w	- Corrosponding Fluctuating Velocities
u_i	- Parametric Local Generalised Co-ordinates
$U(i)$	- Parametric Global Generalised Co-ordinates
X, Y, Z	- Global Cartesian Co-ordinates
x, y, z	- Local Cartesian Co-ordinates
$Y\|_{0.5}$	- The Ordinate at which $U = \frac{1}{2}U_m$

(continued)

α - The Jet Angle of Spread

β - The Jet Half Angle

γ - The Intermittancy

δ - Steplength

ϵ - The Dissipation Term in The Energy Equation

λ - Parametric Coefficient in General Approximating Function

μ - Dynamic Fluid Viscosity

ν - Kinematic Fluid Viscosity

π - Parametric Generalised Co-ordinate

ρ - Fluid Density

σ_K, σ_{KL} - Constant Effective Prandtl Numbers

τ - Shear Stress

ϕ - Square Root of Kinetic Energy of Turbulence

ψ - Stream Function

Subscripts

e - Relating to Local Element

fb - Free Boundary

m - Maximum

o - Relating to Efflux Section (or zero time)

sb - Symmetry Boundary

t - Turbulent

APPENDIX IV

BIBLIOGRAPHY.

1. The Oxford English Dictionary.
   Oxford University Press, 1971.

2. Diffusion of Submerged Jets.
   M L Albertson et al.
   A.S.C.E., 74, 1948.

3. The Turbulent Spreading of the Water Jet.
   A M Binnie.
   Engineering, 153, 1942.

4. Hot-wire Measurements in a Plane Turbulent Jet.
   G Heskestad.
   J. Appl. Mech., 23, 1965.

5. Fluid Dynamics of Jets.
   S I Pai.
   van Nostrand, 1954.

6. Turbulent Jet Expansion.
   E Förthmann.
   Ingenieur-Archiv., V, 1934.

7. Investigations of the Turbulent Mixing Regions Formed by Jets.
   A M Kuethe.
   J. Appl. Mech., 2, 1935.

8. The Calculation of the Length Scale of Turbulence in Some Shear Flows Remote From Walls.
   D B Spalding.
   Imp. Coll. Rep. TWF/TN/31, 1967.

9. Jets, Wakes and Cavities.
G Birkhoff and E H Zarontonello.
Academic Press, 1957.

10. The Theory of Turbulent Jets.
G N Abramovich.
M.I.T. Press, 1963.

11. Energy Spectrum and Turbulence Scales in a Circular Water Jet.
V W Ggoldschmidt and S C Chuang.
Trans. A.S.M.E., J. Basic Eng., 1972.

12. Momentum Diffusion from a Slot Jet into a Moving Secondary.
A S Weinstein et al.
J. Appl. Mech., 23, 1956.

13. The Stability and Transition of a Two-dimensional Jet.
H Sato.
J. Fluid Mech., 7, 1959.

14. Measurements of Velocity Distribution in a Plane Turbulent Jet of Air.
and
15. Measurements of Turbulence in a Plane Jet of Air by the Diffusion and Hot-wire Methods.
B G van Der Hegge Zijnen
Appl. Sci. Res., 7, 1958.

16. The Structure of a Self-preserving Turbulent Plane Jet.
L J S Bradbury.
J. Fluid Mech., 23, 1965.

17. Foundations of Fluid Mechanics.
S W Yuan.
Prentice-Hall, 1967.

18. Boundary Layer Theory.
H Schlichting.
McGraw-Hill, 1960.

19. Mechanics of Fluids.
W J Duncan et al.
Arnold, 1960.

20. The Structure of Turbulent Shear Flow
A A Townsend.
Cambridge University Press, 1956.

21. Simple Expressions for the Spread of Turbulent Jets.
L J S Bradbury.
Aero. Quart., XVIII, 1967.

22. Static Pressure Distribution in the Free Turbulent Jet.
D R Miller and E W Comings.
J. Fluid Mech., 3, 1957.

23. Some Measurements in the Self-preserving Jet.
I Wygnanski and H Fiedler.
Boeing Sci. Res. Lab. Rep. D1-82-0712.

24. On the Theory of the Turbulent Boundary Layer.
J Rotta.
N.A.C.A., TM 1344, 1950.

25. The Understanding and Prediction of Turbulent Flow.
P Bradshaw.
Aero. Journal, July, 1972.

26. Jets and Wall Jets in Uniform Streaming Flow.
I S Gartshore.
McGill Univ., Mech. Eng. Rep. TWF/TN/37, 1968.

27. An Introduction to Turbulence and its Measurement.
P Bradshaw.
Pergamon Press, 1971.

28. Shear flow Turbulence.
O M Phillips.
Annual Review of Fluid Mechanics, 3, 1969.

29. The History of Hydraulics.
H Rouse and S Ince.
Iowa Inst. Hydraulic Res., 1957.

30. A History and Philosophy of Fluid Mechanics.
G A Tokaty.
Foulis, 1971.

31. Science in History.
J D Bernal.
Watts, 1954.

32. Hydrodynamics and Hydraulics.
D Bernoulli and J Bernoulli.
Dover, 1968.

33. Osborne Reynolds and his Work in Hydraulics and Hydrodynamics.
A H Gibson.
Longmans, 1946.

34. Jet Flow and its Effect on Aircraft.
H B Squire.
Aircraft Eng., 22, 1950.

35. The Turbulent Jet in a Moving Fluid.
G N Abramovich.
R.A.E. Rep. 778, 1958.

36. The Plane Jet.
W Bickley.
Phil. Mag., 23, 1937.

37. The Structure and Development of a Plane Turbulent Free Jet.
A Robins.
PhD Thesis, 1971.

38. An Investigation into the Structure of a Turbulent Plane Jet.
L J S Bradbury.
PhD Thesis, 1963.

39. The Planar Turbulent Jet.
E Gutmark and I Wygnanski.
J. Fluid Mech., 73, 1976.

40. Mathematical Models of Turbulence.
B E Launder and D B Spalding.
Academic Press, 1972.

41. Air Jet and Ground Effects Apparatus.
Flint & Partners.
Technical Memorandum, TE 88.

42. Experiments on Pitot Tubes in Shear Flow.
F A MacMillan.
A.R.C., R and M, 3028, 1956.

43. Statistical Theory of Non-homogeneous Turbulence.
J Rotta.
Imp. Coll. Rep. HTS/62/18, 1968.

44. A Two-parameter Model of Turbulence and its Application to Free Jets.
W Rodi and D B Spalding.
Warme-und Stoffubertragung, Bd.3, 1970.

45. Numerical Turbulence Modelling.
M W Rubesin.
A.G.A.R.D. LS; 86, 1977.

46. Calculation of Boundary Layer Development Using the Turbulent Energy Equation.
P Bradshaw et al.
J. Fluid Mech., 28, 1967.

47. A Reynolds Stress Model of Turbulence and its Application to Asymmetric Boundary Layers.
K Hanjalic and B E Launder.
Imp. Coll. Rep. TM/TN/A/8, 1971.

48. Uber eine Methode zur Berechnung Turbulenter Scherstromungen.
J Rotta.
Aerodynamische Versuchsanstalt Gottingen Rep. 69A, 14, 1969.

49. The Structure of Turbulence in Fully developed Pipe Flow.
J Laufer.
N.A.C.A. Rep. 1110, 1952.

50. Engineering Analysis; a Survey of Numerical Procedures.
S H Crandall.
McGraw-Hill, 1956.

51. The Numerical Treatment of Differential Equations.
L Collatz.
Springer-Verlag, 1959.

52. Discrete Methods in Structural Analysis.
N W Taylor.
PhD Thesis, 1975.

53. The Finite Element Method in Structural and Continuum Mechanics.
O C Zienkiewicz.
McGraw-Hill, 1967.

54. The Method of Weighted Residuals - A Review.
B A Finlayson and L E Scriven.
Appl. Mech. Reviews, 19, 9, 1966.

55. Approximations to Functions and to the Solutions of Differential Equations.
R A Frazer et al.
N.P.L. Rep. 1799, 1937.

56. Stiffness and Deflection Analysis of Complex Structures.
M J Turner et al.
Aero. Journal, 23/9, 1956.

57. Localised Raleigh Functions for Stuctural and Stress Analysis.
J M T Thompson.
Int. Journal Solids and Structures, 3, 1967.

58. Hermitian Methods for the Approximate Solution of Partial Differential Equations.
J G A Croll.
J. Inst. Math. Applics., 6,1970.

59. Convergence of Hypar Finite Difference Solutions.
J G A Croll and J C Scrivener.
A.S.C.E. J. Struct. Div., May, 1969.

60. A Finite Difference Procedure for the Integration of the Navier-Stokes Equations.
A K Runchal and M Wolfshtein.
Imp. Coll. Rep. SF/TN/1, 1966.

61. The Flow Past Circular Cylinders at Low Speeds.
A Thom.
Proc. Roy. Soc., 141, 1933.

62. Numerical of a Viscous Fluid Past a Circular Cylinder.
M Kawaguti and P Jain
Univ. Winsconsin Rep. MRC TSR 590, 1965.

63. Numerical Methods for Fluid Dynamics; an Annotated Bibliography.
F H Harlow.
Los Alamos Sci. Lab. Rep. LA-4281, 1969.

64. The Prediction of Two-dimensional, Steady, Turbulent Elliptic Flows.
D B Spalding.
Imp. Coll. Rep. EF/TN/A/16, 1969.

65. A Finite Difference Procedure for Solving the Equations of the Two-dimensional Boundary Layer.
S V Patankar and D B Spalding.
Int. J. Heat and Mass Transfer, 10, 1967.

66. Finite Element Applications in Fluid Dynamics.
J T Oden.
A.S.C.E., J. Eng., Mech. Div., 95, 1969.

67. Finite Element Analysis of Fluid Flows.
H C Martin.
Proc. 2nd Conf. on Matrix Methods in Struct. Mech., 1968.

68. The Application of Finite Element Method Technique to Potential Flow Problems.
G de Vries and D H Norrie.
Trans. A.S.M.E. App. Mech. Div. 71-APM-22, 1971.

69. A Survey of the Theory and Applications of the Finite Element Method in the Analysis of Viscous Incompressible Newtonian Flow.
A G Hutton.
C.E.G.B. Rep. RD/B/N3049, 1974.

70. A Block Iterative Finite Element Algorithm for the Numerical Solution of the Steady State Compressible Navier-Stokes Equations.
C H Cooke and D K Blanchard.
Int. J. Num. Meth. in Eng., II, 1977.

71. An Efficient Solution Procedure for the Incompressible Navier-Stokes Equations.
J D Murphy.
A.I.A.A. Journal, 15, 1977.

72. A Finite Element Approach to the Viscous Incompressible Flow Round a Circular Cylinder.
C W Luchi.
A.I.A.A. Journal, 15,1977.

73. A Hybrid Method for Nonlinear Equations.
and
74. A Fortran Subroutine for Solving Systems of Nonlinear Algebraic Equations.
M J D Powell.
Numerical Methods for Nonlinear Equations.
Ed. P Rabinowitz.
Gordon and Breach, 1970.

75. Numerical Methods.
R A Buckingham.
Pitman, 1962.

76. Advanced Engineering Mathematics.
E Krysig.
Wiley, 1962.

77. Heat Transfer.
A J Chapman.
Macmillan, 1974.

to Film Cooling.
S C Kacker et al.
Prog. Heat Mass Transfer, Pergamon Press, 1969.

79. A Finite Difference/Galerkin Finite Element Solution of a Turbulent Boundary Layer.
M N Bismarck-Nasr.
A.I.A.A. Journal Tech. Notes, 15, 12, 1977.

80. Instruments for Motion Measurement Using Laser Doppler Heterodyning Techniques
R C Watson et al.
I.S.A. Transactions, 8, 1969.

81. D.I.S.A Instruction Manual For Mark I Laser Doppler Anemometer.

82. Localised Fluid Flow Measurements with an He-Ne Laser Spectrometer.
Y Yeh and H Z Cummins.
Appl. Phys. Letters 4, 1964.

83. Measurement of Localised Flow Velocities in Gases with a Laser Doppler Flowmeter
J W Foreman et al.
Appl. Phys. Letters 7, 1965.

84. Turbulent Flow Measurements Utilising the Doppler Shift of Scattered Laser Radiation
Phys. Fluids, 10, 1967.
Goldstein and Hagen

85. Measurement of Turbulent Velocities From the Doppler Shift in Scattered Laser Light
E R Pike et al
J Sci. Inst., Series 2, 1, 1968.

86. A New Theoretical Model for the Laser Doppler Meter
M J Rudd.
J. Sci. Instr., 2, 2, 1969

87. Optimisation of Optical Anemometers
F Durst and J H Whitelaw.
Imp. Coll. Rept. ET/TN/A/1, 1970

88. Integrated Optical Units for Laser Anemometry
F Durst and J H Whitelaw.
J. Phys. E, 4, 1971.

89. Laser Velocimeter for Wind Tunnel Measurements
A Boutier et al.
Paper Presented at 7th Int. Conf. Sci. Instr., Shrivenham, 1977

APPENDIX V

COURSES OF POSTGRADUATE STUDY

1) The Finite Element Method - A Basic Introduction.

Course held at -

Department of Civil and Structural Engineering,

University College, Cardiff.

16 - 20 September, 1974 .

2) Turbulence and Anemometry.

Course held at -

School of Mechanical Engineering,

Cranfield Institute of Technology, Bedfordshire.

30 July - 1 August, 1975.